Behavioral and synaptic circuit analysis in models of neuropsychiatric disorders

Dissecting the *in vivo* role of the postsynaptic density proteins nArgBP2 and Shank3 using genetic engineered mice

Cátia Gisela Rebordelo Marques Feliciano

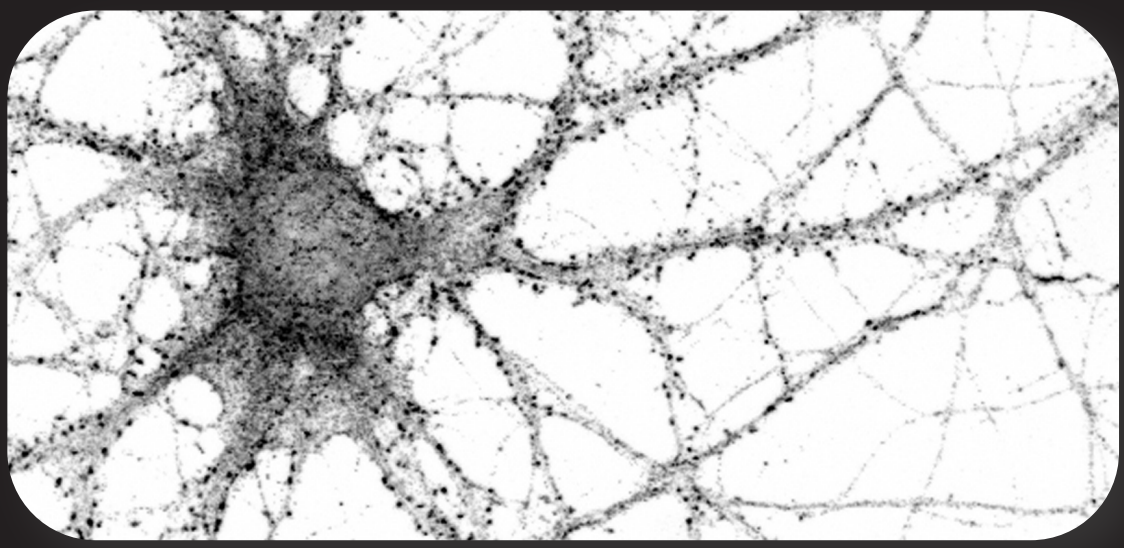

Dissertation presented to obtain the Ph.D degree in Biology

Instituto de Tecnologia Química e Biológica | Universidade Nova de Lisboa

Oeiras,
September, 2011

INSTITUTO
DE TECNOLOGIA
QUÍMICA E BIOLÓGICA
/UNL

Knowledge Creation

Behavioral and synaptic circuit analysis in models of neuropsychiatric disorders

Dissecting the *in vivo* role of the postsynaptic density proteins nArgBP2 and Shank3 using genetic engineered mice

Cátia Gisela Rebordelo Marques Feliciano

Dissertation presented to obtain the Ph.D degree in Biology

Instituto de Tecnologia Química e Biológica | Universidade Nova de Lisboa

Research work coordinated by:

FUNDAÇÃO CALOUSTE GULBENKIAN
Instituto Gulbenkian de Ciência

Oeiras,
September, 2011

INSTITUTO
DE TECNOLOGIA
QUÍMICA E BIOLÓGICA
/UNL

Knowledge Creation

Behavioral and synaptic circuit analysis in models of neuropsychiatric disorders

Dissecting the in vivo role of the postsynaptic density proteins nArgBP2 and Shank3 using genetic engineered mice

Cátia Gisela Rebordelo Marques Feliciano

Dissertação apresentada para obtenção do grau de doutor em Biologia pelo Instituto de Tecnologia Química e Biológica da Universidade de Nova de Lisboa

Orientação do Professor Doutor Guoping Feng

Duke University Medical Center and Massachusetts Institute of Technology

Co-orientação do Professor Doutor Sukalyan Chatterjee

Director do Programa Gulbenkian de Doutoramento em Biomedicina (PGDB)

Investigador Principal no Centro de Neurociências e Biologia Celular (CNC)

Esta tese foi desenvolvida com apoio financeiro da FCT e do FSE no âmbito do Quadro Comunitário de Apoio (SFRH/BD/15855-2005)

FCT Fundação para a Ciência e a Tecnologia
MINISTÉRIO DA CIÊNCIA E DO ENSINO SUPERIOR

Ciência.Inovação 2010

Financiamento no âmbito do III Quadro Comunitário de Apoio, comparticipado pelo Fundo Social Europeu e por fundos nacionais do MCES

Oeiras

2011

Table of Contents

Acknowledgments

I am sure I will never be able to completely thank everyone who supported me throughout this journey. Nonetheless, I will take this opportunity to express my gratitude to those whose friendship, mentoring and support were critical at the personal and academic level.

First and foremost I would first like to thank my Ph.D. supervisor Dr. Guoping Feng for taking me as a student and integrating me in his team. I thank him for being an enthusiastic leader and mentor, for the stimulating discussions, for his patience, his tireless energy, encouragement and insightful advices. I also thank my Ph.D. supervisor Dr. Sukalyan Chatterjee for making me push myself and enriching my scientific horizon since my first day in graduate school. I am very thankful for his support and ideas concerning my future.

I would like to gratefully acknowledge my professors at Universidade da Beira Interior; especially Dr. João Queiroz, Dr. Ignacio Verde, Dra. Graça Baltazar and Dr. José Francisco Cascalheira, for their teaching excellence and for providing a first contact with outstanding research.

I thank all the members of the Feng lab, for the stimulating and fun work environment and for all their help and advices. I am particularly thankful to Jonathan, Zhonghua, Shengli, Molly and Dongqing. I also would like to acknowledge Li Qiu, Jimmy Gross and Qun Liu for technical support and assistance with the injection of ES cells and Dr. Ramona Rodriguiz and Dr. William Wetzel for advice in behavioral experiments. Finally, I am particularly grateful to João Peça for his endless patience, encouragement and support during every step of graduate school.

I am also indebted to the Portuguese community at Duke for making Durham a familiar and enjoyable environment in which to grow as a person and as a scientist. I am especially grateful to Albino Jorge Oliveira-Maia, Teresa Carona Maia, Susana Silva, Rui Peixoto, Ana Oliveira and Catarina Cunha. Finally, Dr. Rui Costa was a very good friend, first welcoming in me to North Carolina and always providing outstanding scientific advices and encouragement.

I wish to thank my great friends Catarina Martins, Catarina Dias, Irene Oliveira, Saudade Lopes, Ana Luísa, Ana Isabel e Vera Enes for keeping Portugal a wonderful

place to go back to. Molly Heyer, Marek Łaska, Michael Wells, Katie King and Thais Vinholo for making my stay in North Carolina happier and full of good memories.

Agradeço ao IGC e ao PGDB pela oportunidade conferida e pela excepcional formação científica e pedagógica durante os cursos leccionados e o apoio financeiro. Agradeço também à Fundação para a Ciência e a Tecnologia pelo financiamento através de uma bolsa individual de doutoramento (SFRH/BD/15855-2005). I would also like to thank the National Institute of Mental Health and the Simons Foundation Autism Research Initiative for the financial support to the projects I was involved.

As minhas palavras finais vão para a minha família. Aos meus irmãos, cunhadas e sobrinhos pelo apoio emocional, por me ajudarem a ultrapassar todos os momentos difíceis e pelo ambiente familiar de amor, compreensão e felicidade. Aos meus pais por estarem sempre disponíveis, nas alegrias e nas tristezas, pela dedicação, paciência e encorajamento e, acima de tudo, por me amarem incondicionalmente e fazerem de mim quem eu sou, a eles eu dedico esta tese.

Sumário

Um ambicioso objectivo em neurociências consiste em compreender como os genes afectam a biologia neuronal, a função sináptica e o comportamento. Os genes que se pensam estar envolvidos em doenças psiquiátricas atraem maior atenção devido à alta probabilidade da sua perturbação originar alterações salientes em processos neurobiológicos. Desta forma, estes genes permitem também uma melhor compreensão de questões biomédicas relevantes. Usando o ratinho (murganho) como animal modelo pode acelerar este processo de descoberta pois trata-se de uma espécie capaz de padecer de manipulações ao nível genético, permitindo assim a recriação ortóloga de mutações humanas. Ao mesmo tempo, o conhecimento actual da neurobiologia comportamental em ratinhos pode conectar certos endofenótipos como sendo reminiscentes de perturbações humanas.

No meio pós-sináptico de neurónios glutamatérgicos encontra-se um aglomerado de proteínas essenciais para o funcionamento sináptico. Esta estrutura conhecida como densidade pós-sináptica, contém um vasto número de receptores de neurotransmissores, proteínas adaptadoras, proteínas de sinalização e proteínas de adesão, que desempenham um papel crucial na regulação da comunicação neuronal. Mais ainda, nos recentes anos, muitos dos genes que codificam estas proteínas da densidade pós-sináptica têm sido associados a um vasto leque de doenças psiquiátricas. No entanto, os mecanismos celulares envolvidos, os circuitos afectados *in vivo* e como estas mutações se traduzem em comportamentos anormais, permanece um fenómeno desconhecido para a vasta maioria destes mesmos genes.

O trabalho apresentado nesta tese tem como objectivo compreender melhor a função de duas proteínas pós-sinápticas, a nArgBP2 (*neural Arg-binding protein 2*) e a Shank3 (*SH3 and multiple ankyrin repeat domains protein 3*). Estas proteínas foram seleccionadas pois ambas podem formar interacções directas com a proteína SAPAP3 (*SAP90/PSD-95-associated protein 3*), a qual desempenha uma função crucial na densidade pós-sináptica. Por sua vez, em humanos, o gene Shank3 está fortemente associado ao desenvolvimento de autismo, enquanto o gene que codifica a nArgBP2 está localizado numa região cromossomal que foi sugerida como uma região de susceptibilidade para a doença maníaco-depressiva. Utilizando uma estratégia multidimensional, este trabalho caracteriza a expressão e localização destes dois

genes no cérebro do ratinho e, através de engenharia genética, descreve as linhagens de ratinhos mutantes que foram produzidas para avaliar *in vivo* as consequências da disrupção de Shank3 e nArgBP2.

A caracterização detalhada do RNAm do gene nArgBP2 no cérebro do ratinho mostra que este é expresso na parte frontal do cérebro. Um anticorpo anti-nArgBP2 foi gerado para caracterizar a expressão proteica ao longo do desenvolvimento e isto levou à observação de que existe um forte enriquecimento da proteína nArgBP2 na camada externa do giro dentado do hipocampo. Animais mutantes com uma disrupção da nArgBP2 apresentam comportamentos hiperactivos em ambientes novos e familiares, aumento de estereotipias, redução de comportamentos-tipo depressão e uma disfunção acentuada nos ritmos circadianos, todos estes endofenótipos característicos de comportamento-tipo maníaco. Para testar se estes comportamentos-tipo maníacos poderiam ser revertidos foi administrado lítio, que se mostrou efectivo em melhorar vários dos comportamentos anormais, incluindo as disfunções nos ritmos circadianos e a redução de comportamentos-tipo depressão. Usando técnicas de electrofisiologia e bioquímica, descobriu-se um fortalecimento na sinalização glutamatérgica e também um aumento no nível de subunidades de receptores do glutamato. No conjunto, estes dados sugerem que a nArgBP2 pode desempenhar um papel importante na regulação do comportamento e das sinapses glutamatérgicas.

Mutações e lesões no gene Shank3 estão na origem das complicações neurológicas presentes em pacientes afectados pela síndrome de Phelan-McDermid (SPM). Adicionalmente, mutações neste gene estão também presentes em doentes autistas que não apresentam SPM. Os fundamentos neurobiológicos e as disfunções sinápticas originadas pela perturbação do gene Shank3 são exploradas neste trabalho ao nível sináptico, dos circuitos neuronais e do comportamento. Por fim, das duas linhagens de ratinhos mutantes geradas para o gene Shank3, a mutação mais severa leva a que os animais exibam comportamentos repetitivos e injuriosos, e défices em interacções sociais, duas das três complicações comportamentais comummente observadas em pacientes autistas. Adicionalmente, uma análise celular, electrofisiológica e bioquímica, revela defeitos nas sinapses estriatais e nos circuitos cortico-estriatais em ratinhos mutantes para o gene Shank3. Este trabalho propõe que a Shank3 é um gene essencial para o desenvolvimento normal da conectividade

neuronal e apoia o modelo de que mutações no gene Shank3 levam ao desenvolvimento de doenças do espectro do autismo.

Summary

Understanding how discrete genes affect neuronal biology, synaptic function and, ultimately, behavior is a major goal in neuroscience. Not surprisingly, genes believed to be involved in human psychiatric and developmental brain disorders garner the most attention due to the likelihood that their disruption will promote salient changes in neurobiological functions. They also promise to nurture further understanding of relevant biomedical questions. Using the mouse as a model organism accelerates this discovery process because the species is amenable to manipulation at the genetic level, allowing for the orthologous recreation of human mutations. Simultaneously, our understanding of murine behavioral outputs can now be linked to particular endophenotypes reminiscent of human disorders.

One large cluster of proteins important for synaptic function is situated at the postsynaptic site of glutamatergic neurons. This structure, known as the postsynaptic density, contains large numbers of neurotransmitter receptors, scaffolding, signaling and adhesion proteins that play a critical role in the regulation of neuronal communication. Moreover, several of the genes which code for proteins of the postsynaptic density have in recent years been implicated in a wide spectrum of neuropsychiatric disorders. Nevertheless, the cellular mechanism involved, the neuronal circuits affected *in vivo* and the manner in which discrete mutations translate into behavioral abnormalities remain unknown for a large number of these genes.

This project aimed at increasing our understanding of the function of two postsynaptic proteins, nArgBP2 (neural Arg-binding protein 2) and Shank3 (SH3 and multiple ankyrin repeat domains protein 3). These proteins were selected because both can form dyadic interaction with SAPAP3 (SAP90/PSD-95-associated protein 3), a key protein at the postsynaptic density. In humans, Shank3, in particular, has been strongly linked with the development of autism, while nArgBP2 sits in a chromosomal region possibly linked to bipolar disorder. Using a multi-level approach, this provides a detailed characterization of the localization and expression of these genes in the mouse brain. By means of genetic engineering, mutant mouse lines were also generated to probe the *in vivo* consequences of their disruption.

A detailed characterization of nArgBP2 mRNA expression in the mouse brain demonstrates that it is widely expressed in the forebrain. Additionally, an anti-nArgBP2

antibody generated to characterize protein expression across development led to the observation of a striking enrichment of nArgBP2 in the outer molecular layer of the dentate gyrus. Furthermore, nArgBP2 disruption is shown to generate animals that display hyperactivity in novel environments and in the home cage, increased stereotypies, reduced depressive-like behaviors and a pronounced disruption in circadian rhythms, all endophenotypes of manic-like behavior. To test if the manic-like behaviors might be reversed, lithium was administered and shown to ameliorate several behavioral abnormalities including the circadian rhythm dysfunction and the reduced depressive-like behaviors. Probing the mutant animals at the electrophysiological and biochemical level uncovered an increase in glutamatergic signaling and in levels of glutamate receptor subunits at the synapse. Together, these results suggest that nArgBP2 may play an important role in the regulation of glutamatergic synapses and behavior.

Mutations and lesions in the Shank3 gene are thought to be the main source of the neurological deficits seen in Phelan-McDermid syndrome (PMS) patients. Additionally, mutations in this gene are also present in autistic patients outside of diagnosed PMS. The neurobiological substrates and synaptic dysfunctions arising from the perturbation of the Shank3 gene are explored in this work at the synaptic, circuit and behavioral level. From the two Shank3 mutant mice lines generated, the most severe mutation led to animals that exhibited self-injurious repetitive grooming and deficits in social interaction, two of the three behavioral abnormalities seen in autistic individuals. Additionally, cellular, electrophysiological and biochemical analyses uncovered defects at striatal synapses and cortico-striatal circuits in the Shank3 mutant mice. This work suggests that Shank3 is a critical gene for the normal development of neuronal connectivity and further supports the involvement of mutations in the Shank3 gene in autistic spectrum disorders.

Abbreviations

AMPA	α-amino-3-hydroxy-5-methyl-4-isoxazolepropionic acid
AOB	Accessory olfactory bulb
Arc	Arcuate hypothalamic nucleus
ARNTL, or BMAL1	Aryl hydrocarbon receptor nuclear translocator-like protein
ASDs	Autism spectrum disorders
BAC	Bacterial artificial chromosome
BDNF	Brain-derived neurotrophic factor
BLA	Basolateral anterior amygdaloid nucleus
BLP	Basolateral posterior amygdaloid nucleus
BMP	Basomedial amygdaloid nucleus
BPD	Bipolar Disorder
Clock	Circadian Locomotor Output Cycles Kaput
CREB	cAMP response element-binding
Cry	Cryptochrome
CT	Circadian time
D1R	Dopamine D1 Receptor
D2R	Dopamine D2 Receptor
DAOA	D-amino acid oxidase activator
DISC1	Disrupted-in-Schizophrenia 1
fMRI	functional magnetic resonance imaging
gcl	Granule cell layer
Gl	Glomerular layer
GSK-3β	Glycogen synthase kinase-3 beta
Hb	Habenula
KO	Knockout
LSD	Lateral septal nucleus, dorsal
MAGUK	Membrane-associated guanylate kinase
NRC/MASC	NMDA receptor complex/MAGUK-associated signaling complex
MDD	Major Depressive Disorder
MDMA	3,4-methylenedioxymethamphetamine
mGluRs	Metabotropic glutamate receptors

MH	Medial hypothalamus
ML	Mitral cell layer
NAc	Nucleus Accumbens
nArgBP2	neural Arg-binding protein 2
NMDA	N-Methyl-D-aspartic acid
NR1	NMDA receptor subunit 1
NR2A	NMDA receptor subunit 2A
NR2B	NMDA receptor subunit 2B
PCR	Polymerase chain reaction
Per gene	Period gene
PFC	Prefrontal cortex
Pir	Piriform cortex
PKCI	Protein kinase C interacting protein
PMS	Phelan-McDermid syndrome (22q13.3 deletion syndrome)
PSD	Postsynaptic Density
PSD-93	Postsynaptic density protein 93
PSD-95	Postsynaptic density protein 95
SAP102	Synapse-associated protein 102
SAPAP 1-3	SAP90/PSD95-associated protein 1-3
SCN	Suprachiasmatic Nucleus
SPON	Superior paraolivary nucleus
SHANK 1-3	SH3 and multiple ankyrin repeat domains protein 1-3
SORBS2	Sorbin and SH3 domain-containing protein 2
SPM	Synaptosomal plasma membrane
St	Striosomes
TPH	Tryptophan hydroxylase protein
UPD	Unipolar Depression
VTN	Ventral thalamic nuclei
WT	Wildtype

Chapter 1

General Introduction

Neuropsychiatric Disorders

Overview of Neuropsychiatric Disorders

The World Health Organization has estimated that 20 to 25% of all individuals will experience some form of mental or behavioral disorder during their lifetime. Assessments from 2001 show that neuropsychiatric disorders have a point prevalence of 10% in the general adult population, which in that year corresponded to approximately 450 million afflicted individuals (WHO, 2001).

In terms of "years lost to a disability", neuropsychiatric disorders are at the top of disability-causing diseases or disorders together and represent over a third of time lost while disabled. In 2004, the leading cause for disability was Unipolar Depressive Disorder which corresponded to 8.3% of the total disabilities for males and 13,4% for females. Schizophrenia and bipolar disorder, each representing 2 to 3% of years lost to a disability also rank consistently among the top leading global causes of medical burden for non-fatal disabling conditions (WHO, 2004b).

These disorders also play an important role in economic cost to society. The aggregate yearly cost in the United States was pointed to be as high as 2.5% of the gross domestic product (Rice, 1990), while in the European Union it is situated between 3% and 4%. Furthermore, the expenditure on health related mental disorders accounts for approximately 10-20% of the total health care costs in most European countries (Meerding et al., 1998; OECD, 2008; Patel and Knapp, 1998).

Two large epidemiological studies summarized on Table 1, representing data collected in the 1980's (NIMH, 1992) and 1990's (Kessler et al., 1994), highlight the prevalence of discrete disorders in the US general adult population. Finally, in the more than 32,000 suicides in the United States in 2005, 90% of these were believed to be associated with a neuropsychiatric disorder (Insel, 2009).

	ECA* Prevalence (%)	NCS** Prevalence (%)	Best*** Estimate* (%)
Any Anxiety Disorder	13.1	18.7	**16.4**
Simple Phobia	8.3	8.6	**8.3**
Social Phobia	2	7.4	**2**
Agoraphobia	4.9	3.7	**4.9**
GAD	—	3.4	**3.4**
Panic Disorder	1.6	2.2	**1.6**
OCD	2.4	—	**2.4**
PTSD	—	3.6	**3.6**
Any Mood Disorder	7.1	11.1	**7.1**
MD Episode	6.5	10.1	**6.5**
Unipolar MD	5.3	8.9	**5.3**
Dysthymia	1.6	2.5	**1.6**
Bipolar I	1.1	1.3	**1.1**
Bipolar II	0.6	0.2	**0.6**
Schizophrenia	1.3	—	**1.3**
Nonaffective Psychosis	—	0.2	**0.2**
Somatization	0.2	—	**0.2**
ASP	2.1	—	**2.1**
Anorexia Nervosa	0.1	—	**0.1**
Severe Cognitive Impairment	1.2	—	**1.2**
Any Disorder	**19.5**	**23.4**	**21**

Table 1. – 1-year prevalence of neuropsychiatric disorders in 18-54 year olds. *ECA study, Epidemiologic Catchment Area from 1980-1985 (NIMH, 1992). **NCS study, National Comorbidity Survey 1990-1992 (Kessler et al., 1994). ***Adapted from the "Report of the Surgeon General on mental health" (Satcher, 2000). GAD, generalized anxiety disorder; OCD, obsessive-compulsive disorder; PTSD, post-traumatic stress disorder; MD, major depression; ASP, antisocial personality disorder.

Mood Disorders

Mood disorders encompass a number of psychiatric diagnoses which describe "disorders in which the fundamental disturbance is a change in affect or mood to depression (with or without associated anxiety) or to elation" (WHO, 2004a). Changes in the underlying mood are hypothesized to be the main feature in these disorders. These diagnosis broadly encompass both the manifestation of single episodes of depressive or manic diagnoses to a combination or oscillations between altered mood states (American Psychiatric Association, 2000).

One end of the mood spectrum is occupied by Unipolar Depression (UPD or Major Depressive Disorder, MDD), a mental disorder characterized by a generalized low mood accompanied by low self-esteem and anhedonia. Patients in a depressive state experience strong emotions of sadness and grief which in contrast to a healthy individual do not remit when the external cause of these emotions is ameliorated. Additionally, these emotions can also be disproportionate to their underlying cause or occur without any triggering external effects (Belmaker and Agam, 2008; Wakefield et al., 2007). Clinically, the diagnosis for UPD requires the observation of distinct altered emotional state and the presence of several psychophysiological changes. These primarily include a depressed mood (subjective or reported by others) and a markedly diminished interest in pleasurable activities (anhedonia). Physiological signs can include significant weight loss or weight gain, disturbed sleep patterns with episodes of insomnia or hypersomnia, extreme fatigue, psychomotor agitation and slowing of speech and action. Other common symptoms described by patients include: feelings of worthlessness, guilt, indecisiveness, diminished ability to think and concentrate and recurrent suicidal thoughts. Diagnostic for UPD is usually attained when several of these symptoms persist for a minimum of 2 weeks and interfere considerably with work and family relations (American Psychiatric Association, 2000). Depressive episodes in UPD are also highly recurrent. Of the individuals who suffer a single episode, 60% of them go on to develop a second, and of those, 70% recur in a third episode (American Psychiatric Association., 2000). Depression also tends to emerge early in adolescence and progress into adulthood suggesting a developmental course in neuropathogenesis (Kim-Cohen et al., 2003; Pine et al., 1998).

Milder or circumstantial forms of depression include Dysthymic Disorder, Psychotic Major Depression, Postpartum Depression and Seasonal Affective Disorder.

Dysthymia originates from the ancient Greek word for “bad mood”. This disorder is defined by milder, non-disabling symptoms that persist for two years or longer (Akiskal, 1983; American Psychiatric Association, 2000). Dysthymia is an independent diagnosis but can also be present in the course of a major depressive state. Specifically, a long term study has shown that patients with major depressive disorder spent on average 44% of their course in a low-grade depressive state (dysthymic) and only 15% of time in major depressive episodes (Judd et al., 1998).

Psychotic depression is characterized by the presence of delusions or hallucinations and specific biological alterations, including a chronic over-activation in the production of glucocorticoids (Schatzberg et al., 1985). This latter observation has led to the successful treatment of Psychotic Major Depression with glucocorticoid receptor antagonists (Belanoff et al., 2001; Schatzberg et al., 1983). Furthermore, Psychotic Major Depression is more resistant to classic pharmacological treatments than non-psychotic MDD while on the other hand, electroconvulsive therapy was reported as more effective for Psychotic Major Depression (Buchan et al., 1992; Petrides et al., 2001).

Postpartum dysphoric mood states comprise a range of severity, from the commonly denominated “baby blues” (a highly prevalent disorder of a mild and transient nature) to the more severe and persistent Postpartum Affective Psychosis and Postpartum Depression. In Western countries the incidence of Postpartum Depression, in particular, has been reported to be as high as 10-20% (Grace et al., 2003; Hopkins et al., 1984).

Lastly, and originally described by Rosenthal and colleagues at the NIH, Seasonal Affective Disorder is also described as change in mood. Most commonly associated with depression affect occurring during the winter (or less frequently in the summer) (Rosenthal et al., 1984), Seasonal Affective Disorder is also positively correlated to latitude and diminished duration of daytime light (Rosen et al., 1990; Vera, 1998).

Mood disorders also include the Bipolar Spectrum Disorders; these are characterized by a combination of clinical manifestation of elevated moods (mania or hypomania if symptoms are milder), depressive episodes, or mixed episodes (simultaneous characteristics of mania and depression). In manic episodes a psychotic state can also be present with symptoms of delusions and hallucinations (American

Psychiatric Association, 2000). Bipolar and unipolar disorders share overlapping symptomatology; namely in the presence of episodes of depression in certain forms of bipolar illness. However, the distinction in nosological diagnosis between these two types of mood disorders is supported by distinct differences in disease outcome, response to pharmacological treatment and genetic studies (Farmer and McGuffin, 1989; Kendell, 1987).

Bipolar Spectrum Disorders are also subdivided into several categories: for Bipolar I Disorder (BPDI), a positive diagnostic includes at least one manic or mixed episode (i.e. dysphoric mania or agitated depression) with or without concurrent episodes of hypomania or major depression. Bipolar II Disorder (BPDII) is diagnosed with the occurrence of at least one hypomanic episode and one major depressive episode. Additionally, in BPDII, depressive episodes are more frequent and more intense than manic episodes. Furthermore, some individuals can undergo what is known as “rapid cycling”, a condition in which depressive (dysthymic) and manic (euphoric) states rapidly alternate (Dunner et al., 1977). Interestingly, tricyclic antidepressants can induce rapid cycling in bipolar patients (Wehr and Goodwin, 1979). Finally, another bipolar-like state includes Cyclothymia, a condition considered to be the most milder form of the bipolar spectrum, where affected patients exhibit both hypomanic and mild depressive states (Akiskal et al., 1977).

Historically, depression and mania are some of the oldest known forms of mental disorder. Predating psychiatry by several centuries, Hippocrates was the first to describe these illnesses as disconnected from mysticism and supernatural causes, but instead linked them to a biological cause originating in the brain (Zarate and Manji, 2009). Recently, with the contemporary advent of human genetics, epidemiological studies and heightened clinical awareness, the potential genetic influences that precipitate these disorders have garnered substantial interest.

Heritability of Mood Disorders

The heritability of UPD and BPD was originally addressed from quantitative data obtained from interviews of affected patients and family members (James and Chapman, 1975; McGuffin et al., 1988; Reich et al., 1987; Smeraldi et al., 1977; Trzebiatowska-Trzeciak, 1977). The prevalence of similar disorders in first degree relatives was found to be consistently higher than the expected value for the general population. For UPD, in particular, incidences as high as 15% and 20% have been reported for first degree relatives (Shih et al., 2004; Sullivan et al., 2000). A meta-analysis study on familial transmission, twin studies and environmental influences led Sullivan and colleagues to propose that: “Major depression is a familial disorder, and its familiality mostly or entirely results from genetic influences.” (Sullivan et al., 2000).

In terms of gender, although there is strong evidence that UPD affects more women than men (Kessler et al., 1993; Weissman et al., 1993), most studies do not find significant differences in the genetic heritability between males and females (Kendler and Prescott, 1999; Lyons et al., 1998; McGuffin et al., 1996), suggesting that both genders share the majority, but not totality of genetic influences for UPD (Kendler and Prescott, 1999; Sullivan et al., 2000).

Genetic heritability also plays a major role in the development of Bipolar Disorder (Andreasen et al., 1987; Goldin et al., 1983; Reich et al., 1969; Weissman et al., 1984). Interestingly, the lifetime risk of mood disorders for relatives of bipolar patients was reported to be higher than that for unipolar probands (24% versus 20%) (Ciaranello and Ciaranello, 1991; Meltzer, 1987). Furthermore, the lifetime risk of bipolar disorder in relatives of bipolar probands is 40-70% for monozygotic twins and 5-10% for first degree relatives, whereas an overall risk in the general population of 0.5-1% suggests a 10-20 fold increase in risk for first degree relatives of afflicted individuals (Craddock and Jones, 1999).

The precise model for the genetic transmission of bipolar and unipolar disease, however, remains somewhat elusive. Some studies have supported the hypothesis of some disease causing loci, arguing in favor of Mendelian inheritance. Nevertheless, most studies have not excluded the possibility for polygenic or multifactorial models. This suggests the possibility of a mixed model of inheritance or a combination between single gene mutations and disease predisposition due to the interaction between multiple genes (Ciaranello and Ciaranello, 1991; Craddock and Jones, 1999; Lau and

Eley, 2010; Zarate and Manji, 2009). Additional factors play a role confounding the interpretation of genetic inheritance, these include: assortative pairing (*defined by the tendency for individuals with related phenotypes to mate more commonly than what would be expected by random chance*) (Baron et al., 1981; Mathews and Reus, 2001; Merikangas et al., 1988), genetic anticipation (*surfacing of symptoms at an earlier age in familial transmission as it is passed on to the next generation*) (Lange and McInnis, 2002; McInnis et al., 1993; Nylander et al., 1994), genomic imprinting (McMahon et al., 1995; Ohara et al., 1998) or potential effects from mitochondrial genes (Clay et al., 2010; Kato and Kato, 2000; McMahon et al., 1995).

It is therefore clear that bipolar disorder is a complex genetic disorder. However, the high heritability of this condition has attracted intensive research activity aiming at identifying disease causing mutations or mutations associated with increased susceptibility to BPD. Surprisingly, large quantities of data from human genetics, in the form of linkage and association studies have identified a multitude of putative regions of interest for BPD susceptibility in virtually every human chromosome except the Y chromosome (Figure 1). These results have muddled a strong conclusion as far as precise genetic influences on the etiology of this disorder but have, nonetheless, put forward a few “hot spot” regions, which have been reproducibly identified by independent groups of researchers (Serretti and Mandelli, 2008).

Linkage and association studies suffer from a major confound in the form of reports which are not reproduced across different populations, as well as deficiencies in attaining wide statistical significance in several studies. These can be in part due to limited sample sizes and/or high degree of genotypical heterogeneity. Recently, more encompassing genome-wide studies are able to identify single nucleotide polymorphisms across the entire genome of each individual. Up to 2011, six genome-wide association studies have been published for bipolar disorder (Baum et al., 2008; Ferreira et al., 2008; Scott et al., 2009; Sklar et al., 2008; Smith et al., 2009; WTCCC, 2007). These studies present the upside of providing an unbiased identification of putative novel target genes, but at the same time may miss important rare causative mutations. On the other hand, genome-wide approaches often identify targets whose disease mechanisms remain obscure and only a few targets ascribed to neurobiological relevant pathways (Soronen et al., 2010). Conversely, the approach more commonly explored in neurobiology research, known as “candidate gene approach”, devotes

specific attention to genes that are known to be involved in biological pathways relating to the disease. Importantly, the synergy between unbiased genomic approaches and target based approach has put forward several promising targets that may be involved in the neuropathology of BPD.

Bipolar Disorder

Candidate Genes for Bipolar Disorder

Mutations in the promoter region of the serotonin transporter -SLC6A4- in the 17q11 region have been implicated in several studies into BPD. Multiple groups have identifying a 44 base pair insertion/deletion and another polymorphism in the second intron of the gene as potentially being involved in BPD (Anguelova et al., 2003; Heils et al., 1996; Lasky-Su et al., 2005; Lesch et al., 1996; Rotondo et al., 2002). The tryptophan hydroxylase (TPH) protein is the rate-limiting enzyme in the synthesis of serotonin. In humans, TPH1 and TPH2 proteins are coded by two separate genes with only TPH2 (in chromosome 12q21) being strongly expressed in the brain (Walther et al., 2003). TPH2 polymorphisms have also been implicated in susceptibility to BPD (Cichon et al., 2008; Grigoroiu-Serbanescu et al., 2008; Harvey et al., 2007; Lopez et al., 2007; Van Den Bogaert et al., 2006).

Dopamine, like serotonin, is a monoaminergic neurotransmitter, and genes involved in the dopamine signaling pathway have also been implicated in mood disorders. The Dopamine Receptor D4 (11p15), the Dopamine Receptor D1 (5p35) and the Dopamine Transporter -SLC6A3-(5p15) have all been suggested to be linked to BPD (Del Zompo et al., 2007; Greenwood et al., 2001; Greenwood et al., 2006; Lopez Leon et al., 2005).

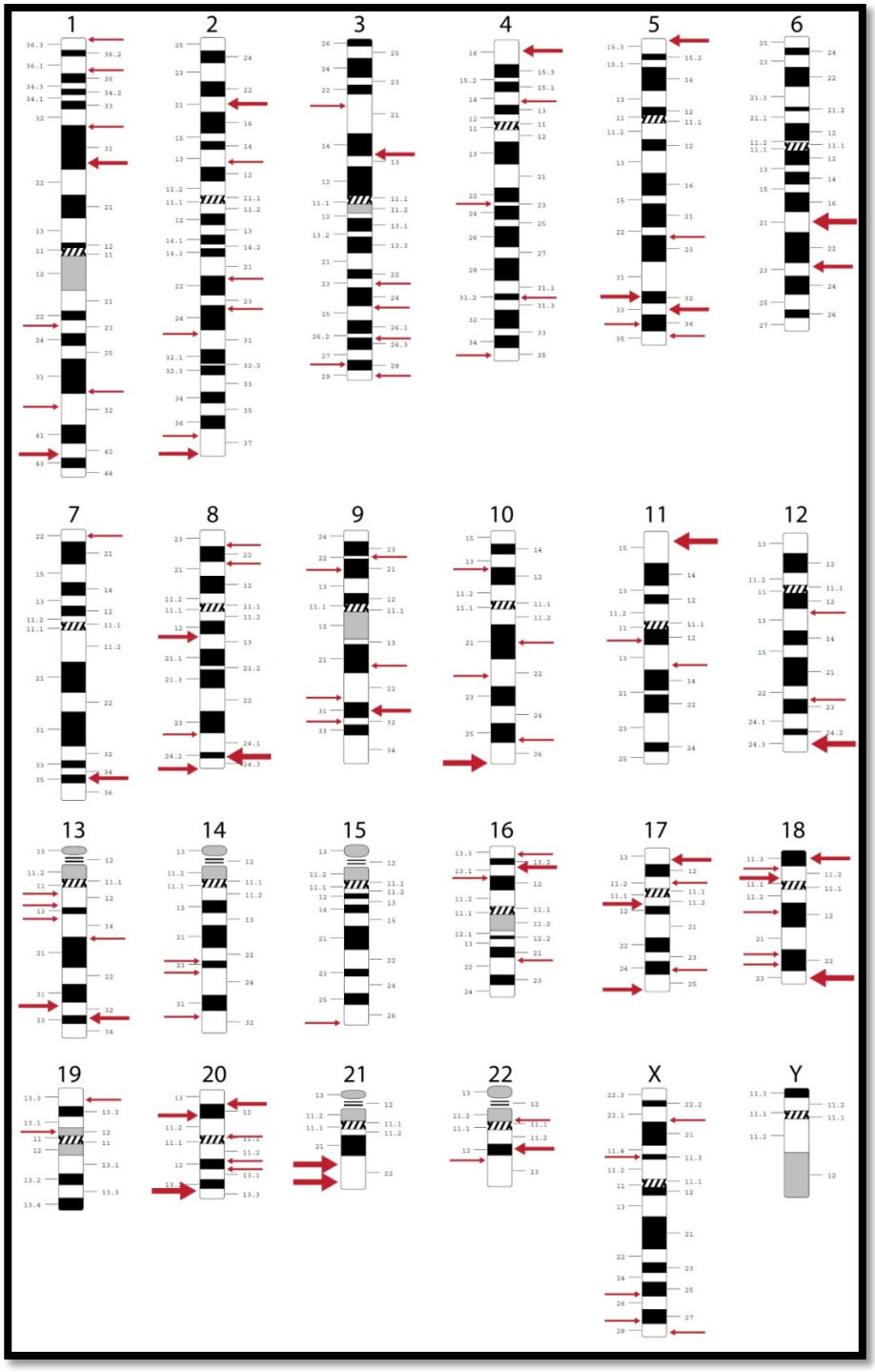

Figure 1. – Chromosomal regions associated with bipolar disorder. Thicker arrows indicate stronger evidence (multiple reports). Figure adapted from (Serretti and Mandelli, 2008) and chromosome ideograms from (David Adler, Univ. of Washington).

The Disrupted-in-Schizophrenia-1 (DISC1) gene (1q42) is another candidate gene for which there is strong evidence implicating its dysfunction in BPD (Blackwood et al., 2001; Hodgkinson et al., 2004; Palo et al., 2007). This clear overlap in a gene potentially involved in schizophrenia as well as BPD is perhaps not surprising given the endophenotypical similarities between the two disorders (Zarate and Manji, 2009). Other strongly implicated genes include the D-amino acid oxidase activator (DAOA) (13q33) (Detera-Wadleigh and McMahon, 2006), FAT1 (4q35) (Abou Jamra et al., 2008; Blair et al., 2006), the Brain-derived neurotrophic factor (BDNF) (11p14) (Kanazawa et al., 2007; Sklar et al., 2002) and interestingly, the aryl hydrocarbon receptor nuclear translocator-like protein (ARNTL, also known as Bmal1) (11p15) which heterodimerizes with the CLOCK gene as part of the molecular regulation of circadian rhythms (discussed below) (Mansour et al., 2006; Nievergelt et al., 2006).

Gene	Cellular role	Chromosome location
SLC6A4	*Serotonin reuptake*	17q11
TPH2	*Rate-limiting enzyme in the synthesis of serotonin*	12q21
DRD4	*Dopamine receptor*	11p15
DRD1	*Dopamine receptor*	5p35
SLC6A3	*Dopamine reuptake*	5p15
DISC1	*Multiple cellular roles*	1q42
DAOA	*Indirectly involved in the activation of NMDA receptors*	13q33
FAT1	*Adhesion molecule and/or signaling receptor (Cadherin-related family)*	4q35
BDNF	*Neurotrophin*	11p14
ARNTL (Bmal1)	*Circadian clock*	11p15

Table 2. – Genes strongly implicated in the Bipolar Disorder which have also been explored at the neurobiological level in potentially relevant cellular and signaling pathways.

Sleep and Bipolar Disorder

Sleeping disorders have long been associated with mood disorders. Disturbances in sleep are included as part of the symptomatology for the diagnoses of both MDD (when present as hypersomnia or insomnia) and BPD, where reduced need for sleep can be part of a positive diagnostic for manic episodes (American Psychiatric Association, 2000). Classically, sleep deregulation has often been considered an epiphenomena of mood disorders and not necessarily a causal or primary driving force for either UPD or BPD, but more so, a consequence of the individuals' altered mood. Recently, however, a shift in paradigm is emerging whereby a deeper understanding of the biology of circadian rhythms and their relationship to mood disorders is seen as an important mechanism contributing to the genesis and/or maintenance of mood disorders (Harvey, 2001; Harvey, 2011; McCrae and Lichstein, 2001; NIH, 2005).

Both insomnia or hypersomnia are highly prevalent in UPD, with 60% to 84% of patients reporting sleep related symptoms (Ford and Kamerow, 1989). Insomnia is also hypothesized to precede and constitute a risk factor for depression (Riemann and Voderholzer, 2003). Interestingly, in a 20 year study from a representative sample of the Swiss population (Vollrath et al., 1989), researchers uncovered that long lasting insomnia predicted major depressive episodes. Specifically, 17% to 50% of subjects with insomnia lasting more than 2 weeks developed a major depressive episode at a later time (Riemann and Voderholzer, 2003).

In BPD, 69 to 99% of patients experiencing manic episodes report a reduction in time spent sleeping. Furthermore, in the course of a depressive episode 23-78% experience hypersomnia (Harvey, 2008). Finally, in the inter-episode periods, BPD patients report sleep disturbances with a higher degree of fragmentation in the sleep/wake rhythm when comparing to healthy patients (Jones et al., 2005).

Additionally, sleep disturbances have been described as an early warning signal for both manic and depressive bipolar episodes. In a meta-analysis of seventy-three publications of prodromal symptoms in BPD and UPD covering a total of 1191 subjects, it was uncovered that most patients were able to identify early symptoms of mood deregulation relapse. Specifically, the most robust early symptom of mania was sleep disturbance, as reported by 77% of BPD patients (Jackson et al., 2003). Moreover, bipolar patients are generally more capable of accurately detecting prodromal symptoms of relapse into manic episodes than they are of identifying relapses into

depressive episodes (Jackson et al., 2003; Sierra et al., 2007). Additionally, sleep disturbances not only predate recurrence into manic episodes, but they can also predict the first onset into BPD. A study performed in high-risk offspring (i.e. children coming from families in which one parent was diagnosed with BPD) concluded that sleep disturbances and anxiety disorders were antecedent conditions to develop BPD (Duffy et al., 2007).

Interestingly, sleep deprivation (partial or total), or circadian phase advances in the sleep-wake cycle have long been known to produce an antidepressant effect in bipolar patients undergoing depressive episodes (Barbini et al., 1998; Wehr et al., 1979; Wu et al., 2009). This effect has been hypothesized to be linked to different mechanism, including the serotonergic system (Benedetti et al., 2008), the dopaminergic system (Ebert and Berger, 1998) or as a consequence of a rebound or reset in the Process S (slow wave sleep) sleep stage (Endo et al., 1998; Endo et al., 1997).

Sleep is one of the biological processes controlled by circadian rhythms. The understanding of the molecular underpinnings of mammalian circadian rhythms has seen a surge in recent years. The circadian control of sleep and wakefulness, the genes and molecules involved and the understanding of the neural circuits that play a role in these processes are paving new discoveries into the neurobiology of mood disorders. Therefore, it is acknowledged that a deeper comprehension in the molecular biology of circadian rhythms can provide new clues into the etiology of Bipolar Disorder as well as new avenues for treatment (Jones, 2001).

Circadian Rhythms

Circadian rhythms regulate not only sleep and wakefulness but also body temperature, feeding, drug metabolism, hormone secretion, cell-cycle progression and glucose homeostasis. Circadian cycles themselves synchronize with the natural environment through the light-dark cycle. The circadian period length refers to the real-time duration from a reference point during the course of a full cycle. In laboratory animals entrained to a 12h/12h light-dark cycle, the period duration is 24h. However, in the absence of the photonic entrainment cues, the internal clock usually displays

subjective period lengths that usually deviates from a 24h duration (Schwartz and Zimmerman, 1990) and although light is the predominant *Zeitgeber* (time giver), entrainment to a 24h cycle can also occur with other stimuli, such as food availability (Lax et al., 1999) or social cues (Goel and Lee, 1997).

The "master clock" for the mammalian brain is present in the Suprachiasmatic Nucleus (SCN). Synchronization through daily dark-light cycle originates in photosensitive retinal ganglion cells which function independently of photoreceptor cones and rods and project to the SCN via the retinohypothalamic tract and thus initiate photonic entrainment (Berson, 2007; Berson et al., 2002). However, humans that are completely blind and display "free-running" circadian rhythms, melatonin can be administered to promote circadian entrainment (Sack et al., 2000).

The discovery of the molecular networks involved in circadian pacemaking was originally tackled using random induced-mutagenesis in the fruit fly. This led to the identification of the *per* (period) gene which, depending on the mutation, generated both longer, shorter or arrhythmic periods (Konopka and Benzer, 1971). In wildtype flies it was later discovered that the levels of the per gene undergo an oscillation which approximates the circadian period (Hardin et al., 1990). More recently, advances in mouse molecular genetics have permitted the unraveling of mammalian circadian biology. One landmark study was the identification of the *Clock* gene (Circadian Locomotor Output Cycles Kaput) (Vitaterna et al., 1994). Using forward genetics, Vitaterna and colleagues induced random mutations in the gametes of male mice using ENU (N-ethyl-N-nitrosourea), and subsequently phenotyped 304 mice for disrupted circadian behavior. From these, they identified one mutant animal with a period 1 hour longer that its founder parent. Homozygocity of the mutated locus led to a disrupted, arrhythmic circadian period. Cloning of the gene and functional rescue of the Clock-mutant mice using bacterial artificial chromosome (BAC) transgenic rescue was also accomplished by the same group (Antoch et al., 1997; King et al., 1997). Interestingly, however, the ENU induced mutation produces a single nucleotide change in a splice acceptor region in intron 19 ($Clock^{\Delta 19}$) which induces an exon skipping and 51 amino acid deletion (King et al., 1997). More recently, a targeted deletion of exon 4 and 5 in the Clock gene generated a mouse line with a null allele for this gene (Debruyne et al., 2006). Surprisingly, this line of mice displayed minimal aberrations in circadian patterns, suggesting that the $Clock^{\Delta 19}$ may function as a dominant negative.

In contrast, homozygous mice for a deletion of Bmal1, a critical binding partner for Clock and an essential molecule in the molecular circadian regulation, display a complete loss of circadian rhythmicity in free-running conditions at both the behavioral and molecular level (Bunger et al., 2000). CLOCK and BMAL1 heterodimerize in the cytoplasm before entry into the nucleus, this is followed by phosphorylation events which promote their function as a transcriptional complex. With the above observations from mouse molecular genetics, this suggests that BMAL1 is essential for the transcriptional control and circadian oscillations, whereas, Clock can be functionally substituted by another protein (Debruyne et al., 2006). One possible candidate is Npas2, which has been suggested as having an overlapping role with Clock in the mouse brain (DeBruyne et al., 2007). At the molecular level, CLOCK interacts with BMAL1 to activate *Per (period homologue)* and *Cry (cryptochrome)* genes. PER and CRY can then heterodimerize, translocate to the nucleus, interact with the CLOCK:BMAL1 complex to inhibit self-expression (i.e. PER and CRY). During subjective evening, the PER:CRY repressor complex is degraded and the CLOCK:BMAL1 complex initiates a new cycle of transcription (Takahashi et al., 2008). Although these molecular pathways are central to circadian biology there are other known pathways that intersect this protein expression and degradation cycles which are summarized in Figure 2.

Interestingly, the link between circadian rhythms and bipolar disorder has also been explored using the $Clock^{\Delta 19}$ mice (Roybal et al., 2007). These mice display a strong preference for rewarding stimuli when compared to controls, a symptom present in bipolar patients during manic episodes, and also display less time immobile in the forced swim test (a measure of depression) as well as other behavioral abnormalities consistent with a model for mania.

Symptoms of mania	Clock mutant mice
Disrupted circadian rhythms	Disrupted circadian rhythms
Hyperactivity	Hyperactivity
Decreased sleep	Decreased sleep
Feelings of extreme euphoria	Hyperhedonia/less helplessness
Increased risk-taking	Reduced anxiety
Propensity toward drug abuse	Increased preference for cocaine

Table 3. – Clock display behavioral abnormalities consistent with symptoms from bipolar patients in the manic state.

Moreover, lithium salts, which are administered as a mood stabilizer for BPD patients, ameliorates several of the behavioral abnormalities in the Clock$^{\Delta 19}$ mice in measures of anxiety- and depression-related behavioral tasks (Roybal et al., 2007).

Therefore, it is now acknowledged that circadian biology is well positioned to play a major role in BPD. Moreover, human genetic data and mouse modeling have implicated several of the genes crucial for normal circadian to susceptibility to BPD.

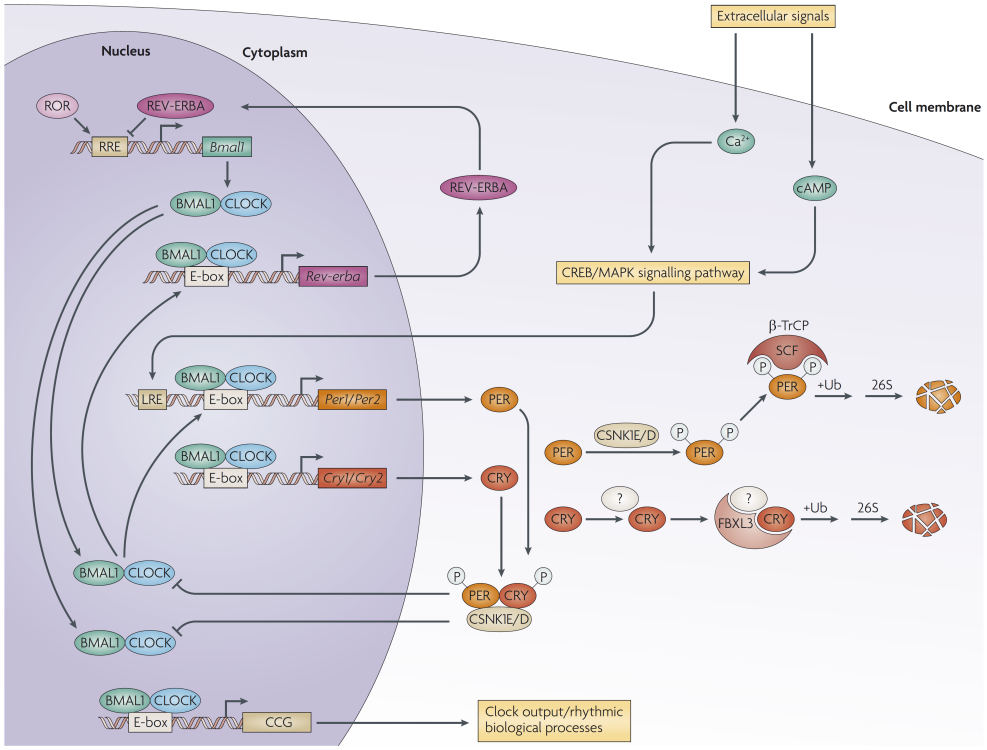

Figure 2. – The mammalian circadian clock is composed of a transcriptional–translational feedback network. The circadian clock is composed of a primary negative feedback loop involving several genes, these include: Clock (and Npas2), Bmal1, Per1, Per2, Cry1 and Cry2. CLOCK (or NPAS2) and BMAL1 are transcription factors that activate transcription of Per and Cry. The resulting PER and CRY proteins heterodimerize, translocate to the nucleus and interact with the CLOCK:BMAL1 complex to inhibit their own transcription. After a period of time, the PER:CRY repressor complex is degraded and CLOCK:BMAL1 initiate a new cycle of transcription. A secondary autoregulatory feedback loop is composed of Rev:erba, which is another direct target of the CLOCK:BMAL1 transcription complex. REV:ERBA represses Bmal1 transcription and competes with a retinoic acid-related orphan receptor (ROR) to bind ROR response elements (RREs) in the Bmal1 promoter. Post-translational modification and degradation are another mechanism playing a role in circadian periodicity. Casein kinase 1 delta (CSNK1D) and CSNK1E are proteins involved in the phosphorylation of clock proteins, which in turn targets these proteins for polyubiquitylation and degradation by the proteosomal system. PER and CRY proteins are targeted for degradation by the β-TrCP1 and FBXL3 E3 ubiquitin ligase complexes. Legend: CCG (clock-controlled genes); CREB (cAMP response element-binding); E-box (BMAL1:CLOCK consensus binding regions); MAPK (mitogen-activated protein kinase); SCF (SCF E3 ubiquitin ligase); Ub (ubiquitin). *Reprinted with permission from Macmillan Publishers Limited, ref 2579550687171, (Takahashi et al., 2008).*

Modeling Bipolar Disorder

Although mouse models of BPD have been proposed, the critical feature of bipolar cycling between mania and depression has not been successfully observed for genetic mouse models. It is unknown if this limitation is inherent to the murine model or if the manipulations performed have yet to tap on a truly cyclic pathological pendulum capable of pushing mice from depressive-like into manic-like behavior. Nevertheless, useful models of depression and of mania have been reported which replicate several of the features of both types of episodes.

Several pharmacological models of BPD have been proposed in rodents. Amphetamines and other psychostimulants, such as D-amphetamine, 3,4-methylenedioxymethamphetamine (MDMA) and cocaine can induce psychomotor hyperactivity in mammals (Koob and Bloom, 1988). Administration of psychostimulants, amphetamines or methamphetamines, have been used to simulate manic episodes and a concomitant administration of therapies, such as lithium, valproic acid or transcranial magnetic stimulation can successfully rescue pathological behaviors (Frey et al., 2006a; Frey et al., 2006b; Gould et al., 2001; Shaldivin et al., 2001). Repeated administration of methamphetamines, cocaine or morphine can produce behavioral sensitization and be used as a model of bipolar disorder which produces some cyclical manic-depressive activity. Again, the behavioral effect produced by these drugs are reversed or prevented by administration of lithium (Antelman et al., 1998; Kucinski et al., 1998; Namima et al., 1999). Of particular interest, in one study, a model of repeated high-dose cocaine administration produces behavioral hyperactivity response on some days and behavioral hypoactivity on alternating days (Antelman et al., 1998). Another pharmacological model for BPD includes the combination of amphetamine and chlordiazepoxide to induce hyperactivity, which can be rescued by lithium treatment (Vale and Ratcliffe, 1987). The drug ouabain, an inhibitor of the sodium-potassium pump, has also been used to model mania. This drug is known to induce hyperactivity in rodents, again an effect which can be countered by administration of lithium (El-Mallakh et al., 2003; Li et al., 1997).

The Nucleus Accumbens (NAc) and the prefrontal cortex (PFC) contain a central part of the neural circuitry that controls the expression of conditioned responses to amphetamine and cocaine-related motor hyperactivity (Franklin and Druhan, 2000). Several of these psychostimulants are known to increase dopamine content in the NAc.

The acute locomotor hyperactivity due to amphetamines and metamphetamine can be suppressed by Dopamine D1 and D2 receptor antagonists or Dopamine D2 Receptor (D2) agonist –quinpirole- (Kuribara and Uchihashi, 1993; Steketee and Kalivas, 1992). Amphetamines and cocaine tap into the dopamine neurotransmission by promoting an increase of presynaptic dopamine release (Jones et al., 1998; Kokoshka et al., 1998) and cocaine by blocking the reuptake of dopamine (Kitayama et al., 1992; Ritz et al., 1987). Therefore, strong evidences suggest this neurotransmitter may be involved in the development of mania (Diehl and Gershon, 1992).

One interesting behaviorally-induced model for mania involves inducing sleep-deprivation. Originally developed to study sleep deprivation in cats (Jouvet et al., 1964), a common version of this test in rodents prevents sleep by stationing the animal in a platform covered in water. At the onset of REM sleep, muscle relaxation puts the animal in contact with water and induces awakening. This test, compounds sleep deprivation with other stressors such as social isolation, immobilization and contact with water, which impart several behavioral responses similar to idiopathic mania. Interestingly, haloperidol and lithium treatment reduced the sleep deprivation induced manic behavioral manifestations (Gessa et al., 1995).

Another behavioral model is the dominant–submissive test to study mania and depression. Animals screened in this test display mania-like or depression-like behavior depending on their social position. Interestingly, this effect was determined to be reversed by anti-manic or anti-depressive drugs (Malatynska and Knapp, 2005; Malatynska et al., 2007).

With the above described Clock$^{\Delta 19}$ mice, other genetically manipulated animals have also been proposed to model aspects of BPD. At the most basic level, these include the analysis of the inbred strains of laboratory mice (Einat, 2007). Others include the Disrupted-in-Schizophrenia 1 gene (DISC1) originally identified in a Scottish family strongly afflicted by schizophrenia and mood disorders. Although not thoroughly explored, mutant mice for DISC1 remains an interesting putative model for bipolar disorder (Ishizuka et al., 2006; Lipina et al., 2010; O'Tuathaigh et al., 2007).

Glucocorticoid receptors modulate stress response and cognitive functions linked to mood disorders (Yehuda et al., 1993). Animal models designed to perturb glucocorticoid receptor function have been generated and shown to display several endophenotypes relevant to BPD and UPD. An antisense RNA transgenic mouse for

the glucocorticoid receptor displays obesity and increased activity in the HPA (Hypothalamic–pituitary–adrenal) axis, consistent with severe depression (Pepin et al., 1992). Treatment of these animals with moclobemide, a monoamine oxidase type A inhibitor, reverted both behavioral and hormonal alterations (Montkowski et al., 1995). Another mouse model includes a forebrain specific over-expression of the glucocorticoid receptor. These animals displayed increased depression-like behaviors, anxiety-like behaviors, hypersensitivity to cocaine administration and a high sensitivity to anti-depressants (Wei et al., 2004). In addition to the above, there are other manipulations on this same gene which promote relevant phenotypes to depression in the mouse. Interestingly, one group simultaneously examined two lines of mutant mice, one with a heterozygous reduction in glucocorticoid receptor expression, and the other with an overexpression of the receptor. Similarly to the other loss of function mutants, the reduction in expression generated an animal prone to depression, while the overexpression produced an animal resistant to depression (Ridder et al., 2005); however, this is different from what was seen in an earlier model of glucocorticoid receptor overexpression (Wei et al., 2004).

The 22q11 deletion in humans is associated with a conserved deletion of approximately 40 genes which impart a high risk for mental disorders, most notably schizophrenia and early onset BPD (Papolos et al., 1996). The prevalence of 22q11 deletion syndrome is estimated to be approximately 1:6000 in the live births, making this syndrome the second most common chromosomal disorder (after Down's syndrome) and the most common microdeletion syndrome (Botto et al., 2003; Devriendt et al., 1998; Paylor and Lindsay, 2006). One of the most robust findings in a mouse model of 22q11 microdeletion are deficiencies in sensory motor gating (Kimber et al., 1999). This endophenotype is mostly linked to schizophrenia in humans (Braff and Geyer, 1990; Braff et al., 2001), but nevertheless may also be strongly linked to bipolar disorder since BPD patients also display sensory motor gating deficits (Perry et al., 2001).

The Glycogen synthase kinase 3 gene which produces the two isoforms, GSK-3α and GSK-3β, is intimately linked with the glycogen metabolism but is also important in several downstream signaling pathways of neuronal receptors (e.g. growth factors, neurotransmitters and neurotrophins). GSK-3β in particular has been implicated in bipolar disorder and also as a potential target for lithium's therapeutic effect in mood

stabilization (Gould et al., 2004). GSK-3β has also been linked to regulation of the circadian rhythm (Kaladchibachi et al., 2007). Pharmacologically, GSK-3β is efficiently inhibited by lithium and valproate, both of which are used to treat BPD (Chen et al., 1999; Klein and Melton, 1996). Interestingly, transgenic mice overexpressing GSK-3β express several features reminiscent of mania when tested behaviorally, these included, hypophagia, increased locomotor activity and decreased habituations in the open field test and increased acoustic startle response with decreased habituation (Prickaerts et al., 2006).

The Protein kinase C interacting protein (PKCI) is a small protein belonging to the histidine triad family proteins. In a meta-analysis of 12 microarray studies of bipolar disorder, this gene was found to be decreased in the dorsolateral PFC (Elashoff et al., 2007). Relevant for mood disorders, the PKCI/HINT1 mutant mice display less immobility in the forced swim and the tail suspension tests, both of which are indicative of lower levels of depression. These animals are also less anxious than their wildtype littermates, at the same time as the HPA axis activity was reported to be potentiated in the knockouts (Barbier and Wang, 2009).

Electrophysiological kindling has also been used to model aspects of BPD (Post et al., 2001). This procedure has been used to indirectly address illness progression and development of new BPD episodes (Machado-Vieira et al., 2004). A typical kindling paradigm involves a daily subthreshold stimulation of the amygdala. With the progression of stimulations, same intensity depolarization leads to motor seizures and, subsequently, the occurrence of spontaneous seizures in the absence of stimulation (Goddard et al., 1969; Racine, 1972). Phenotypically, kindled rats display an increase in "emotionality" and increased resistance to capture in an open field test (Kalynchuk et al., 1998). On a similar paradigm hippocampal kindling induces increased locomotor activity, which can be suppressed by the injection of a D2 receptor antagonist in the NAc (Leung et al., 2000). Nevertheless, the validity of the kindled model directly relating to the pathophysiological mechanisms of BPD is controversial (Post and Weiss, 1998).

As detailed above, there are a considerable number of avenues to model bipolar disorder in laboratory animals. Validation of these models according to set criteria is therefore a necessity to establish which procedures garner the best approximation to the human condition. The rationale for this validation is generally broken in three categories, face validity, construct validity and predictive validity. Face validity is

attained when phenomenological similarities are seen between the model and the studied phenomena (i.e. the animal displays behavioral responses reminiscent of the human condition). Construct validity references to a strong theoretical support for the model (i.e. targeting a gene which is implicated in a human disorder). Predictive validity pertains at correcting abnormalities in the model after treatments or manipulations which replicate what is seen in affected individuals after homologous treatments (e.g. correction of behavioral defects in a model of BPD following a treatment with lithium) (Boulton et al., 1991).

In BPD research, most models only approximate neuropathogenesis to a certain degree. Most pharmacological models display a good level of face validity but are somewhat lacking in construct validity (i.e. most bipolar onsets are not brought about by amphetamine or cocaine administration). On the other hand, genetic models display in some cases robust construct validity but only moderately approximate face validity (e.g. none of the genetic models display cyclic manic-depressive episodes). Predictive validity however is somewhat robustly attained across most modalities when measuring responsiveness to conventional treatment in reverting phenotypical manifestations (e.g. lithium or other pharmacological treatments successfully correct several abnormal phenotypes in the majority of models).

Together, the models exemplified above detail important aspects of behavioral alterations related to face validity. Nevertheless, although a substantial amount of information is still lacking on the neurobiological and synaptic subtracts involved in bipolar pathogenesis, recent advances in studying both human patients and the aforementioned models provide some indications on potential commonalities in synaptic dysfunctions, neural circuit dysfunction and how drug treatments like lithium may affect the underlying mechanisms of this disorder.

Model	Main effects	Relevant Reference
Amphetamine	Hyperactivity/ Reversibility and prevention of symptoms by Li, valproic acid or transcranial magnetic stimulation	(Frey et al., 2006a; Frey et al., 2006b; Gould et al., 2001; Shaldivin et al., 2001)
Metamphetamines	Hyperactivity/ reversibility of symptoms by Li	(Namima et al., 1999)
Cocaine	Potential cycling model of BPD	(Antelman et al., 1998)
Morphine	Oscillatory effects on shock induced hypoalgesia/ Li attenuates phenotype	(Kucinski et al., 1998)
Amphetamine & chlordiazepoxide	Hyperactivity/ reversibility of symptoms by Li	(Vale and Ratcliffe, 1987)
Ouabain	Hyperactivity/ reversibility of symptoms by Li	(El-Mallakh et al., 2003; Li et al., 1997)
Sleep deprivation	Insomnia, hyperactivity, irritability, aggressiveness, hypersexuality and increased stereotypies/ Behavioral effects reverted by haloperidol or lithium	(Gessa et al., 1995)
Dominance-submission	Drugs used to treat mania inhibit the dominant behavior| Antidepressants counteract the behavioral consequences of encounter defeats	(Malatynska et al., 2007)
Clock$^{\Delta 19}$	Hyperactivity, decreased sleep, lowered depression-like behavior, lower anxiety, increase in the reward value for cocaine and sucrose/lithium rescues phenotypes	(Roybal et al., 2007)
DISC1	Hyperactivity, deficits in PPI, deficits in sociability	(Ishizuka et al., 2006; Lipina et al., 2010; O'Tuathaigh et al., 2007)
22q11 deletion	Deficits in sensory motor gating	(Paylor and Lindsay, 2006; Paylor et al., 2001)
GSK-3β overexpression	Hypophagia, increased locomotor activity with decreased habituations, increased acoustic startle response with decreased habituation	(Prickaerts et al., 2006)
PKCI mutant mice	Less anxious, less prone to depression, increased HPA axis activity	(Barbier and Wang, 2009)
Amygdala and hippocampal kindling	Increase in emotionality response/increased activity in the open field reverted by D2 antagonist	(Kalynchuk et al., 1998; Leung et al., 2000)

Table 4. – Bipolar models, main face and main predictive validity and relevant references.

Circuit Dysfunctions in Bipolar Disorder

The neural networks most strongly implicated as dysfunctional in BPD patients are comprised of the prefrontal cortical-striatal-limbic circuits. These regions form a key system in the control of complex socio-emotional behaviors (Cerullo et al., 2009; Strakowski et al., 2005). Broadly, prefrontal cortical areas are involved in executive function, decision-making and attention. Most notably, damage to orbitofrontal cortex is known to affect patients and produce impairments in everyday decisions-making, whilst simultaneously not affecting most other cognitive abilities (Wallis, 2007). Perhaps the two most well studied examples of damage to frontal cortical regions are the case of Phineas Gage and patient EVR. Both men were reported to display intact functioning in higher cognition (memory, reading and writing, verbal communication, sensorial processing, facial recognition and fine motor function) but an extremely damaged decision-making process profoundly altered their personalities and behaviors (Damasio, 2005; Eslinger and Damasio, 1985). In terms of circuitry, the PFC receives afferent connections from all sensorial modalities (Carmichael and Price, 1995b; Cavada et al., 2000). Conversely, projections from the PFC extend to synapse onto premotor cortical neurons as well as somatosensory association cortical structures. Additionally, the PFC is known to heavily converge onto limbic regions (amygdala, cingulate gyrus, hippocampus and thalamus) (Carmichael and Price, 1995a) and the striatum (Haber et al., 1995; Kemp and Powell, 1970).

The second brain area involved in BPD is the striatum. The striatum is a major component of the basal ganglia which is comprised of a group of forebrain nuclei that receive inputs from the cortex and that in turn project to the thalamus. This circuit delineates the cortical-striatal-thalamic-cortical loop and is the canonical circuit involved in motor control planning and execution (Albin et al., 1989). Notably, both Parkinson and Huntington's disease involve a perturbation in the main type of striatal neurons, the medium spiny neurons, either due to their loss in the case of Huntington's disease or dysfunctionality due to lack of dopamine in the case of Parkinson's disease (Albin et al., 1989; DeLong, 1990). The striatum, and more broadly the basal ganglia in general, is also critically involved in the neuronal processes of habit formation, procedural memory formation, regulation of stereotypical behaviors and regulation of social interactions (Graybiel, 2008; Krach et al., 2010).

Lastly, the limbic system is also hypothesized to be involved in the broad neuronal circuitry potentially dysfunctional in BPD. Even though this structure is comprised of several well defined brain sub-regions, there is no precise neuroanatomical consensus as to which of these compose the limbic system (LeDoux, 2000). The amygdala, cingulate gyrus, hippocampus, thalamus and hypothalamus are some of the more "consensual limbic areas". Functionally, the limbic system is classically described as an important hub for memory formation, arousal and autonomic nervous system (Stephen et al., 1997).

The cortical-striatal-limbic circuits were the focus of several neuroimaging studies, such as magnetic resonance imaging (MRI) and positron emission tomography. These approaches provide clues into the neuroanatomical abnormalities that may underlay BPD. Largely, most studies using imaging approaches analyzing whole brain volumes, report either normal size or a small decrease in whole brain volume in BPD patients (Arnone et al., 2009; Strakowski et al., 2005). Nevertheless, more circumscribed regional differences have been observed in prefrontal cortical regions, limbic areas and in the basal ganglia nuclei. The subgenual prefrontal cortex was reported to be smaller in patients with mood disorders (Drevets et al., 1997; Hirayasu et al., 1999). In the basal ganglia, however, some reports have pointed to a larger striatal size in bipolar patients (Aylward et al., 1994; Noga et al., 2001; Strakowski et al., 1999) or no significant differences (Brambilla et al., 2001; Strakowski et al., 2005), while other reports have shown an anisotropy in discrete basal ganglia structures (Haznedar et al., 2005; Hwang et al., 2006). Interestingly, when comparing between BPD and UPD patients with healthy controls, structural enlargement of the basal ganglia and amygdala have been observed in BPD, whereas these structures appear to be smaller in UPD patients (Strakowski et al., 2002a). The hippocampus is also implicated in BPD; however, studies looking at this region display conflicting reports in the literature, with both smaller (Blumberg et al., 2003; Frazier et al., 2005; Strakowski et al., 2002b; Strasser et al., 2005; Swayze et al., 1992) and larger hippocampal volumes (Beyer et al., 2004; Strakowski et al., 1999) having been reported. Importantly, one confounding factor that may explain these discrepancies (not only for hippocampus but also other regions under investigation) is the medication history and how that may play a role in brain volume. This was best addressed in one influential work where the authors analyzed unmedicated BPD patients, BPD patients

on a lithium treatment, BPD patients under a different drug treatment (the anticonvulsantes valproic acid or lamotrigine) and healthy controls. In this work, there was a trend for a smaller hippocampal region in untreated BPD patients when compared to controls, but conversely, an increased hippocampal volume in lithium treated patients when compared to healthy controls (Yucel et al., 2008). This finding highlights the potential neuronal effects of this drug in humans and addresses some of the conflicting evidences in the field pertaining to anatomical brain volume.

Nevertheless, even though structural abnormalities provide some clues into affected neural circuits, functional MRI (fMRI) has also been used to probe how brain regions are affected in terms of neuronal activity. One work found an increase in amygdala activation and a reduction in dorsolateral prefrontal cortex activation in response to fearful facial stimuli (Yurgelun-Todd et al., 2000). The same group however, found an increase in dorsolateral prefrontal cortex and decrease anterior cingulate cortex (limbic system) activation during a cognitive test (Gruber et al., 2004). BPD patients also display increased activation in the amygdala, thalamus, hypothalamus (limbic system) and medial globus pallidus (basal ganglia) (Malhi et al., 2004). Qualitatively similar results were found by a separate group where patients observing hostile faces had greater activation in the limbic regions (left amygdala) and the basal ganglia region (nucleus accumbens and putamen) (Rich et al., 2006).

Interestingly, some researchers have proposed that UPD and BPD can perhaps be distinguished based on fMRI activation patterns. Specifically, responses to positive and negative emotional expressions in BPD patients revealed increased subcortical and ventral PFC responses, when comparing to healthy controls or UPD patients (Lawrence et al., 2004). It is worth noting however, that even though these studies are informative, they carry some limitations in interpretation. Confounding factors include not only the effect of medication on neuronal activation patterns, but also the contaminating effect that comorbid conditions may have on neuronal activity. Also, while some studies look at whole brain during imaging, many only analyze discrete regions of interest. Finally, experimental differences in the tasks performed by patients during fMRI analysis make a combined analysis of data across multiple research groups difficult to attain (Yurgelun-Todd and Ross, 2006).

Nevertheless, fMRI studies in BPD patients have provided an interesting framework to understand and identify the neural circuits disrupted in this disorder.

(Yurgelun-Todd and Ross, 2006). At the same time, this information provides important and complementary information when attempting to model BPD with genetic mouse model and broadly point to an over-activation of neuronal circuits in BPD.

Synaptic Dysfunctions in Bipolar Disorder

At the most fundamental level, the behavioral manifestations in neuropsychiatric disorders are a direct consequence of dysfunction in neuronal communication. Specifically, schizophrenia, autism and mood disorders are an example of disorders which have accrued significant converging evidence implicating synaptic dysfunction to their respective etiological basis (Bourgeron, 2009; Sanacora et al., 2008; Sodhi et al., 2008). For BPD, key findings pertaining to molecular dysfunctions are postulated to affect either the neurons as a whole or specifically the signaling networks at the postsynaptic site. Therefore, the molecular complexity of the postsynaptic site may be of key interest in understanding BPD and how synaptic dysfunction may contribute to the development of this disorder.

Chemical synapses are by far the most abundant types of synapses in the mammalian brain (Kandel et al., 2000). These specialized cell-cell junctions mediate the assymetrical flow of information from the pre-synaptic neuron to the postsynaptic cell. Notably, neurotransmitters exert specialized effects in the downstream cell but can in some cases influence the releasing neuron itself (Starke, 1981). The varied types of neurotransmitters available in the central nervous system provide a substantial pool for combinatorial information processing in neurons. For mood disorders in particular, the monoaminergic systems (serotonin, noradrenalin and dopamine) have been the focus of intense research; nevertheless, growing evidence implicates the glutamatergic system as potentially underlying the molecular pathways for these disorders (Sanacora et al., 2008). One interesting hypothesis is that even though monoaminergic neurotransmitters play an important role in the amelioration of symptoms in UPD and BPD, glutamatergic regulation of synaptic and neural plasticity is central to the etiology and treatment of these neuropsychiatric disorders (Manji et al., 2000; Payne et al., 2002; Sanacora et al., 2008).

In the mammalian brain, glutamate is the most abundant excitatory neurotransmitter (Purves, 2008). Glutamatergic synapses form the prototypical junctions and the ones that best represent the asymmetric nature of information flow between neurons in the central nervous system. In these types of synapses, glutamate is released from the axonal presynaptic bouton onto the synaptic cleft. The neurotransmitter then transverses the synaptic cleft to bind and activating glutamate receptors on the postsynaptic neuron and generate excitatory postsynaptic currents (EPSCs) or changes in intracellular biochemical processes (Kandel et al., 2000). The glutamate receptors which effect this communication are subdivided into two major subtypes, ionotropic and metabotropic glutamate receptors. Metabotropic glutamate receptors (mGluRs) are G-protein-coupled receptors further subdivided into three groups, group I (mGluR1a–d, mGluR5a,b), group II (mGluR2 and mGluR3) and group III (mGluR4, mGluR6–8). These transmembrane receptors transduce neurotransmitter binding to intracellular activation of phospholipase C, modulation of adenylyl cyclase and through other second messengers (Conn and Pin, 1997). Glutamate ionotropic receptors are also subdivided according to their physiological and pharmacological properties into three groups, the N-Methyl-D-aspartic acid (NMDA) glutamate receptors; the α-amino-3-hydroxy-5-methyl-4-isoxazolepropionic acid (AMPA) glutamate receptors and kainate receptors (Dingledine et al., 1999). Ionotropic glutamate receptors are ligand gated channels which depending on physiological conditions and selective permeability, allow the passage of ions across the cell membrane.

In recent decades a large body of research has been devoted to the understanding of the proteinaceous synaptic machinery at both the presynaptic and postsynaptic site (Kennedy, 2000; Trimble et al., 1991). In the postsynaptic site, glutamate receptors cluster at high densities in the postsynaptic membrane through the action of a complex network of proteins known as the postsynaptic density (PSD) (Kennedy, 2000; O'Brien et al., 1998). The PSD was originally observed under electron microscopy of brain tissue as an electron dense material present beneath the plasma membrane of most postsynaptic sites (Palay, 1956a; b; Palay and Palade, 1955). This structure was latter characterized as being composed of several different proteins serving a multitude of intracellular functions (Carlin et al., 1983; Collins et al., 2006; Kennedy et al., 1983; Okabe, 2007). Using a combination of biochemical purification of

PSDs and proteomic analysis, over 1000 different types of proteins at varying stoichiometric ratios have been identified at the PSD (Sheng and Hoogenraad, 2007). Interestingly, many of these proteins are not only present at the PSD, but are also biochemically enriched at this structure, when comparing the relative abundance between the PSD and the synaptic cytoplasm (Collins et al., 2006). By function, some of the best characterized types of PSD protein include: glutamate neurotransmitter receptors; scaffolding and adaptor proteins involved in the anchoring, trafficking and regulation of postsynaptic receptors; cell-adhesion molecules, which form contact across the synaptic cleft; kinases involved in downstream signaling and proteins involved in interaction and remodeling of the actin cytoskeleton (Sheng and Hoogenraad, 2007).

The molecular function of many of these proteins revolves around the formation of defined macro-molecular complexes which orchestrate biochemical function in discrete sub-networks. The NMDA glutamate receptors, known to play an important role for synaptic plasticity and cellular information processing (Daw et al., 1993; Malenka and Nicoll, 1993), form one of the largest complexes within the PSD (Husi and Grant, 2001; Husi et al., 2000). One example is the NMDA receptor/MAGUK-associated signaling complex (MASC), named after the receptors and their primary interaction proteins, the “membrane associated guanylate kinase” (MAGUK) family of proteins. The MASC complex is composed of at least 186 different proteins which form a 2000 KDa structure within the larger PSD (Collins et al., 2006; Husi and Grant, 2001). Other large complex is formed by mGluRs which can associate with at least 64 other types of proteins (Farr et al., 2004) and AMPA receptors complex which directly or indirectly associate with at least 9 other proteins in the PSD (Collins et al., 2006).

Abnormalities in glutamatergic biology in patients affected by mood disorders have been found in the cerebral spinal fluid, serum, plasma and brain tissue (Altamura et al., 1993; Francis et al., 1989; Frye et al., 2007; Kim et al., 1982; Levine et al., 2000; Mauri et al., 1998; Mitani et al., 2006). However, the majority of these studies were performed with samples from UPD patients. In one study however, increased levels of glutamate were observed in the frontal cortex of UPD and BPD patients (Hashimoto et al., 2007). Nevertheless, one important cavet with most studies performed in human patients, is the confounding effect of the medications prescribed affecting glutamate or glutamate receptor levels. Nevertheless, the alterations brought about by mood

disorder therapeutics can themselves be informative on the underlying mechanisms surrounding BPD.

Mood stabilizer drugs, such as lithium and valproic acid, are generally prescribed to BPD patients to alleviate manic episodes and also to prevent recurrent manic-depressive oscillations. In cultured neurons, lithium displays a protective effect on NMDA mediated excitotoxicity due to calcium influx (Hashimoto et al., 2002; Nonaka et al., 1998). Indirectly, this suggests that abnormality in glutamatergic neurotransmission may underlay certain cellular aspects of BPD. Also, AMPA receptor function is known to be modulated by both lithium and valproic acid. It is interesting that although these two drugs are structurally dissimilar, both are able to affect AMPA receptor synaptic expression (Du et al., 2004). Specifically, both drugs lead to a downregulation of AMPA receptor GluR1 and GluR2 subunits, while conversely, the antidepressant drug imipramine, which can trigger manic episodes, increases synaptic expression of GluR1 in hippocampus *in vivo* (Du et al., 2008; Du et al., 2004).

It is therefore not surprising that synaptic and postsynaptic proteins directly or indirectly involved in the anchoring, regulation and trafficking of glutamate receptors may play a role in psychiatric disorders in general or in BPD in particular. In fact, several canonical PSD scaffolding proteins are strongly implicated in a multitude of disorders, such as mental retardation (SAP102 – synapse associated protein 102 a MAGUK), autism (Shank3 – SH3 and multiple ankyrin repeat domains protein 3) or obsessive-compulsive disorder (SAPAP3 - SAP90/PSD95-associated protein 3) (Bienvenu et al., 2009; Durand et al., 2007; Tarpey et al., 2004; Welch et al., 2007).

Shank/SAPAP/nArgBP2 protein network at the PSD

The Shank family of proteins is a group of PSD proteins coded by three independent genes, Shank1-3 (Lim et al., 1999). Shank proteins (Shank1-3) bind to SAPAP and participate in the PSD95/SAPAP/Shank complex (Kim et al., 1997; Takeuchi et al., 1997). This complex functions as a scaffold and is involved in the assembly of macromolecular signaling complexes and trafficking of ionotropic glutamate receptors (Malinow and Malenka, 2002; Nicoll et al., 2006; Prybylowski and Wenthold, 2004). This complex is also involved in the formation and maintenance of

dendritic spines (Elias and Nicoll, 2007; Hung et al., 2008; Roussignol et al., 2005; Welch et al., 2007). Importantly, genetic disruption of *Shank3* is thought to be a primary cause for the deficits in the 22q13.3 deletion syndrome (Phelan-McDermid syndrome), a syndrome characterized by the presence of autistic symptoms in a high percentage of affected individuals (Discussed in next section) (Abrahams and Geschwind, 2008).

The SAPAP family of proteins is another group of proteins involved in the regulation of the PSD and glutamate receptors (Takeuchi et al., 1997; Welch et al., 2007; Welch et al., 2004). SAPAP3, in particular, binds to Shank3 and has also been demonstrated to affect NMDA receptors at the PSD (Welch et al., 2007). *In vivo,* mutant mice for the SAPAP3 gene display OCD-like behaviors which are ameliorated by the administration of fluoxetine (Welch et al., 2007). In humans, mutations in the SAPAP3 gene have also been identified in OCD patients (Bienvenu et al., 2009; Boardman et al., 2010; Zuchner et al., 2009). Interestingly, both SAPAP3 and Shank3 proteins are enriched in the striatum and both mutant animals display cortico-striatal defects (Peca et al., 2011; Welch et al., 2007).

nArgBP2 (neural Arg-binding protein 2) is another binding partner to SAPAP3 identified using a Yeast Two-hybrid screening (Kawabe et al., 1999). This protein is the neuronal specific form of ArgBP2, a protein which associates and is a phosphorylation target for Abl and Arg protein-tyrosine kinases (Wang et al., 1997). ArgBP2 and nArgBP2 are reported to closely regulate multiple mechanisms converging on the cytoskeleton (Cestra et al., 2005; Ronty et al., 2005). At the same time, ArgBP2 was also identified to be present at the nucleus (Kioka et al., 2002; Wang et al., 1997). nArgBP2 however, is specifically expressed in the brain, much like SAPAP3 and Shank3, and is also highly enriched in the PSD. Therefore, nArgBP2 is well positioned to bridge the interaction between the PSD and the actin cytoskeleton (Cestra et al., 2005; Kawabe et al., 1999). In terms of structure, nArgBP2 is composed of a conserved Sorbin homology domain (which was demonstrated to target proteins to lipid rafts) (Kimura et al., 2001), a zinc finger domain in the brain specific section of the protein and three SH3 domains near the C-terminus (Kawabe et al., 1999).

Even with the above, much of the *in vivo* functions of nArgBP2 remain unknown. However, the association of nArgBP2 in a complex of PSD protein involved in other neuropsychiatric disorder (SAPAP3-OCD and Shank3-Autism) highlights a potential

role for this gene in related neuropsychiatric disorders. Importantly, the concept of a human *phenome* supports the functional analysis of genes and their association with similar disorders in a landscape of interrelated diseases which may originate from an overlapping molecular causation (Barabasi et al., 2011; Goh et al., 2007; Linghu et al., 2009; Oti and Brunner, 2007; Oti et al., 2008; van Driel et al., 2006). This is particularly relevant to diseases which share common endophenotypes that may be brought about by functionally related genes which produce proteins that, at the cellular level, associate in a multiprotein complex (e.g. the complexes in the PSD) in the same pathway, or as part of the same subcellular organelle (Linghu et al., 2009; Oti and Brunner, 2007). This is particularly relevant for the study of nArgBP2 since the interaction of this protein with SAPAP3 and its enrichment at the PSD promotes an association of nArgBP2 with a cluster of proteins that are strongly implicated in the pathogenesis of several neuropsychiatric disorders.

Finally, nArgBP2 is coded from the SORB2 gene which is present in chromosome 4q35, a region identified in BPD susceptibility. Therefore, the *in vivo* characterization and the exploration of the cellular roles of nArgBP2 are underexplored, at the same time as the potential involvement of this gene in neuropsychiatric disorders remains an interesting hypothesis.

Autism Spectrum Disorders

Overview of Autism Spectrum Disorders

Leo Kanner (1943) and Hans Asperger (1944) independently identified and characterized the dysfunctional behavioral patterns present in autistic children. The term autism derives from the Greek word *autós* (meaning “self”) and was originally coined to describe how schizophrenic patients withdrew to self-generated fantasies. However, autism is now almost exclusively used to characterize the combination of the three main components in autism spectrum disorders (ASDs): 1) impairments in language and communication; 2) repetitive behaviors, interests or routines; and 3) deficits in social interaction and social behaviors (American Psychiatric Association, 2000). Epidemiological studies estimate that approximately 1% of the human population displays some form of ASD (Baird et al., 2006; Bertrand et al., 2001; Chakrabarti and

Fombonne, 2005). Autism is also comorbid with other conditions and a large percentage of autistic individuals display intellectual disability (70%), sleep disturbances (50%), epilepsy (20-30%) or mood disorders (10-20%) (Geschwind, 2009; La Malfa et al., 2004; Leyfer et al., 2006; Tuchman and Rapin, 2002). ASDs are also highly heritable with reported concordance rates of 30% in dizygotic twins but 90% in monozygotic twins (Bailey et al., 1995; Rosenberg et al., 2009). Nevertheless, even though there is a very high degree of confidence for the genetic causation of autism, evidences suggest that paradoxically it is not necessarily inherited, but instead due in large percentage to *de novo* mutations (Beaudet, 2007). Moreover, recent work suggest that in 10-20% cases it is possible to identify the underlying genetic cause in ASD patients (Jacquemont et al., 2006; Sebat et al., 2007).

In addition, there are a large numbers of genes associated with ASDs (Abrahams and Geschwind, 2008) and an emerging hypothesis centers on the fact that several of the known genes associated with ASDs code for proteins that are involved in synaptic function (van de Lagemaat and Grant, 2010; Zoghbi, 2003). Some of the most promising targets include the complex of trans-synaptic proteins formed by Neurexin/Neuroligin/PSD-95/SAPAP/Shank (Bourgeron, 2009; van de Lagemaat and Grant, 2010). Several of these genes have been linked to ASDs, including Shank2 and Shank3 (Berkel et al., 2010; Bonaglia et al., 2001; Bonaglia et al., 2006; Durand et al., 2007; Gauthier et al., 2009; Pinto et al., 2010), SAPAP2 (Pinto et al., 2010), neurexin-1 (Kim et al., 2008; Wisniowiecka-Kowalnik et al., 2010) and neuroligin-3 and -4 (Jamain et al., 2003).

Neuroligins and Neurexins in Autism

Neuroligins are cell-adhesion molecules located at the postsynaptic membrane and neurexins are their presynaptic binding partners (Shapiro et al., 2007). The neurexins are a family of proteins originally identified as one of the receptors for alpha-latrotoxin (a component in black widow spider poison) (Ushkaryov et al., 1992). Neuroligin-1, in turn, was identified through its interaction with β-neurexins (Ichtchenko et al., 1995). Neurexins (1-3) genes are known to be alternatively spliced into thousands of different isoforms broadly subdivided into two groups, (1) α-neurexins,

characterized by the presence of a large extracellular portion containing six laminin/neurexin/sex-hormone-binding globulin (LNS) domains (Rudenko et al., 1999) and three interleaved epidermal growth factor (EGF)-like domains; and (2) β-neurexins, which only include the sixth LNS domain (Missler et al., 1998). Neuroligins, which are coded by 4 different genes, are endogenous neurexin ligands that express a signal sequence, a large extracellular domain functionally similar to an acetylcholinesterase domain, one transmembrane region, and a C-terminal cytoplasmic domain which contains a PDZ recognition sequence (Ichtchenko et al., 1995; Missler et al., 1998). Postsynaptically, the PDZ recognition sequence interacts with downstream scaffolding proteins PSD-95 (Irie et al., 1997; Sudhof, 2008).

Ectopic expression of neuroligin promotes postsynaptic differentiation *in vitro* (Chih et al., 2005) and similarly neurexins may induce the assembly of presynaptic terminals (Dean et al., 2003). The significant role played by these genes in the formation and regulation of synaptic function in the central nervous system is further enhanced by findings relating these genes to human disorders. Specifically, the identification of a missense mutation (R451C) in the Neuroligin-3 gene in two siblings afflicted by ASDs and a frameshift inducing mutation in Neuroligin-4 present in two probands from a different family (Jamain et al., 2003). Moreover, one different group has also positively linked a mutation in neuroligin-4 with mental retardation and autism (Laumonnier et al., 2004).

Importantly, mutant mice for neuroligins and neurexins have been used to model autism. Mice engineered to express the R451C mutation in the neuroligin-3 gene were shown to display impaired social behaviors, enhanced spatial learning and an in increase in inhibitory transmission. However, neuroligin-3 knockout mice did not manifest relevant autism-like behaviors, suggesting that a “gain-of-function” occurring with the amino acid substitution is the leading cause for the behavioral deficits (Tabuchi et al., 2007). Moreover, knockout mice for the neuroligin-4 gene do display behavioral deficits and abnormal vocalizations, suggesting phenotypical similarities to autism-like behaviors (Jamain et al., 2008). Murine genetic studies of the neurexin family of genes through targeted mutations are complicated due to the large number of isoforms. Nevertheless, converging evidences arrive from the studies in neurexin1α knockout mutant mice showing that these animals display increased repetitive grooming behavior and deficient nest building (a measure of sociability in mice) associated with a

functional decrease in glutamatergic synaptic strength in hippocampal neurons (Etherton et al., 2009).

Phelan-McDermid Syndrome and Shank3

Phelan-McDermid syndrome (PMS), also known as 22q13.3 microdeletion syndrome, is characterized by severe deficits in language delay, deficits in social behaviors and the presence of stereotypical behaviors. Several patients also display neonatal hypotonia, minor dysmorphic features and seizures (Phelan et al., 2001). Originally identified as a cytogenetic abnormality, several genes are eliminated with the deletion of the q13 tail of chromosome 22 (Prasad et al., 2000; Precht et al., 1998). From the multiple genes deleted in 22q13, Bonaglia and colleagues first proposed that the Shank3 gene deletion is the proximal cause for the origination of the main symptom in PMS (Bonaglia et al., 2001). Later, the same group also identified a recurrent breakpoint in the Shank3 gene which may lay at the basis for the chromosomal instability that leads to the 22q13 deletion (Bonaglia et al., 2006). A more refined view by gene sequencing has also confirmed that indeed Shank3 is the key gene responsible for the main neurological defects in PMS (Durand et al., 2007; Wilson et al., 2003). Additionally, several mutations in Shank3 have been identified in ASD patients not clinically diagnosed with PMS, suggesting that Shank3 may indeed be responsible for a monogenic form of autism (Gauthier et al., 2009; Moessner et al., 2007).

Shank family proteins (Shank1-3) are key elements at the postsynaptic density. Together with SAPAP proteins, Shank forms a dyadic interaction which organizes into a trans-synaptic complex of linearly interacting partners composed of Neurexin/Neuroligin/PSD-95/SAPAP/Shank (Bourgeron, 2009; van de Lagemaat and Grant, 2010) with several directly implicated in ASDs (Berkel et al., 2010; Jamain et al., 2003; Kim et al., 2008; Pinto et al., 2010; Wisniowiecka-Kowalnik et al., 2010).

At the protein level Shank genes give rise to several isoforms. The longest isoform of the Shank genes exhibit a multitude of protein-protein interaction domains, including ankyrin repeat domains, an SH3 domain, a PDZ domain, a proline-rich region and a SAM domain (Lim et al., 1999). Shank proteins are also a part of the PSD core (Naisbitt et al., 1999) and orchestrate a complex network with several other proteins, including α-Fodrin and Sharpin, which are binding partners at the N-terminal ankyrin repeat domain (Bockers et al., 2001; Lim et al., 2001). The SH3 domain of Shank binds

to Densin-180 (Quitsch et al., 2005). The PDZ domain of Shank binds to the SAPAP-PSD95-NMDA complex (Naisbitt et al., 1999) and the proline-rich region to Homer (Tu et al., 1999) and Cortactin (Du et al., 1998). Finally the SAM domain of Shank is known to undergo homo-oligomerization, which has been proposed to form a platform for the organization of the broader PSD network (Baron et al., 2006; Hayashi et al., 2009; Naisbitt et al., 1999).

Converging evidences also arise from mouse models for Shank3 mutations. Our own work and from other groups have proposed Shank3 mutant mice as valid models for ASDs. Specifically, we characterized two Shank3 knockout mouse lines and found that mice with a genetic lesion in the PDZ domain of Shank3 (exons 13-16) exhibit severe impairments in social interaction and increased repetitive behaviors (Peca et al., 2011). Together with other research groups we have shown that Shank3 mutation provide strong converging evidence that mutations in this gene lead to: a) impaired glutamatergic signaling; b) increased repetitive behaviors; c) dysfunction in social behaviors (Bangash et al., 2011; Bozdagi et al., 2010; Peca et al., 2011; Wang et al., 2011). In our work we also found that Shank3 is the only Shank family member highly expressed in the striatum and that the cortico-striatal circuit is abnormal in these mice. The striatum is a brain region implicated both in OCD (repetitive actions) (Graybiel, 2008; Modell et al., 1989) and ASDs (response to social stimuli) (Scott-Van Zeeland et al., 2010), supporting a role for the basal ganglia as a focal point for the dysfunction in neurological circuits of autism (Damasio and Maurer, 1978). Interestingly, in humans there is also a link between social interaction and activity in this region. Specifically, ventral striatal activation is seen during functional imaging studies under a variety of rewarding social stimuli, such as observing beautiful faces, positive emotional expressions, images of maternal and romantic love and during the anticipation of a positive social feedback (Aharon et al., 2001; Bartels and Zeki, 2000; 2004; Rademacher et al., 2010; Spreckelmeyer et al., 2009). Conversely, this region is under-activated in autistic patients in response to social stimuli (Scott-Van Zeeland et al., 2010). Therefore, the Shank3 mutant mice provide a powerful tool to dissect the neural circuitry mechanisms underlying the abnormal behaviors relevant to human ASD and simultaneously a platform to test novel treatments.

Objectives and Thesis Outline

The study of neuropsychiatric disorders offers the possibility to explore to a higher degree of confidence what are the parameters for “normal” functioning of the brain and therefore convey a better understanding of this still mysterious organ. While we are gaining a better understanding of which brain regions may be responsible for discrete operant neuronal functions, conclusive evidences are often gained from the observation of lesions and studying behavioral output. This is perhaps best illustrated from the advances made in understanding functional compartmentalization thought the study of brain lesions (Blumenfeld, 2010) or more recently with targeted transcranial magnetic stimulation (Hallett, 2000). Nevertheless, tracing the direct influence of genes and gene mutations, their role in pathogenesis of electrophysiological, biochemical and ultimately behavioral deficits, is only possible using animal models.

To this end, we started by studying the SAPAP3 gene (Appendix 1 (Welch et al., 2007)) and identified a critical role played by this gene in the regulation of glutamatergic signaling, cortical striatal circuitry and mouse behavior. From this study we hypothesized that genes interacting with SAPAP3 could share the phenotypical landscape of neuropsychiatric disorders. We therefore defined the scope of our thesis to center on the role of other genes coding for proteins that are directly binding partners to SAPAP3. Specifically, we used a combination of database mining and bioinformatics to cross reference targets with their potential involvement in human genetic and neuropsychiatric disorders. This screen led us to focus on two particular genes: nArgBP2 and Shank3.

We aimed at the characterization of the expression patterns of these genes in the mouse brain and performed disruptions by homologous recombination in ES cells to studied the biochemical, electrophysiological and behavioral consequences of disrupting Shank3 (Chapter 2) or nArgBP2 (Chapter 3 and 4) *in vivo*.

Chapter 2

Shank3 mutant mice as a model for ASDs

In the ensuing manuscript, Cátia Feliciano made the following contributions:

Planned the research and designed the experiments

Generated ES constructs, targeted ES cells and produced mutant mice

Collected, analyzed and interpreted:

Behavioral tests, in situ hybridization, biochemistry, cell fill data and electron microscopy

Analyzed and interpreted:

Golgi staining data

Interpreted electrophysiology data

Wrote the paper

This work was publication with equal contribution from Peça, J. and Feliciano, C.

ARTICLE

doi:10.1038/nature09965

Shank3 mutant mice display autistic-like behaviours and striatal dysfunction

João Peça[1,2]*, Cátia Feliciano[1,3]*, Jonathan T. Ting[1], Wenting Wang[1], Michael F. Wells[1], Talaignair N. Venkatraman[4], Christopher D. Lascola[1,4], Zhanyan Fu[1,5,6] & Guoping Feng[1,6,7]

Autism spectrum disorders (ASDs) comprise a range of disorders that share a core of neurobehavioural deficits characterized by widespread abnormalities in social interactions, deficits in communication as well as restricted interests and repetitive behaviours. The neurological basis and circuitry mechanisms underlying these abnormal behaviours are poorly understood. SHANK3 is a postsynaptic protein, whose disruption at the genetic level is thought to be responsible for the development of 22q13 deletion syndrome (Phelan–McDermid syndrome) and other non-syndromic ASDs. Here we show that mice with *Shank3* gene deletions exhibit self-injurious repetitive grooming and deficits in social interaction. Cellular, electrophysiological and biochemical analyses uncovered defects at striatal synapses and cortico-striatal circuits in *Shank3* mutant mice. Our findings demonstrate a critical role for SHANK3 in the normal development of neuronal connectivity and establish causality between a disruption in the *Shank3* gene and the genesis of autistic-like behaviours in mice.

Autism and autism spectrum disorders (ASDs) are neurodevelopmental disorders diagnosed based on a triad of criteria: deficits in communication, impaired social interaction, and repetitive or restricted interests and behaviours[1]. ASDs are highly heritable disorders with concordance rates as high as 90% for monozygotic twins[2]. Recent genetic and genomic studies have identified a large number of candidate genes for ASDs[3], many of which encode synaptic proteins[4–6], indicating synaptic dysfunction may have a critical role in ASDs[7,8]. One of the most promising ASD candidate genes is *Shank3*, which codes for a key postsynaptic density (PSD) protein at glutamatergic synapses. Disruption of *Shank3* is thought to be the cause of core neurodevelopmental and neurobehavioural deficits in the 22q13 deletion syndrome (Phelan–McDermid syndrome), an autism spectrum disorder[9–11]. Furthermore, recent genetic screens have identified several mutations/rare variants of the *Shank3* gene in ASD patients outside of diagnosed 22q13 deletion syndrome[12,13].

The Shank family of proteins (SHANK1–3) directly bind SAPAP (also known as DLGAP) to form the PSD-95–SAPAP–SHANK complex[14,15] (PSD-95 is also known as DLG4). This core of proteins is thought to function as a scaffold, orchestrating the assembly of the macromolecular postsynaptic signalling complex at glutamatergic synapses. Currently, however, little is known about the *in vivo* function of SHANK3 at the synapse and how a disruption of *Shank3* may contribute to ASDs. Here we demonstrate that genetic disruption of *Shank3* in mice leads to compulsive/repetitive behaviour and impaired social interaction, resembling two of the cardinal features of ASDs. Biochemical, morphological and electrophysiological studies revealed synaptic dysfunction at cortico-striatal synapses, part of the neural circuits strongly implicated as dysfunctional in ASDs. Our studies provide a synaptic and circuitry mechanism underlying *Shank3* disruption and ASD-like behaviours.

Shank3B$^{-/-}$ mice display repetitive grooming

The *Shank3* gene codes for large proteins with multiple protein–protein interaction domains (Fig. 1a). We generated two different alleles of SHANK3 mutant mice. In *Shank3A* mutant mice, we targeted a portion of the gene encoding the ankyrin repeats (Supplementary Fig. 1b). This resulted in a complete elimination of SHANK3$_\alpha$, the longest SHANK3 isoform (Fig. 1b). However, the other two isoforms were not affected (here named SHANK3$_\beta$ and SHANK3$_\gamma$). In *Shank3B* mutants, we targeted the fragment encoding the PDZ domain (Supplementary Fig. 1c). This led to the complete elimination of both SHANK3$_\alpha$ and SHANK3$_\beta$ isoforms and a significant reduction of the putative SHANK3$_\gamma$ isoform at the PSD ($-42.12\% \pm 9.27\%$ of control, $n = 3$, $P < 0.05$) (Fig. 1b). Our analysis is mainly focused on the *Shank3B*$^{-/-}$ mutants due to their more pronounced behavioural and physiological defects.

We used mice with a hybrid genetic background to avoid the potential contribution to behavioural phenotypes of homozygous genetic variants on a pure inbred background[7,16]. Initially, F1 hybrids from heterozygous × heterozygous matings were generated and homozygous mice were born at an expected Mendelian rate. However, homozygous knockout mice from this type of mating are smaller than their wild-type littermates, presumably due to inadequate competition for resources during early postnatal days leading to different developmental trajectories. We postulated that this size difference would influence our behavioural tests. To alleviate this confound, heterozygous animals were crossed in direct brother-sister matings for five generations from which we derived F5 isogenic hybrids in a mixed background. These isogenic animals were then used to generate time-mated homozygous × homozygous breeding pairs to obtain wild-type and mutant animals used in the experiments. F5 *Shank3A* and F5 *Shank3B* knockouts from these matings are reared to weaning age with body weights similar to those from F5 control animals.

Shank3B$^{-/-}$ mice did not display any gross anatomical or histological brain abnormality, but on rare occasions exhibited seizures during handling in routine husbandry procedures. However, spontaneous seizures were never observed. By the age of 3–6 months, *Shank3B*$^{-/-}$

[1]Department of Neurobiology, Duke University Medical Center, Durham, North Carolina 27710, USA. [2]PhD Programme in Biomedicine and Experimental Biology (BEB), Center for Neuroscience and Cell Biology, University of Coimbra, Coimbra, Portugal. [3]Gulbenkian PhD Programme in Biomedicine, Gulbenkian Science Institute, 2781-901 Oeiras, Portugal. [4]Department of Radiology, and Brain Imaging and Analysis Center, Duke University Medical Center, Durham, North Carolina 27710, USA. [5]Department of Psychiatry and Behavioral Science, Duke University Medical Center, Durham, North Carolina 27710, USA. [6]McGovern Institute for Brain Research, Department of Brain and Cognitive Sciences, Massachusetts Institute of Technology, Cambridge, Massachusetts 02139, USA. [7]Stanley Center for Psychiatric Research, Broad Institute, Cambridge, Massachusetts 02142, USA.
*These authors contributed equally to this work.

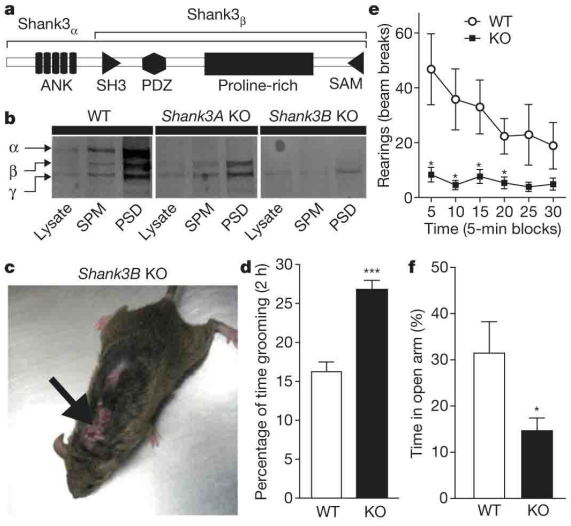

Figure 1 | Excessive grooming, skin lesions and anxiety-like behaviour in *Shank3B*$^{-/-}$ mice. **a**, SHANK3 protein structure. **b**, Western blot showing a pan-SHANK3 antibody staining in brain lysate, synaptosomal plasma membrane (SPM) and 2× Triton X-100-washed PSD (PSD) fraction in wild-type (WT), *Shank3A*$^{-/-}$ and *Shank3B*$^{-/-}$ mice. **c**, Four-month-old *Shank3B*$^{-/-}$ mice display neck and head lesions (arrows). **d**, Pre-lesion *Shank3B*$^{-/-}$ (KO) mice spent more time in self-grooming than WT. **e**, In the open field test, *Shank3B*$^{-/-}$ mice, when compared to controls, display decreased rearing activity. **f**, In the zero maze test, *Shank3B*$^{-/-}$ mice spent less time in the open area than wild-type controls. $*P < 0.05$, $***P < 0.001$, two-tailed *t*-test for **d** and **f**, two-way repeated measures ANOVA with post hoc two-tailed *t*-test for **e**; all data are presented as means ± s.e.m. from 6–9 mice per genotype.

mice developed pronounced skin lesions with varying degrees of phenotypical penetrance: approximately 35% in the general holding colony (Fishers exact test, $P < 0.0001$), and 100% in mating females that have produced 4–6 litters. The lesions tend to appear first on the back of the neck or on the face (Fig. 1c) and usually progressed bilaterally to cover large areas of the body. The lesions were self-inflicted, as they were present in animals socially isolated at weaning age, and not due to excessive allogrooming, as no lesions were found in wild-type or *Shank3B*$^{+/-}$ mice housed from birth with *Shank3B*$^{-/-}$ animals. Furthermore, 24 h videotaping in pre-lesion animals revealed that *Shank3B*$^{-/-}$ mice showed an increase in time spent grooming when compared to wild-type controls (Fig. 1d). These observations indicate that *Shank3B*$^{-/-}$ mice display excessive grooming and self-injurious behaviour.

We characterized the animals further in a battery of behavioural tests. In the rotarod motor test, *Shank3B*$^{-/-}$ and control animals performed at similar levels (Supplementary Fig. 2). In the open field test, when compared to controls, *Shank3B*$^{-/-}$ mice showed similar levels of activity and thigmotaxis (Supplementary Fig. 2). However, rearing, which is a form of vertical exploration considered to be anxiogenic for mice, was significantly reduced in the mutants (Fig. 1e). In the elevated zero maze, the *Shank3B*$^{-/-}$ mice spent less time exploring the open arms of the maze versus the closed arms (Fig. 1f). In the light-dark emergence test, the *Shank3B*$^{-/-}$ mice displayed an increased latency to cross into the brightly lit area, although the time spent in each side of the box was similar between mutant animals and controls (Supplementary Fig. 2). Thus, the *Shank3B*$^{-/-}$ mice display an anxiety-like behaviour and excessive, self-injurious grooming. In contrast, *Shank3A*$^{-/-}$ mice displayed no lesions or anxiety-like behaviour (Supplementary Fig. 3).

Social interaction deficits in *Shank3B*$^{-/-}$ mice

Deficits in social interaction are the most recognizable manifestation of autistic behaviours in humans. We used a modified version of a three-chamber social arena[17] to probe animals for their voluntary initiation of social interaction and their ability to discriminate social novelty. Initially, the test animal was left to explore and initiate social contact with a partner ('Stranger 1') held inside a wired cage or an identical but empty wired cage ('Empty cage'). In this test, the *Shank3B*$^{-/-}$ mice displayed dysfunctional social interaction behaviour, as measured by observing both time spent in the compartment containing the social partner (Fig. 2a, b) or in close interaction (Fig. 2d). Notably, *Shank3B*$^{-/-}$ mice exhibited a clear preference for interacting with the empty cage rather than with the social partner (Fig. 2a, d). In a subsequent trial, a novel social partner ('Stranger 2') was introduced into the previously empty wired cage. Wild-type mice displayed a preference for the novel animal, as shown by the increase in time spent in the compartment containing 'Stranger 2'. The *Shank3B*$^{-/-}$ mutants markedly spent more time in the centre chamber (Fig. 2c) and a reduced amount of time closely interacting with either social partner (Fig. 2e). In an identical test, the *Shank3A*$^{-/-}$ mice displayed normal initiation of social interaction, but perturbed recognition of social novelty (Supplementary Fig. 4).

Additionally, in an open arena test, freely interacting dyadic pairs of wild-type–*Shank3B*$^{-/-}$ mice displayed less time spent in reciprocal interaction, a lower frequency of nose-to-nose interaction and anogenital sniffing when compared to wild-type–wild-type pairs (Supplementary Fig. 5). Thus, data from both social interaction tests indicate that *Shank3B*$^{-/-}$ mice display abnormal social interaction as well as deficits in discriminating social novelty.

In our breeding scheme, *Shank3B*$^{-/-}$ mice and wild-type mice were nurtured by *Shank3B*$^{-/-}$ and wild-type dams, respectively. To assess the impact of maternal rearing on the observed sociability defects, we performed time-mated cross-fostering of *Shank3B*$^{-/-}$ mice and controls. Cross-fostering of *Shank3B*$^{-/-}$ neonatal pups with wild-type dams (KO_{cf}) revealed qualitatively equivalent social defects in the mutant mice as compared to those observed in mutant mice nurtured by *Shank3B*$^{-/-}$ dams. Additionally, rearing wild-type neonatal pups by *Shank3B*$^{-/-}$ dams (WT_{cf}) did not perturb normal sociability in wild-type animals (Supplementary Fig. 6). These data further indicate a genetic origin of the abnormal social behaviours in the *Shank3* mutant mice.

Altered PSD composition in the striatum

The basal ganglia are one of the brain regions implicated as dysfunctional in ASD. The repetitive/compulsive grooming behaviour in *Shank3B*$^{-/-}$ mice also suggests defects in cortico-striatal function. Furthermore, *Shank3*, but not *Shank1* or *Shank2*, is highly expressed in the striatum (Fig. 3a) (Supplementary Fig. 7 and Supplementary Table 1). Therefore, we focused our analyses on striatal neurons and cortico-striatal synapses.

Shank family members have been proposed as key regulators of the PSD at glutamatergic synapses[18]. To determine how the disruption of *Shank3* may affect the PSD protein network, we used biochemically purified PSDs from the striatum of wild-type and *Shank3B*$^{-/-}$ mice and performed semiquantitative western blotting for several scaffolding proteins (Fig. 3b) and glutamate receptor subunits (Fig. 3c). At the PSD level, we observed reduced levels of SAPAP3, Homer-1b/c and PSD-93 (also known as HOMER1 and DLG2, respectively; Fig. 3b) as well as a reduction in the glutamate receptor subunits GluR2, NR2A and NR2B (also known as GRIA2, GRIN2A and GRIN2B, respectively; Fig. 3c). These results suggest an altered molecular composition of postsynaptic machinery in the striatum and a possible disruption of glutamatergic signalling.

Morphological defects of medium spiny neurons

To test whether disruption of SHANK3 affects neuronal morphology, we traced Golgi-stained striatal medium spiny neurons (MSNs) and

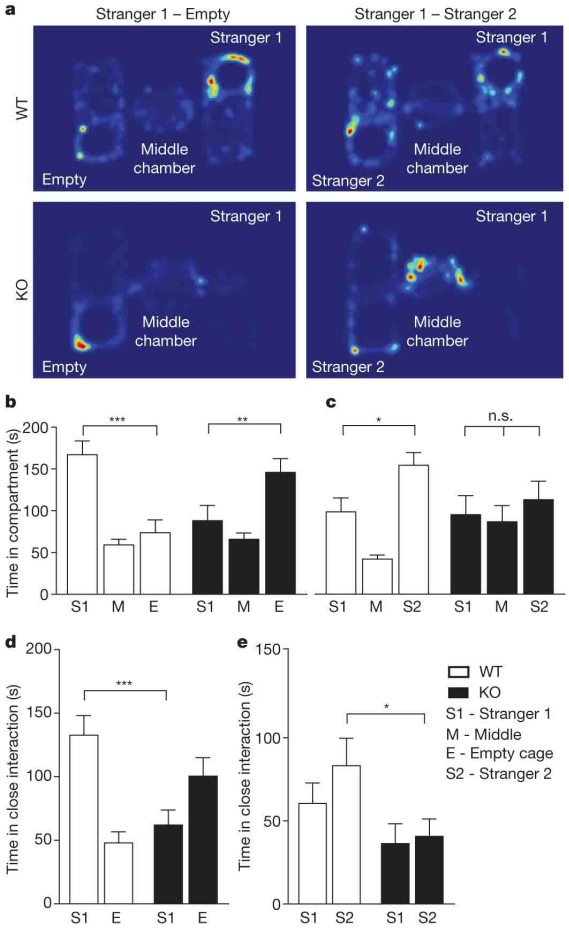

Figure 2 | Reduced social interaction and abnormal social novelty recognition in *Shank3B*$^{-/-}$ mice. **a**, Representative heat map analysis from 'Stranger 1 – Empty' and 'Stranger 1 – Stranger 2' trials from *Shank3B*$^{-/-}$ mice and controls. **b**, In the social interaction test, *Shank3B*$^{-/-}$ mice (closed bars) spent less time in the chamber containing the social partner (Stranger 1) and more time in the chamber containing the empty wire cage when compared to controls (open bars). **c**, In the social novelty test, *Shank3B*$^{-/-}$ mice do not display a preference for the novel social partner (Stranger 2), and spent more time in the middle chamber. **d**, **e**, When analysing social interaction by close proximity (within 5 cm) to either 'Stranger 1', 'Empty Cage' (**d**), or 'Stranger 1', 'Stranger 2' (**e**), *Shank3B*$^{-/-}$ mice displayed a clear reduction in social interaction when compared to controls (**d**); whereas under a social novelty paradigm (**e**), *Shank3B*$^{-/-}$ mice displayed a clear reduction in time spent with 'Stranger 2' *P<0.05, **P<0.01, ***P<0.0001; one-way ANOVA, with Bonferroni post hoc t-test for **b**–**e**; all data presented as means ± s.e.m.; 12–14 mice per group.

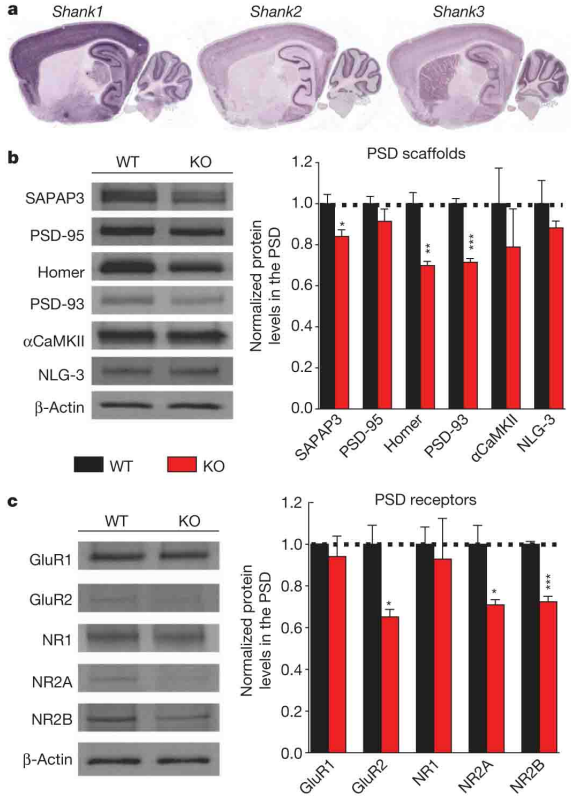

Figure 3 | Biochemical changes in striatal synapses of *Shank3B*$^{-/-}$ mice. **a**, Only *Shank3* mRNA is highly expressed in the striatum. **b**, Protein levels of the scaffolding proteins SAPAP3, Homer and PSD-93 are reduced in striatal PSD fractions from *Shank3B*$^{-/-}$ mice. αCaMKII and NLG-3 are also known as CAMK2A and NLGN3, respectively. **c**, Protein levels of glutamate receptor subunits GluR2, NR2A and NR2B are reduced in striatal PSD fractions from *Shank3B*$^{-/-}$ mice. GluR1 and NR1 are also known as GRIA1 and GRIN1, respectively. Each lane was loaded with 3 μg of protein with β-actin as loading control and normalized to wild-type levels. *P < 0.05, **P < 0.01, ***P < 0.001, two-tailed t-test; all data are presented as means ± s.e.m.; n = 3 samples per group, with each sample being a combined pool of striatal tissue from three animals.

their dendrites to investigate the cellular morphology and complexity of these cells. Sholl analysis revealed neuronal hypertrophy as measured by an increase in complexity of dendritic arborizations (Fig. 4a), total dendritic length (Fig. 4b) and also an increase in surface area (Fig. 4c) in *Shank3B*$^{-/-}$ MSNs.

Next, we performed patch-assisted Lucifer Yellow cell filling of MSNs and measured spine density in control and *Shank3B*$^{-/-}$ mice. *Shank3B*$^{-/-}$ mice displayed a significant reduction in spine density (Fig. 4d, e). We did not observe significant changes in spine length or head diameter; however, the neck width of *Shank3B*$^{-/-}$ MSN spines was slightly larger than that of controls (Supplementary Fig. 8).

Finally we analysed PSD morphology by electron microscopy (Fig. 4f). We found a significant reduction in mean thickness (Fig. 4g) of PSDs from *Shank3B*$^{-/-}$ mice relative to controls. Additionally, PSD length was also significantly reduced in the *Shank3B*$^{-/-}$ mice (Fig. 4h). Taken together, these results highlight a critical *in vivo* role for *Shank3* in the normal development of medium spiny neurons and striatal glutamatergic synapses.

Striatal hypertrophy in *Shank3B*$^{-/-}$ mice

Even though there is no clear correlation between brain size or neuronal hypertrophy specifically for *Shank3* disruptions in humans, a potential link between enlarged brain size, neuronal hypertrophy and autism has been suggested previously[19]. In particular, increased caudate volume in autism patients has been proposed to be linked to repetitive behaviours[20,21]. We measured striatal volume using three-dimensional magnetic resonance imaging in the intact brain of *Shank3B*$^{-/-}$ and control mice. We found that there was no significant difference in overall brain size between the genotypes. However, measurement of caudate volume in the same animals revealed a small but

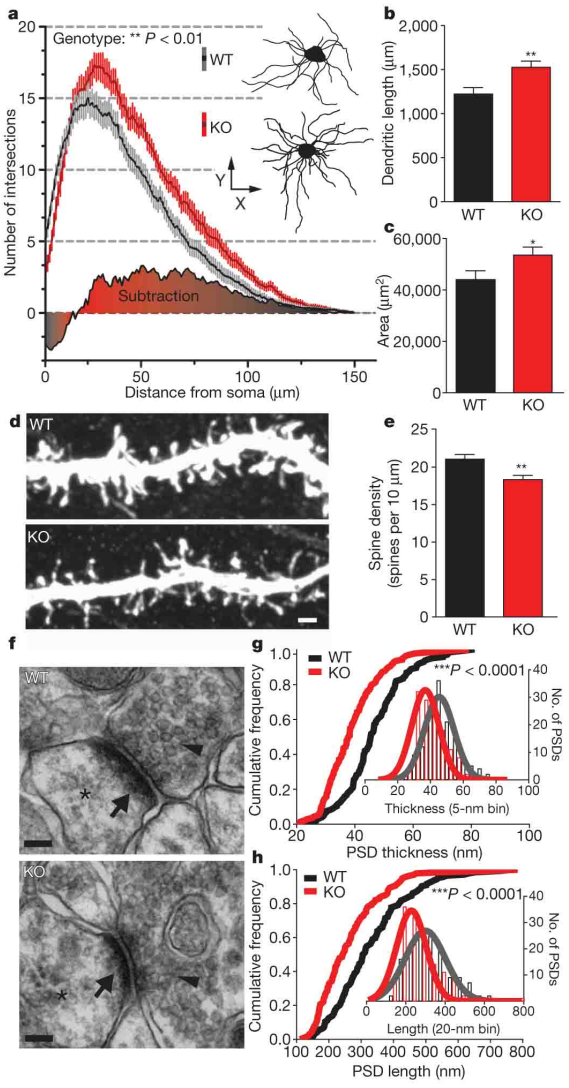

Figure 4 | Morphological and ultrastructural neuronal abnormalities in *Shank3B*$^{-/-}$ mice. **a**, Sholl analysis reveals an increased neuronal complexity of *Shank3B*$^{-/-}$ MSNs (red) when compared to MSNs from wild-type mice (grey); example neurons are shown as insets (top, WT–; bottom, KO–). **b**, **c**, MSNs from *Shank3B*$^{-/-}$ mice show an increase in total dendritic length (**b**) and surface area (**c**) when compared to controls. **d**, Representative confocal stacks of dye-filled MSNs from KO and WT mice; scale bar; 1 μm. **e**, Spine density in MSNs from *Shank3B*$^{-/-}$ mice is lower than that of wild-type MSNs. **f**, Examples of electron micrographs depicting the synaptic contacts with presynaptic vesicles (arrowheads), postsynaptic densities (arrow) and dendritic spine (asterisk); scale bar, 100 nm. **g**, *Shank3B*$^{-/-}$ PSDs are thinner than wild-type PSDs. **h**, *Shank3B*$^{-/-}$ PSDs are shorter than wild-type PSDs. $*P < 0.05$, $**P < 0.01$, $***P < 0.0001$; two-way repeated measures ANOVA for **a**; two-tailed *t*-test for **b**, **c** and **e**; two-sample Kolmogorov–Smirnov test for **g** and **h**. Data in **g** and **h** are presented as cumulative frequency plot with histogram distribution and Gaussian curve fit for the insets. Data from **b**, **c** and **e** are presented as means ± s.e.m.; $n = 36$ from 3 wild-type mice and $n = 36$ from 3 *Shank3B*$^{-/-}$ mice for **a**–**c**; $n = 41$ dendritic segments from 3 wild-type mice and $n = 36$ dendritic segments from 3 *Shank3B*$^{-/-}$ mice for **e**; $n = 144$ PSDs from three wild-type mice and $n = 140$ PSDs from three *Shank3B*$^{-/-}$ mice for **g**, **h**.

significant volumetric enlargement of this structure in *Shank3B*$^{-/-}$ mice (Supplementary Fig. 9). These data suggest a correlation between neuronal hypertrophy and brain volume, consistent with studies from other mouse models of ASD[22,23].

Perturbation of striatal postsynaptic function

To elucidate the functional consequences of a disruption in *Shank3* on synaptic function, we performed recordings of cortico-striatal synaptic circuitry in acute brain slices of 6–7-week-old animals. We found that field population spikes were significantly reduced in *Shank3B*$^{-/-}$ mice when compared with controls (Fig. 5a). Presynaptic function was not altered, as indicated by the relationship of stimulation intensity to the amplitude of the action potential component of the response termed negative peak 1 (NP1) and the paired-pulse ratio (PPR; Supplementary Fig. 10). These results indicate that the reduction in total field responses was most likely due to a postsynaptic impairment in synaptic function and/or a reduction in the number of functional synapses. Consistent with their mild behavioural phenotypes *Shank3A*$^{-/-}$ mice displayed minimal disruption at cortico-striatal synapses (Supplementary Fig. 11).

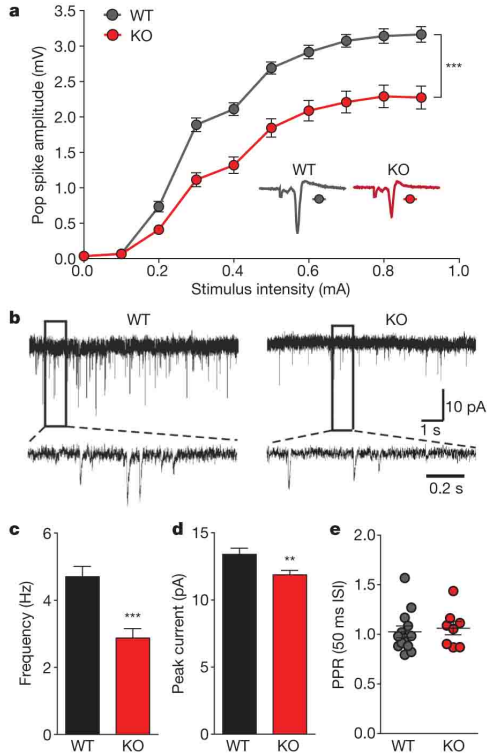

Figure 5 | Reduced cortico-striatal synaptic transmission in *Shank3B*$^{-/-}$ MSNs. **a**, Cortico-striatal pop spike amplitude is decreased in *Shank3B*$^{-/-}$ mice (red trace) as measured by extracellular field recordings. Inset, example traces for *Shank3B*$^{-/-}$ (KO) and wild-type (WT). **b**, mEPSC example traces from wild-type and *Shank3B*$^{-/-}$ MSNs recorded with whole-cell voltage clamp. **c**, **d**, Reduced mEPSC frequency (**c**) and amplitude (**d**) in *Shank3B*$^{-/-}$ MSNs when compared to wild-type. **e**, PPR is unaltered in *Shank3B*$^{-/-}$ MSNs. $**P < 0.01$, $***P < 0.001$; two-way repeated measures ANOVA, with Bonferroni post hoc test for **a**; two-tailed *t*-test for **c**, **d**; all data presented as means ± s.e.m. For field recordings, $n = 13$ slices from four mice per group; for mEPSCs, $n = 29$ MSNs from wild-type mice, $n = 32$ MSNs from Shank3B$^{-/-}$ mice.

We next performed whole-cell voltage clamp recordings of α-amino-3-hydroxy-5-methyl-4-isoxazolepropionic acid receptor-miniature excitatory postsynaptic currents (AMPAR-mEPSCs) in dorsolateral striatal MSNs. We found that the frequency of mEPSCs was significantly reduced in *Shank3B*$^{-/-}$ MSNs (Fig. 5b, c), indicating a reduction in the number of functional synapses in *Shank3B*$^{-/-}$ MSNs because we did not observe defects on presynaptic function by measuring PPR (Fig. 5e). We also found a significant reduction of peak mEPSC amplitude in *Shank3B*$^{-/-}$ MSNs (Fig. 5b, d), indicating a reduction in the postsynaptic response from the available synapses. We did not observe significant differences in *N*-methyl-D-aspartate receptor (NMDA)/AMPA receptor-mediated current ratio in *Shank3B*$^{-/-}$ neurons (Supplementary Fig. 12). Finally, similar defects in mEPSC frequency and amplitude were observed in *Shank3B*$^{-/-}$ and wild-type littermate mice obtained from heterozygous matings (Supplementary Fig. 13). Together, these data demonstrate a critical role for SHANK3 in postsynaptic function in cortico-striatal circuitry.

To assess if the defects arising from *Shank3* dysfunction were specific to striatal circuitry or due to a more broad CNS perturbation, we performed a Morris water maze task for hippocampal-dependent learning and memory. We found that *Shank3B*$^{-/-}$ mice performed at the same levels as controls in both learning and probe trials (Supplementary Fig. 14a–c). Reversal learning and probe trials again demonstrated similar levels of performance between *Shank3B*$^{-/-}$ mice and controls (Supplementary Fig. 14d–f). Concomitantly, we performed electrophysiological recordings from the hippocampal CA1 sub-region and found no obvious difference in field recordings of population spikes or PPR between genotypes (Supplementary Fig. 15a–c). In addition, we found no significant differences in mEPSC frequency or mEPSC amplitude (Supplementary Fig. 15d–f). These data suggest that the observed behavioural and synaptic defects are specific to discrete brain regions and are not part of an overall CNS dysfunction.

Discussion

Despite recent advances in the understanding of autism spectrum disorder genetics, the underlying neurobiological substrates and neural circuits involved in these disorders remain largely unknown. The *Shank3* gene has become the focus of substantial interest, with an increasing body of evidences suggesting *Shank3* as the causative gene of the major neurological symptoms in the 22q13 deletion syndrome[9,11–13,24]. Our present study with *Shank3* mutant mice not only sheds light on a critical *in vivo* role for SHANK3 in striatal glutamatergic synaptic structure and function, but also demonstrates causality between a disruption in this gene and the development of autistic-like behaviours in mice.

In this study, we generated two mutant alleles for the *Shank3* gene. These two lines of mice showed different levels of severity in synaptic defects and phenotypes. In humans, multiple mutations/variants of *Shank3* gene have been identified to coalesce at the ankyrin repeats and downstream of PDZ domain[9,13]. Our data indicate that disruptions of different locations of the *Shank3* gene can lead to varying degrees of functional defects, which may in part contribute to phenotypic heterogeneity in *Shank3*-related ASDs. We should note that, in clinical conditions, the 22q13 deletions and the autism-associated *Shank3* mutations are heterozygous, whereas in our current study, we used homozygous mutant mice to get a clear understanding of the physiological role of the *Shank3* gene and the underlying functional consequences of its disruption. Further studies will be needed to elucidate potential functional deficits resulting from *Shank3* haploinsufficiency in *Shank3B*$^{-/-}$ mice.

PSD-95–SAPAP–SHANK proteins form a key postsynaptic scaffold at glutamatergic synapses which interacts with many synaptic proteins, including the neurexin–neuroligin complex[25]. In addition to *Shank3* (ref. 9), it is worth noting that *Shank2* (refs 6, 8), *SAPAP2* (ref. 6), neurexin-1 (ref. 26) and neuroligin-3 and -4 (ref. 27) have all been implicated in human ASDs. Therefore, the dysfunction of neurexin–neuroligin–PSD-95–SAPAP–SHANK complex could underlie a common synaptic mechanism for a subset of ASDs.

The precise circuitry defects involved in autistic behaviours are poorly understood. Neuroimaging studies provide evidence that caudate and frontal-striatal circuitries are dysfunctional areas in ASD[28–30]. Cortico-striatal circuitry dysfunction has also been strongly implicated in repetitive/compulsive behaviours in obsessive-compulsive disorder (OCD)[31–33]. We previously found that deletion of *SAPAP3*, which directly interacts with SHANK3 and is highly expressed in the striatum, leads to cortico-striatal circuitry dysfunction and OCD-like behaviours including repetitive/compulsive grooming in mice[31]. Repetitive behaviours are also often seen in autistic patients and in some mouse models of ASDs[34–36]. SHANK3 is the most abundant SHANK family member expressed in the striatum and *Shank3B*$^{-/-}$ mice exhibit excessive/repetitive grooming leading to skin lesions. Our data support the hypothesis that repetitive behaviours in OCD and ASD may share a common circuitry mechanism.

The regulation of social behaviours and social interaction is thought to be controlled by several brain regions and circuits[37]. Similarly, genetic makeup is thought to have a key role in the phenotypical manifestation of social behaviours[38]. The robust social interaction deficits in *Shank3B* mutant mice demonstrate a casual role for the disruption of this gene in the genesis of social dysfunction and provide a valuable experimental system for future genetic dissection of the neuronal basis of social behaviour.

METHODS SUMMARY

Behavioural analysis. Young adult mice 5–6-weeks old were used for all behavioural analyses except lesion scores which were performed in 4–5-month-old mice. All experiments were done blind to genotypes. All experimental procedures were reviewed and approved by the Duke University Institutional Animal Care and Use Committee and the MIT Committee on Animal Cares.

Statistical analysis. Analyses were performed using Prism (GraphPad Software) and MATLAB (MathWorks). Details on particular tests used are described in the main text and in the methods section; a summary of statistical analysis for the behavioural data are presented in Supplementary Table 2.

Full Methods and any associated references are available in the online version of the paper at www.nature.com/nature.

Received 7 September 2010; accepted 22 February 2011.
Published online 20 March 2011.

1. American Psychiatric Association Task Force on DSM-IV. *Diagnostic and statistical manual of mental disorders: DSM-IV-TR* (American Psychiatric Association, 2000).
2. Rosenberg, R. E. *et al.* Characteristics and concordance of autism spectrum disorders among 277 twin pairs. *Arch. Pediatr. Adolesc. Med.* **163,** 907–914 (2009).
3. Abrahams, B. S. & Geschwind, D. H. Advances in autism genetics: on the threshold of a new neurobiology. *Nature Rev. Genet.* **9,** 341–355 (2008).
4. Bourgeron, T. A synaptic trek to autism. *Curr. Opin. Neurobiol.* **19,** 231–234 (2009).
5. Zoghbi, H. Y. Postnatal neurodevelopmental disorders: meeting at the synapse? *Science* **302,** 826–830 (2003).
6. Pinto, D. *et al.* Functional impact of global rare copy number variation in autism spectrum disorders. *Nature* **466,** 368–372 (2010).
7. Tabuchi, K. *et al.* A neuroligin-3 mutation implicated in autism increases inhibitory synaptic transmission in mice. *Science* **318,** 71–76 (2007).
8. Berkel, S. *et al.* Mutations in the *SHANK2* synaptic scaffolding gene in autism spectrum disorder and mental retardation. *Nature Genet.* **42,** 489–491 (2010).
9. Durand, C. M. *et al.* Mutations in the gene encoding the synaptic scaffolding protein SHANK3 are associated with autism spectrum disorders. *Nature Genet.* **39,** 25–27 (2006).
10. Prasad, C. *et al.* Genetic evaluation of pervasive developmental disorders: the terminal 22q13 deletion syndrome may represent a recognizable phenotype. *Clin. Genet.* **57,** 103–109 (2000).
11. Wilson, H. L. *et al.* Molecular characterisation of the 22q13 deletion syndrome supports the role of haploinsufficiency of *SHANK3/PROSAP2* in the major neurological symptoms. *J. Med. Genet.* **40,** 575–584 (2003).
12. Moessner, R. *et al.* Contribution of *SHANK3* mutations to autism spectrum disorder. *Am. J. Hum. Genet.* **81,** 1289–1297 (2007).
13. Gauthier, J. *et al.* Novel de novo SHANK3 mutation in autistic patients. *Am. J. Med. Genet. B. Neuropsychiatr. Genet.* **150B,** 421–424 (2009).
14. Kim, E. *et al.* GKAP, a novel synaptic protein that interacts with the guanylate kinase-like domain of the PSD-95/SAP90 family of channel clustering molecules. *J. Cell Biol.* **136,** 669–678 (1997).

15. Takeuchi, M. *et al.* SAPAPs. A family of PSD-95/SAP90-associated proteins localized at postsynaptic density. *J. Biol. Chem.* **272,** 11943–11951 (1997).
16. Zoghbi, H. Y. & Warren, S. T. Neurogenetics: advancing the "next-generation" of brain research. *Neuron* **68,** 165–173 (2010).
17. Moy, S. S. *et al.* Sociability and preference for social novelty in five inbred strains: an approach to assess autistic-like behavior in mice. *Genes Brain Behav.* **3,** 287–302 (2004).
18. Hung, A. Y. *et al.* Smaller dendritic spines, weaker synaptic transmission, but enhanced spatial learning in mice lacking Shank1. *J. Neurosci.* **28,** 1697–1708 (2008).
19. Redcay, E. & Courchesne, E. When is the brain enlarged in autism? A meta-analysis of all brain size reports. *Biol. Psychiatry* **58,** 1–9 (2005).
20. Langen, M. *et al.* Changes in the developmental trajectories of striatum in autism. *Biol. Psychiatry* **66,** 327–333 (2009).
21. Hollander, E. *et al.* Striatal volume on magnetic resonance imaging and repetitive behaviors in autism. *Biol. Psychiatry* **58,** 226–232 (2005).
22. Bourgeron, T. A synaptic trek to autism. *Curr. Opin. Neurobiol.* **19,** 231–234 (2009).
23. Kwon, C. H. *et al.* Pten regulates neuronal arborization and social interaction in mice. *Neuron* **50,** 377–388 (2006).
24. Bonaglia, M. C. *et al.* Identification of a recurrent breakpoint within the *SHANK3* gene in the 22q13.3 deletion syndrome. *J. Med. Genet.* **43,** 822–828 (2006).
25. Irie, M. *et al.* Binding of neuroligins to PSD-95. *Science* **277,** 1511–1515 (1997).
26. Kim, H. G. *et al.* Disruption of neurexin 1 associated with autism spectrum disorder. *Am. J. Hum. Genet.* **82,** 199–207 (2008).
27. Jamain, S. *et al.* Mutations of the X-linked genes encoding neuroligins NLGN3 and NLGN4 are associated with autism. *Nature Genet.* **34,** 27–29 (2003).
28. Silk, T. J. *et al.* Visuospatial processing and the function of prefrontal-parietal networks in autism spectrum disorders: a functional MRI study. *Am. J. Psychiatry* **163,** 1440–1443 (2006).
29. Horwitz, B., Rumsey, J. M., Grady, C. L. & Rapoport, S. I. The cerebral metabolic landscape in autism. Intercorrelations of regional glucose utilization. *Arch. Neurol.* **45,** 749–755 (1988).
30. Sears, L. L. *et al.* An MRI study of the basal ganglia in autism. *Prog. Neuropsychopharmacol. Biol. Psychiatry* **23,** 613–624 (1999).
31. Welch, J. M. *et al.* Cortico-striatal synaptic defects and OCD-like behaviours in *Sapap3*-mutant mice. *Nature* **448,** 894–900 (2007).
32. Shmelkov, S. V. *et al.* Slitrk5 deficiency impairs corticostriatal circuitry and leads to obsessive-compulsive-like behaviors in mice. *Nature Med.* **16,** 598–602 (2010).
33. Graybiel, A. M. Habits, rituals, and the evaluative brain. *Annu. Rev. Neurosci.* **31,** 359–387 (2008).
34. McFarlane, H. G. *et al.* Autism-like behavioral phenotypes in BTBR T+tf/J mice. *Genes Brain Behav.* **7,** 152–163 (2008).
35. Blundell, J. *et al.* Neuroligin-1 deletion results in impaired spatial memory and increased repetitive behavior. *J. Neurosci.* **30,** 2115–2129 (2010).
36. Etherton, M. R., Blaiss, C. A., Powell, C. M. & Sudhof, T. C. Mouse neurexin-1α deletion causes correlated electrophysiological and behavioral changes consistent with cognitive impairments. *Proc. Natl Acad. Sci. USA* **106,** 17998–18003 (2009).
37. Insel, T. R. & Fernald, R. D. How the brain processes social information: searching for the social brain. *Annu. Rev. Neurosci.* **27,** 697–722 (2004).
38. Ebstein, R. P., Israel, S., Chew, S. H., Zhong, S. & Knafo, A. Genetics of human social behavior. *Neuron* **65,** 831–844 (2010).

Supplementary Information is linked to the online version of the paper at www.nature.com/nature.

Acknowledgements We thank C. Duarte, S. Chaterjee and A. Oliveira-Maia for discussions; L. Kruger and Q. Liu for technical assistance; A. Hadiono for assistance in behavioural annotation; D. Bredt for the PSD-93 antibody; T. Boeckers for the anti-SHANK3 antibody; S. Miller and P. Christopher for advice and assistance with electron microscopy techniques; J. Crawley for the demonstration of social behaviour tests; N. Calakos and Y. Wan for advice on electrophysiology studies; A. Graybiel for critical comments of the manuscript; D. Wang and the other members of the G.F. laboratory for their support. We thank The Poitras Center for Affective Disorders Research. This work was funded by a grant from NIMH/NIH (R01MH081201), a Hartwell Individual Biomedical Research Award from The Hartwell Foundation, and a Simons Foundation Autism Research Initiative (SFARI) grant Award to G.F.; a NARSAD Young Investigator Award and NIH Ruth L. Kirschstein National Research Service Award (F32MH084460) to J.T.T.; a NIH (R03MH085224) grant to Z.F.; and doctoral fellowships from the Portuguese Foundation for Science and Technology to J.P. (SFRH/BD/15231/2004) and C.F. (SFRH/BD/15855/2005). C.F. would like to acknowledge the support from the "Programa Gulbenkian de Doutoramento em Biomedicina" (PGDB, Oeiras, Portugal) and J.P. the "Programa Doutoral em Biologia Experimental e Biomedicina" (CNC, Coimbra, Portugal).

Author Contributions J.P., C.F., J.T.T., W.W., M.F.W., T.N.V., C.D.L. and Z.F. participated in the execution and analysis of experiments. J.P., C.F., J.T.T., C.D.L, Z.F. and G.F participated in the interpretation of the results. J.P., C.F. and G.F. designed the experiments and wrote the paper.

Author Information Reprints and permissions information is available at www.nature.com/reprints. The authors declare no competing financial interests. Readers are welcome to comment on the online version of this article at www.nature.com/nature. Correspondence and requests for materials should be addressed to G.F. (fengg@mit.edu).

METHODS

Mice. *Shank3* mutant mice were generated by homologous recombination in R1 embryonic stem cells and implanted in C57 blastocysts using standard procedures. One targeting vector (Shank3A) was designed to replace exon 4–7 (containing the ankyrin repeat domains) and another vector (Shank3B) was designed to replace exon 13–16 (containing the PDZ domain) of the *Shank3* gene with a NEO cassette. Genotypes were determined by PCR of mouse tail DNA, using: for Shank3A, primer F1a (GGTTGAGGATGAGCAAGCTAG) and R1a (GGGAC ATAAGTGAAGGTTAGG) for the wild-type allele (318 base pairs), and F1a and R2 (TCAGGGTTATTGTCTCATGAGC; in the neo cassette) for the mutant allele (361 base pairs); for Shank3B, primer F1b (GAGCTCTACTCCCTT AGGACTT) and R1b (TCCCCCTTTCACTGGACACCC) for the wild-type allele (316 base pairs), and F1b and R2 (TCAGGGTTATTGTCTCATGAGC; in the neo cassette) for the mutant allele (360 base pairs). The NEO cassette was not removed.

Chimaeric mice were crossed to C57 females (Jackson Labs). Initially, F1 hybrids from heterozygous × heterozygous matings were generated. However, homozygous knockouts mice from this type of mating are smaller than their wild-type littermates, presumably due to an inadequate competition for resources during early postnatal days leading to different developmental trajectories. We postulated that this size difference would influence our behavioural tests. To alleviate this confound, heterozygous animals were crossed in direct brother-sister matings for five generations from which we derived F5 isogenic hybrids in a mixed background. These isogenic animals were then used to generate time-mated homozygous × homozygous breeding pairs to obtain wild-type and mutant animals used in the experiments. F5 *Shank3A* and F5 *Shank3B* knockouts from these matings are reared to weaning age with weights similar to those from F5 control animals.

Animals were housed at a constant 23 °C in a 12 h light/dark cycle (lights off at 19:00), with food and water available *ad libitum*. Mice were housed 3–5 by genotype per cage with the exception of the animals individually housed for grooming measurements. Only aged-matched male mice were used for behavioural experiments, all other tests included age-matched males and females in proportional contribution across groups. Unless otherwise noted, all tests were conducted with naive cohorts of mice. All experimental procedures were reviewed and approved by the Duke University Institutional Animal Care and Use Committee and the MIT Committee on Animal Cares..

Grooming behaviour[31]. Young adult male mice 5–6-week-old were used for analysis of grooming behaviour. Habituated, individually housed animals were video-taped for 24 h under 700 lx (day, 12 h) and ~2 lx (red light at night, 12 h) illumination. Grooming behaviours were coded from 19:00–21:00 h (that is, 2 h beginning at the initiation of the dark cycle); this segment was analysed using Noldus Observer software and the total amount of time in the 2-h segment spent grooming was determined. Grooming included all sequences of face-wiping, scratching/rubbing of head and ears, and full-body grooming. The observer was blinded to genotype during the scoring of the videotapes.

PSD preparation and western blot. PSD fractions of the striatum were prepared as previously described[31], separated on SDS–PAGE and probed with specific antibodies. The relative amount of β-actin was used as loading control. Antibodies used in these experiments include rabbit antibodies against PSD-93 (gift from D. Bredt) and Shank3 (gift from T. Boeckers). The antibody for SAPAP3 has been previously described[39]. Commercial antibodies used include monoclonal antibodies against NR1 (Transduction Laboratories), NR2B (Millipore), CaMKII (Transduction Laboratories), NR2A (Millipore), and β-actin (Sigma), as well as polyclonal antibodies against GluR1 (Abcam), Homer (Chemicon), GluR2 (Abcam), neuroligin-3 (Synaptic Systems) and PSD-95 (Abcam).

***In situ* hybridization.** mRNA *in situ* hybridization was performed as described elsewhere[39]. Briefly, reactions were performed with 20 μm cryosections from freshly frozen 5-week-old brain mouse tissue using digoxigenin (DIG)-labelled riboprobes against mouse *Shank1* cDNA (NM_001034115; base pairs 4107–4924), *Shank2* cDNA (NM_001081370; base pairs 2063–2876) and *Shank3* (NM_021423; base pairs 3159–3959). The complementary DNAs used were all verified by sequencing compared to the following sequences GenBank accession numbers: (*Shank1*: NM_001034115), (*Shank2*: NM_001081370) and (*Shank3*: NM_021423). The hybridization signal was detected using an alkaline phosphatase (AP)-conjugated anti-DIG antibody (Roche) and developed using 5-bromo-4-cloro-indolylphosphate/nitroblue tetrazolium (BCIP/NBT; Roche).

Motor and anxiety-like behaviours[31]. Zero maze: an elevated zero maze was indirectly illuminated at 100 lx. Testing commenced with an animal being introduced into a closed area of the maze. Behaviour was video-taped for 5 min and subsequently scored by a trained observer using Noldus Observer software. Anxiety-like behaviour was deduced based upon the percent time spent in the open areas. The observer was blinded to genotype. The animals used in the zero maze test, both $Shank3A^{-/-}$, $Shank3B^{-/-}$ and respective controls were previously tested in the open field test with a 2-day period in between tasks.

Open field: spontaneous locomotor activity was evaluated over 30 min in an automated Omnitech Digiscan apparatus (AccuScan Instruments) as described[31]. Locomotor activity was assessed as total distance travelled (m). Anxiety-like behaviour was defined by number of rearings and time spent in the centre as compared to time spent in the perimeter (thigmotaxis) of the open field.

Dark-light emergence test: mice were habituated in an adjacent room to low light conditions (~40 lx) and the test room was initially under similar illumination. Testing was conducted in a two-chambered test apparatus (Med Associates), with one side draped in black cloth (that is, dark-chamber) and the other illuminated at ~1,000 lx (that is, light-chamber) with a high intensity house light and overhead fluorescent lamps. Upon placing the mice into the dark chamber, the light chamber was illuminated and the door between the two chambers was opened. The mice were allowed to freely explore the apparatus for 5 min. The latency to emerge from the darkened into the lighted chamber and the percentage of time spent in the illuminated chamber were used as indices of anxiety-like behaviours.

Social interaction paradigm. Three-chamber social test: sociability and response to social novelty test was performed as previously described[17] with minor modifications. Briefly, 5–6-week-old male animals were used across all tests. Target subjects (Stranger 1 and Stranger 2) were 5–6-week-old males habituated to being placed inside wire cages for 5 days before beginning of testing. Test mice were habituated to the testing room for at least 45 min before the start of behavioural tasks. The social test apparatus consisted of a transparent acrylic box with removable floor and partitions dividing the box into three chambers. Here, the middle chamber (20 cm × 17.5 cm) is half the width of Chamber 1 (20 cm × 35 cm) and Chamber 2 (20 cm × 35 cm) with the overall dimensions of the box being 60 cm (length) × 35 cm (width) with 5 cm openings between each chamber which can be closed or open with a lever operated door. The wire cages used to contain the stranger mice were cylindrical, 11 cm in height, a bottom diameter of 10.5 cm with the bars spaced 1 cm apart (Galaxy Cup, Spectrum Diversified Designs). An inverted transparent cup was placed on the top of the cage to prevent the test mice from climbing on the top of the wire cage.

For the sociability test, the test animal was introduced to the middle chamber and left to habituate for 5 min, after which an unfamiliar mouse (Stranger 1) is introduced into a wire cage in one of the side-chambers and an empty wire cage on the other side-chamber. The dividers are then raised and the test animal is allowed to freely explore all three chambers over a 5 min session. Following the 5 min session, the animal remains in the chamber for an extra 5 min (post-test) to better acquire the identification cues from Stranger 1 animal. Following this, a novel stranger mouse (Stranger 2) is inserted in the wire cage previously empty and again the test animal is left to explore for a 5 min session. Time spent in each chamber, time spent in close proximity and heat maps were calculated using the automated software Noldus Ethovison. The release of the animals and relative position of social and inanimate targets was counterbalanced. However, for each individual test animal the location of Stranger 1 was maintained during Stranger 1 – E and Stranger 1 – Stranger 2 testing of the social behaviour.

Dyadic social interaction: animals were acclimatized to the test room for at least 1 h before the experiment. Target mice were wild-type and $Shank3B^{-/-}$ of 6 weeks of age. Stimulus mice were conspecific age-matched wild-type mice socially naive to the target mice. At least 3 h before the beginning of the test, stimulus mice were given identifiable markings on the tails using a black marker pen. A pair of target and stimulus mice were introduced in a transparent Plexiglas arena (40cm × 40cm × 30cm) covered with fresh bedding and the session recorded for 10 min. Quantification of social behaviours was performed using Noldus Observer software by a researcher blinded to the genotype of the target animals. Quantifications included: reciprocal social interaction, as determined by any sequence or combination of sequences involving close huddling, sniffing (for example, nose-to-nose, anogenital sniffing) or allogrooming by the target and stimulus mouse; the frequency of nose-to-nose sniffing; and the frequency of anogenital sniffing initiated by the target animal towards the stimulus mouse. Statistical tests were performed using unpaired two-tailed *t*-test.

Rotarod. Motor coordination was assessed in an accelerating rotarod test (4–40 r.p.m.). Briefly, animals were introduced in the apparatus (Med Associates) and the latency to fall was determined. Animals were tested for three trials in a single day with an inter-trial interval of 10 min.

Morris water maze. Morris water maze testing was conducted as describe elsewhere[40] with minor modifications. Male mice (4–5-weeks old) selected for the test were individually handled daily for 5 days before beginning the experiment. Testing pool was 120 cm in diameter and the platform 8 cm in diameter. The platform was submerged 1 cm below the water surface. Pool water was maintained at 23.0 ± 0.5 °C and made opaque by mixing-in white non-toxic tempera paint. During training, 90 s duration trials were used, if the animals did not find

the platform within 90 s the experimenter guided the animal to the platform. After reaching the platform the animals were left for 15 s on top of the platform before being removed. Trials were administered for 5 days with four trials per animal per day with the platform located in the south-west quadrant. On the sixth day a 60 s probe trial was performed. On the seventh day, the reversal training commenced with the platform in the north-east quadrant, and proceeded as described above. The experimenter followed the animals' progress using tracking software outside of the testing room. Tracking and analysis were performed using the Noldus Ethovison software.

Golgi staining and Sholl analysis. All brains and collected sections were coded in order to blind the experimenter of the genotype until after all data was collected and analysed. Brains from 5-week-old, gender-matched *Shank3B*$^{-/-}$ and control mice were prepared using standard Golgi–Cox impregnation technique using the FD Rapid GolgiStain Kit (NeuroTechnologies). Serial coronal sections of 100 μm were collected from controls and *Shank3B* mutant animals. A total of 12 cells per animal were traced across the dorsal striatum as to sample representatively from this structure for a final number of 36 cells per genotype. For each animal, sections were selected to be between rostral-caudal bregma 1.18 mm and 0.86 mm. Criteria to identify medium spiny neurons were, (1) presence within the caudate putamen; (2) full impregnation of the neuron along the entire length of the dendritic arborization; (3) relative non-overlap with surrounding neurons and isolation from astrocytes and blood vessels and (4) morphologically, by the presence of high number of spines and relatively short neuronal arborizations as characteristics of MSNs. For each selected neuron the entire neuronal arbor was reconstructed under a ×100 oil lens in a motorized microscope with a digital CCD camera connected to a computer running Neurolucida Software (MBF Bioscience). The three-dimensional analysis of the reconstructed neurons was performed using NeuroExplorer software (MBF Bioscience) and data from branch length, number of branches and neuronal complexity was measured and analysed in Prism (Graph Pad). Two-way repeated measures ANOVA was used for Sholl analysis. Statistical significance was accepted when $^{*}P < 0.05$, $^{**}P < 0.01$ and $^{***}P < 0.0001$.

Cortico-striatal electrophysiology. Brain slice preparation for extracellular field recording: acute brain slices were prepared from 6–7-week-old mice. Slices were prepared from one WT and one KO pair each day and the experimenter was blinded to the genotype. The mice were deeply anesthetized by intra-peritoneal injection of avertin and then transcardially perfused with carbogenated (95% O_2, 5% CO_2) ice-cold protective cutting artificial cerebrospinal fluid (aCSF) with the composition (in mM): 119 glycerol, 2.5 KCl, 1.25 NaH_2PO_4, 26 $NaHCO_3$, 25 glucose, 2 thiourea, 5 L-ascorbic acid, 3 Na-pyruvate, 0.5 $CaCl_2.4H_2O$, 10 $MgSO_4.7H_2O$. Mice were then decapitated and the brains were removed into ice-cold cutting solution for an additional 1 min. The brains were then rapidly blocked for coronal sectioning at 300-μm thickness on a VF200 model compresstome (Precisionary Instruments) using either a sapphire or zirconium ceramic injector style blade. Slices containing the dorsal striatum were initially recovered for 30 min at room temperature (23–25 °C) in a carbogenated protective recovery aCSF (same composition as the cutting aCSF except that glycerol was replaced with *N*-methyl-D-glucamine (NMDG)-Cl as a substitute for NaCl to prevent initial excitotoxic swelling during re-warming). After this initial 30 min period the slices were transferred into a holding chamber containing carbogenated normal aCSF of the composition (in mM): 119 NaCl, 2.5 KCl, 1.25 NaH_2PO_4, 26 $NaHCO_3$, 12.5 glucose, 2 $CaCl_2.4H_2O$, 1 $MgSO_4.7H_2O$. The holding aCSF was supplemented with (in mM): 2 thiourea, 1 L-ascorbic acid, 3 Na-pyruvate to improve slice health and longevity, and slices were stored for 1–6 h before transfer to the recording chamber for use. The osmolarity of all solutions was measured at 300–310 mOsm and the pH was maintained at ~7.3 after equilibration under constant carbogenation.

Supplementary Fig. 11 shows summary data for corticostriatal field recordings from acute coronal brain slices of Shank3A mutant versus WT mice. The method of slice preparation differed significantly in these earlier experiments. Mice were transcardially perfused with carbogenated ice-cold protective sucrose aCSF with the composition (in mM): 185 sucrose, 2.5 KCl, 1.25 NaH_2PO_4, 26 $NaHCO_3$, 25 glucose, 0.5 $CaCl_2.4H_2O$, 4 $MgSO_4.7H_2O$ (pH 7.3, 300–310 mOsm) without supplementation of antioxidants. Slices were immediately transferred into a holding chamber containing carbogenated normal aCSF of the composition (in mM): 119 NaCl, 2.5 KCl, 1.25 NaH_2PO_4, 26 $NaHCO_3$, 12.5 glucose, 2 $CaCl_2.4H_2O$, 1 $MgSO_4.7H_2O$ (pH 7.3, 300–310 mOsm) without supplementation of antioxidants, and slices were stored for 1–4 h before transfer to the recording chamber. The absence of the initial 30 min recovery period in 'protective' aCSF in addition to the absence of antioxidant supplementation in the cutting aCSF and in the aCSF in the holding chamber results in more rapid deterioration of slice health and smaller evoked population spike amplitudes on average, indicating reduced overall slice viability compared to slices prepared with a 30 min NMDG aCSF recovery protocol described above. However, WT and KO brain slices were always subjected to identical procedures on any given day of recording and the procedures were always standardized for each discrete experimental data set so that these factors would not introduce any potential confounds.

Extracellular field recording. A platinum iridium concentric bipolar stimulating electrode (CBAPC75, 25 μm inner pole diameter; FHC) was placed on the inner border of the corpus callosum between the cortex and dorsolateral striatum. This electrode position was chosen to predominantly activate cortical axons within the corpus callosum which heavily converge upon striatal MSNs to form excitatory corticostriatal synaptic connections. Although there is ample evidence on which to base our assertion that stimulation of the corpus callosum predominantly results in activation of cortical axons[41,42], we are unable to exclude the possibility of a relatively smaller contribution arising from activation of thalamostriatal axons that have distal terminals in dorsolateral striatum nearby to the stimulated region. Thus, although we refer to our measurements as primarily reflecting corticostriatal transmission, our measurements are not 'pure' corticostriatal responses. Borosilicate glass recording electrodes filled with 2 M NaCl were placed in the dorsolateral striatum approximately 400–450 μm away from the stimulating electrode. Corticostriatal field population spikes were evoked with 0.15 ms step depolarizations at 0.5 mA intensity at a frequency of 0.05–0.1 Hz. Paired pulses were evoked with a 100 ms inter-stimulus interval. Baseline responses were monitored to ensure stable population spike amplitude for a minimum of 5 min. Input-output functions were then determined for the negative peak 1 (NP1; presynaptic fibre volley) and population spike amplitude by three consecutive rounds of stimulation from 0–1.0 mA in 0.1 mA increments. All recordings were performed at room temperature and acquired using pCLAMP 10 software (Axon Instruments/Molecular Devices). Data analysis was performed blind to genotype in Clamp fit (Axon Instruments/Molecular Devices). Population spike amplitude was measured as the average of the early peak positivity to the peak negativity and from the peak negativity to the late peak positivity. This standard method takes into account the fact that the downward population spike is superimposed on an upward field excitatory postsynaptic potential (fEPSP). Paired pulse ratio (PPR) was calculated as the ratio of the 2nd population spike amplitude to the 1st population spike amplitude for responses to paired pulse stimulation at 0.5 mA fixed intensity with a 100 ms inter-stimulus interval for the pair.

Extracellular field recordings and whole-cell mEPSC recordings in the hippocampal CA1 region were conducted in 300 μm thick acute brain slices from 6–9-week-old WT and Shank3B mutant mice. For measurement of hippocampal CA1 population spikes, a concentric bipolar stimulating electrode was placed in the stratum radiatum to stimulate the Schaffer collateral pathway, and a borosilicate glass recording electrode (~2–3 MΩ) filled with recording aCSF was placed in the CA1 pyramidal cell layer approximately 400 μm from the stimulation site. The recording electrode was placed at the depth in the slice that gave the largest population spike amplitude, and a stable baseline was established for <10 min. Input-output recordings were conducted by increasing the stimulation intensity from 0 to 160 μA in 20 μA increments. Three successive rounds were collected and values at each intensity represent the average of the three measurements. CA1 population spike amplitude was quantified exactly as described previously for cortico-striatal population spikes. For CA1 pyramidal neuron whole-cell recordings, pyramidal neurons in CA1 were identified under infrared-differential interference contrast (IR-DIC) visualization. Cells were patched with a Caesium-gluconate-based internal solution containing (in mM): 110 Caesium-gluconate, 15 KCl, 4 NaCl, 5 TEA-Cl, 20 HEPES, 0.2 EGTA, 5 lidocaine *N*-ethyl chloride, 4 ATP magnesium salt, and 0.3 GTP sodium salt. The pH was adjusted to 7.25 with D-gluconic acid and osmolarity was adjusted to 290–300 mOsm with sucrose as necessary. The recording aCSF contained 1 μM TTX, 100 μM picrotoxin, 5 μM CGP55845, and 50 μM D-APV to isolate pure AMPAR-mediated mEPSCs. CA1 neurons were voltage-clamped at −80 mV to amplify the smallest spontaneous miniature synaptic events that might otherwise escape detection. Criteria for acceptance were uncompensated stable $R_a < 25$ MΩ and holding current < -300 pA. mEPSCs were detected using MiniAnalysis software (Synaptosoft) as described for striatal MSNs. All recordings were carried out at room temperature (23–25 °C). Slices were prepared in a 20–30 degree off-horizontal cutting angle (optimal for CA1 region) from one WT and one KO pair each day and the experimenter was blind to the genotypes of the animals.

Striatal slice preparation for whole-cell recording. Mice 5–6-week-old were used for all whole-cell electrophysiology procedures by an experimentalist blinded to genotype. Acute coronal striatal slices were prepared as follows. Briefly, mice were anesthetized with Avertin solution (20 mg/ml, 0.5 mg/g body weight) and perfused through the heart with a small volume (about 20 ml) of ice-cold and oxygenated (95% O_2, 5% CO_2) cutting solution containing (mM): 105 NMDG, 105 HCl, 2.5 KCl, 1.2 NaH_2PO_4, 26 $NaHCO_3$, 25 Glucose, 10 $MgSO_4$, 0.5 $CaCl_2$, 5 L-Ascorbic Acid, 3 Sodium Pyruvate, 2 Thiourea (pH 7.4, with osmolarity of 295–305 mOsm). The brains were rapidly removed and placed in ice-cold and oxygenated cutting solution. The coronal slices (300 μm) were prepared

using a slicer (Vibratome 1000 Plus, Leica Microsystems, USA) and then transferred to an incubation chamber (BSK4, Scientific System Design Inc., USA) at 32 °C with carbogenated cutting solution, which was gradually replaced with aCSF in 30 min through a peristaltic pump (Rainin, RP-1) allowing a precise regulation of flowing rates. The slices were then kept in the aCSF that contained (mM): 119 NaCl, 2.3 KCl, 1.0 NaH_2PO_4, 26 $NaHCO_3$, 11Glucose, 1.3 $MgSO_4$, 2.5 $CaCl_2$ (pH was adjusted to 7.4 with HCl, with osmolarity of 295–305 mOsm) at room temperature for at least 30 min.

Whole-cell patch-clamp. The slice was placed in a recording chamber (RC-27L, Warner Instruments) and constantly perfused with oxygenated aCSF at 24 °C (TC-324B, Warner Instruments) at a rate of 1.5–2.0 ml min^{-1}. The striatum and individual MSNs were visualized and identified with a microscope equipped with IR-DIC optics (BX-51WI, Olympus) by location, shape and size (ovoid cell body with major axis of 10 to 14 μm). Two additional measures were used to distinguish them from similar sized GABAergic interneurons. First, GABAergic interneurons show smaller membrane capacitance (C_m) and membrane time constant (τ_m) (at least two times less) when compared to that of MSNs. In the case of recordings done with Cs^+ internal, these membrane properties were measured immediately after membrane rupture when the Cs^+ internal has not been dialysed and taken effect yet. Second, AMPA receptor–mediated mEPSCs showed much faster kinetics (including both rise time and decay time constant, τ decay) in GABAergic interneurons. Whole-cell patch-clamp recordings were obtained from MSNs using recording pipettes (King Precision Glass, glass type 8250) pulled in a horizontal pipette puller (P-87, Sutter Instruments) to a resistance of 3–4 MΩ, when filled with the internal solution containing (in mM): 107 $CsMeSO_3$, 10 CsCl, 3.7 NaCl, 5 TEA-Cl, 20 HEPES, 0.2 EGTA, 5 lidocaine *N*-ethyl chloride, 4 ATP magnesium salt, and 0.3 GTP sodium salt. pH was adjusted to 7.3 with KOH and osmolarity was adjusted to 298–300 mOsm with 15 mM K_2SO4.

To record AMPA receptor-miniature excitatory postsynaptic currents (mEPSCs), the cells were held in voltage clamp at −70 mV in the presence of 50 μM APV (DL-2-amino-5-phosphono-valeric acid), 25 μM BMR (1(*S*),9(*R*)-(−)-bicuculline methbromide), 10 μM D-serine and 1 μM TTX (all from Tocris). The miniature events were not recorded until 5 min after entering whole cell patch clamp recording mode to allow the dialysis of Cs^+ internal solution for a relatively complete block of the potassium channels in the MSNs. The mEPSCs were detected and analysed with MiniAnalysis (Synaptosoft).

For paired-pulse stimulation experiments, AMPAR mediated excitatory postsynaptic currents (EPSCs) were evoked by a local concentric bipolar stimulating electrode (CBARC75, FHC) that was placed in the inner edge of corpus callosum within the dorso-lateral region of the striatum. Recordings were made in the presence of picrotoxin (100 μM) and APV (50 μM) to block activation of $GABA_A$ receptors and NMDA receptors. Stimulation was current-controlled (ISO-Flex, A.M.P.I.). The stimulus intensity was set at a level that could evoke 300–400 pA AMPAR-mediated response for all the cells measured and delivered with an inter-stimulus interval of 50 ms. The paired-pulse measurements were obtained for 15–20 consecutive traces and only those traces with stable evoked first current response were used for data analysis. The PPR was calculated with the peak current response to the second pulse divided by that of the first response.

NMDAR- and AMPAR- mediated synaptic current ratio (NMDA/AMPA ratio) was recorded in the presence of picrotoxin at holding potentials of +40 mV and −70 mV, respectively. The NMDA/AMPA ratios were measured according to previously described methods[43]. Briefly, the stimulus intensity was set at a level that could evoke 300–400 pA AMPAR-mediated response with a holding potential at −70 mV. Each evoked response was repeated for 15–20 times with an inter-stimulus interval of 20 s for all the cells measured. The time point of the peak current at –70 mV, considered to be fully mediated by AMPARs, was used to establish the time window for measuring the AMPA peak at +40 mV. The decay to baseline of the AMPA current at –70 mV was used to select a time window for measurement of the NMDA current; a 10-ms measurement window beginning 40 ms after the stimulus artefact was used. This current amplitude at this point was designated as the NMDAR mediated synaptic current response. (I_{NMDA} at +40 mV/I_{AMPA} at –70 mV) was taken as the NMDA/AMPA ratio.

Data acquisition and analysis. A Multiclamp 700B amplifier (Molecular Devices Corporation) and digidata 1440A were used to acquire whole cell signals. The signals were acquired at 20 kHz and filtered at 2 kHz. The series-resistance was <20 MΩ. Values are expressed as means ± s.e.m. Data were tested for significance using either an unpaired *t*-test or a two-way repeated measures ANOVA.

Cell filling. Mice were assigned a code previous to dissection, as to maintain a blinded genotype across all procedures, including dissection, cell filling, imaging and quantification. Mice were deeply anesthetized with an overdose of isofluorane and transcardially perfused with PBS (pH 7.4) followed by ice-cold 4% paraformaldehyde/PBS (PFA) (pH 7.4). The brains were removed and post-fixed overnight in PFA 4%. After post-fixation, the brain was sliced at 200-μm thickness coronal sections in a vibratome and kept in PBS at 4 °C. For cell filling injections, selected brain slices immersed in PBS were mounted in a tissue stage. Dorsal striatal medium cells were targeted with post hoc confirmation of being medium spiny neurons (morphology and spine density). Using a micromanipulator, micropipettes loaded with Lucifer Yellow dye (Sigma L-0259, 8% solution in 0.05 M Tris buffer, pH 7.4) were used to impale the cell body. A micropipette containing a solution of 0.1 M LiCl was used to deliver the dye with a continuous 10 nA current for 5 min. Following cell filling, a post-staining was used to amplify the fluorescent signal. Briefly, sections were transferred to blocking solution (5% sucrose, 2% BSA, and 1% Triton X-100 in PBS) containing 1:500 rabbit anti-Lucifer Yellow antibody (Invitrogen A5750) and incubated gently for 3 days at 4 °C. Sections were washed three times for 5 min in blocking solution and incubated 2 h at room temperature with 1:400 biotinylated goat anti-rabbit antibody (Vector Laboratories BA-1000). Next, sections were washed three times for 5 min in PBS. A tertiary incubation was performed by incubating sections for 2 h at room temperature in streptavidin-conjugated Alexa 488 (Invitrogen S11223) diluted 1:1,000 in PBS. Finally, sections were washed three times in PBS, mounted on slides using Fluoro-Gel (EMS, 17985-10) and imaged by confocal microscopy. Spine density was calculated automatically using NeuronStudio (Mount Sinai School of Medicine) and manually curated by an observer using a three-dimensional analysis of the dendritic image stack. All spine counts began 30 μm away from the outer edge of the soma and extended for an additional 10–60 μm away from the starting point. The data from spine density passed the Lilliefors normality test and D'Agostino & Pearson omnibus normality test. Spine metrics relating to spine length, spine neck diameter and spine neck width were collected using ImageJ (NIH). All analyses of spine metrics were performed by observers that were blinded to the genotypes of the animals.

Electron microscopy. Mice were assigned a code previous to dissection, as to maintain a blinded genotype across all procedures, including dissection, sample processing, imaging and quantification. Mice were deeply anesthetized with an overdose of isofluorane and transcardially perfused with PBS (pH 7.4) followed by ice-cold 4% paraformaldehyde (PFA) in phosphate buffer (pH 7.4). The brains were removed, the striatum dissected and post-fixed overnight in PFA 4%, then transferred into a 4% glutaraldehyde solution and kept at 4 °C for 3 days. The samples were washed twice, 20 min each, in 7.5% sucrose, 0.1 M sodium cacodylate buffer, then post-fixed in 1% osmium tetroxide for 2 h with initial microwave treatment for 6 min. Next, the samples were washed twice in 0.11 M veronal acetate buffer for 20 min each. Following en-block staining in 1% uranyl acetate in distilled water for 1 h the samples were washed twice in 0.11 M veronal acetate buffer for 20 min each. Samples were dehydrated using serial dilutions of ethanol (70%, 95%, 2× 100%) for 20 min each, with initial microwave treatment of 2 min. Samples were then treated for 20 min twice with propaline oxide and impregnated with 50:50 propaline oxide:Epon resin overnight at 4 °C, with initial microwave treatment for 3 min. Next, the samples were impregnated with 100% Epon resin, three changes of 2 h each, with initial microwave treatment for 3 min each. Tissue samples were embedded in moulds and incubated for 48 h at 60 °C. Afterwards, semi-thin sections (0.5 μm) were cut on a Leica UltraCut S ultramicrotome and stained with Toluidine (0.8%) stain. From these, thin striatal sections (70 nm) were cut on an UltraCut S, mounted on 200 mesh Metaxaform Copper Rhodium grids and post-stained in 2% uranyl acetate in distilled water for 15 min and Sato's Lead citrate stain for 7 min. Grids were examined on a Philips (FEI) CM 12 transmission electron microscope. Images were acquired at ×40,000 magnification using an AMT 2Vue system, with an ORCA HR High resolution digital camera 7 megapixels, a Hamamatsu DCAM board for acquisition and AMT Image Capture Engine software version 600.335f. Images were saved as 7.5 megapixels 8 bit TIFF format files. PSD measurements were performed using ImageJ (NIH) by an observer that was blinded to the genotype of the samples.

Magnetic resonance image acquisition. Animals were assigned a blinding code, which was maintained during magnetic resonance (MR) data acquisition and analysis. MR mouse brain imaging was performed on a 7T Bruker Biospec 70/30 horizontal bore system (Billerica). Animals were lightly anesthetized under isofluorane with continuous monitoring and maintenance of physiological parameters throughout the imaging session (~60 min for each animal). Axial two-dimensional T2-weighted fast spin echo images (TURBO-RARE, TE/TR = 11/4,200 ms with 1 mm slice thick, matrix = 256 × 256 and FOV of 2.4 cm × 2.4 cm, five averages, 0.0 mm interslice gap) images were first obtained for screening purposes and supplemental anatomic information. For directed striatal and brain volumetric analysis, 64 contiguous 500-μm thick three-dimensional FSE proton density images (TURBO-RARE, TE/TR = 9/1,500 ms, matrix = 256 × 256 × 64 and FOV 2.2 cm × 2.2 cm × 2.2 cm, 25 min duration) were acquired.

MR volumetry measurements. Volumetric analysis of MR data sets was performed in OsiriX software, an open source image processing application

developed and maintained by Pixmeo. The left caudate-putamen was manually segmented in each animal by an investigator blinded to genotype. Each caudate-putamen was traced on contiguous axial slices from the three-dimensional volume acquisition with reference to a high-resolution age-matched mouse brain atlas (The Mouse Brain Atlas, The Mouse Brain Library at http://www.mbl.org). Selected areas were reviewed for consistency on coronal and sagittal representations, and cross-correlated with axial two-dimensional FSE images. Volumes were computed within OsiriX. Two separate striatal segmentations were obtained for each animal, with the average volume then taken. Intrarater reliability (kappa value) was = 0.97.

Volume normalization. Unilateral caudate-putamen volumes were normalized to brain volume measurements obtained from the same three-dimensional volume sets. Because of susceptibility distortions within the posterior fossa, and variable inclusion from animal to animal of posterior fossa contents at the caudal end of the 64 slice three-dimensional volume set, 'whole' brain volumes for normalization were obtained in each animal from traces beginning rostrally at the olfactory bulbs and ending caudally through the cerebral aqueduct at the roof of the fourth ventricle. As with striatal volumes, brain volumes were computed in OsiriX from the average of two segmentations. Intrarater reliability (kappa value) was >0.99. Statistical analysis was performed with unpaired two-tailed *t*-test.

39. Welch, J. M., Wang, D. & Feng, G. Differential mRNA expression and protein localization of the SAP90/PSD-95-associated proteins (SAPAPs) in the nervous system of the mouse. *J. Comp. Neurol.* **472,** 24–39 (2004).
40. Vorhees, C. V. & Williams, M. T. Morris water maze: procedures for assessing spatial and related forms of learning and memory. *Nature Protocols* **1,** 848–858 (2006).
41. Yin, H. H., Davis, M. I., Ronesi, J. A. & Lovinger, D. M. The role of protein synthesis in striatal long-term depression. *J. Neurosci.* **26,** 11811–11820 (2006).
42. Malenka, R. C. & Kocsis, J. D. Presynaptic actions of carbachol and adenosine on corticostriatal synaptic transmission studied *in vitro*. *J. Neurosci.* **8,** 3750–3756 (1988).
43. Myme, C. I., Sugino, K., Turrigiano, G. G. & Nelson, S. B. The NMDA-to-AMPA ratio at synapses onto layer 2/3 pyramidal neurons is conserved across prefrontal and visual cortices. *J. Neurophysiol.* **90,** 771–779 (2003).

doi:10.1038/nature09965

Shank3 mutant mice display autistic-like behaviours and striatal dysfunction

João Peça, Cátia Feliciano, Jonathan T. Ting, Wenting Wang, Michael F. Wells, Talaignair N. Venkatraman, Christopher D. Lascola, Zhanyan Fu and Guoping Feng

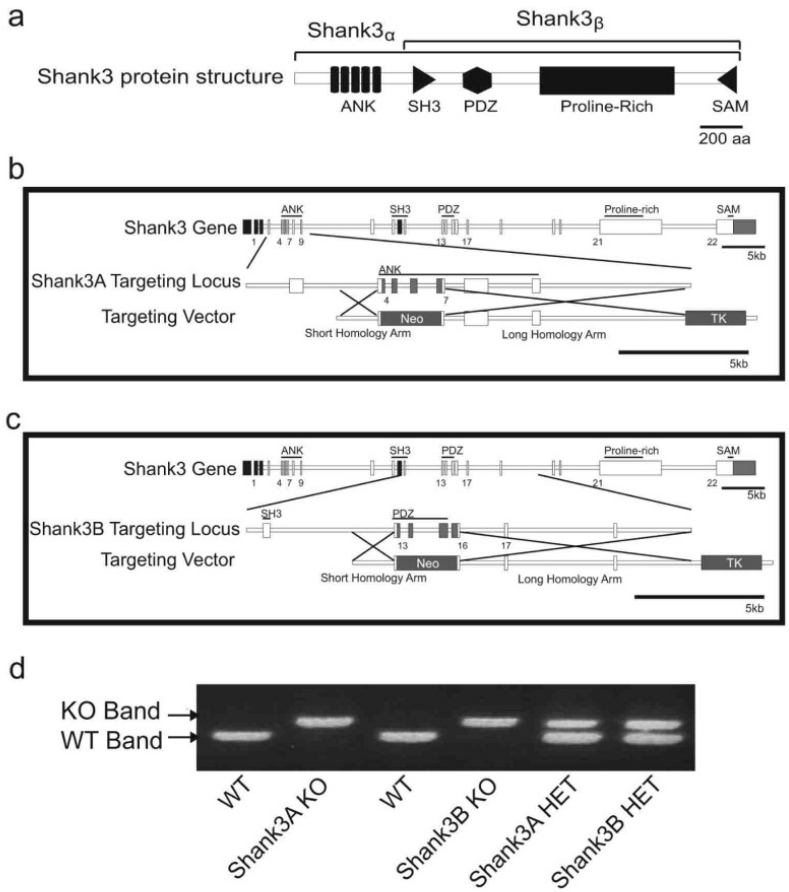

Supplementary Figure 1 | Shank3 protein structure, gene structure and targeted disruptions.a,Shank3 protein structure, with known isoforms highlighted.**b**, **c**, Targeting strategy and targeting vector for Shank3A-mutant mice (**b**), and Shank3B-mutant mice (**c**). **d**, PCR genotyping for Shank3A$^{+/+}$, Shank3A$^{+/-}$, Shank3A$^{-/-}$, Shank3B$^{+/+}$, Shank3B$^{+/-}$ and Shank3B$^{-/-}$ mice.

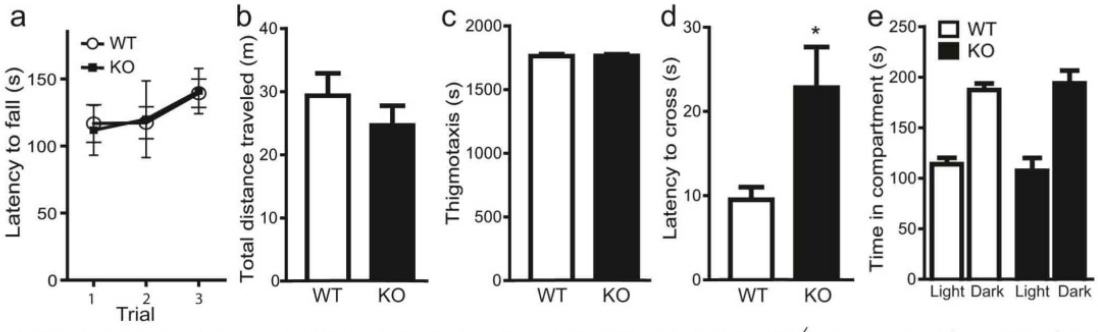

Supplementary Figure 2 | Motor learning and anxiety tests in *Shank3B*$^{-/-}$ mice. a, In the rotarod test, *Shank3B*$^{-/-}$ mice and controls display similar levels of motor coordination. **b, c,** In the open field test, *Shank3B*$^{-/-}$ mice, when compared to controls, display similar levels of total distance traveled (**b**) and thigmotaxis (**c**). **d, e,** In the dark-light box emergence test, *Shank3B*$^{-/-}$ mice display an increased latency to initially cross from the dark into the brightly lit chamber (**d**), but spend a similar amount of time in either chamber when compared to controls (**e**). * $p<0.05$, two-tailed *t*-test for **d**; all data are presented as means ± s.e.m; n=5 mice per genotype for **a,** and 8-9 mice per genotype for **b-e**.

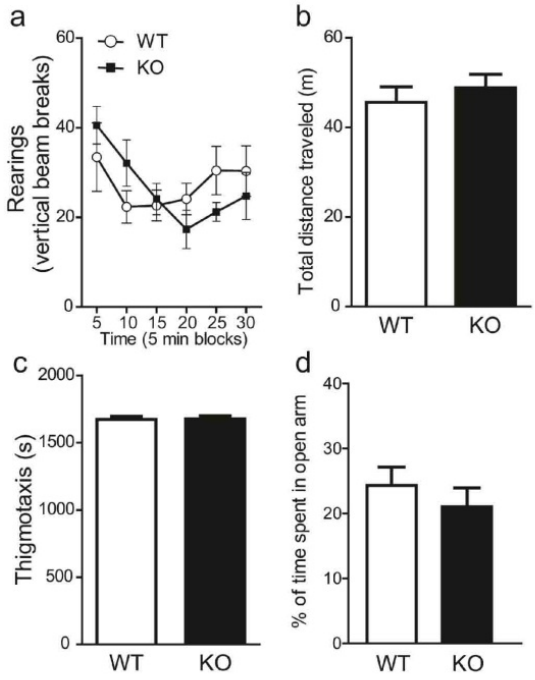

Supplementary Figure 3 | Anxiety levels and exploratory behaviours in *Shank3A*$^{-/-}$ mice. a-c, In the open field test *Shank3A*$^{-/-}$ rearing (**a**), total distance traveled (**b**), and time spent close to the chamber walls (thigmotaxis) (**c**) is not significantly different from controls. **d,** In the zero maze test, *Shank3A*$^{-/-}$ mice spent a similar amount of time in the open area when compared to wildtype controls. Two-tailed *t*-test for **b-d**;Two-way repeated measures ANOVA for **a**; all data presented as means ± s.e.m. n = 8 mice per genotype.

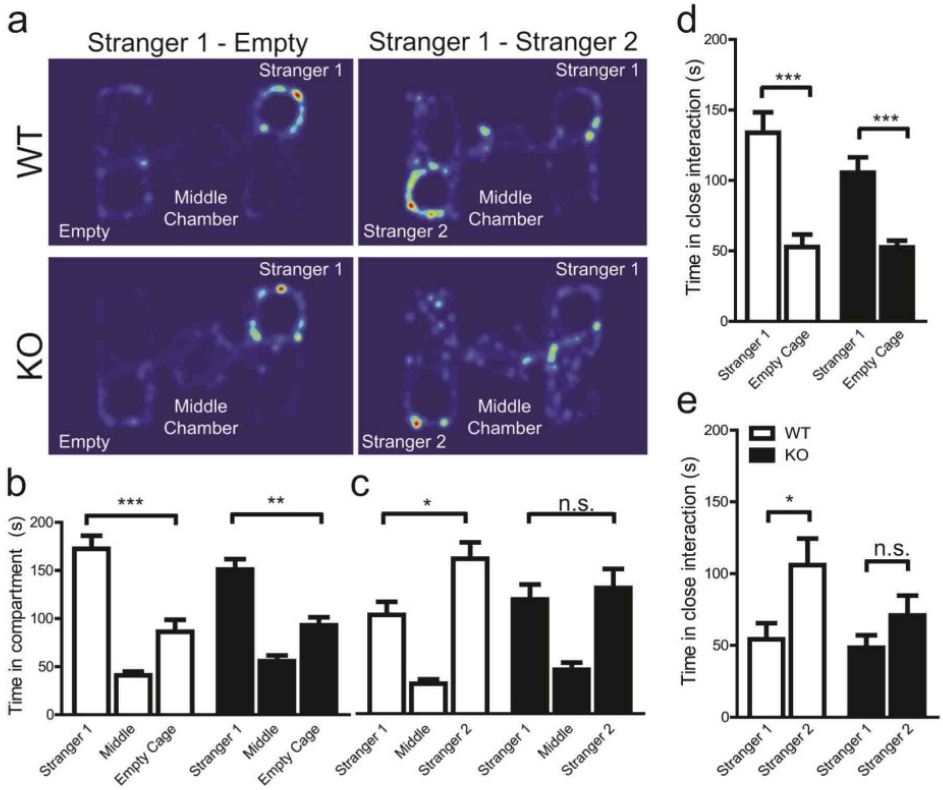

Supplementary Figure 4 | Social interaction and social novelty recognition tests in *Shank3A*$^{-/-}$ mice.a, Representative heat map analysis from "Stranger 1 – Empty" and "Stranger 1 – Stranger 2" trials from *Shank3A*$^{-/-}$ mice and controls. **b,** In the social interaction test, both *Shank3A*$^{-/-}$ mice (KO – black bars) and wildtype controls (WT – white bars) spent more time in the chamber containing the social partner (Stranger 1) than in the chamber containing the empty wire cage (Empty Cage).**c,** In the social novelty test, *Shank3A*$^{-/-}$ mice do not display preference for the novel social partner (Stranger 2). **d, e,** When analyzing social interaction by close proximity (within 5cm) to either "Stranger 1", "Empty Cage" (**d**), or "Stranger 1", "Stranger 2" (**e**), *Shank3A*$^{-/-}$ mice again display a preference for close social interaction with "Stranger 1"than "Empty cage" (**d**); however, under a social novelty paradigm (**e**), *Shank3A* mutantsdisplay abnormal social novelty recognition, as indicated by reduced preference for the novel social partner (Stranger 2). * $p<0.05$, ** $p<0.01$, *** $p<0.0001$, One-way ANOVA, with Bonferroni *post hoc t*-test; data are presented as means ± s.e.m. from 12-13 mice per group.

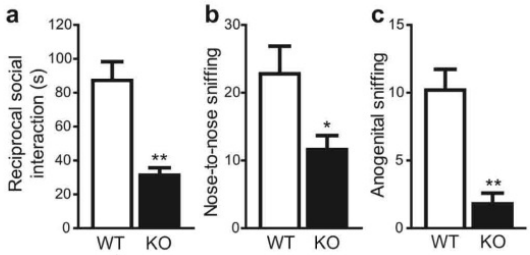

Supplementary Figure 5 | *Shank3B*$^{-/-}$ mice display social deficits during dyadic interaction in an open arena test. a, Unfamiliar pairs ofwildtype-*Shank3B*$^{-/-}$ mice (black bars) spend less time in reciprocal social interaction when compared to unfamiliar pairs of wildtype-wildtype mice (white bars). **b, c,** Quantification of nose-to-nose sniffing (**b**) and anogenital sniffing (**c**) by the target animal (wildtype or *Shank3B*$^{-/-}$) towards a stimulus animal (wildtype) demonstrates that the *Shank3B*$^{-/-}$mice (black bars) display a reduction in the frequency of social exploratory events when compared to wildtype controls (white bars). * $p<0.05$, ** $p<0.01$, two-tailed *t*-test;all data presented as means ± s.e.m;n=5 mice per group.

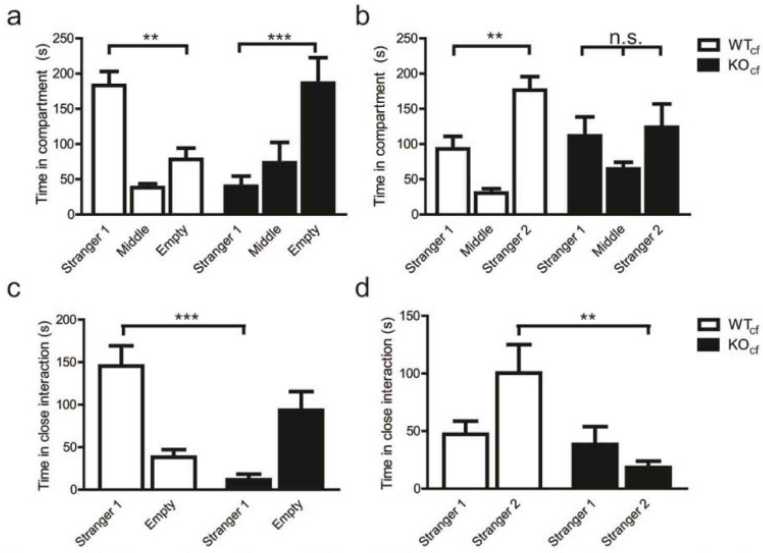

Supplementary Figure 6 | Cross-fostering of Shank3B mutants and wildtype mice does not rescue the sociability phenotype in *Shank3B*$^{-/-}$mice and does not impact social interaction and social recognition in wildtype mice.Wildtype and *Shank3B*$^{-/-}$ neonatal pups from homozygous x homozygous mating were cross-fostered at postnatal day 1 and reared by dams of the opposite genotype (wildtype mice with *Shank3B*$^{-/-}$ dams "WT_{cf}" and *Shank3B*$^{-/-}$ mice with wildtype dams "KO_{cf}"). **a,** In the three-chamber social interaction test, cross-fostered *Shank3B*$^{-/-}$ mice (KO_{cf} – black bars) spent less time in the chamber containing the social partner (Stranger 1) and more time in the chamber containing the empty wire cage (Empty Cage), cross-fostered wildtype mice display normal sociability levels (WT_{cf} – white bars). **b,** In the social novelty test, cross-fostered *Shank3B*$^{-/-}$ mice do not display a preference for the novel social partner (Stranger 2). **c, d,** When analyzing social interaction by close proximity (within 5cm) to either "Stranger 1", "Empty Cage" (**c**), or "Stranger 1", "Stranger 2" (**d**), cross-fostered *Shank3B*$^{-/-}$ mice displayed a clear reduction in social interaction(**c**); while under a social novelty paradigm (**d**), cross-fostered *Shank3B*$^{-/-}$ mice displayed a clear reduction in time spent with "Stranger 2". ** $p<0.01$, *** $p<0.001$, One-Way ANOVA, with Bonferroni *post hoct*-test; all data are presented as means ± s.e.m. from 7 mice per group.

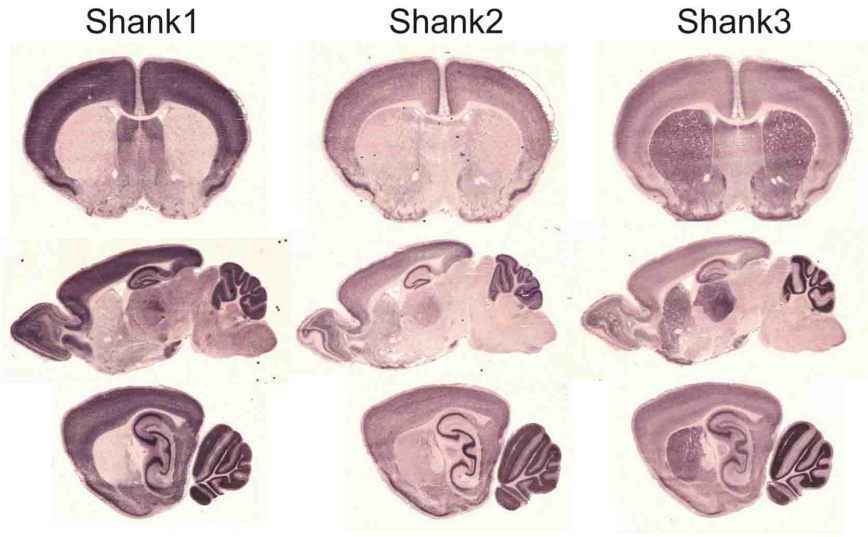

Table 1

Expression of Shank family of proteins in the CNS

	Shank1	Shank2	Shank3
Cortex	++++++	+++	+++
Thalamus	+++	+	+++++
Striatum	-	-	+++++
Amygdala	+++	+	+
Hippocampus	+++++	+++	+++
CA1	+++++	+++	++
CA3	++++	+++	++++
Dentate Gyrus	+++	+++	+
Cerebellum	+++	+++	+++
Purkinje cells	++++	+++++	-
Granule cells	++	-	++++
Colliculus	++	-	+
Brain Stem	++	-	+
Dendritically targeted	Yes	No	Yes

Supplementary Figure 7 | mRNA *in situ* characterization of *Shank* family of genes. a, *Shank1*, *Shank2* and *Shank3* mRNA *in situ* hybridization of coronal, medial parasagittal and lateral parasagittal mouse brain section from 5 week old mice. *Shank3* is the only Shank family member highly expressed in the striatum.

Supplementary Table 1 | Expression of *Shank* family of proteins in the CNS.Relative expression levels of *Shank1, Shank2* and *Shank3* in different areas of the central nervous system in serial sections from 5 week old mice (++++++ highest expression; - no detectable expression).

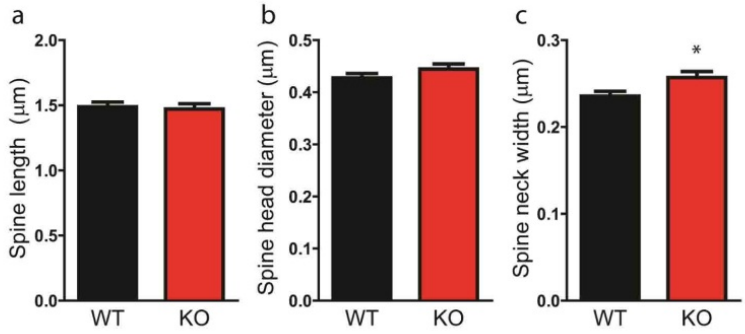

Supplementary Figure 8 | Morphological spine metrics from *Shank3B*$^{-/-}$ and control MSNs. a-c, Spine length and spine head diameter are not significantly different between *Shank3B*$^{-/-}$and wildtype medium spiny neurons (**a, b**), whereas spine neck width is larger in *Shank3B*$^{-/-}$spines (**c**). * p<0.05, two-tailed *t*-test; all data are presented as means ± s.e.m; n = 140 spines per genotype.

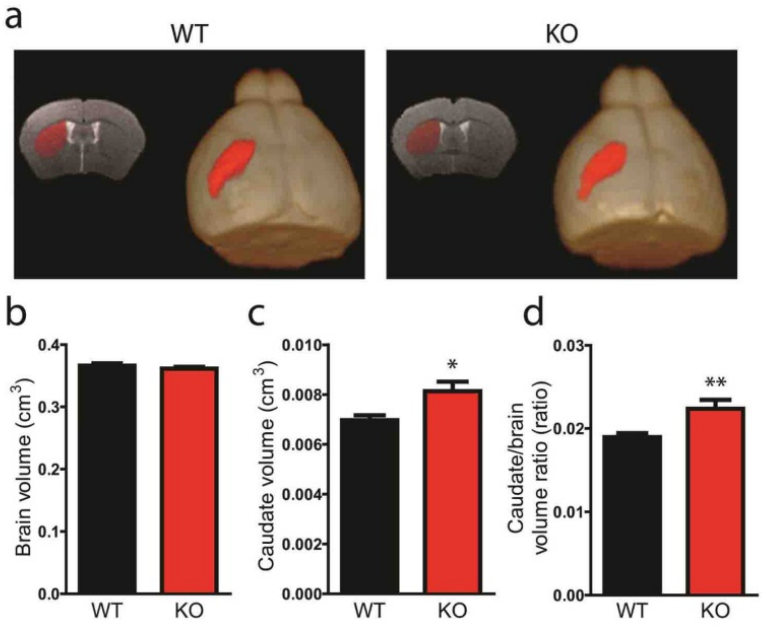

Supplementary Figure 9 | Increased striatal volume in *Shank3B*$^{-/-}$mice.a-c, Striatum and whole brain volumes measured by MRI. **a,** A 3D reconstruction of the brain is used for striatal and whole brain volumetric analysis as depicted for both WT and KO. **b,** Whole brain volume is not significantly different between control (WT) and *Shank3B*$^{-/-}$ mice (KO). **c,** Striatal volume is significantly larger in the *Shank3B*$^{-/-}$ mice. **d**, Striatum/brain volume ratio is increased in the *Shank3B*$^{-/-}$ mice.* p<0.05, ** p<0.01, two-tailed *t*-test. Data are presented as means ± s.e.m, n = 12 mice per genotype.

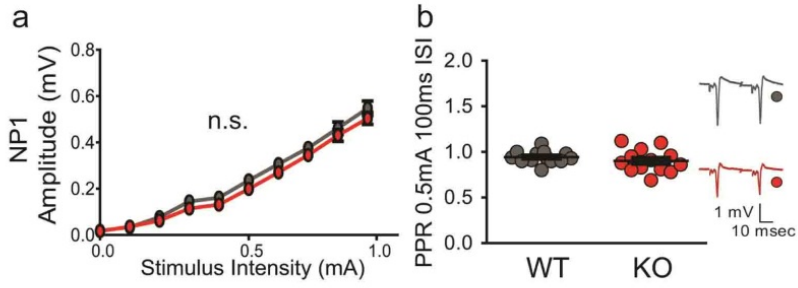

Supplementary Figure 10 | Normal presynaptic function in*Shank3B*$^{-/-}$ mice. Presynaptic function was measured by the relationship of stimulation intensity to the amplitude of the action potential component of the response termed negative peak 1 (NP1, **a**), and the paired-pulse ratios (PPR, **b**). NP1 amplitude (**a**) and PPR (**b**) are not significantly different between *Shank3B*$^{-/-}$ and control mice; example traces are shown as an inset for *Shank3B*$^{-/-}$ mice (red) and wildtype (grey). All data are presented as means ± s.e.m; n=13 slices from 4 mice per group.

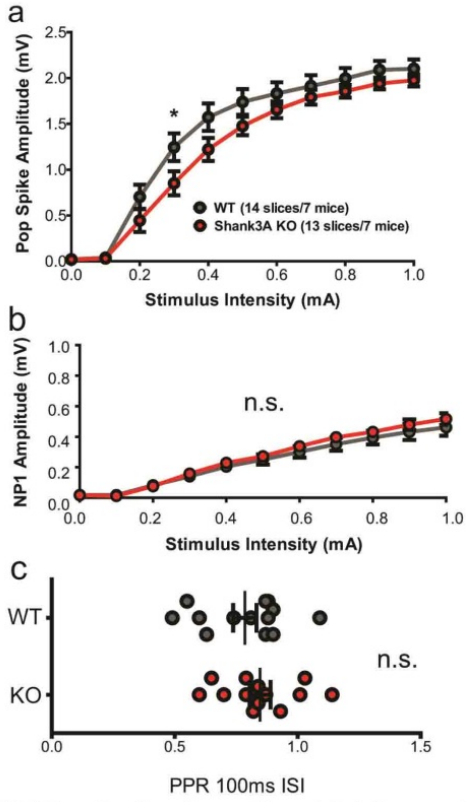

Supplementary Figure 11 | Slight reduction in cortico-striatal synaptic transmission in *Shank3A*$^{-/-}$ mice.a, Cortico-striatal pop spike amplitude is only statistically significantly decreased at one point in the stimulus intensity range for the *Shank3A*$^{-/-}$ mice (red trace) when compared to controls. **b**, **c**, NP1 amplitude (**b**) and PPR (**c**) are not significantly altered between *Shank3A*-mutant and controls. * p<0.05; Two-way

repeated measures ANOVA (p>0.05, not statistically significant), with Bonferroni *post hoc* test for **a** and**b;** two-tailed *t*-test for **c**; all data presented as means ± s.e.m; field recordings n=13-14 from 7 mice per group.

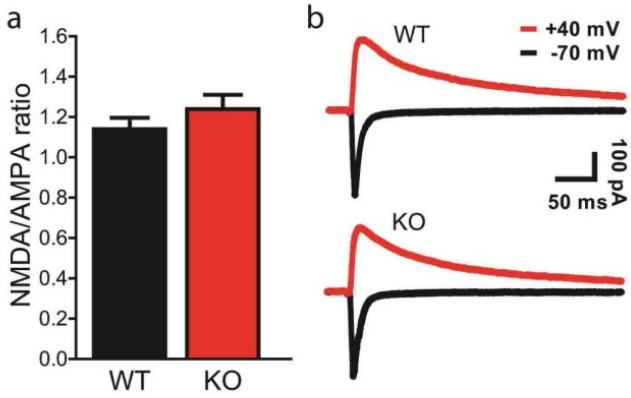

Supplementary Figure 12 | NMDA/AMPA ratio is not changed in *Shank3B*$^{-/-}$ MSNs. a, NMDA/AMPA ratio from MSNs is not changed when comparing *Shank3B*$^{-/-}$to controls. **b,** Example trace recordings from wildtype and *Shank3B*$^{-/-}$ MSNs at a stimulus intensity that evokes a ~300pA AMPA mediated response. Two-tailed *t*-test, data are presented as means ± s.e.m; n=15 from wildtype, n=13 from *Shank3B*$^{-/-}$ mice.

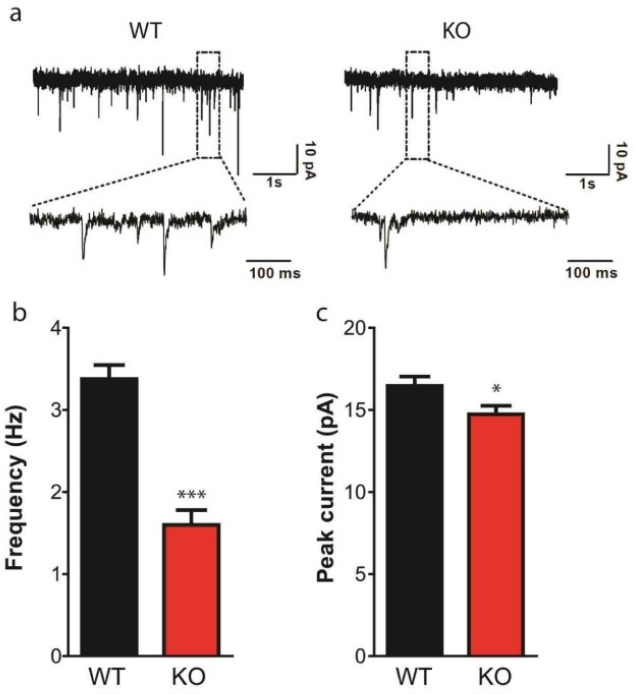

Supplementary Figure 13 | Reduced synaptic transmission inMSNs of *Shank3B*$^{-/-}$mice from heterozygous matings. a, mEPSC example traces fromwildtypeand *Shank3B*$^{-/-}$ MSNs recorded with whole cell voltage clamp. **b**, mEPSC event frequency in *Shank3B*$^{-/-}$ MSNs (red) is lower when compared to

wildtype (black).**c**, Peak current from mEPSC is smaller in*Shank3B*$^{-/-}$ than in wildtype MSNs. * p<0.05, *** p<0.001; unpaired two-tailed *t*-test;n=15cells per genotype; all data presented as means ± s.e.m.

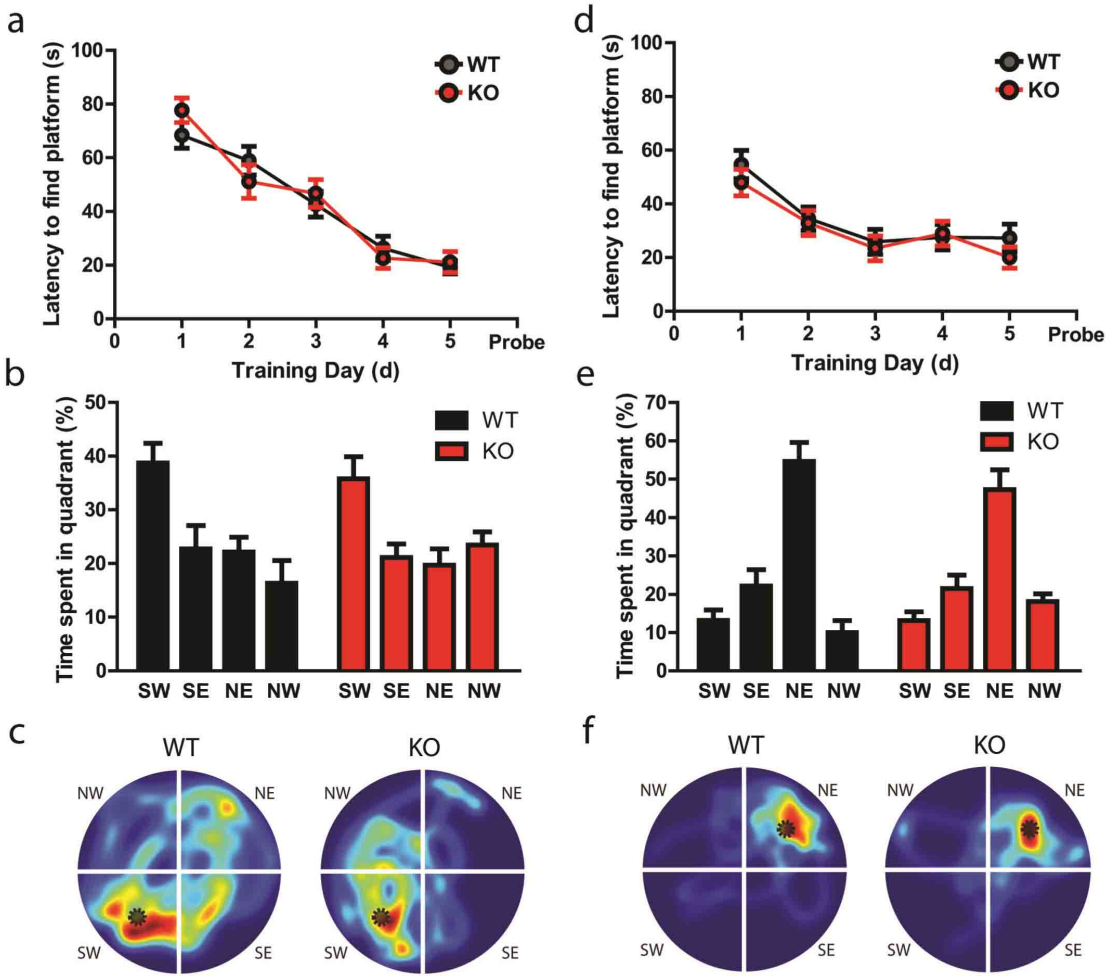

Supplementary Figure 14 | Morris Water Maze learning and memory test in *Shank3B*$^{-/-}$mice.a-b, Latency to find the platform decreases significantly across 5 days of training for both wildtype and *Shank3B*$^{-/-}$mice (**a**). In the probe trial, when compared to controls, *Shank3B*$^{-/-}$ mice spent a similar amount of time in target quadrant (SW) (**b**). **c**, Representative example heat maps from control (WT) and *Shank3B*$^{-/-}$mice (KO) during the probe trial. **d-e,** Latency to find the platform decreases significantly across subsequent 5 days of reversal training (platform switched to NE) for both wildtype and *Shank3B*$^{-/-}$mice (**d**). In the reversal probe trial, when compared to controls, *Shank3B*$^{-/-}$ mice spent a similar amount of time in target quadrant (NE) (**e**). **f**, Representative example heat maps from control (WT) and *Shank3B*$^{-/-}$mice (KO) during the reversal probe trial. Two-way repeated measures ANOVA (effect of genotype not statistically significant, p>0.05), all data are presented as means ± s.e.m; n=9 for wildtype, n=8 for *Shank3B*$^{-/-}$mice.

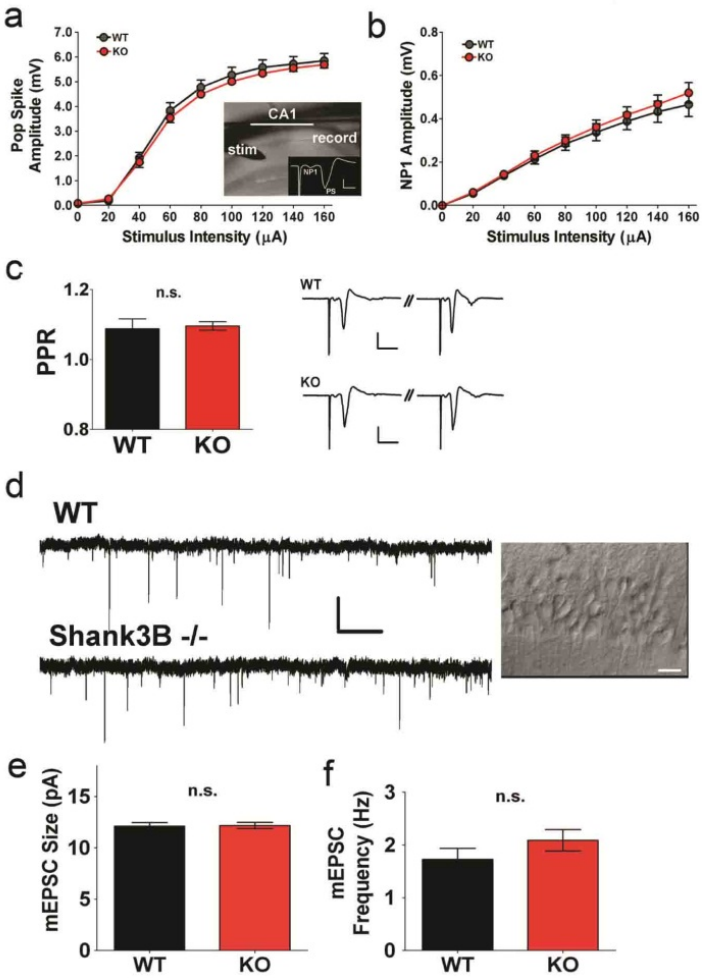

Supplementary Figure 15 | Hippocampal CA1 pyramidal neuron synaptic function is not significantly altered in *Shank3B*$^{-/-}$ mice. a, No significant difference in input-output functions of hippocampal CA1 population spikes measured from acute brain slices from wildtype (WT – black trace) and *Shank3B*$^{-/-}$(KO – red trace) mice. Inset, example DIC image of an acute hippocampal slice showing stimulation electrode and recordings electrode positioning. Lower right, example trace showing fiber volley component (NP1) and population spike (PS). Scale bars, 2 mV/3 msec. **b**, Fiber volley (NP1) amplitude is not significantly different between *Shank3B*$^{-/-}$and WT slices. $p>0.05$, Two-way repeated measures ANOVA, with Bonferroni *post hoc* test. **c**, Summary data for 100 msec interstimulus interval PPR (100 μA stimulus) of CA1 population spikes. Right, example traces of population spike paired pulses. Scale bars: 2 mV / 10 msec PPR is not significantly altered between *Shank3B*$^{-/-}$ and WT slices. $p>0.05$, two-tailed *t*-test. Data from **a-c** are presented as means ± s.e.m; field recordings n=10 slices from 4 mice per group. **d**, Example traces of mEPSCs recorded from CA1 pyramidal neurons (WT – top trace, *Shank3B*$^{-/-}$ – bottom trace). Scale bars: 20 pA / 2 sec. Right inset, 40X IR-DIC image of a recorded CA1 pyramidal neuron. Scale bar: 20 μm. **e**, Summary data for mEPSC size. **f**, summary data for mEPSC frequency. Whole-cell recordings, n=20 neurons for WT and n=20 neurons for *Shank3B*$^{-/-}$. n.s., not significant, two-tailed *t*-test; data are presented as means ± s.e.m.

doi:10.1038/nature09965

Supplementary Table 2

Shank3B — Summary of behavioural statistical data

Test	Duration	Measurement	# of animals	Values	Statistical Test	p value	*Post hoc* test	p value	Figure
Lesion Score	-	Presence/Absence of skin lesions	WT=38 KO=29	WT=0/38 KO=10/19	Fisher's exact test	< 0.0001***	-	-	-
Grooming Score	2 hours	Time spent grooming (% of total)	WT=6 KO=6	WT = 16.24 ± 1.252 KO = 26.83 ± 1.142	Unpaired two-tailed t-test	< 0.0001***	-	-	1d
Open Field	30 minutes (5 minute bins)	Vertical beam-breaks	WT = 9 KO = 9	5min - WT = 46.78 ± 12.92 KO = 8.333 ± 2.646	Two-way repeated measure ANOVA	Genotype < 0.05* Time bin <0.001***	Unpaired two-tailed t-test (WT v KO)	< 0.05*	1e
		Vertical beam-breaks		10min - WT = 35.78 ± 11.12 KO = 4.556 ± 1.709				< 0.05*	1e
		Vertical beam-breaks		15min - WT = 33.00 ± 9.814 KO = 7.667 ± 2.522				< 0.05*	1e
		Vertical beam-breaks		20 min - WT = 22.33 ± 6.451 KO = 5.333 ± 2.147				< 0.05*	1e
		Vertical beam-breaks		25 min - WT = 22.89 ± 11.03 KO = 3.889 ± 1.679				> 0.05	1e
		Vertical beam-breaks		30 - WT = 18.89 ± 8.448 KO = 4.889 ± 2.214				> 0.05	1e
	30 minutes	Total distance travelled (m)		WT = 29.34 ± 3.552 KO = 24.67 ± 3.111	Unpaired two-tailed t-test	> 0.05	-	-	Supplementary Fig 2b
		Thigmotaxis (s)		WT = 1758 ± 17.22 KO = 1770 ± 12.17	Unpaired two-tailed t-test	> 0.05	-	-	Supplementary Fig 2c
Zero Maze	5 minutes	Time spent in open arm (% of total)	WT = 9 KO = 9	WT = 31.46 ± 6.802 KO = 14.66 ± 2.740	Unpaired two-tailed t-test	< 0.05*	-	-	1f
Light-Dark box	5 minutes	Duration in Light (s)	WT = 8 KO = 8	WT = 113.8 ± 6.401 KO = 107.3 ± 12.72	Unpaired two-tailed t-test	> 0.05	-	-	Supplementary Fig 2e
		Duration in Dark (s)		WT = 187.3 ± 6.396 KO = 193.8 ± 12.69	Unpaired two-tailed t-test	> 0.05	-	-	Supplementary Fig 2e
		Latency to Light (s)		WT = 9.513 ± 1.494 KO = 22.83 ± 4.837	Unpaired two-tailed t-test	< 0.05*	-	-	Supplementary Fig 2d

doi:10.1038/nature09965

Social Interaction	5 minutes	Time in compartment (s)	WT=12 KO=14	WT - Stranger 1 = 167 ± 16.65 Middle = 59.15 ± 6.77 Empty = 73.74 ± 15.27 KO - Stranger 1 = 88.01 ± 18.42 Middle 65.98 ± 7.47 Empty = 145.9 ± 16.63	One-way ANOVA	< 0.0001***	Bonferroni's Multiple Comparison Test (Strg1 v Empty)	< 0.0001*** < 0.01**	2b 2b
Social Novelty	5 minutes	Time in compartment (s)		WT - Stranger 1 = 100.3 ± 16.85 Middle 42.83 ± 4.765 Stranger 2 = 156.7 ± 15.51 KO - Stranger 1 = 96.8 ± 23.15 Middle = 88 ± 19.8 Stranger 2 = 115 ± 22.49	One-way ANOVA	< 0.01**	Bonferroni's Multiple Comparison Test (Strg1 v Strg 2)	< 0.05* > 0.05	2c 2c
Social Interaction	5 minutes	Time spent in close proximity (s)		Stranger 1 - WT = 132.7 ± 15.46 KO = 62.06 ± 11.72 Empty Cage WT = 47.95 ± 8.743 KO = 100.5 ± 14.53	One-way ANOVA	< 0.0001***	Bonferroni's Multiple Comparison Test (Strg 1 v Strg 1) (Empty v Empty)	< 0.0001*** < 0.05*	2d 2d
Social Novelty	5 minutes	Time spent in close proximity (s)		Stranger 1 - WT = 60.39 ± 12.27 KO = 35.59 ± 11.43 Stranger 2 - WT = 83.21 ± 16.46 KO = 40.68 ± 10.52	One-way ANOVA	< 0.05*	Bonferroni's Multiple Comparison Test (Strg1 v Strg 1) (Strg2 v Strg 2)	> 0.05 < 0.05*	2e 2e
Dyadic Test	5 minutes	Time spent in reciprocal social interaction (s)	WT = 5 KO = 5	WT = 87.28 ± 11.02 KO = 31.30 ± 4.389	Unpaired two-tailed t-test	< 0.01**	-	-	Supplementary Fig 5a
		Frequency of nose-to-nose sniffing		WT = 22.80 ± 4.05 KO = 11.60 ± 2.09	Unpaired two-tailed t-test	< 0.05*	-	-	Supplementary Fig 5b
		Frequency of anogenital sniffing initiated by the test animal		WT = 10.20 ± 1.53 KO = 1.80 ± 0.8	Unpaired two-tailed t-test	< 0.01**	-	-	Supplementary Fig 5c

Social Interaction (Cross Fostering)	5 minutes	Time in compartment (s)	WT=7 KO=7	WT - Stranger 1 = 183.3 ± 19.61 Middle = 38.24 ± 5.38 Empty = 78.31 ± 15.86 KO - Stranger 1 = 40.00 ± 14.50 Middle = 73.29 ± 29.01 Empty = 186.6 ± 36.07	One-way ANOVA	< 0.01**	Bonferroni's Multiple Comparison Test (Strg1 v Empty)	< 0.01** < 0.001***	Supplementary Figure 6a Supplementary Figure 6a
Social Novelty (Cross Fostering)	5 minutes	Time in compartment (s)		WT - Stranger 1 = 93.06 ± 17.81 Middle = 30.32 ± 6.31 Stranger 2 = 176.40 ± 19.19 KO - Stranger 1 = 111.7 ± 26.69 Middle = 64.45 ± 9.59 Stranger 2 = 123.8 ± 33.20	One-way ANOVA	< 0.001***	Bonferroni's Multiple Comparison Test (Strg1 v Strg 2)	< 0.01** > 0.05	Supplementary Figure 6b Supplementary Figure 6b
Social Interaction (Cross Fostering)	5 minutes	Time spent in close proximity (s)		Stranger 1 - WT = 145.4 ± 23.84 KO = 11.70 ± 6.53 Empty Cage WT = 38.20 ± 9.11 KO = 93.67 ± 21.75	One-way ANOVA	< 0.0001***	Bonferroni's Multiple Comparison Test (Strg 1 v Strg 1) (Empty v Empty)	< 0.001*** > 0.05	Supplementary Figure 6c Supplementary Figure 6c
Social Novelty (Cross Fostering)	5 minutes	Time spent in close proximity (s)		Stranger 1 - WT = 47.23 ± 11.50 KO = 38.40 ± 15.43 Stranger 2 - WT = 100.3 ± 24.77 KO = 18.32 ± 5.59	One-way ANOVA	< 0.05*	Bonferroni's Multiple Comparison Test (Strg1 v Strg 1) (Strg2 v Strg 2)	> 0.05 < 0.01**	Supplementary Figure 6d Supplementary Figure 6d
Morris Water Maze - Training	Maximum duration of 90 seconds per trial	Latency to Platform (Day 1; 4 trials per day) Latency to Platform (Day 2; 4 trials per day) Latency to Platform (Day 3; 4 trials per day) Latency to Platform (Day 4; 4 trials per day) Latency to Platform (Day 5; 4 trials per day)		WT = 65.07 ± 5.314 KO = 77.69 ± 4.598 WT =58.85 ± 5.339 KO = 51.11 ± 6.253 WT =42.65 ± 4.795 KO = 46.7 ± 5.143 WT =26.3 ± 4.49 KO = 22.66 ± 3.825 WT =19.22 ± 2.492 KO = 21.12 ± 3.885	Two-way repeated measure ANOVA	Effect of Training p < 0.0001*** Effect of Genotype p > 0.05	Bonferroni's Multiple Comparison Test (WT v KO)	> 0.05 > 0.05 > 0.05 > 0.05 > 0.05	Supplementary 14a

doi:10.1038/nature09965

Morris Water Maze - Reversal Training	Maximum duration of 90 seconds per trial	Latency to Platform (Day 1; 4 trials per day)	WT=9 KO=8	WT =54.62 ± 5.228 KO = 47.95 ± 4.954	Two-way repeated measure ANOVA	Effect of Training p < 0.0001*** Effect of Genotype p > 0.05	Bonferroni's Multiple Comparison Test (WT v KO)	> 0.05	Supplementary 14b
		Latency to Platform (Day 2; 4 trials per day)		WT =34.52 ± 4.376 KO =32.87 ± 4.662				> 0.05	
		Latency to Platform (Day 3; 4 trials per day)		WT =25.85 ± 4.683 KO = 23.43 ± 4.614				> 0.05	
		Latency to Platform (Day 4; 4 trials per day)		WT =27.56 ± 4.697 KO = 28.96 ± 4.588				> 0.05	
		Latency to Platform (Day 5; 4 trials per day)		WT =27.3 ± 5.131 KO = 20 ± 3.959				> 0.05	
Morris Water Maze - Probe Trial	60 seconds	Percent of Time in SW Quadrant		WT = 38.74 ± 3.65 KO = 35.76 ± 4119	Two-way repeated measure ANOVA	Effect of Quadrant p < 0.001*** Effect of Genotype p > 0.05	Bonferroni's Multiple Comparison Test (WT v KO)	> 0.05	Supplementary 14c
		Percent of Time in SE Quadrant		WT = 22.71 ± 4.364 KO = 21.12 ± 2.515				> 0.05	
		Percent of Time in NE Quadrant		WT = 22.16 ± 2.733 KO = 19.69 ± 3.022				> 0.05	
		Percent of Time in NW Quadrant		WT = 16.37 ± 2.733 KO = 19.69 ± 3.022				> 0.05	
Morris Water Maze - Reversal Probe Trial	60 seconds	Percent of Time in SW Quadrant		WT = 13.17 ± 2.732 KO = 13.08 ± 2.334		Effect of Training p < 0.0001*** Effect of Genotype p > 0.05	Bonferroni's Multiple Comparison Test (WT v KO)	> 0.05	Supplementary 14d
		Percent of Time in SE Quadrant		WT = 22.16 ± 4.225 KO = 21.52 ± 3.483				> 0.05	
		Percent of Time in NE Quadrant		WT = 54.65 ± 4.897 KO = 47.3 ± 5.13				> 0.05	
		Percent of Time in NW Quadrant		WT = 10.01 ± 3.081 KO = 18.09 ± 2.024				> 0.05	
Rotorod	Trial 1	Latency to fall (s)	WT=5 KO=5	WT = 116.8 ± 13.92 KO = 111.8 ± 18.59	Two-way repeated measure ANOVA	Effect of Trial p < 0.05* Effect of Genotype p > 0.05	Bonferroni's Multiple Comparison Test (WT v KO)	> 0.05	Supplementary Fig 2a
	Trial 2	Latency to fall (s)		WT = 117.4 ± 11.86 KO = 120 ± 28.6				> 0.05	
	Trial 3	Latency to fall (s)		WT = 139.4 ± 10.51 KO = 141 ± 16.83				> 0.05	
Swim Speed	Trial 1 of MWM	Velocity (cm/s)	WT=9 KO=8	WT = 17.94 ± 0.8249 KO = 18.47 ± 1.268	Unpaired two-tailed t test	> 0.05	-	-	-

Shank3A

Test	Duration	Measurement	# of animals	Values	Statistical Test	p	*Post hoc* test	p	Figure
Open Field	30 minutes (5 minute bins)	Vertical beam-breaks	WT = 8 KO = 8	5min - WT = 33.44 ± 7.627 KO = 40.56 ± 4.187	Two-way repeated measure ANOVA	Time bin <0.05* Genotype p > 0.05	Unpaired two-tailed t-test (WT v KO)	> 0.05	Suplementary 3a
				10min - WT = 22.33 ± 3.603 KO = 32.11 ± 5.16				> 0.05	
				15min - WT = 22.67 ± 3.403 KO = 24.11 ± 3.486				> 0.05	
				20min - WT = 24.11 ± 3.506 KO = 17.33 ± 4.282				> 0.05	
				25min - WT = 30.44 ± 5.409 KO = 21.22 ± 2.093				> 0.05	
				30min - WT = 30.33 ± 5.6 KO = 24.78 ± 5.23				> 0.05	
	30 minutes	Total distance travelled (m)		WT = 45.62 ± 3.459 KO = 48.82 ± 3.02	Unpaired two-tailed t-test	> 0.05	-	-	Suplementary 3b
		Thigmotaxis (s)		WT = 1673 ± 23.58 KO = 1676 ± 23.6	Unpaired two-tailed t-test	> 0.05	-	-	Suplementary 3c
Zero Maze	5 minutes	Time spent in open arm (% of total)	WT = 8 KO = 8	WT = 24.35 ± 2.809 KO = 21.02 ± 2.951	Unpaired two-tailed t-test	> 0.05	-	-	Suplementary 3d
Social Interaction	5 minutes	Time in compartment		WT - Stranger 1 = 172 ± 13.72 Middle = 41.12 ± 3.781 Empty = 86.32 ± 12.43	One-way ANOVA	< 0.0001***	Bonferroni's Multiple Comparison Test (Strg 1 v Empty)	< 0.0001***	Suplementary 4b
				KO - Stranger 1 = 151 ± 10.73 Middle 55.69 ± 5.847 Empty = 93 ± 8.178				< 0.01**	
Social Novelty	5 minutes	Time in compartment	WT=12 KO=13	WT - Stranger 1 = 104.5 ± 13.57 Middle 31.7 ± 4.527 Stranger 2 = 163.6 ± 17.31	One-way ANOVA	< 0.0001***	Bonferroni's Multiple Comparison Test (Strg 1 v Strg 2)	< 0.05*	Suplementary 4c
				KO - Stranger 1 =120.6 ± 15.79 Middle = 46.36 ± 7.503 Stranger 2 = 132.7 ± 20.03				> 0.05	

doi:10.1038/nature09965

Social Interaction	5 minutes	Time Spent in close proximity	WT - Stranger 1 = 133.8 ± 14.52 Empty = 52.77 ± 8.891 KO - Stranger 1 = 105.6 ± 10.97 Empty = 52.52 ± 4.811	One-way ANOVA	< 0.0001***	Bonferroni's Multiple Comparison Test (Strg 1 v Empty)	< 0.0001*** < 0.001***	Suplementary 4d
Social Novelty	5 minutes	Time Spent in close proximity	WT - Stranger 1 = 54.25 ± 11.22 Stranger 2 = 105.9 ± 18.4 KO - Stranger 1 = 48.39 ± 8.624 Stranger 2 = 70.87 ± 13.83	One-way ANOVA	< 0.05*	Bonferroni's Multiple Comparison Test (Strg 1 v Strg 2)	< 0.05* > 0.05	Suplementary 4e

Chapter 3

Characterization of nArgBP2 expression in the mouse brain

In the ensuing work (manuscript in preparation), Cátia Feliciano made the following contributions:

Designed experiments

Produced DIG-RNA probes, anti-nArgBP2 antibody, performed *in situs,* protein stainings and characterized the anti-nArgBP2 antibody.

Wrote the manuscript

Characterization of nArgBP2 mRNA localization and protein expression in the mouse brain

Cátia Feliciano[1,2], João Peça[1], Qiangge Zhang[3], Michael F. Wells[3] & Guoping Feng[1,3†]

1 - Department of Neurobiology, Duke University Medical Center, Durham, NC 27705, USA

2- Gulbenkian PhD Programme in Biomedicine, Gulbenkian Science Institute, 2781-901 Oeiras, Portugal

3 - McGovern Institute for Brain Research, Department of Brain and Cognitive Sciences, Massachusetts Institute of Technology, Cambridge, MA, 02139

† - Corresponding author – Guoping Feng (fengg@mit.edu)

Abstract

The postsynaptic density at glutamatergic synapses is a macromolecular complex essential for proper synaptic function. In the postsynaptic density, membrane-bound receptors are functionally connected to the cellular cytoskeleton through multiple protein-protein layers of interactions. Several of the core synaptic scaffolding proteins have been characterized in recent years. The neuronal Arg binding protein-2 (nArgBP2) interacts with actin regulatory proteins and is a binding partner to the SAP90/PSD-95 associated proteins (SAPAP) at the postsynaptic density. However, the expression pattern of nArgBP2 in the mouse brain and the relative contribution of nArgBP2 to total ArgBP2 expression in neuronal tissue remains unclear. Here, we present a detailed characterization of ArgBP2/nArgBP2 mRNA expression in the mouse brain and demonstrate that nArgBP2 is the main form expressed in the mouse forebrain while ArgBP2 forms are predominantly expressed in the cerebellum. Using an anti-nArgBP2 specific antibody, we characterize protein expression across development and observe that nArgBP2 is enriched in discrete brain nuclei and at glutamatergic synapses.

Introduction

Excitatory glutamatergic transmission depends heavily on the correct assembly of the postsynaptic density (PSD) (Kennedy, 2000). The PSD is a macromolecular structure which clusters neurotransmitter receptors, signaling enzymes, adhesion complexes and scaffolding proteins all within a few nanometers of the postsynaptic membrane and in direct apposition to the presynaptic terminal (Sheng and Hoogenraad, 2007). Additionally, several proteins present at the PSD are known to associate with and regulate the synaptic actin cytoskeleton. This continuous link, from membrane bound receptor to the downstream cellular cytoskeleton is thought to be important for normal synaptic function and for the morphological changes occurring at dendritic spines (Dillon and Goda, 2005; Ehlers, 2002; Fischer et al., 2000). Also, substantial attention has been given to characterize and understand the role of core PSD scaffolding proteins, their molecular partners, expression patterns and synaptic role. Among others, these include the PSD-95-, the Shank- and the SAPAP-family of proteins (Bockers et al., 2004; Fukaya and Watanabe, 2000; Sala et al., 2001; Tu et al., 1999; Welch et al., 2004).

ArgBP2 is a member of the Vinexin/Ponsin/ArgBP2 family of proteins which are thought to participate in signal transduction and in the regulation of the actin cytoskeleton (Kioka et al., 2002). ArgBP2 was originally identified as a phosphorylation target and binding partner to the Arg and Abl protein-tyrosine kinases (Wang et al., 1997). The neuronal specific form of ArgBP2 (nArgBP2), was identified in a yeast two-hybrid screen as a binding partner to SAPAP (Kawabe et al., 1999). In neuronal tissue, nArgBP2 is known to coordinate multiple mechanisms converging on the actin cytoskeleton and was shown to interact with actin regulatory proteins, suggesting it may lay downstream of SAPAP proteins in the PSD (Cestra et al., 2005; Ronty et al., 2005). At the cellular level, ArgBP2 is also present in cytoskeletal stress fibers and the cellular nucleus (Wang et al., 1997). In terms of structure, both ArgBP2 and nArgBP2 feature a sorbin homology domain near the N-terminus and three SH3 domains at the C-terminus. The sorbin homology domain is highly homologous to the sorbin peptide originally identified in the lumen of porcine duodenum (Vagne-Descroix et al., 1991). In humans, it is hypothesized that the sorbin peptide originates from an alternative splicing of the SORBS2 gene (ArgBP2) (Hand and Eiden, 2005). When present as part of a protein domain, the sorbin homology domain is thought to promote the targeting of proteins to lipid rafts (Kimura et al., 2001). The C-terminal SH3 domains have been characterized to mediate protein-protein interactions between ArgBP2/nArgBP2 and binding partners such as, Abl, Arg, Cbl, Pyk2, vinculin and afadin (Haglund et al., 2004; Kawabe et al., 1999; Soubeyran et al., 2003; Wang et al., 1997). Finally, nArgBP2 contains a zinc finger domain in its neuronal-specific exon. This exon is highly conserved across mammalian species and gives rise to a 606 amino-acid portion of the protein (Kioka et al., 2002).

As a first step towards understanding the *in vivo* role of nArgBP2 we have performed a sub-cellular and histological characterization of nArgBP2 in the mouse brain. To assess the presence of cellular transcripts for ArgBP2 and nArgBP2 we used in situ mRNA hybridization across serial sections the mouse brain. To evaluate the translation of the nArgBP2 mRNA products into functional protein, we generated an anti-nArgBP2 specific antibody and explored the brain and sub-cellular localization of nArgBP2 in the murine central nervous system.

Materials and Methods

In situ hybridization

ArgBP2 (nucleotide #3449-4239, ENSMUST00000135336, Sorbs2-004) and nArgBP2 (nucleotide #1856-2857, ENSMUST00000135336, Sorbs2-004) cDNA fragments were amplified by polymerase chain reaction (PCR) from an adult cDNA library and cloned into pBluescript II SK+ (Stratagene, La Jolla, CA, USA). Plasmids were linearized with restriction enzymes (NotI or XhoI, New England BioLabs, Ipswich, MA, USA) that generated 5' overhangs. The transcription reactions and Digoxigenin (DIG)-labeling of RNA probes were performed using the MAXIscript in vitro RNA synthesis kit (Ambion, Austin, TX, USA). For both ArgBP2 and nArgBP2, the sense strands were generated by T7 RNA polymerase and the antisense strands by T3 RNA polymerase. Quantification of DIG-labeled probes was done by dot blotting and probing with alkaline phosphatase-conjugated anti-DIG antibody, using a DIG-RNA standard (Roche, Indianapolis, IN, USA). P21 and adult (3 months-old) mice were deeply anesthetized with isofluorane, and perfused with PBS followed by 4% paraformaldehyde/PBS (PFA, Electron Microscopy Sciences, Hatfield, PA, USA). Brains were dissected, embedded in OCT compound (TissueTek, Torrance, CA, USA) and frozen in ethanol/dry ice slush. Blocks were mounted for coronal and sagittal planes and 20 µm thick sections were cut on a Leica CM1850 cryostat (Leica Microsystems, Richmond Hill, Ontario, Canada). Brain sections were collected onto Superfrost Plus slides (Fisher Scientific, Swanee, GA, USA) and air dried at room temperature (RT) for 1 hour. The sections were then fixed in 4% (PFA) in PBS for 10 minutes at RT, washed 3 times with PBS for 3 minutes each, acetylated for 10 minutes at RT in TEA buffer (4 ml triethanolamine and 0.525 ml 12.1 M HCl were added to 295 ml H2O and stirred; 0.75 ml acetic anhydride was added just before sections were immersed) and again washed 3 times with PBS for 3 minutes each. For prehybridization, sections were incubated with hybridization buffer (50% formamide [Sigma, St. Luis, MO, USA], 5X SSC [750 mM NaCl, 75 mM Na-Citrate], 5X Denhardt's solution [Sigma], 250 µg/ml yeast tRNA [Roche], 500 µg/ml salmon sperm DNA [Sigma], 50 µg/ml heparin [Sigma] in DEPC-dH2O for 1 hour at RT. DIG-labeled RNA probes were diluted in hybridization solution to a working concentration of 1000 ng/ml, heated at 70°C for 10 minutes and chilled on ice. The prehybridization solution was

removed and hybridization mixture was added to the sections. The sections were covered with parafilm. The hybridization was done overnight at 68°C in a humidified chamber containing 50% formamide/2XSSC. After hybridization, parafilm was removed by dipping the sections in 2XSSC at RT. Sections were washed 4 times in 0.2XSSC at 68°C for 3 hours, then adjusted to RT in 0.2XSSC for 5 minutes and washed 2X5 minutes with TBS (150 mM NaCl, 10 mM Tris-HCl, pH 7.4). For immunological detection, sections were incubated with blocking buffer (10% normal sheep serum, 0.2% blocking reagent [Roche]) for 1 hour at RT, followed by incubation with alkaline phosphatase-conjugated anti-DIG antibody (1:2000 in blocking buffer) overnight at 4°C. Sections were washed 4X10 minutes with TBS and incubated with color detection buffer (100 mM NaCl, 50 mM MgCl2, 0,24 mg/ml levamisole, 100 mM Tris-HCl, pH 9.5) for 5 minutes. The color reaction was performed in the presence of nitroblue tetrazolium (NBT; 0.35 mg/ml) and 5-bromo-4-chloro-3-indolyl-phosphate (BCIP; 0.175 mg/ml) in detection buffer at RT in the dark. Incubation depended on how quickly signal from the antisense probe appears versus background signal in the sense probe. Sections were then washed in TBS, water and then mounted with 90% glycerol/H2O. Images were collected on a Zeiss Axioskop 2 Plus (Carl Zeiss, Thornwood, NY, USA) with a Zeiss Neofluar 4X objective using a Zeiss Axiocam digital camera (Carl Zeiss). Images were assembled and processed using Adobe Photoshop (Adobe Systems, San Jose, CA, USA).

Antibody production and purification

The sequence of the mouse nArgBP2 gene (ENSMUST00000135336, Sorbs2-004) was used to design PCR primer sets to amplify a region unique and of suitable antigenicity, encoding a 201 amino acids region (404-604, ENSMUSP00000114286, SORBS2-004), corresponding to the brain specific exon of SORBS2. The nArgBP2 selected region was amplified by PCR from an adult cDNA library using Pfu Turbo DNA Polymerase (Stratagene, La Jolla, CA, USA) and cloned in frame into the bacterial expression vector pET-23b (+). A histidine-tagged fusion protein (His-nArgBP2$_{404-604}$) was produced with the pET overexpression system (Novagen, Madison, WI, USA). Transformed BL21(DE3) bacteria were grown, lysed and separated into soluble and insoluble fractions. Isopropylthio-β-galactoside (IPTG) induced bacterial expression of the fusion protein. To determine the relative solubility of the fusion protein, both

fractions were run out on SDS-PAGE and stained with Coomassie blue. The fusion protein His-nArgBP2$_{404-604}$ was insoluble. The preparation of the insoluble fusion protein was done under denaturing conditions, by solubilization of the inclusion bodies with 6 M Guanidine hydrochloride (Guanidine-HCl, Sigma) and purification on a HisBind Quick Column (Novagen), with all the solutions containing 6 M Guanidine-HCl. The Quick column eluates were dialyzed against 6 washes of 4L PBS/0.02% sodium azide at 4°C (6X 12 hours) and collected at the end of the dialysis. The histidine column-purified fusion proteins were run out via SDS-PAGE and the gel was stained using 0.05% Coomassie stain in H_2O. After several washes with H_2O, the band corresponding to the size of the fusion protein was cut from the gel and sent to Washington Biotechnology (Baltimore, MD, USA). Approximately 2.2 mg of fusion protein was sent. Polyclonal antibodies were prepared by immunizing two rabbits with the fusion protein present in the polyacrylamide gel material. Upon receipt of the serum bleeds (nArgBP2-A and nArgBP2-B, corresponding to each immunized rabbit), the antibodies were affinity-purified. More fusion protein (approximately 2 mg) was generated and purified as above. The band was excised from the gel and minced, and the fusion protein was electroeluted (model 422 Electro-Eluter, Bio-Rad, Hercules, CA, USA) and then dialyzed against coupling buffer (CB) solution (0.1 M NaHCO3, 0.1 M NaCl, pH 8.4) for 4 times with change of buffer every 12 hours, to remove Tris-containing buffer. The fusion protein was collected and concentrated to a final volume of 0.5 ml using a Centriprep column (Ultracel YM-3 membrane of 3,000 Nominal Molecular Weight Limit, Millipore, Bedford, MA, USA). 0.5 ml of 2X CB and then 4 ml CB with 1.25% SDS were added (the final concentration of SDS is 1%). 20 µl were kept as control for determination of protein concentration before coupling. 0.2 g of cyanogen bromide-activated Sepharose 4B beads (Sigma) were weighed out and allowed to swell on ice for 1 hour with 50 ml of 1 mM HCl. After shaking, the bead-acid gel was poured into an empty HisBind quick column and washed with 10 ml of cold water 5 times. The column was then washed with 5 ml of CB and the fusion protein was immediately added. The column was stopped at the top and bottom and placed sideways on a rotator for 2 hours at room temperature to allow the fusion protein to couple with the beads. The protein/SDS solution was drained into a tube and saved for determination of coupling efficiency. The column was washed 5 times with CB and then unreacted groups were blocked overnight at 4°C with 0.2 M glycine, pH 8.0. The column was then washed 5

times alternatively with CB and acetate buffer (0.1 M acetic acid, 0.1 M NaCl, pH 4.0) and then with 20 ml of PBS/0.02% sodium azide. The gel was transferred to a polyprep column (Bio-Rad) with 5 ml PBS/0.02% sodium azide. The sealed column was kept at 4°C until antibody purification. Protein solutions before and after coupling were compared by reading OD280. Protein concentration was also determined using BCA protein assay (Pierce Thermo Scientific, Rockford, IL, USA). Serum from the immunized rabbits was thawed and first purified by ammonium sulfate precipitation. Briefly, ammonium sulfate was slowly added to serum while stirring until 50% volume. The mixture was stirred overnight at 4°C and then centrifuged at 5,000 g for 30 minutes. The pellet was resuspended in 0.4 volumes of the starting serum volume and filtered (0.2 μm). The filtrate was collected and dialyzed versus three changes of PBS/0.02% sodium azide overnight at 4°C. Just prior to column purification, the column was washed with 10 bed volumes of 10 mM Tris (pH 7.5), followed by 10 bed volumes of 100 mM glycine (pH 2.2) and 10 bed volumes of 10 mM Tris buffer (pH 8.8). When the last bed volume was confirmed with litmus paper to be at pH 8.8, 10 bed volumes of 100 mM triethylamine (pH 11.5, prepared fresh) were added and then the column was washed again with 10 mM Tris Buffer (pH 7.5) until the pH reached 7.5. Serum was passed through the column 3 times, followed by 30 bed volumes of 10 mM Tris (pH 7.5) and 30 bed volumes of 10 mM Tris/500 mM NaCl (pH 7.5). Acid-sensitive antibody-antigen interactions were broken with 10 bed volumes of 100 mM glycine (pH 2.2) and eluted into a tube containing 30% of the elution volume of 1 M Tris (pH 8.0). The column was then washed with 10 mM Tris (pH 8.8) until a pH of 8.8 was recorded at the outflow. The antibodies bound by base-sensitive interactions were eluted by passing 10 bed volumes of 100 mM triethylamine (pH 11.5, prepared fresh) through the column. The antibodies were collected in a tube containing 15% of the elution volume of 1 M tris (pH 6.0). Antibody fractions were combined, dialyzed against PBS/0.02% sodium azide (4X 12 hours) and collected. Antibody concentration was determined by BCA protein assay (Pierce Thermo Scientific) and the antibody was diluted to 250 μg/ml in 0.2% bovine serum albumin (BSA, Sigma)/PBS.

Evaluation of antibody specificity

In order to confirm that the rabbit polyclonal antibody generated is able to recognize the nArgBP2 protein, HEK cells were plated in 6-well plates and transfected

with a total of 2 µg DNA and 2 µl Lipofectamine 2000 (Invitrogen, Carlsbad, CA, USA) per well. 36 hours after transfection, cells were lysed with SDS-PAGE loading buffer. nArgBP2-A and nArgBP2-B rabbit polyclonal antibodies (1:1000, incubation overnight at 4°C) were tested on lysates from HEK cells that were either non-transfected, transfected with pCINeo-Myc-nArgBP2 or empty vector (control). Secondary antibody Peroxidase-conjugated Donkey Anti-Rabbit IgG (Jackson ImmunoResearch Lab, West Grove, PA, USA) was added at 1:20000 dilution and incubated 4 hours at RT. Western development was perform by incubating the membrane with ECL Plus (Amersham) and imaged in a STORM 860 (GE Healthcare). Only nArgBP2-A recognized a specific band.

Fluorescent immunohistochemistry

P14, P21 and adult (3 months-old) mice were deeply anesthetized with isofluorane and perfused with Lactated Ringer's solution followed by 4% PFA (in PBS). Brains were dissected and post-fixed overnight in the same solution. 50 µm sagittal sections were cut using a vibratome (Pelco 102, Ted Pella, Redding, CA). Sections were washed 3X 5 minutes in PBS and then blocked for 1 hour with blocking buffer (5% normal goat serum [Sigma], 2% BSA [Sigma] and 0.2% triton X-100 (Sigma) in PBS). Sections were incubated with primary antibody (nArgBP2-A, 1:100) overnight at 4°C, washed 3X 20 minutes in PBS and then incubated for 4 hours with Alexa Fluor 488 goat anti-rabbit secondary antibody (Invitrogen/Molecular Probes, Carlsbad, CA, USA) diluted 1:1000 in blocking solution. Following secondary antibody incubation, sections were washed 3X 20 minutes in PBS and mounted with PPD solution (1mg/mL para-phenylenediamine [ICN, Aurora, OH] in 90% glycerol/PBS). For P0 and P7 brains, 10 µm sections were cut from freshly frozen brains on a cryostat at -19°C and mounted on gelatin-coated Superfrost Microscope slides (Fisher Scientific). The sections were fixed in 4% (PFA) in PBS for 10 minutes at RT. From this step on, the procedure is similar as above. Images were collected on a Zeiss Axioskop 2 Plus (Carl Zeiss, Thornwood, NY, USA) with a Zeiss Neofluar 4X objective using a Zeiss Axiocam digital camera (Carl Zeiss). Images were assembled and processed using Adobe Photoshop (Adobe Systems, San Jose, CA, USA).

Neuron Culture and Fluorescent immunocytochemistry

Hippocampal neurons from P2 mice were co-cultured with rat astrocytes in a "sandwich" format at the density of 12,500 cells/cm2 as described previously (Kaech and Banker, 2006). Neurons were fixed in 4% PFA, 4% sucrose in PBS solution for 20 minutes at 4°C and subsequently permeabilized with 0.2% Triton X-100 in PBS for 10 minutes at 4°C. Neurons were then blocked with 5% BSA, 15% normal goat serum in PBS solution for 1 hour at RT. Primary antibodies diluted in blocking buffer were added and incubated overnight at 4°C. Neurons were then washed four times with blocking buffer for 5 minutes each. Secondary antibodies (Invitrogen/Molecular Probes) were diluted 1:1000 in blocking buffer and incubated with neurons for 1 hour at RT. Coverslips were then washed four times with PBS, one time with water and then mounted on glass slides using ProLong Gold Antifade Reagent (Invitrogen). The primary antibodies were diluted in blocking buffer and used at the following dilutions: nArgBP2-A rabbit polyclonal, 1:200; anti-PSD-95 mouse monoclonal IgG2a (clone 6G6-1C9, Thermo Scientific), 1:400; anti-synapsin 1/2 guinea pig polyclonal antiserum (Synaptic Systems, Göttingen, Germany), 1:1000; anti-gephyrin mouse monoclonal, hybridoma supernatant from mAb7a cell line (Synaptic Systems), 1:800. These primary antibodies were recognized by the following secondary antibodies: goat anti-rabbit Alexa488, goat anti-mouse Alexa555 and goat anti-guinea pig Alexa647.

Images were captured by using Olympus Fluoview FV1000 confocal microscope with 60x objective (UPlanSApo, 1.35 oil) at the 1024x1024 pixel resolution. Images were acquired as a Z-stack with 0.50 um interval for a total depth of 2 μm. Maximum intensity projections were then formed from the Z-stacks.

Postsynaptic density isolation

The PSD fraction of forebrain was prepared as described (Welch et al., 2004; Ehlers, 2003) with slight alterations. All the steps in the protocol are done at 4°C. Approximately 200 mg of mouse forebrain was homogenized in 3 ml of a solution containing HEPES-buffered sucrose (HBS, 4 mM HEPES, 0.32 M sucrose, pH 7.4) with a protease inhibitor cocktail (Roche, 11873580001) and two phosphatase inhibitor cocktails (Sigma, P2850, P5726) using a motor driven glass-teflon homogenizer for 30 strokes at ± 900 rpm. The homogenates were then centrifuged at 700 g for 15 minutes

to remove the pelleted nuclear fraction (P1). The supernatant was collected (S1) and this step was repeated, collecting the supernatant again (S2). This fraction corresponds to the Brain Lysate. The resulting supernatant (S1) was centrifuged at 18,000 g for 15 minutes to yield a pellet corresponding to the crude synaptosomal membrane (P2). The pellet was resuspended in 1 ml HBS and centrifuged at 18,000 g for 15 minutes to yield the pelleted washed crude synaptosomal fraction (P2'). The pellet was then lysed by osmotic shock by adding 3 ml of cold 4 mM HEPES, pH 7.4 and by applying 8 strokes of glass-teflon homogenizer to pooled samples followed by mixing in an orbital shaker for 1 hour. Samples were centrifuged at 25,000 g for 20 minutes to yield a supernatant (crude synaptic vesicle fraction, S3) and a pellet (lysed synaptosomal membrane fraction, P3). P3 was then well resuspended in 100 µl of HBS. P3 was then layered on top of a discontinuous sucrose gradient of 0.8, 1.0 and 1.2 M (500 µl each layer) and centrifuged at 150,000 g for 2 hours. The synaptic plasma membrane (SPM) fraction was obtained by extracting the layer between the 1.0 and 1.2 M sucrose gradient, diluted by adding 2.5 volumes of 4 mM HEPES, pH 7.4 (with protease and phosphatase inhibitors) and pelleted by centrifugation at 150,000 g for 30 minutes. Pellet (SPM) was resuspended in 500 µl of 50 mM HEPES, 2 mM EDTA, pH 7.4 (with protease and phosphatase inhibitors) and Triton X-100 was added to 0.5% and mixed. After rotating at 4°C for 15 minutes, samples were centrifuged at 32,000 g for 20 minutes to yield the PSD-1T fraction (pellet). PSD-1T was resuspended in 500 µl of 50 mM HEPES, 2 mM EDTA, pH 7.4 (with protease and phosphatase inhibitors), Triton X-100 was added to 0.5% and mixed. After rotating at 4°C for 15 minutes, samples were centrifuged at 200,000 g for 20 minutes to yield the PSD-2T fraction (pellet). PSD-2T was recovered is 100 µl of 50 mM HEPES, 2 mM EDTA, pH 7.4 (with protease and phosphatase inhibitors). Protein concentration was determined using BCA protein assay (Pierce Thermo Scientific).

Results

Expression of ArgBP2 and nArgBP2 in the mouse brain

To assess the expression of the different ArgBP2 isoforms by mRNA *in situ* hybridization, we designed one probe for a region in common among ArgBP2 mRNA isoforms in order to detect the expression of both neuronal and non-neuronal forms, and a second probe to specifically identify the neuronal specific form - nArgBP2- . This was achieved by taking advantage of the unique region expressed in this isoform. Bioinformatic analysis reveals that there is no unique region exclusively expressed in non-neuronal forms of ArgBP2; therefore, a “non-neuronal” probe could not be generated. To comparatively assess mRNA expression in the adult mouse brain we collected serial sections from adult mice and performed probe incubations and signal development in parallel for both probes. In situ mRNA hybridization of adult mouse sections revealed that ArgBP2 is highly expressed in several brain regions (Fig. 1A). Expression of nArgBP2 was largely equivalent and most areas displayed a signal intensity comparable to that of the common region probe (Fig. 1E).

ArgBP2 labeling in the olfactory bulb was abundant in glomerular cell layer (Gl) and mitral cell layer (ML) (Fig. 1B). Labeling for nArgBP2 in the same regions was present but the signal intensity was slightly less intense when compared to the probe for the common region (Fig. 1F). High levels of expression of ArgBP2/nArgBP2 were seen in cortical layers II/III and VI, but only few cells in cortical layer V express these transcripts (Fig. 1C, G). Very high levels of expression of ArgBP2/nArgBP2 are present in the hippocampal formation, including CA1 and CA3 pyramidal neurons and dentate gyrus granule cells (Fig. 1D, H). Both probes detect high levels of mRNA expression in the striatum. In the thalamus, sparse but strong labeling was observed for individual cells using both probes (Fig. 1A, E). Differential expression was observed between the two probes in the cerebellum. In this region, ArgBP2 but not ArgBP2 was strongly expressed in the granule cell layer (gcl) (Fig. 1A, E). Dendritic targeting of ArgBP2/nArgBP2 mRNA was not observed, since no signal was detected in cortical layer I or in the molecular layer in the hippocampal formation.

nArgBP2 is the main neuronal form in the mouse brain with the exception of the cerebellum

After observing largely similar expression pattern between ArgBP2 and nArgBP2 probes we postulated that nArgBP2 would be the main isoform in the brain contributing to the overall ArgBP2 signal. To test this, we used serial sections to assess the differential expression of ArgBP2/nArgBP2 in P21 mice (Fig. 2A). A qualitative assessment of these differences was achieved by comparing sections from the same mouse and digitally subtracting the signal of nArgBP2 from the signal of total ArgBP2 (Fig. 2B) (total ArgBP2 minus nArgBP2). This manipulation estimates the signal intensity and regional differential expression of non-neuronal forms of ArgBP2. We observed that the expression of non-neuronal ArgBP2 is mostly concentrated in the mouse cerebellum ganglion cell layer. In all other brain regions, nArgBP2 is the predominant form (Fig. 2B).

Detailed mRNA expression of nArgBP2 across serial mouse brain sections

After determining that nArgBP2 is the main form expressed in the mouse brain we performed a detailed in situ mRNA across coronal and sagittal sections to determine expression in discrete nuclei (Fig. 3). We found that expression in the amygdala was abundant and at high expression levels; including in the anterior (BLA) to posterior (BLP) basolateral and basomedial amygdaloid nucleus (BMP) (Fig. 3A, D, E). Expression of nArgBP2 was also found in the habenula (Hb) and some sparse expression was found in the hypothalamic nuclei (MH) (Fig. 3B, F, G). Finally, strong labeling was observed in the dorsal part of the lateral septal nucleus, dorsal (LSD) (Fig. 3H) and the piriform cortex (Pir) (Fig. 3I).

Characterization of an anti-nArgBP2 specific antibody

nArgBP2 is unique due to the inclusion of a single exon which codes for a 606 amino acid section of the protein. We produced a specific antibody designed to recognize nArgBP2 through the use of a recombinant antigen consisting of the first 201 amino acids of this region (Fig. 4A). Bioinformatic analysis revealed that this protein sequence displays high levels of antigenicity and does not share homology with other known proteins, with the exception of the nArgBP2 mammalian orthologous. To assess

specificity, the antibody was tested against the lysate of HEK cells transfected with a nArgBP2 expression vector (Fig. 4B). The antibody was also used to recognize nArgBP2 after overexpression in high density hippocampal neuron cultures at DIV 8 (Fig. 4C). After overexpression, nArgBP2 was found in the cell body, nucleus, dendritic processes and spines of transfected neurons (Fig. 4C). Endogenous protein expression was also observed in nearby non-transfected neurons (Fig. 4C – star). To assess the recognition of endogenous protein in brain tissue we performed western blotting in samples of brain lysate, synaptosomal plasma membrane (SPM) and twice washed Triton X-100-extracted postsynaptic density (PSD-2T) fraction.

A single protein band of approximately 180kD was detected across all fractions. The apparent molecular weight of this band is consistent with predicted amino acid composition for nArgBP2 (Fig. 4D). We also observed an enrichment of nArgBP2 across the PSD purification gradient (Fig. 4D). Together, these results demonstrate a high specificity for the anti-nArgBP2 antibody and confirm the enrichment of nArgBP2 at the PSD.

Localization and enrichment of nArgBP2 protein in the mouse brain

Using the anti-nArgBP2 specific antibody, we next characterized the expression pattern of nArgBP2 at the protein level in the mouse brain across five developmental time-points: P0, P7, P14, P21 and 3 months-old (Fig. 5 and Fig. 6). Neonatal (P0) expression of nArgBP2 was mostly restricted to the dentate gyrus with some low-level expression in the striatum (Fig. 5A). At P7, there was strong expression in the hippocampus, the striatum and olfactory bulb, but low levels of expression of nArgBP2 in cortical layers (Fig. 5B). In the cortex, expression was mostly prevalent in layer IV cells. Expression in layers I, II/III and VI was low at P7. Notably, layer V cortical neurons and the cerebellum region do not express significant levels of nArgBP2, confirming the results observed from mRNA in situ hybridization. At P14 and P21, nArgBP2 was strongly detected in the hippocampal formation, the striatum and cortical layers I, II/III, IV and VI (Fig. 5C-D). After P14, moderate levels of expression can also be found in several thalamic nuclei (Fig. 5D). We also examined the expression of nArgBP2 across parasagittal and coronal section in adult mice to examine enrichment in specific nuclei (Fig. 6A-B). In the olfactory bulb, low levels of expression were observed in glomeruli (Fig. 6C) and in the accessory olfactory bulb (AOB) (Fig. 6A). In

the adult brain, highest levels of expression were present in cortical layers II/III and IV (Fig. 6D), the striatum (Fig. 6E), the amygdala (Fig. 6F), in the habenula (Hb) (Fig. 6G) and in the superior paraolivary nucleus (SPON) (Fig. 6H). In the striatum, nArgBP2 is particularly enriched in sparse, patch-like islands reminiscent of striosomes (St) (Graybiel, 1984). In the thalamus, low levels of expression were observed in the ventral thalamic nuclei (VTN) (Fig. 6I). Low levels of expression were found in the medial hypothalamus (MH), but high expression levels in the arcuate hypothalamic nucleus (Arc) (Fig. 6J). Finally, one distinct pattern was observed in the strong labeling of nArgBP2 at the outer molecular layer of the dentate gyrus (Fig. 6K).

nArgBP2 is present in excitatory but not inhibitory synapses

We next investigated if, at the cellular level, nArgBP2 localizes to both excitatory and inhibitory synapses. Using low-density DIV 14 hippocampal neuron cultures we performed a triple staining for endogenous nArgBP2, gephyrin and the ubiquitous presynaptic marker synapsin (Fig. 7A-D). Gephyrin is a component of the postsynaptic network in glycinergic and gabaergic synapses (Feng et al., 1998; Jacob et al., 2005). We observed that nArgBP2 does not co-localize with gephyrin (Fig. 7A'-D'). To assess if nArgBP2 is present at excitatory synapses, we performed a triple staining for nArgBP2, the excitatory postsynaptic marker PSD-95 and synapsin (Fig. 8A-D). We observed that nArgBP2 strongly co-localizes with PSD-95 (Fig. 8A'-D'). Moreover, a high magnification analysis, reveals the expected apposition between synapsin and PSD-95 and a superimposition of the nArgBP2 signal on PSD-95 puncta (Fig. 8A''-D''). This result suggests that nArgBP2 is localized to the postsynaptic compartment but is concentrated distally to PSD-95 and the postsynaptic membrane (Fig. 8E). Core PSD proteins, such PSD-95, are usually localized within a few nanometer of the postsynaptic cleft (Petersen et al., 2003). At the same time, the more distal localization of nArgBP2 is consistent with its role in interacting with actin regulatory proteins at the interface of the PSD and the actin cytoskeleton.

Discussion

In this study we have presented a detailed characterization on the expression of ArgBP2 in the mouse brain. We observed that nArgBP2 is the main ArgBP2 isoform present in the central nervous system and that there is a differential expression of this

isoform across development. In the adult brain, nArgBP2 mRNA and protein are specifically enriched in discrete regions and nuclei, such as the habenula, striasomes and the outer molecular layer of the dentate gyrus. We also observed that nArgBP2 is specifically localized to glutamatergic synapses but not to inhibitory gabaergic or glycinergic synapses.

While the functional role of the protein section coded by the brain specific exon is still unknown, this section is selectively included in nArgBP2 transcripts. We also found that nArgBP2 is not significantly expressed in the cerebellum as whole. Interestingly, at the synaptic level it is known that there are striking differences in the composition in cerebellar PSD proteins when comparing to forebrain PSDs. Examples include CAMKII and Shank3, which among other PSD proteins, are known to be differentially expressed between these two anatomical regions (Cheng et al., 2006; Miller and Kennedy, 1985). Interestingly, the Shank family of proteins and nArgBP2 share other similarities. Both are large proteins with multiple protein-protein interaction domains, both interact with the SAPAP family of proteins (Kawabe et al., 1999; Naisbitt et al., 1999) and both mediate the interaction between core PSD proteins and actin regulatory elements (Bockers et al., 2001; Cestra et al., 2005; Park et al., 2003; Ronty et al., 2005). Recently, we have investigated the role these two key proteins in the PSD complex where nArgBP2 is inserted. Characterization of SAPAP3 and Shank3 uncovered an important role for these scaffolding proteins in synaptic function and behavior (Peca et al., 2011; Welch et al., 2007; Welch et al., 2004). Therefore, it will be important to understand if nArgBP2, a member of the Shank3-SAPAP3 complex, may also play a role in the regulation of glutamatergic synapses. Here, we presented a first step into better understanding the role of nArgBP2 in the murine brain though its neuroanatomical characterization.

One interesting finding in this characterization work is the observation of a strong local enrichment of nArgBP2 in the dentate gyrus. Afferent enervation to the dentate gyrus segregates mainly into the lateral perforant pathway from entorhinal cortical neurons which synapses on dendrites extending into the outer molecular layer, and anterior commissure fibers which make connections with proximal synapses in the inner molecular layer of dentate granule cells (Forster et al., 2006). The enrichment of nArgBP2 at the outer molecular layer in the dentate gyrus could signify either enrichment in presynaptic terminals from the lateral perforant pathway or a differential

postsynaptic enrichment in granule cells distal synapses. Evidences supporting the latter come from the observation that nArgBP2 is enriched in postsynaptic density fractions and its co-localization with PSD-95 but not with synapsin. Additionally, at P0 ArgBP2 is highly expressed in the dentate gyrus, but virtually absent from other brain regions, including the entorhinal cortex, suggesting again that this enrichment may arise from a postsynaptic mechanism. Notably, the actin dynamics in the dentate gyrus molecular layer are known to work independently between layers and selectively respond to electrical stimuli originating in different excitatory pathway (Fukazawa et al., 2003). Therefore, it is interesting to speculate that the enrichment of nArgBP2 may mediate the segregation of layer specific postsynaptic mechanisms.

The demonstration that nArgBP2 is not present in inhibitory synapses further supports evidences that inhibitory postsynaptic protein networks specialization are profoundly different in their biochemical composition when compared to PSD network at excitatory synapses (Kneussel and Betz, 2000; Kneussel and Loebrich, 2007; Ryan and Grant, 2009; Sheng and Hoogenraad, 2007). Interestingly, there are increasing evidences pointing to the role of multiple PSD proteins in synaptic dysfunction and disease. Multiple lines of evidences have linked dysfunction in PSD proteins with neural disorders. It is estimated that from the over 1000 different PSD proteins, a large number of these are associated with one or more of 130 neurological phenotypes (Bayes et al., 2011). Interestingly, in silico and meta-analysis studies have shown that proteins known to play a role in disease afford its biochemical interaction partners a higher probability of also playing a pathological role (Barabasi et al., 2011; Goh et al., 2007; Linghu et al., 2009; Oti et al., 2008). Shank3 plays a key role in the development of autism spectrum disorders and also schizophrenia (Durand et al., 2007; Gauthier et al., 2010; Peca et al., 2011). Similarly, SAPAP3 also plays an important role in the normal maturation of glutamatergic PSDs and mutations in this gene may be responsible for a susceptibility to obsessive-compulsive behaviors (Bienvenu et al., 2009; Boardman et al., 2010; Welch et al., 2007; Zuchner et al., 2009). Therefore, studies aimed at understanding the *in vivo* role of nArgBP2 and a possible link to human disorders are critical to address. Our present work established a detailed characterization of this protein and identifies the brain regions where nArgBP2 may exert its endogenous function.

Figure 1

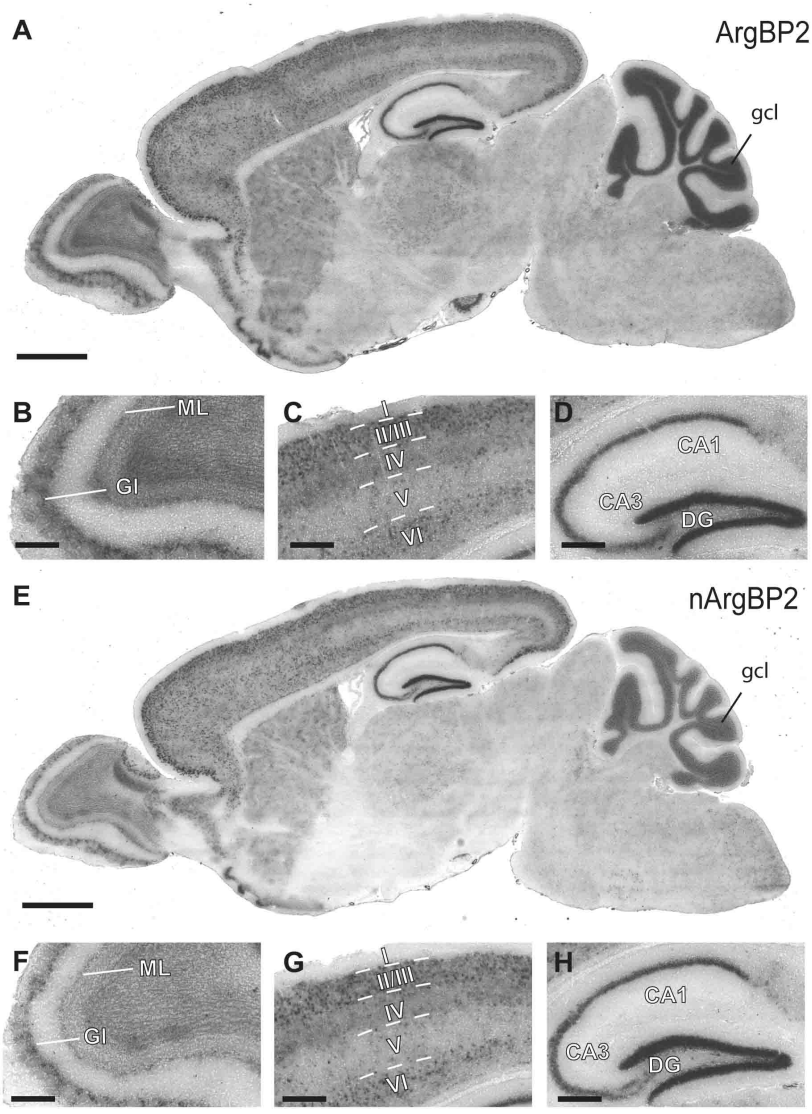
A
ArgBP2
gcl
B
ML
Gl
C
I
II/III
IV
V
VI
D
CA1
CA3
DG
E
nArgBP2
gcl
F
ML
Gl
G
I
II/III
IV
V
VI
H
CA1
CA3
DG

Figure 2

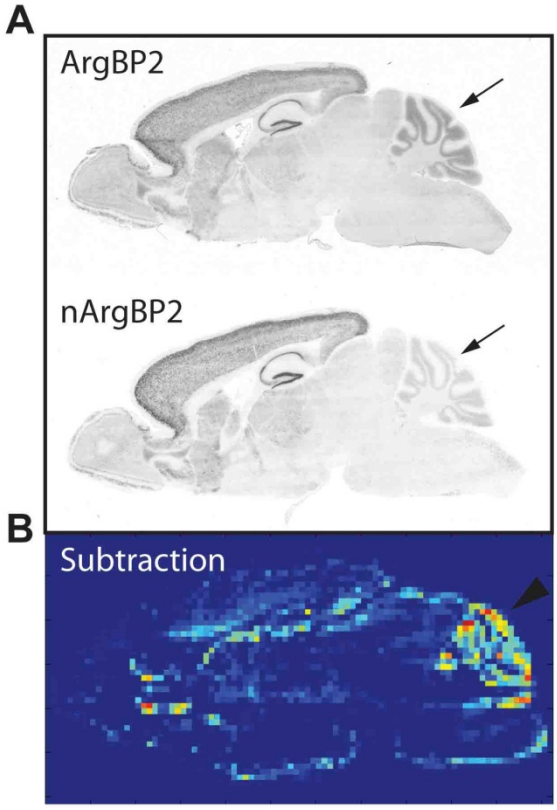

Figure 3

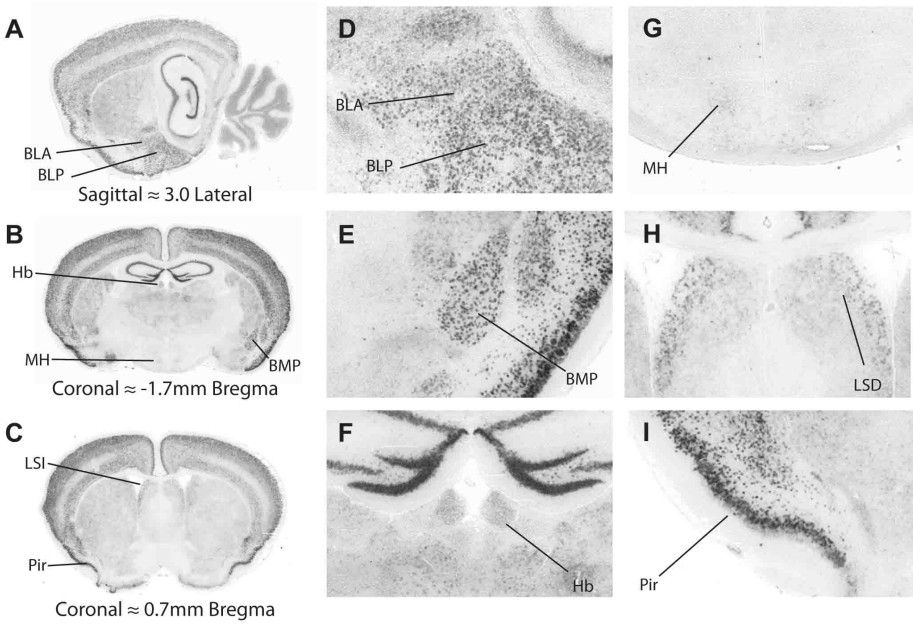
A
BLA
BLP
Sagittal ≈ 3.0 Lateral
B
Hb
MH
BMP
Coronal ≈ -1.7mm Bregma
C
LSI
Pir
Coronal ≈ 0.7mm Bregma
D
BLA
BLP
E
BMP
F
Hb
G
MH
H
LSD
I
Pir

Figure 4

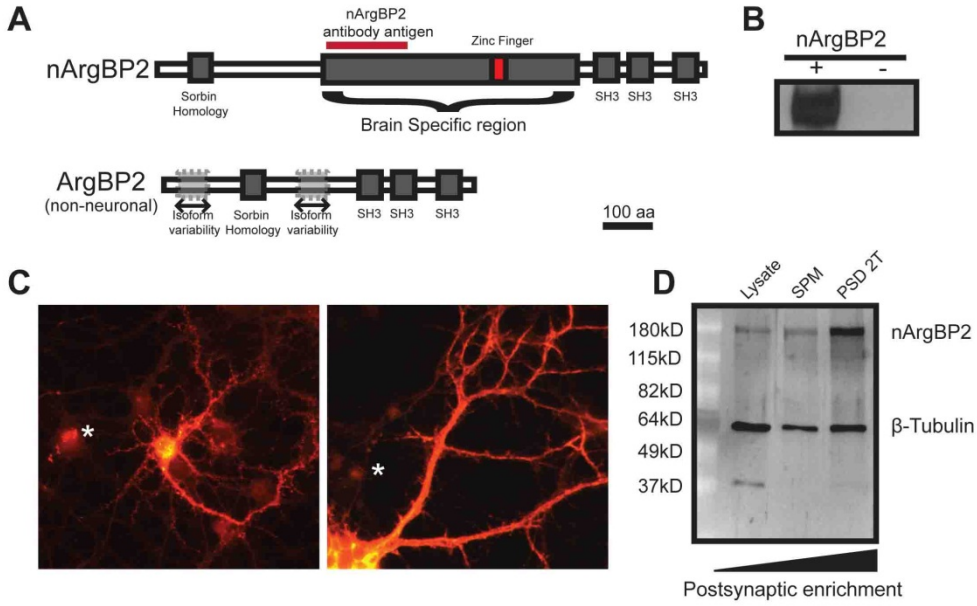
A
nArgBP2
antibody antigen
Zinc Finger
nArgBP2
Sorbin
Homology
SH3 SH3 SH3
Brain Specific region
ArgBP2
(non-neuronal)
Isoform
variability
Sorbin
Homology
Isoform
variability
SH3 SH3 SH3
100 aa
B
nArgBP2
+ -
C
D
Lysate
SPM
PSD 2T
180kD
115kD
82kD
64kD
49kD
37kD
nArgBP2
β-Tubulin
Postsynaptic enrichment

Figure 5

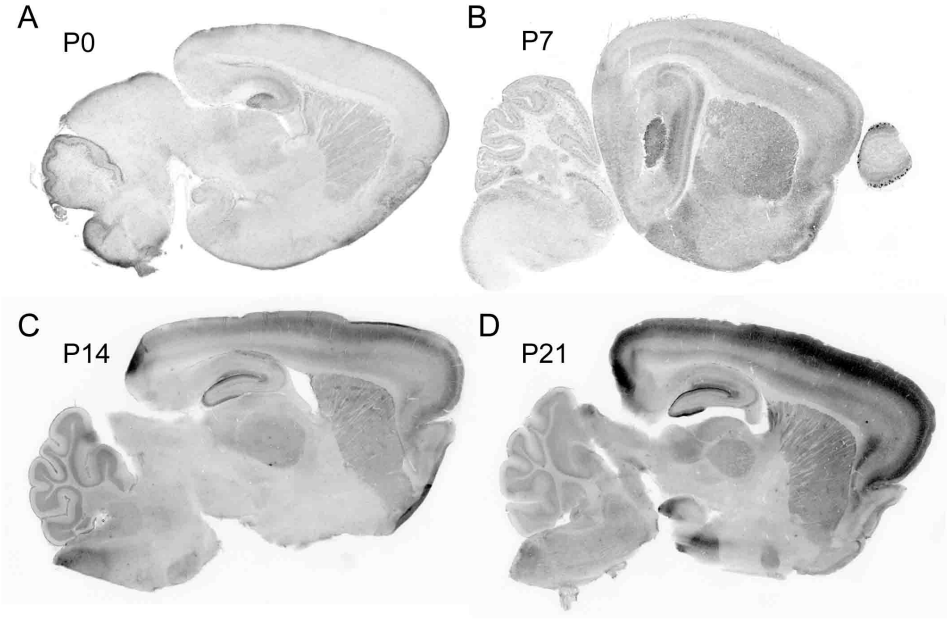

Figure 6

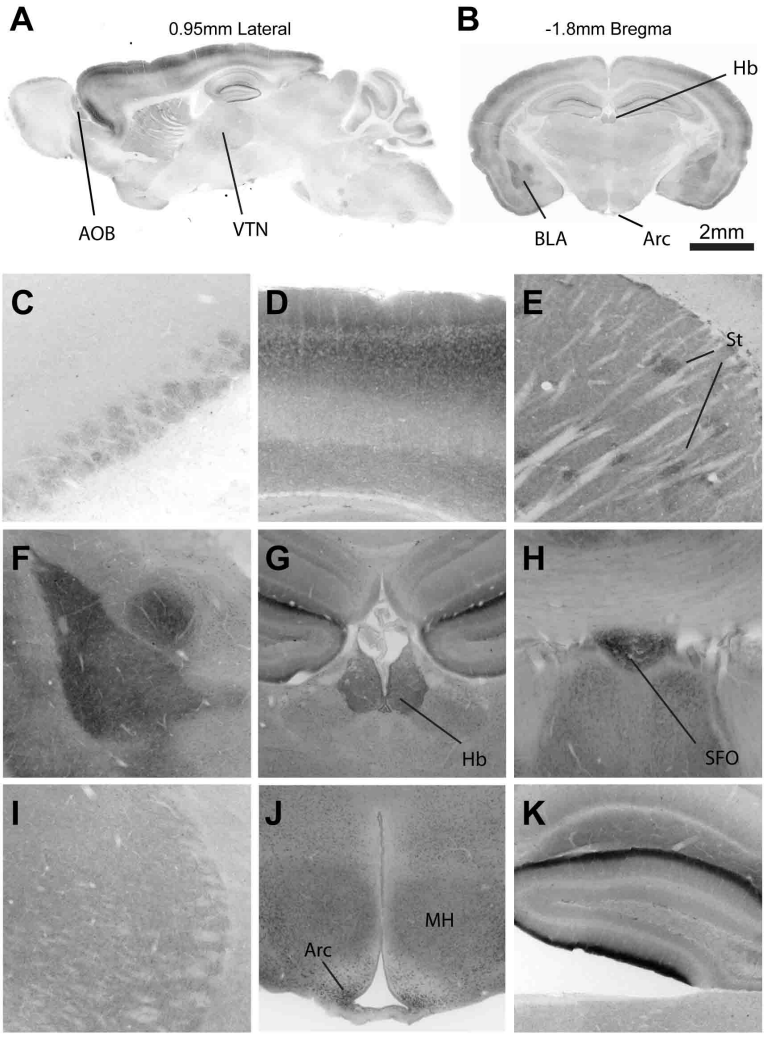
A
0.95mm Lateral
AOB
VTN
B
-1.8mm Bregma
Hb
BLA
Arc
2mm
C
D
E
St
F
G
Hb
H
SFO
I
J
MH
Arc
K

Figure 7

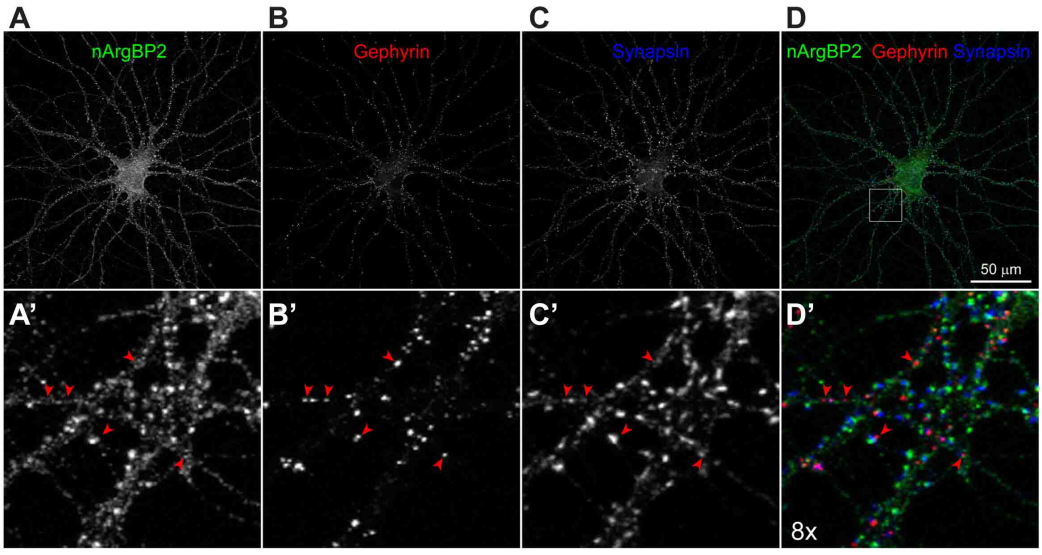
A
B
C
D
nArgBP2
Gephyrin
Synapsin
nArgBP2 Gephyrin Synapsin
50 µm
A'
B'
C'
D'
8x

Figure 8

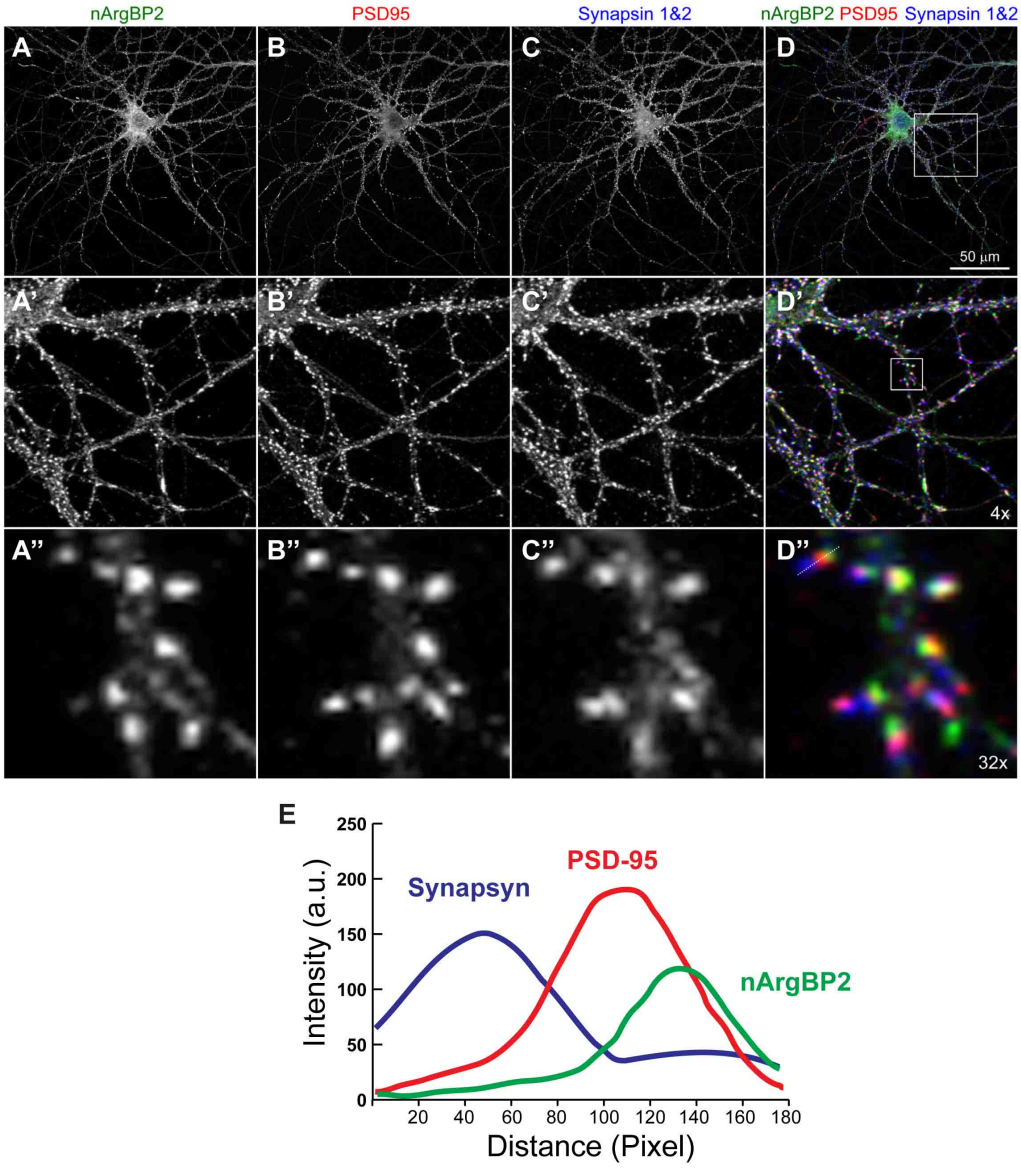
nArgBP2
PSD95
Synapsin 1&2
nArgBP2 PSD95 Synapsin 1&2
A
B
C
D
50 µm
A'
B'
C'
D'
4x
A''
B''
C''
D''
32x
E
PSD-95
Synapsyn
nArgBP2
Intensity (a.u.)
250
200
150
100
50
0
20
40
60
80
100
120
140
160
180
Distance (Pixel)

Figure Legends

Figure 1 – Expression of ArgBP2 and nArgBP2 mRNA in the adult mouse brain. A, In situ mRNA hybridization for ArgBP2 transcripts in a parasagittal whole brain section from a 3 month old C57/B6 mouse. B, The olfactory bulb displays ArgBP2 labeling in the glomeruli layer and mitral cell layer. C, High magnification image from cortical layers demonstrate a dense labeling in layers II/III, IV and VI, but a sparse labeling in layer V. D Hippocampal formation presents strong labeling for ArgBP2 in cell bodies of CA1, CA3 and dentate gyrus granule cell layer. E, In situ hybridization for nArgBP2 mRNA in a parasagittal whole brain section from a 3 month old C57/B6 mouse. F, Olfactory bulb displays some nArgBP2 labeling in the glomeruli layer and mitral cell layer. G, Cortical layers present a dense labeling for nArgBP2 in layers II/III, IV and VI, but a sparse labeling in layer V. H, Hippocampal formation is strongly labeled for nArgBP2 in cell bodies of CA1, CA3 dentate gyrus granule cell layer. Scale bar, 1mm for A and E, and 300 μm for B-D and F-H. For abbreviations see list.

Figure 2 – nArgBP2 is the main ArgBP2 form in the mouse brain with the exception of the cerebellum. A, Sections from a P21 brain were used to detect ArgBP2 and nArgBP2. B, Digital subtraction of ArgBP2 signal minus nArgBP2 signal reveals that non-neuronal ArgBP2 is mainly expressed in the cerebellum (B) (arrow). In remain regions, nArgBP2 is the dominant form. Images were pixelated to smooth cellular level differences.

Figure 3 – Expression of nArgBP2 transcripts in discrete brain nuclei in the adult mouse brain. A-C, nArgBP2 in parasagittal section (A) and coronal sections (B-C). D-I nArgBP2 is strongly expressed in the amygdala, including the anterior basolateral amygdaloid nucleus (BLA) and the posterior basolateral amygdaloid nucleus (BLP) (D-E). nArgBP2 mRNA is strongly detected in the habenula (F), and some expression is detected the hypothalamus (G). In midline coronal sections, nArgBP2 mRNA is expressed in the lateral septal nucleus (H) and the piriform cortex (I).

Figure 4 – Generation and characterization of an anti-nArgBP2 antibody. A, ArgBP2 and nArgBP2 isoforms express a sorbin homology domain and three SH3 domains, additionally; nArgBP2 includes a large region with a zinc finger domain. The anti-nArgBP2 antibody was designed for the brain specific region. B, Antibody immunoblot

against lysates from HEK cells transfect with a nArgBP2 expression plasmid or empty vector. C, Immunocytochemistry of hippocampal neurons in culture transfected with nArgBP2 expression plasmid and non-transfected neurons (asterisk). D, Anti-nArgBP2 antibody detects a single band in brain lysate, synaptosomal plasma membrane (SPM) and twice Triton X-100-extracted postsynaptic density (PSD-2T) fraction purified from mouse brain.

Figure 5 – Protein expression of nArgBP2 across development. A, At P0, nArgBP2 protein is expressed in the hippocampus and in the striatum. B, At P7, nArgBP2 is strongly expressed in the striatum, hippocampus and olfactory bulb and with moderately expressed in the cortex. C-D, nArgBP2 expression at P14 (C) and P21 (D) is concentrated in the hippocampal formation, cortical layers I, II/III, IV and VI, the striatum and several thalamic nuclei.

Figure 6 – Detailed characterization of nArgBP2 protein expression in the adult mouse brain. A-B, Fluorescent immunohistochemistry reveals that nArgBP2 is enriched in several nuclei in the central nervous system. These include the accessory olfactory bulb (AOB), ventral thalamic nuclei (A) and amygdala (B). C-K, nArgBP2 expression is present in the glomeruli in the olfactory bulb (C), and layer II/III, IV and VI in the cortex (D), the striatum (E), amygdala (F), habenula (G), superior paraolivary nuclei (H), low levels of expression in the thalamus (VTN) (I) and hypothalamic nucleus, but high levels of expression in the arcuate nucleus (J). Very high levels of expression of nArgBP2 are seen in the outer molecular layer in the dentate gyrus (K).

Figure 7 – nArgBP2 does not co-localize with gephyrin at inhibitory synapses. A-D, Triple staining for endogenous nArgBP2 (A), gephyrin (B) and synapsin (C) in low density hippocampal neuron cultures. A'-D' High power magnification indicates that puncta from gephyrin and nArgBP2 do not co-localize at postsynaptic sites. Scale bar 50μm.

Figure 8 – nArgBP2 co-localizes with PSD-95 at excitatory synaptic sites. A-D, Triple staining for endogenous nArgBP2 (A), PSD-95 (B) and synapsin (C) in low density hippocampal neuron cultures. A'-D' 4x magnification indicate that nArgBP2 and PSD-95 strongly localize to synaptic sites. A''-D'' Higher power magnification reveals an apposition between synapsin and PSD-95 and a strong overlap between PSD-95 and

nArgBP2 at postsynaptic sites. E, Analysis of signal intensity across pixel distance indicates that the signal peak for synapsin and PSD-95 is segregated, PSD-95 and nArgBP2 strongly co-localize although nArgBP2 signal peak is more distanced from the synapsin peak. Scale bar 50µm.

References

Barabasi AL, Gulbahce N, Loscalzo J. 2011. Network medicine: a network-based approach to human disease. Nat Rev Genet 12(1):56-68.

Bayes A, van de Lagemaat LN, Collins MO, Croning MD, Whittle IR, Choudhary JS, Grant SG. 2011. Characterization of the proteome, diseases and evolution of the human postsynaptic density. Nat Neurosci 14(1):19-21.

Bienvenu OJ, Wang Y, Shugart YY, Welch JM, Grados MA, Fyer AJ, Rauch SL, McCracken JT, Rasmussen SA, Murphy DL, Cullen B, Valle D, Hoehn-Saric R, Greenberg BD, Pinto A, Knowles JA, Piacentini J, Pauls DL, Liang KY, Willour VL, Riddle M, Samuels JF, Feng G, Nestadt G. 2009. Sapap3 and pathological grooming in humans: Results from the OCD collaborative genetics study. Am J Med Genet B Neuropsychiatr Genet 150B(5):710-720.

Boardman L, van der Merweb L, Lochner C, Kinneara CJ, Seedatd S, Steind D, J,, Moolman-Smook JC, Hemmings SMJ. 2010. Investigating SAPAP3 variants in the etiology of obsessive-compulsive disorder and trichotillomania in the South African white population. Comprehensive Psychiatry (in press).

Bockers TM, Mameza MG, Kreutz MR, Bockmann J, Weise C, Buck F, Richter D, Gundelfinger ED, Kreienkamp HJ. 2001. Synaptic scaffolding proteins in rat brain. Ankyrin repeats of the multidomain Shank protein family interact with the cytoskeletal protein alpha-fodrin. J Biol Chem 276(43):40104-40112.

Bockers TM, Segger-Junius M, Iglauer P, Bockmann J, Gundelfinger ED, Kreutz MR, Richter D, Kindler S, Kreienkamp HJ. 2004. Differential expression and dendritic transcript localization of Shank family members: identification of a dendritic targeting element in the 3' untranslated region of Shank1 mRNA. Mol Cell Neurosci 26(1):182-190.

Cestra G, Toomre D, Chang S, De Camilli P. 2005. The Abl/Arg substrate ArgBP2/nArgBP2 coordinates the function of multiple regulatory mechanisms converging on the actin cytoskeleton. Proc Natl Acad Sci U S A 102(5):1731-1736.

Cheng D, Hoogenraad CC, Rush J, Ramm E, Schlager MA, Duong DM, Xu P, Wijayawardana SR, Hanfelt J, Nakagawa T, Sheng M, Peng J. 2006. Relative and absolute quantification of postsynaptic density proteome isolated from rat forebrain and cerebellum. Mol Cell Proteomics 5(6):1158-1170.

Dillon C, Goda Y. 2005. The actin cytoskeleton: integrating form and function at the synapse. Annu Rev Neurosci 28:25-55.

Durand CM, Betancur C, Boeckers TM, Bockmann J, Chaste P, Fauchereau F, Nygren G, Rastam M, Gillberg IC, Anckarsater H, Sponheim E, Goubran-Botros H, Delorme R, Chabane N, Mouren-Simeoni MC, de Mas P, Bieth E, Roge B, Heron D, Burglen L, Gillberg C, Leboyer M, Bourgeron T. 2007. Mutations in the gene encoding the synaptic scaffolding protein SHANK3 are associated with autism spectrum disorders. Nat Genet 39(1):25-27.

Ehlers MD. 2002. Molecular morphogens for dendritic spines. Trends Neurosci 25(2):64-67.

Feng G, Tintrup H, Kirsch J, Nichol MC, Kuhse J, Betz H, Sanes JR. 1998. Dual requirement for gephyrin in glycine receptor clustering and molybdoenzyme activity. Science 282(5392):1321-1324.

Fischer M, Kaech S, Wagner U, Brinkhaus H, Matus A. 2000. Glutamate receptors regulate actin-based plasticity in dendritic spines. Nat Neurosci 3(9):887-894.

Forster E, Zhao S, Frotscher M. 2006. Laminating the hippocampus. Nat Rev Neurosci 7(4):259-267.

Fukaya M, Watanabe M. 2000. Improved immunohistochemical detection of postsynaptically located PSD-95/SAP90 protein family by protease section pretreatment: a study in the adult mouse brain. J Comp Neurol 426(4):572-586.

Fukazawa Y, Saitoh Y, Ozawa F, Ohta Y, Mizuno K, Inokuchi K. 2003. Hippocampal LTP is accompanied by enhanced F-actin content within the dendritic spine that is essential for late LTP maintenance in vivo. Neuron 38(3):447-460.

Gauthier J, Champagne N, Lafreniere RG, Xiong L, Spiegelman D, Brustein E, Lapointe M, Peng H, Cote M, Noreau A, Hamdan FF, Addington AM, Rapoport JL, Delisi LE, Krebs MO, Joober R, Fathalli F, Mouaffak F, Haghighi AP, Neri C, Dube MP, Samuels ME, Marineau C, Stone EA, Awadalla P, Barker PA, Carbonetto S, Drapeau P, Rouleau GA. 2010. De novo mutations in the gene encoding the synaptic scaffolding protein SHANK3 in patients ascertained for schizophrenia. Proc Natl Acad Sci U S A 107(17):7863-7868.

Goh KI, Cusick ME, Valle D, Childs B, Vidal M, Barabasi AL. 2007. The human disease network. Proc Natl Acad Sci U S A 104(21):8685-8690.

Graybiel AM. 1984. Correspondence between the dopamine islands and striosomes of the mammalian striatum. Neuroscience 13(4):1157-1187.

Haglund K, Ivankovic-Dikic I, Shimokawa N, Kruh GD, Dikic I. 2004. Recruitment of Pyk2 and Cbl to lipid rafts mediates signals important for actin reorganization in growing neurites. J Cell Sci 117(Pt 12):2557-2568.

Hand D, Eiden LE. 2005. Human sorbin is generated via splicing of an alternative transcript from the ArgBP2 gene locus. Peptides 26(7):1278-1282.

Jacob TC, Bogdanov YD, Magnus C, Saliba RS, Kittler JT, Haydon PG, Moss SJ. 2005. Gephyrin regulates the cell surface dynamics of synaptic GABAA receptors. J Neurosci 25(45):10469-10478.

Kaech S, Banker G. 2006. Culturing hippocampal neurons. Nat Protoc 1(5):2406-2415.

Kawabe H, Hata Y, Takeuchi M, Ide N, Mizoguchi A, Takai Y. 1999. nArgBP2, a novel neural member of ponsin/ArgBP2/vinexin family that interacts with synapse-associated protein 90/postsynaptic density-95-associated protein (SAPAP). J Biol Chem 274(43):30914-30918.

Kennedy MB. 2000. Signal-processing machines at the postsynaptic density. Science 290(5492):750-754.

Kimura A, Baumann CA, Chiang SH, Saltiel AR. 2001. The sorbin homology domain: a motif for the targeting of proteins to lipid rafts. Proc Natl Acad Sci U S A 98(16):9098-9103.

Kioka N, Ueda K, Amachi T. 2002. Vinexin, CAP/ponsin, ArgBP2: a novel adaptor protein family regulating cytoskeletal organization and signal transduction. Cell Struct Funct 27(1):1-7.

Kneussel M, Betz H. 2000. Receptors, gephyrin and gephyrin-associated proteins: novel insights into the assembly of inhibitory postsynaptic membrane specializations. J Physiol 525 Pt 1:1-9.

Kneussel M, Loebrich S. 2007. Trafficking and synaptic anchoring of ionotropic inhibitory neurotransmitter receptors. Biol Cell 99(6):297-309.

Linghu B, Snitkin ES, Hu Z, Xia Y, Delisi C. 2009. Genome-wide prioritization of disease genes and identification of disease-disease associations from an integrated human functional linkage network. Genome Biol 10(9):R91.

Miller SG, Kennedy MB. 1985. Distinct forebrain and cerebellar isozymes of type II Ca2+/calmodulin-dependent protein kinase associate differently with the postsynaptic density fraction. J Biol Chem 260(15):9039-9046.

Naisbitt S, Kim E, Tu JC, Xiao B, Sala C, Valtschanoff J, Weinberg RJ, Worley PF, Sheng M. 1999. Shank, a novel family of postsynaptic density proteins that binds to the NMDA receptor/PSD-95/GKAP complex and cortactin. Neuron 23(3):569-582.

Oti M, Huynen MA, Brunner HG. 2008. Phenome connections. Trends Genet 24(3):103-106.

Park E, Na M, Choi J, Kim S, Lee JR, Yoon J, Park D, Sheng M, Kim E. 2003. The Shank family of postsynaptic density proteins interacts with and promotes synaptic accumulation of the beta PIX guanine nucleotide exchange factor for Rac1 and Cdc42. J Biol Chem 278(21):19220-19229.

Peca J, Feliciano C, Ting JT, Wang W, Wells MF, Venkatraman TN, Lascola CD, Fu Z, Feng G. 2011. Shank3 mutant mice display autistic-like behaviours and striatal dysfunction. Nature.

Petersen JD, Chen X, Vinade L, Dosemeci A, Lisman JE, Reese TS. 2003. Distribution of postsynaptic density (PSD)-95 and Ca2+/calmodulin-dependent protein kinase II at the PSD. J Neurosci 23(35):11270-11278.

Ronty M, Taivainen A, Moza M, Kruh GD, Ehler E, Carpen O. 2005. Involvement of palladin and alpha-actinin in targeting of the Abl/Arg kinase adaptor ArgBP2 to the actin cytoskeleton. Exp Cell Res 310(1):88-98.

Ryan TJ, Grant SG. 2009. The origin and evolution of synapses. Nat Rev Neurosci 10(10):701-712.

Sala C, Piech V, Wilson NR, Passafaro M, Liu G, Sheng M. 2001. Regulation of dendritic spine morphology and synaptic function by Shank and Homer. Neuron 31(1):115-130.

Sheng M, Hoogenraad CC. 2007. The postsynaptic architecture of excitatory synapses: a more quantitative view. Annu Rev Biochem 76:823-847.

Soubeyran P, Barac A, Szymkiewicz I, Dikic I. 2003. Cbl-ArgBP2 complex mediates ubiquitination and degradation of c-Abl. Biochem J 370(Pt 1):29-34.

Tu JC, Xiao B, Naisbitt S, Yuan JP, Petralia RS, Brakeman P, Doan A, Aakalu VK, Lanahan AA, Sheng M, Worley PF. 1999. Coupling of mGluR/Homer and PSD-95 complexes by the Shank family of postsynaptic density proteins. Neuron 23(3):583-592.

Vagne-Descroix M, Pansu D, Jornvall H, Carlquist M, Guignard H, Jourdan G, Desvigne A, Collinet M, Caillet C, Mutt V. 1991. Isolation and characterisation of porcine sorbin. Eur J Biochem 201(1):53-59.

Wang B, Golemis EA, Kruh GD. 1997. ArgBP2, a multiple Src homology 3 domain-containing, Arg/Abl-interacting protein, is phosphorylated in v-Abl-transformed cells and localized in stress fibers and cardiocyte Z-disks. J Biol Chem 272(28):17542-17550.

Welch JM, Lu J, Rodriguiz RM, Trotta NC, Peca J, Ding JD, Feliciano C, Chen M, Adams JP, Luo J, Dudek SM, Weinberg RJ, Calakos N, Wetsel WC, Feng G. 2007. Cortico-striatal synaptic defects and OCD-like behaviours in Sapap3-mutant mice. Nature 448(7156):894-900.

Welch JM, Wang D, Feng G. 2004. Differential mRNA expression and protein localization of the SAP90/PSD-95-associated proteins (SAPAPs) in the nervous system of the mouse. J Comp Neurol 472(1):24-39.

Zuchner S, Wendland JR, Ashley-Koch AE, Collins AL, Tran-Viet KN, Quinn K, Timpano KC, Cuccaro ML, Pericak-Vance MA, Steffens DC, Krishnan KR, Feng G, Murphy DL. 2009. Multiple rare SAPAP3 missense variants in trichotillomania and OCD. Mol Psychiatry 14(1):6-9.

Acknowledgments

We thank S. Chatterjee for helpful discussion and support. We thank The Poitras Center for Affective Disorders Research. This work was funded by a grant from NIMH/NIH (R01MH081201), a Hartwell Individual Biomedical Research Award from The Hartwell Foundation, a Simons Foundation Autism Research Initiative (SFARI) grant Award to G.F..; and doctoral fellowships from the Portuguese Foundation for Science and Technology to C.F. (SFRH/BD/15855/2005) and J.P. (SFRH/BD/15231/2004). C.F. would like to acknowledge the support from the ‘‘Programa Gulbenkian de Doutoramento em Biomedicina’’ (PGDB, Oeiras, Portugal).

Author Contributions

C.F., J.P., Q.Z. and M.F.W. executed and analyzed the experiments. C.F. and G.F designed the experiments and wrote the paper.

Chapter 4

nArgBP2 mutant mice as a model for BPD

In the ensuing work (manuscript in preparation), Cátia Feliciano made the following contributions:

Generated mutant mouse lines

Designed experiments

Performed behavioral, staining, biochemical experiments

Participated in interpreting electrophysiology recordings and Golgi staining data

Wrote the paper

nArgBP2 mutant mice display manic-like behaviors, disrupted circadian rhythms and enhanced glutamatergic signaling

Cátia Feliciano[1,2], João Peça[1], Jonathan T. Ting[1] & Guoping Feng[1,3†]

1 - Department of Neurobiology, Duke University Medical Center, Durham, NC 27710, USA

2- Gulbenkian PhD Programme in Biomedicine, Gulbenkian Science Institute, 2781-901 Oeiras, Portugal

3 - McGovern Institute for Brain Research, Department of Brain and Cognitive Sciences, Massachusetts Institute of Technology, Cambridge, MA, 02139

† - Corresponding author – Guoping Feng (fengg@mit.edu)

Running Title: nArgBP2 mutant mice as a model for BPD

Abstract

Bipolar disorder (BPD) is a debilitating condition with strong genetic heritability. Both disruptions in circadian rhythms and in the glutamatergic system have been implicated in this disorder. However, the identification of candidate genes and the generation of animal models with face, predictive and construct validity are necessary for a deeper understanding of BPD. Here we characterize the *in vivo* consequences of disrupting the neuronal Arg/Abl-binding protein 2 (nArgBP2), a postsynaptic density protein which interacts with the SAPAP/Shank complex at glutamatergic synapses. We show that mice with a targeted deletion for nArgBP2 exhibit hyperactivity in novel environments and home cage, display increased stereotypies, reduced depressive-like behaviors and a pronounced disruption in circadian rhythms, all endophenotypes of manic-like behavior. Lithium, a drug commonly prescribed to BPD patients successfully ameliorates the circadian rhythm dysfunction and corrects the reduced depressive-like behaviors in nArgBP2 mutant mice. Furthermore, we found that mild chronic stress challenges the nArgBP2 mutants into a depressive-like phenotype. Finally, using electrophysiology and biochemistry we uncover an increase in glutamatergic signaling and in glutamate receptor subunits at the synapse. These findings demonstrate that nArgBP2 plays an important role at glutamatergic synapses and that nArgBP2 mutant animals may be a valuable model to probe BPD.

Introduction

Bipolar disorder (BPD) is a debilitating condition characterized by cyclic alterations in mood, ranging from manic and hypomanic affect to depression (American Psychiatric Association, 2000). BPD is diagnosed in patients after at least one manic episode with or without concurrent episodes of depression. Some individuals can also undergo "rapid cycling" during which manic and depressive states have been reported to alternate up to 20 times in one year (Dunner et al., 1977). Although the triggering pathological events remain unknown, human genetic studies have provided evidences for the strong heritability in BPD (Craddock and Jones, 1999; McGuffin et al., 2003). Notably, in the general population BPD is thought to afflict 0.5-1.0% of individuals (Kessler et al., 1994; Craddock and Jones, 1999). On the other hand, monozygotic twins of BPD probands have a lifetime risk of 40-70% to develop this disorder and first degree relative of probands share a risk of 5-10% (Kessler et al., 1994; Craddock and Jones, 1999). Nevertheless, the identification of causative genes for BPD has been complicated by the presence of susceptibility regions in virtually every human chromosome (Serretti and Mandelli, 2008). Therefore, the diagnostic for BPD remains solely based on behavioral manifestations.

From associated co-morbid conditions, sleep disorders are among the most prevalent in BPD (Jones, 2001). A range of 69 to 99% of patients experiencing manic episodes report a reduction in time spent sleeping and hypersomnia during depressive states (Harvey, 2008). Moreover, sleep disturbances are strong prodromal symptom of relapse into manic episodes and in the prediction of first BPD onset (Jackson et al., 2003; Duffy et al., 2007; Sierra et al., 2007). Furthermore, the link between sleep, circadian rhythms and bipolar disorder has also been modeled in mice. The $Clock^{\Delta 19}$ mutant mice display a disruption in circadian activity and also manifest several phenotypes reminiscent of manic-like behavior (Vitaterna et al., 1994; Roybal et al., 2007). Convergent evidences for the link between BPD and circadian disruption also emerge from the behavioral and molecular effects of lithium on circadian biology. Lithium salts are a common therapeutic prescribed to BPD patients, and lithium is one of the few known substances that influence circadian activity at the behavioral level, possibly through the action on the circadian nuclear receptor Rev-erbα or the signaling protein GSK3β (Abe et al., 2000; Lenox et al., 2002; Jope, 2003; Yin et al., 2006).

At the neuronal and circuit level, dysfunction in glutamatergic signaling has also garnered substantial interest as a potential underlying cause for affective mood disorders (Du et al., 2004; Alt et al., 2006; Wilson et al., 2006; Sanacora et al., 2008; Shaltiel et al., 2008). The postsynaptic density (PSD) is a critical structure in glutamatergic synapses (Kennedy, 2000; Sheng and Hoogenraad, 2007) and mutations in genes coding for PSD proteins are known to give rise to several forms of mental disorders. In particular, the synaptic macromolecular complex composed of Neurexin/Neuroligin/PSD-95/SAPAP/Shank has been linked to a large number of human neuropsychiatric disorders (Bayes et al., 2011), including autism (Durand et al., 2007; Berkel et al., 2010; Pinto et al., 2010), schizophrenia (Sudhof, 2008), obsessive-compulsive disorder (Welch et al., 2007; Zuchner et al., 2009; Boardman et al., 2010) and mental retardation (Tarpey et al., 2004; Berkel et al., 2010). Therefore, the hypothesis that interaction between molecular partners leads to the development of disorders with partially overlapping endophenotypes, suggests a landscape of interrelated disorders which may originate from overlapping molecular causation (Goh et al., 2007; Oti et al., 2008; Barabasi et al., 2011).

nArgBP2, a neuronal specific isoform of the SORBS2 gene, was identified through its interaction with the SAPAP family of proteins (Kawabe et al., 1999). nArgBP2 is phosphorylated by Abl and Arg protein-tyrosine kinases (Wang et al., 1997) and is proposed to regulate mechanisms converging on the actin cytoskeleton. nArgBP2 is synaptically enriched and well positioned to bridge the interaction between the PSD and the actin cytoskeleton (Kawabe et al., 1999; Cestra et al., 2005). At the protein structure level, nArgBP2 is composed of a conserved Sorbin homology domain (Kimura et al., 2001), a zinc finger domain and three SH3 domains near the C-terminus (Kawabe et al., 1999). The association of nArgBP2 to a complex of PSD proteins involved in other neuropsychiatric disorders (SAPAP3 in OCD (Welch et al., 2007) and Shank3 in autism (Peca et al., 2011a) highlights a potential role for this gene in related neuropsychiatric disorders. Moreover, SORBS2 localizes to a region of 4q35 implicated in bipolar disorder (Adams et al., 1998; Blair et al., 2002). Nevertheless, the *in vivo* function of nArgBP2 and its potential role in pathological conditions remains unknown. Therefore, in an effort to characterize the consequences of disrupting nArgBP2, we generated targeted mutant mice by homologous recombination in ES cells. A comprehensive behavioral analysis revealed that the nArgBP2 knockout mice display

spontaneous increased activity, increased explorative behavior, reduced depressive-like behaviors and a disruption in circadian period length. Pharmacological intervention with lithium was shown to ameliorate the behavioral phenotypes reminiscent of manic-like behavior, while conversely, challenging these animals with a paradigm of chronic stress switched them to a depressive-like state. Finally, biochemical and electrophysiological analysis uncovered an increase in glutamatergic synaptic signaling as a potential underlying source for the abnormal behaviors.

Materials and Methods

ES cells and PCR

nArgBP2 mutant mice were generated by homologous recombination in R1 mouse embryonic stem cells (Nagy et al., 1993) using standard procedures (Feng et al., 1998). The targeting vector was designed to disrupt the brain specific exon in the SORB2 gene (exon number 27; NIA mouse gene index #U009304) with the insertion of a NEO cassette. Genotypes were determined by PCR of mouse tail DNA using the primers FrtR2 (GGTTCTTTCCGCCTCAGG) and SAF (CCTGCCATGCCGCTCTGG) for the mutant allele (400 base pairs), and SAF and DelR (GTCTGGGAAGCTGTCGCAG) for the wildtype allele (300 base pairs).

Southern Blot

Southern blot of ES cells was performed according to standard methods(Feng et al., 1998). Briefly, a 1499bp probe, external to the short arm, was amplified with the following primers PF1 (CATGACGGTTCACAGCCATCTG) and PR1 (CAGGCTTGGTGGCGAGTGCC). The probe was then hybridized to XbaI-digested ES cell genomic DNA, yielding a 8kb band for the wildtype allele and a 5kb band for the mutant allele. A similar procedure was repeated for post hoc confirmation of targeting using tissue from heterozygous mutant mice.

PSD preparation and Western blot

Purification of brain lysate, synaptosomal membrane fractions and PSD fractions of mouse brain were prepared as previously described (Welch et al., 2007; Peca et al., 2011b). Briefly, 3 µg of protein sample were ran on SDS-PAGE and probed

with specific antibodies. The relative amounts of β-actin (Sigma, #A5441) or β-tubulin (Sigma, #T4026) were used as loading control. Antibodies used in these experiments include antibodies against nArgBP2 (rabbit anti-nArgBP2 generated in our lab(Feliciano et al., 2011)) PSD-93 (gift from Dr. David Bredt); PSD-95 (Abcam #ab18258); SAP102 (Calbiochem, #573902); SAPAP3 (previously described(Welch et al., 2004)); Shank3 (NeuroMab, #75-109); Homer (Chemicon, #AB5875); NR1 (BD Biosciences, #556308); NR2A (Upstate, #05-901); NR2B (Upstate, #05-920); GluR1 (Abcam, #ab31232); GluR2 (Abcam, #ab20673); mGluR1/5 (Thermo Scientific, #PA1-4663); AKT (Cell Signaling Technology, #4691); AKT-pSer473 (Cell Signaling Technology, #4058); AKT-pThr308 (Cell Signaling Technology, #2965); GSK3β (BD Biosciences, #610202); GSK3β-pSer9 (Cell Signaling Technology, #9336); PAK1 (Cell Signaling Technology, #2602); PAK1-pThr423 (Cell Signaling Technology, #2601). The antibody for SAPAP3 has been previously described (Welch et al., 2004).

Behavioral Tests

All experimental procedures were reviewed and approved by the Duke University Institutional Animal Care and Use Committee (IACUC). Animals were housed 3-5 per cage by genotype, at a constant 23 °C in a 12 h light/dark cycle (lights off at 19:00), with food and water available ad libitum. For behavioral experiments we used age-matched 3-4 months old mice. All experiments were performed by experimenters blinded to the genotype of the animals.

Immunohistochemistry

Adult mouse immunohistochemistry was performed according to standard methods (Welch et al., 2007). Briefly, 50μm thick sections were collected from PFA fixed mouse brain, incubated with the anti-nArgBP2 antibody and an Alexa Fluor 488 goat anti-rabbit secondary antibody (Invitrogen, Carlsbad, CA, USA). Images were collected on a Zeiss Axioskop 2 Plus (Carl Zeiss, Thornwood, NY, USA) with a Zeiss Neofluar 4X objective using a Zeiss Axiocam digital camera (Carl Zeiss). Images were assembled and processed using Adobe Photoshop (Adobe Systems, San Jose, CA, USA).

Motor and explorative behavior

Open field: spontaneous locomotor activity was evaluated over 60 min in an automated Omnitech Digiscan apparatus (AccuScan Instruments) as described (Peca et al., 2011b). Locomotor activity was assessed as total distance traveled (m). Anxiety-like behavior was defined by number of rearings and the time spent in the center as compared to time spent in the perimeter (thigmotaxis) of the open field. An automated measure of stereotypies in the open field test was defined as multiple breaks in the same beam (or set of beams), repeatedly and separated by less than 1 seconds (e.g. grooming).

Running wheels: 3-4 months old animals were individually housed in a home cage containing a running wheel (Coulbourn Instruments, PA, USA). Multiple sets of running wheel cages were enclosed in an environment isolation chamber, which allowed the attenuation of sound, smells and permitted the control of the light/dark cycle (custom built). Activity counts were recorded using the ClockLab software (Actimetrics, IL, USA) and processed using MATLAB (MathWorks, MA, USA). Measures for activity were determined across 15 days in a 12-hour light/ 12-hour dark cycle. Each complete wheel turn corresponded to one activity count.

Circadian rhythm

Circadian rhythms: Identical equipment to the one described above. After a 2-3 week period in a light/dark cycle, the animals were released into constant darkness. Animals were checked for health, food and water availability every week; bedding was changed every 2 weeks. For animals undergoing lithium treatment, and their controls, monitoring was performed every 5 days and the cage bedding was replaced every 10 days. The monitoring of the animals and husbandry procedures were performed with minimal perturbation to the animals and under low intensity red-light (<50 lux). Determination of circadian period length was performed using a continuous interval of at least 10 days and calculated using the Lomb-Scargle periodogram.

Light pulses: Sensitivity to photonic cues and circadian resetting was performed with a simplified Aschoff method(Aschoff, 1965; Refinetti, 2006) with only two time points, CT14 (circadian time 14) and CT24. In nocturnal animals, CT12 is the subjective night, hence, the start of activity. Briefly, using ClockLab, calculation of the subjective

circadian time was determined for each individual mouse and a 300 lux light exposure of 15min was administered at CT14, CT24 and the phase shifts calculated in ClockLab.

Chronic mild stress: We adapted our circadian apparatus to induce a form of chronic mild stress by maintaining constant illumination for a period of 8 weeks. The animals were monitored for health status, food and water availability every week.

Drug treatment

Lithium treatment for running wheels: Mice were introduced in the running wheel apparatus and maintained on a LD cycle. During the first week the animals were fed a chow contained a low dose of lithium carbonate (1.2 g/kg) to reduce lithium toxicity. During the second week of LD, the animals were switch to a chow containing lithium carbonate at 2.4 g/kg. This dose was previously calculated to yield serum drug levels at concentrations similar to the therapeutic window for BPD patients (0.6 -1.2 mEq/L) (Du et al., 2008). Treatment continued for an additional 8 weeks under DD conditions. Lithium-containing chow and control chow were identical with the exception of the added drug (Bio-Serv, NJ, USA).

Valproic acid treatment for running wheels: Chow containing sodium valproate was administered in a similar paradigm as described for lithium treatment; however, drug concentration in the chow was 10 g/kg for the low dose and 20 g/kg for the high dose (Bio-Serv, NJ, USA). Sodium valproate at 20 g/kg in the chow was previously determined to yield serum drug levels (bound + unbound) at concentrations similar to the therapeutic window for human patients (50 - 100 µg/mL) (Du et al., 2008).

Lithium treatment for Forced Swim Test: Control and mutant mice were tested under the Forced Swim test (described below). The same cohort of animals was then treated for 1 week with low dose lithium carbonate-containing chow (1.2 g/kg) followed by 3 weeks of chow with lithium carbonate at 2.4 g/kg.

Serum blood levels of lithium and valproic acid: Animals were deeply anesthetized, decapitated and trunk blood was collected for analysis of drug levels. Determination of drug serum levels was performed by Medtox (St. Paul, MN, USA).

Forced Swim (Porsolt) Test

The test animals were acclimatized to the testing room for 60 min prior to the trial and assigned a code to maintain blinded genotyping information. Mice were then

placed in a glass beaker (18 cm in diameter) containing water at 23-24 °C and their behavior videotaped for 10 min. Next, the mice were removed and placed in an empty cage to dry before being transferred to their home cage. The water was changed and the beaker cleaned between each subject. From the 10 min recorded for each animal, only the last 6 min of the test were scored for total time spent in immobility. The experimenter scoring the behavior was blinded to the animal genotype. Immobility was defined as the absence of volitional body or limb movement.

Brain Slice preparation for extracellular field recording

Acute brain slices were prepared from 3-4 month old mice. Slices were prepared from one WT and one nArgBP2 KO pair each day and the experimenter was blind to the genotypes. The mice were deeply anesthetized by intra-peritoneal injection of Avertin and then transcardially perfused with 25 mL of carbogenated ice-cold protective cutting artificial cerebrospinal fluid (aCSF) with the composition (in mM): 185 sucrose, 2.5 KCl, 1.25 NaH2PO4, 26 NaHCO3, 25 glucose, 5 L-ascorbic acid, 3 Na-pyruvate, 0.5 CaCl2.4H2O, 4 MgSO4.7H2O. Mice were then decapitated and the brains were removed into ice-cold cutting solution for an additional 1-minute. The brains were then rapidly blocked and embedded in low gel point agarose (Sigma type I-B) for horizontal sectioning at 300 μM thickness on a VF200 model Compresstome (Precisionary Instruments) using either a sapphire or zirconium ceramic injector style blade. Slices containing the middle 1/3 of the hippocampus (8 hemi-slices per brain) were immediately transferred to a holding chamber containing carbogenated aCSF (23-25°C) of the composition (in mM): 119 NaCl, 2.5 KCl, 1.25 NaH2PO4, 26 NaHCO3, 12.5 glucose, 2 CaCl2.4H2O, 1 MgSO4.7H2O. The holding aCSF was supplemented with (in mM): 5 L-ascorbic acid, 3 Na-pyruvate to improve slice health and longevity, and slices were recovered for a minimum of 1.5 hours and stored for a maximum of 6 hours prior to transfer to the recording chamber for use. The recording aCSF did not contain L-ascorbic acid or Na-pyruvate. The osmolarity of all solutions was measured at 300-310 mOsm and the pH was maintained at ~7.3 after equilibration under constant carbogenation.

Extracellular field recording

A pencil-tipped platinum iridium concentric bipolar stimulating electrode (CBAPC75, 25uM inner pole diameter; FHC) was placed on the outer 1/3 of the molecular layer of the suprapyramidal blade of the dentate gyrus. This electrode position was chosen to predominantly activate the lateral perforant pathway axons that originate from the entorhinal cortex and terminate onto the distal dendrites of hippocampal dentate granule cells. A borosilicate glass recording electrode filled with 2M NaCl was also placed within the outer 1/3 of the molecular layer at a separation of 250-275 μm from the stimulating electrode tip. The recording electrode was lowered into the slice to the depth that produced that maximal response size. The outer, middle, and inner portions of the molecular layer are easily distinguished under low power magnification (4X) using differential interference contrast (DIC) optics. Electrode placement was further validated under high power magnification (40X) with the aid of 900 nm infra-red DIC optics as needed. Lateral perforant pathway to dentate gyrus extracellular field excitatory postsynaptic potentials (LPP-DG fEPSPs) were evoked with 0.15 ms step depolarizations at 30 μA test intensity at a baseline frequency of 0.050 Hz. Paired pulses were evoked with a 100 ms inter-stimulus interval. LPP-DG fEPSPs exhibited PPF under these conditions, whereas medial perforant pathway responses (MPP-DG fEPSPs) exhibit PPD, as reported previously. In preliminary recording we also verified the specificity of the electrode configuration for LPP-DG fEPSPs versus MPP-DG fEPSPs by examining the sensitivity to mGluR agonists. LPP-DG fEPSPs were reduced by the group III mGluR-selective agonist L-AP4 whereas MPP-DG fEPSPs were not affected. Conversely, MPP-DG fEPSPs were reduced by the group II mGluR-selective agonist DCGIV whereas LPP-DG fEPSPs were not affected. Thus, collectively we used morphological (visualization by DIC optics), electrophysiological (PPF vs. PPD), and pharmacological (sensitivity to mGluR agonists) criteria to confirm that the measured synaptic responses originated from selective stimulation of the lateral perforant pathway.

After establishing a suitable recording configuration, evoked responses were monitored for a baseline period of 5 minutes to ensure stable LPP-DG fEPSP amplitude. Care was taken to ensure that no population spike contamination occurred at the baseline intensity. Input-output functions were then determined for the

presynaptic fiber volley (negative peak 1, NP1) and fEPSP amplitude by conducting three consecutive rounds of stimulation over a complete dynamic range from 0-80 μA in 10 μA increments. All recordings were performed at 30-32°C.

Data acquisition and analysis

Signals were acquired with custom protocols designed using pClamp 10 software to control a Multiclamp 700B amplifier and Digidata 1440A (Axon Instruments/Molecular Devices). Data analysis was performed blind of the genotype of the experimental animals using Clamp Fit software (Axon Instruments/Molecular Devices). Response size for fEPSPs was measured as the absolute peak amplitude. Paired pulse ratio was calculated as the ratio of the 2nd population spike amplitude to the 1st population spike amplitude for responses to paired pulse stimulation at 30 μA fixed intensity with a 100 msec interstimulus interval for the pair. Values are expressed as means ± s.e.m. and data were tested for significance using either an unpaired t-test or two-way repeated measures ANOVA using Prism software (Graph Pad).

Morris water maze

Morris water maze testing was performed as described with minor alterations (Peca et al., 2011b). Briefly, 3-4 months old mice were tested in a 120 cm diameter pool and the hidden platform was 8 cm in diameter. Pool water was maintained at 23 ± 0.5 °C and made opaque by mixing-in white non-toxic tempera paint. During training and reversal training, 90 s duration trials were used. The probe trial was 30s in duration. The experimenter followed the animals' progress using tracking software while situated outside of the testing room. Tracking and analysis were performed using the Noldus Ethovision software.

Golgi staining and Sholl analysis.

Golgi staining and Sholl analysis were performed as described(Peca et al., 2011b). All brains and collected sections were coded in order to blind the experimenter of the genotype until after all data was collected and analyzed. Brains from 3-4 months old mice were prepared with standard Golgi–Cox impregnation techniques using the FD Rapid GolgiStain Kit (NeuroTechnologies). Granule cells in in the upper blade of the dentate were traced using a motorized microscope with a digital CCD camera

connected to a computer running Neurolucida Software (MBF Bioscience). The three-dimensional analysis of the reconstructed neurons was performed using NeuroExplorer software (MBF Bioscience) and data from total dendritic length and neuronal complexity was analyzed in Prism (GraphPad).

Hematoxylin & Eosin; Thionin and Timm Staining

Hematoxylin & Eosin staining and thionin staining were performed according to standard methods(Welch et al., 2007). Timm staining was performed in 25 µm thick section using the FD Rapid TimmStain Kit according to manufacturers' instructions (NeuroTechnologies).

Results

nArgBP2$^{-/-}$ mice display increased levels of spontaneous activity and explorative behavior

In neurons, nArgBP2 is coded by the inclusion of a highly conserved exon normally not expressed outside of the brain (Cestra et al., 2005; Feliciano et al., 2011) (Fig. 1a). We targeted this brain specific exon in mouse ES cells to generate a perturbation in nArgBP2 (Fig. 1a) and confirmed our genetic manipulation through southern blotting of targeted ES cells (Fig. 1b), by PCR (Fig. 1c) and through western blotting in WT and nArgBP2$^{-/-}$ brain samples (Fig. 1d). Mice homozygous for the targeted deletion were born at the expected Mendelian ratio, were fertile and did not display any gross anatomical brain abnormalities; however, slightly enlarged ventricles were often present in nArgBP2 homozygous mutant mice (Supplementary Fig. 1). An initial behavioral screen designed to test exploration in a novel environment revealed that nArgBP2 mutant mice displayed an increase in spontaneous locomotor activity (Fig. 1e-f). Distance traveled in the open field test was significantly greater when compared to WT controls (Fig. 1e: 60min, WT 33.35 ± 3.160m, n=18; KO = 51.67 ± 4.908m, n=18; $p<0.001$, mean ± s.e.m.). nArgBP2 mutant mice also displayed an increase in rearing, which is a form of vertical exploration anxiogenic to mice (Fig. 1f: 60min, WT 124.94 ± 42.855; KO 288.22 ± 47.977, n=18; $p<0.01$, mean ± s.e.m.). However, distance traveled in the center of the open field was similar across genotypes (Fig. 1g: 60min, WT 11.06 ± 1.865m, n=18; KO 12.09 ± 2.016m; n=18, $p>0.05$, mean ±

s.e.m.). Additionally, time spent in stereotypical behaviors was increased in nArgBP2$^{-/-}$ mice (Fig. 1h: 60min, WT 911.69 ± 84.552s, n=18; KO 1118.63 ± 79.600s, n=18; $p<0.05$, mean ± s.e.m.). These results suggest that nArgBP2$^{-/-}$ mice display an increase in spontaneous activity and exploratory behavior in a novel environment.

Disrupted circadian rhythms in nArgBP2$^{-/-}$ mice

Our results suggesting a spontaneous hyperactivity in the open field prompted us to investigate if nArgBP2$^{-/-}$ mice also displayed increased levels of activity over longer periods of time. To this purpose, we tested singly housed, nArgBP2$^{-/-}$ and nArgBP2$^{+/+}$ mice in a home cage setting each containing a running wheel. We found that across a 15 day period, nArgBP2 mutants displayed higher levels of activity in the running wheels, as measured by total number of wheel turns per 24h period (Fig. 2a). In the span of this analysis, we also interrogated the circadian function in nArgBP2$^{-/-}$ mice and uncovered a reduction in circadian period length during “free-running” trials. Mammals entrain biological functions such as sleep, activity and body temperature to external environmental cues. Among the most powerful influencing factors for the oscillation in circadian activity (i.e. a zeitgeber) is the day-night cycle. However, in the absence of zeitgebers (total darkness and absence of any rhythmic perturbation), sleep and activity patterns reveal the periodicity of the internal circadian clock (Lowrey and Takahashi, 2000). Using an apparatus isolated from external cues we found that both genotypes normally entrained to a 12h light-dark cycle (Fig. 2b-d). However, in dark-dark conditions nArgBP2$^{-/-}$ mice displayed a significant reduction in period length (Fig. 2e: WT: 24.18 ± 0.07157 h, n=10; KO: 23.37 ± 0.1049, n=10; $p<0.001$, mean ± s.e.m.). Occasionally, nArgBP2$^{-/-}$ mice exposed to long periods of dark-dark condition also lost rhythm periodicity (Fig. 2d). During dark-dark periods both genotypes remained respondent to phase shifts induced by photonic stimuli (Fig. 2e; Circadian Time 14h, WT: -2.164 ± 0.2h, n=10; KO: -1.941 ± 0.1699 h, n=10; $p>0.05$, mean ± s.e.m.). Our data suggests that nArgBP2$^{-/-}$ may display manic-like behaviors as measured by hyperactivity, increased explorative behavior and a dysfunction in internal circadian clock.

Lithium rescues the circadian period reduction in nArgBP2$^{-/-}$ mice and reverts the resistance to depressive-like behavior

To attempt a pharmacological rescue of the manic-like behaviors and circadian abnormalities in the nArgBP2$^{-/-}$ mice, we treated mutants and controls with two drugs commonly prescribed to BPD patients: lithium, a mood stabilizer and valproic acid, an anticonvulsant. We chronically treated cohorts of animals during the light-dark entrainment period for 4 weeks before switching to a dark-dark environment and assessing internal clock function. Drugs were administered in the chow at concentrations that yield stable blood-level concentrations within therapeutic ranges ((Du et al., 2008) and Supplementary Table 1). The six groups of animals consisted of naïve, lithium- or valproic acid-treated nArgBP2$^{+/+}$ and nArgBP2$^{-/-}$ mice (Fig. 3a-f). Lithium treatment, but not valproic acid, significantly ameliorated the circadian period length dysfunction in the nArgBP2$^{-/-}$ mice (Fig. 3d-f). In these mice, lithium treatment produced an increase in period length by approximately 0.7h, while in control mice lithium produced an increase of only 0.16h. In both genotypes, valproic acid treatment led to a small, but not statistically significant reduction in period length (ANOVA, naïve vs treated, $p>0.05$).

To determine if the manic-like behavior of nArgBP2$^{-/-}$ mice was accompanied by an inverse relationship in measures of rodent depressive-like behaviors we performed a Porsolt forced swim test. In this paradigm, nArgBP2$^{-/-}$ mice spent less time in immobility when compared to controls (Fig. 4a –left-). We again performed a pharmacological intervention and observed that chronic lithium treatment successfully rescued this phenotype (Fig. 4a – right-). Additionally, when analyzing animals that were tested before and after lithium treatment, we observed an inverse trend between genotypes, suggesting an anti-depressive effect of lithium in wildtype mice but an anti-manic effect on the mutant nArgBP2 mice (Fig. 4b).

After testing, animals were sacrificed and the blood concentration of both drugs was found to be similar across genotypes and within proposed therapeutic levels (Supplementary Table 1). Together, our data of increased spontaneous activity, dysfunction in circadian rhythms, reduced depressive-like behavior and pharmacological rescue after lithium treatment, suggests that the nArgBP2 knockout mice display manic-like behaviors.

nArgBP2$^{-/-}$ mice display enhanced depressive-like behaviors after chronic mild stress

Finally, we also explored the possibility that chronic mild stress would differentially affect nArgBP2$^{-/-}$ and control mice. To test this, we maintained a cohort of nArgBP2$^{+/+}$ and nArgBP2$^{-/-}$ mice in the running wheel apparatus under constant illumination for 8 weeks (Fig. 4c). During the period of light/light, both genotypes lost circadian rhythmicity. After this period of extended stress, we removed the animals from the apparatus and performed the forced swim test. Under these conditions we observed that nArgBP2 mutant mice displayed an increase in time spent in immobility when compared to controls (Fig. 4d; WT: 148.0 ± 11.88s, n=9; KO: 216.4 ± 20.77s, n=9; $p<0.05$, mean ± s.e.m.). This data indicate that nArgBP2 mutant mice are prone to display depressive-like phenotypes after chronic, stress-induced challenges.

Behavior inflexibility in nArgBP2$^{-/-}$ mice

Behavioral inflexibility is a common clinical manifestation in humans undergoing manic episodes. To test if naïve nArgBP2 mutant mice also display behavioral rigidity or deficits in behavioral plasticity, we performed a Morris water maze paradigm with reversal training in 3-4 months old animals (Fig. 5). We observed that during the initial training (Day 1), nArgBP2$^{-/-}$ mice displayed a shorter latency to find the platform (Fig. 5a). This was most likely due to a higher average swim velocity in the mutants during the first training day and not due to enhanced learning, since during the first trials the animals are unaware of the presence of the hidden platform (Trial 1-2 Day 1; WT: 16.20 ± 1.241 cm/s, n=9; KO: 19.62 ± 0.6035 cm/s, n=10). However, this difference was eliminated with repeated exposure to the water maze and the development of search patterns by both genotypes, suggesting that there is no enhancement/deficiency in spatial memory learning in the mutant animals (Fig. 5a). At day six we tested the animals in a probe trial (hidden platform removed) and determined that both genotypes spent a similar percent of time in the quadrant that previously contained the hidden platform, suggesting no overt perturbation in spatial memory formation (Fig. 5b-c). During reversal training, the platform was reintroduced, its location switched and the animals re-trained (Fig. 5d). In the reversal probe trial both genotypes again displayed an increase in time spent in the new target quadrant (Fig. 5e-f); however, nArgBP2$^{-/-}$

mice displayed a small but significant larger percent of time spent in the previously correct quadrant (Fig. 5e SW; WT: 16.78 ± 2.678s, n=9; KO: 27.89 ± 3.716 s, n=10; $p<0.05$, mean ± s.e.m.). These data suggest that nArgBP2$^{-/-}$ mice display normal spatial learning and spatial memory formation but a deficiency in behavioral plasticity during the reversal process of memory extinction.

Evidence for enhanced excitatory synaptic function at lateral perforant pathway to granule cell synapses in acute hippocampal brain slices from nArgBP2$^{-/-}$ mice

Initial immunostaining experiments with our newly developed anti-nArgBP2 antibody revealed that the nArgBP2 protein is highly enriched in the outer 1/3 of the dentate gyrus molecular layer corresponding to the lateral perforant pathway (LPP) inputs to dentate granule cells of the hippocampus (Fig. 6a). In light of this striking localization pattern, we analyzed dentate granule cell morphology by Golgi staining and the patterning of the dentate gyrus by Timm staining but did not uncover any overt morphological abnormalities (Supplementary Fig. 2).

To probe the functional consequences of nArgBP2 deletion, we next performed extracellular field recordings from the outer 1/3 of the dentate gyrus molecular layer while stimulating LPP axons using the acute hippocampal brain slice preparation (Fig. 6b). This configuration allowed us to assess the functional status of excitatory synapses formed by LPP axons onto the distal dendrites of dentate gyrus granule cells (denoted as LPP-DG). We recorded LPP-DG fEPSPs over a full dynamic range of stimulation intensities (0-60 µA) from 3-4 month old adult mice in standard aCSF at 29-32^{0}C. Importantly, acute brain slices were prepared from one nArgBP2$^{-/-}$ mouse and one age-matched wild-type control mouse each day, and the experimenter was blinded to the genotypes of the animals. We found that LPP-DG fEPSPs were significantly increased in brain slices from nArgBP2$^{-/-}$ mice when compared to controls (at maximal 60 µA stimulation intensity: nArgBP2 $^{-/-}$ = 1.68 ± 0.06 mV, wild-type = 1.43 ± 0.04 mV, $p<0.001$; Fig. 6c). In contrast, there was no significant difference in the fiber volley amplitude (negative peak 1 or NP1), a measure of axonal excitability, or paired-pulse ratio (PPR), a measure that is inversely proportional to presynaptic release probability (Fig. 6d,e). These findings are consistent with a postsynaptic origin of the increased synaptic responses. Together, these data suggest that nArgBP2 may play a role in the

regulation of glutamatergic synapses and that deletion of nArgBP2 in mice leads to enhanced postsynaptic glutamatergic responsiveness at LPP-DG synapses.

Increased levels of glutamate receptor subunits in the PSD of nArgBP2$^{-/-}$ mice

Next we assessed if the observed enhancement of glutamatergic signaling was accompanied by biochemical alterations in the composition of the PSD. Because PSD isolation from the outer molecular layer in dentate gyrus is impractical, we focused on the striatum since nArgBP2 is expressed both homogenously and at high levels in this region (Fig. 6a). We biochemically isolated PSDs from the striatum of 3-4 months old control and nArgBP2 mutant mice and performed semi-quantitative western blotting for PSD scaffolding proteins (Fig. 7a-b), glutamatergic receptor subunits (Fig. 7c-d) and signaling molecules (Fig. 7e-f). We found that several ionotropic glutamate receptor subunits displayed increased levels in the mutant mice when compared to controls (Fig. 7b). These included NR1 and NR2B subunits of NMDA receptors and the GluR1 and GluR2 subunits of AMPA receptors. These results converge with the findings from dentate electrophysiology in suggesting an up-regulation in glutamatergic signaling as a consequence of the disruption in nArgBP2.

Discussion

The synaptic macromolecular complex composed of PSD-95/SAPAP/Shank and interaction partners has been shown to be important for the normal functioning of the mammalian brain. Mutations in the genes coding for these proteins and their molecular partners have been linked to a large variety of human psychiatric and developmental disorders (Tarpey et al., 2004; Durand et al., 2007; Welch et al., 2007; Sudhof, 2008; Zuchner et al., 2009; Berkel et al., 2010; Boardman et al., 2010; Pinto et al., 2010). We recently characterized the consequences of disrupting SAPAP3 and Shank3 in mice (Welch et al., 2007; Peca et al., 2011b) and we hypothesized that other binding partners to SAPAP3 at the postsynaptic site could also reveal important roles. Here, we focused on elucidating the *in vivo* function of nArgBP2, a protein known to interact with the SAPAP proteins at the PSD (Kawabe et al., 1999). After generating a mutation in the mouse genome to disrupt the production of nArgBP2 we performed a behavioral characterization in homozygous mutant mice. We observed that mutant nArgBP2 mice display several phenotypes reminiscent of manic behavior, including: increased

explorative behavior in a novel environment, increased stereotypies; hyperactivity in the home cage, reduction in circadian rhythm length, behavioral inflexibility and reduced depressive-like behavior. This led us to conclude that nArgBP2$^{-/-}$ mice display strong face validity towards manic-like behaviors. Interestingly, challenging these animals with a form of chronic mild stress led the nArgBP2$^{-/-}$ mice to display an increase in measures of depression when compared to controls, suggesting that these animals can alternate to a depressive state. Finally, to test predictive validity in modeling manic-like behaviors, we administered two drugs commonly prescribed to BPD and we found that lithium treatment successfully ameliorated several of the manic-like behavioral manifestations in nArgBP2$^{-/-}$ mice. Interestingly, nArgBP2 also displays construct validity to manic-depressive behavior since the region containing the nArgBP2 gene in humans -4q35- has been linked to susceptibility to BPD (Adams et al., 1998; Blair et al., 2002). Finally, at the synaptic level we found converging evidences from electrophysiological recordings and biochemical data pointing to an increase in glutamatergic signaling in nArgBP2 knockout mice.

Despite recent progress, the neurobiological substrates underlying BPD are still poorly understood. The identification of susceptibility genes and the generation of animal models are crucial to provide a better understanding on the molecular and synaptic pathways involved in pathological states. The animals we describe here provide a good starting point to dissect the mechanisms involved in BPD. Additionally, our results combined with previous evidences from human genetic linkage data call for a deep sequencing of the SORB2/nArgBP2 gene in BPD patients.

.

Figure 1

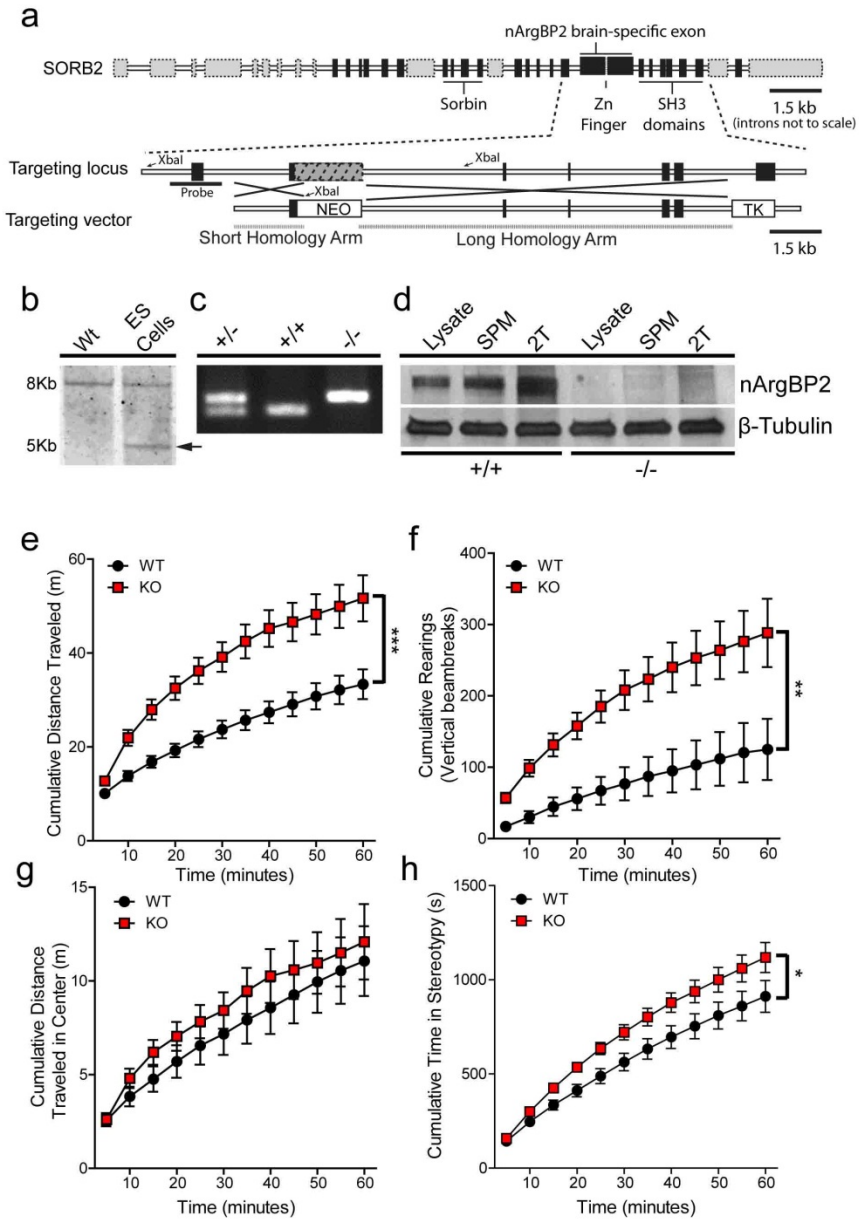
a
nArgBP2 brain-specific exon
SORB2
Sorbin
Zn Finger
SH3 domains
1.5 kb (introns not to scale)
Targeting locus
XbaI
Probe
NEO
TK
Targeting vector
Short Homology Arm
Long Homology Arm
1.5 kb
b
Wt
ES Cells
8Kb
5Kb
c
+/-
+/+
-/-
d
Lysate
SPM
2T
nArgBP2
β-Tubulin
+/+
-/-
e
Cumulative Distance Traveled (m)
WT
KO
***
Time (minutes)
f
Cumulative Rearings (Vertical beambreaks)
**
g
Cumulative Distance Traveled in Center (m)
h
Cumulative Time in Stereotypy (s)
*

Figure 2

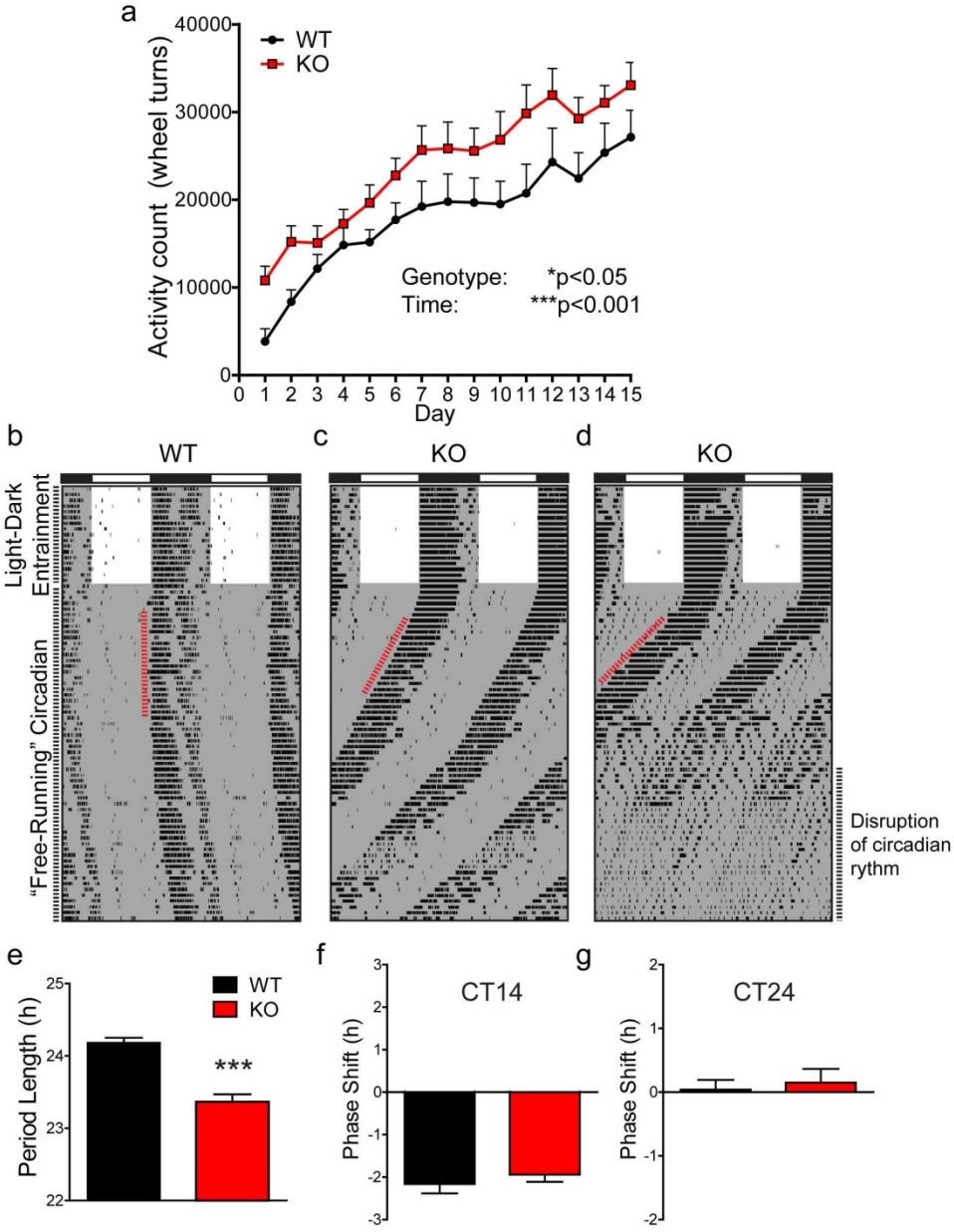
a
Activity count (wheel turns)
40000
30000
20000
10000
0
WT
KO
Genotype: *p<0.05
Time: ***p<0.001
0 1 2 3 4 5 6 7 8 9 10 11 12 13 14 15
Day
b
WT
c
KO
d
KO
Light-Dark Entrainment
"Free-Running" Circadian
Disruption of circadian rythm
e
Period Length (h)
25
24
23
22
WT
KO
***
f
CT14
Phase Shift (h)
3
2
1
0
-1
-2
-3
g
CT24
Phase Shift (h)
2
1
0
-1
-2

Figure 3

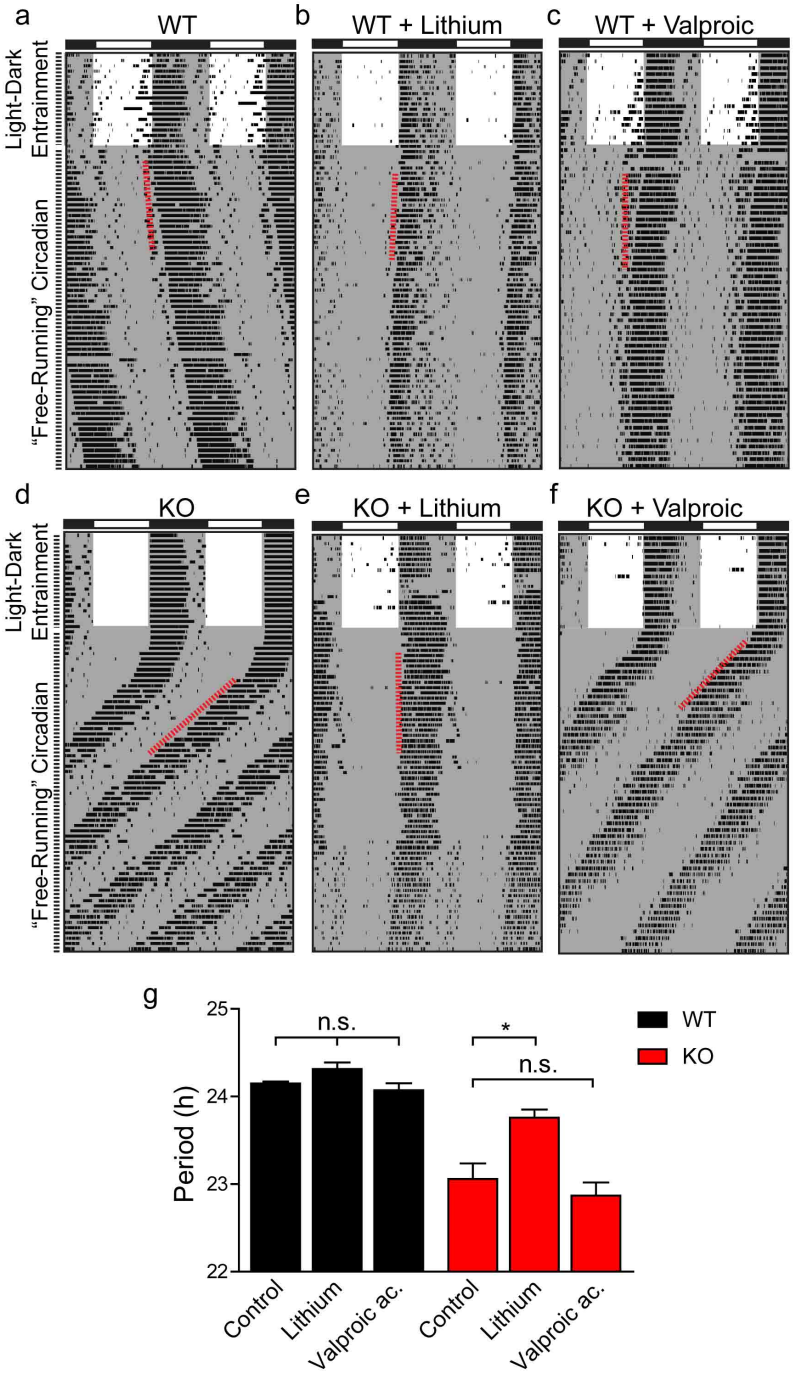
a
WT
b
WT + Lithium
c
WT + Valproic
Light-Dark Entrainment
"Free-Running" Circadian
d
KO
e
KO + Lithium
f
KO + Valproic
Light-Dark Entrainment
"Free-Running" Circadian
g
Period (h)
25
24
23
22
n.s.
*
n.s.
WT
KO
Control
Lithium
Valproic ac.
Control
Lithium
Valproic ac.

Figure 4

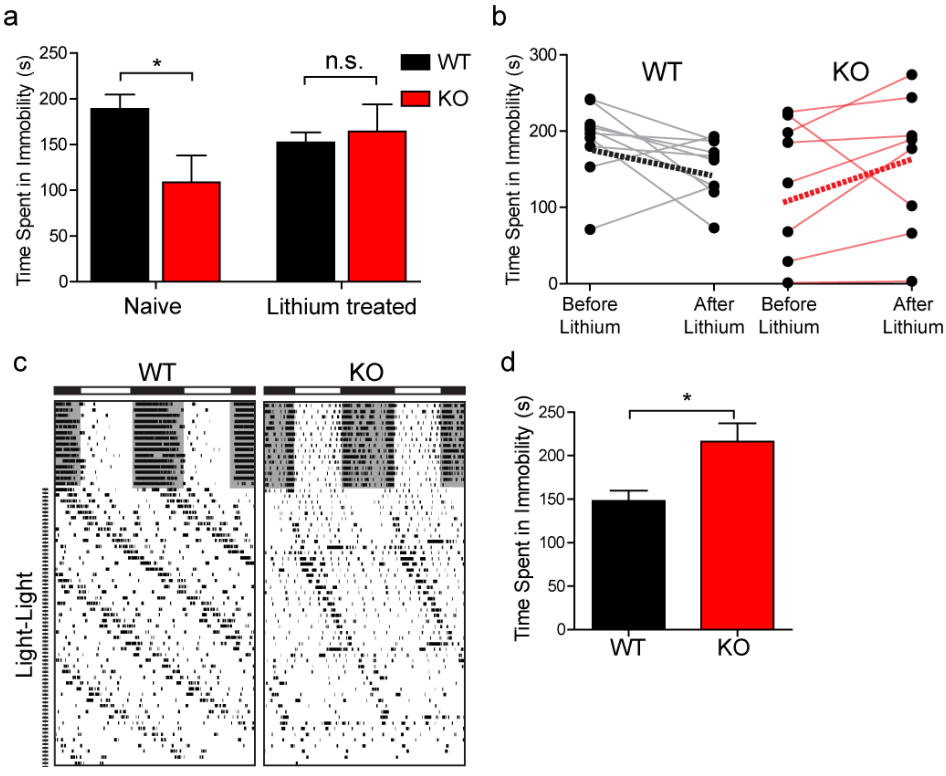
a
Time Spent in Immobility (s)
250
200
150
100
50
0
*
n.s.
WT
KO
Naive
Lithium treated
b
Time Spent in Immobility (s)
300
200
100
0
WT
KO
Before Lithium
After Lithium
Before Lithium
After Lithium
c
WT
KO
Light-Light
d
Time Spent in Immobility (s)
250
200
150
100
50
0
*
WT
KO

Figure 5

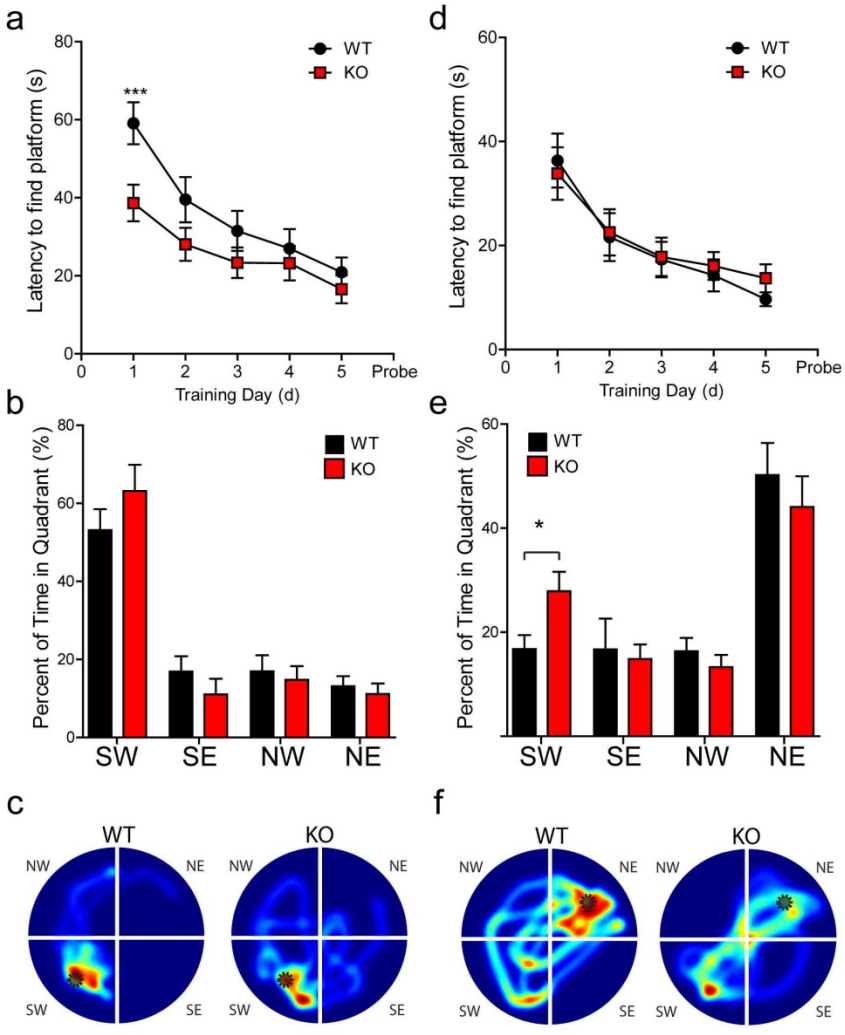
a
Latency to find platform (s)
WT
KO
***
Training Day (d)
Probe
d
Latency to find platform (s)
WT
KO
Training Day (d)
Probe
b
Percent of Time in Quadrant (%)
WT
KO
SW
SE
NW
NE
e
Percent of Time in Quadrant (%)
WT
KO
*
SW
SE
NW
NE
c
WT
KO
NW
NE
SW
SE
f
WT
KO
NW
NE
SW
SE

Figure 6

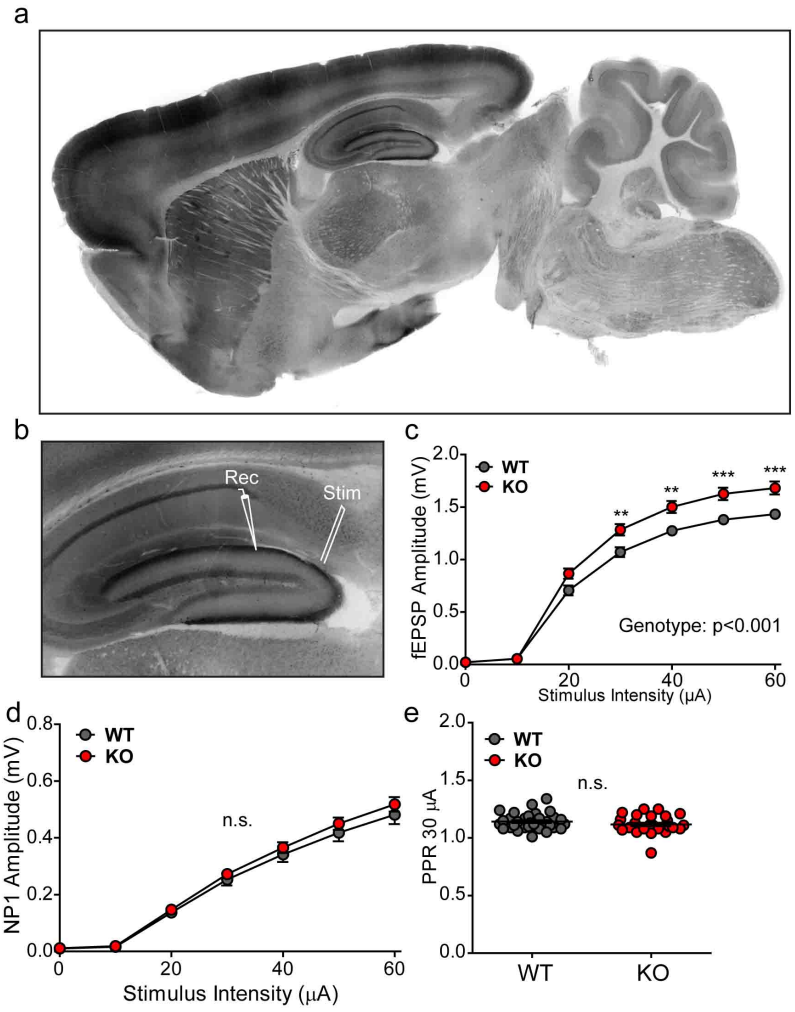
a
b
Rec
Stim
c
WT
KO
fEPSP Amplitude (mV)
2.0
1.5
1.0
0.5
0.0
**
**
***
***
Genotype: p<0.001
0
20
40
60
Stimulus Intensity (μA)
d
WT
KO
NP1 Amplitude (mV)
0.8
0.6
0.4
0.2
0.0
n.s.
0
20
40
60
Stimulus Intensity (μA)
e
WT
KO
PPR 30 μA
2.0
1.5
1.0
0.5
0.0
n.s.
WT
KO

Figure 7

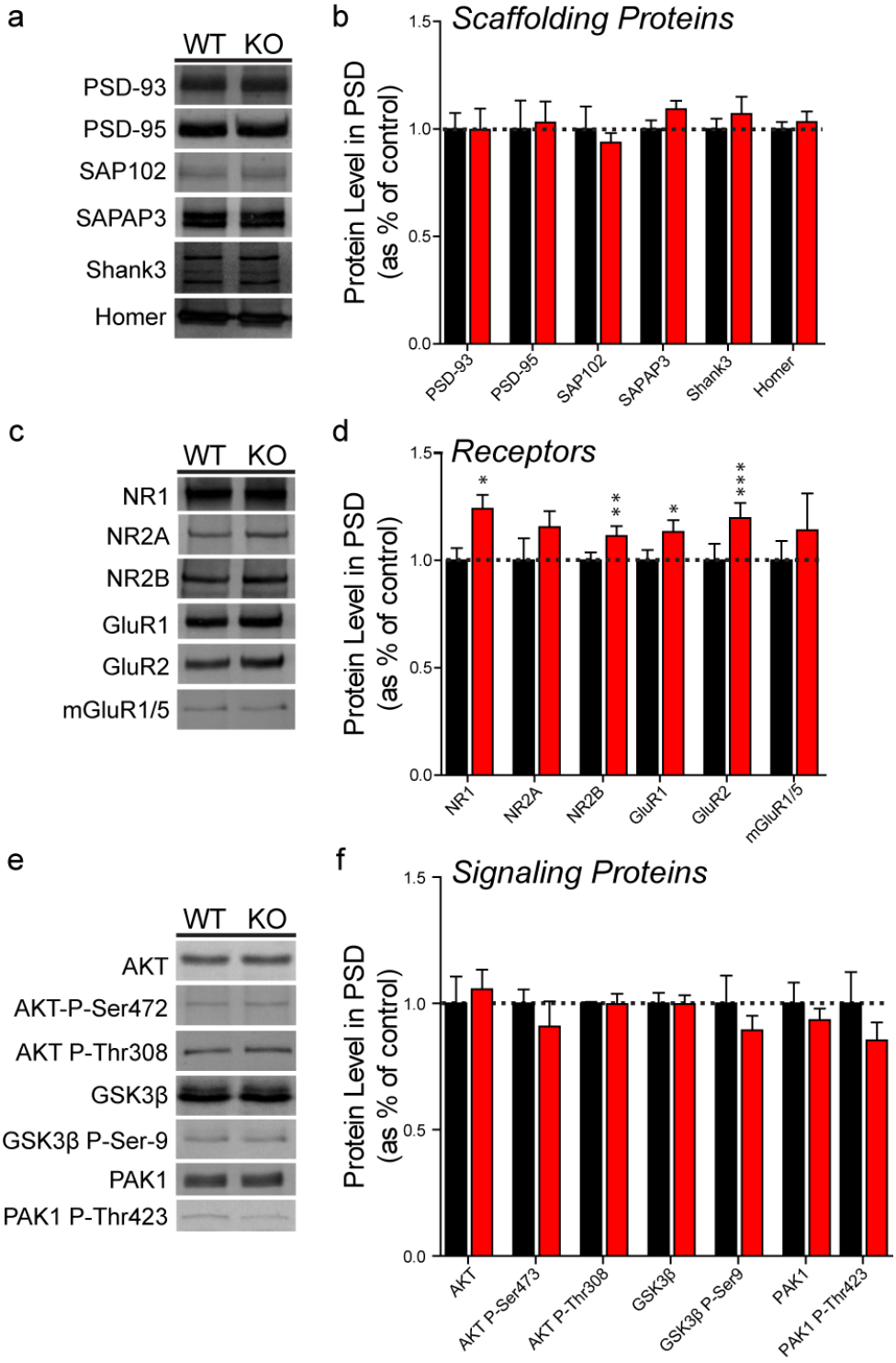
a
WT KO
PSD-93
PSD-95
SAP102
SAPAP3
Shank3
Homer
b
Scaffolding Proteins
Protein Level in PSD (as % of control)
1.5
1.0
0.5
0.0
PSD-93
PSD-95
SAP102
SAPAP3
Shank3
Homer
c
WT KO
NR1
NR2A
NR2B
GluR1
GluR2
mGluR1/5
d
Receptors
Protein Level in PSD (as % of control)
*
**
*
***
NR1
NR2A
NR2B
GluR1
GluR2
mGluR1/5
e
WT KO
AKT
AKT-P-Ser472
AKT P-Thr308
GSK3β
GSK3β P-Ser-9
PAK1
PAK1 P-Thr423
f
Signaling Proteins
Protein Level in PSD (as % of control)
AKT
AKT P-Ser473
AKT P-Thr308
GSK3β
GSK3β P-Ser9
PAK1
PAK1 P-Thr423

Supplemental Figure 1

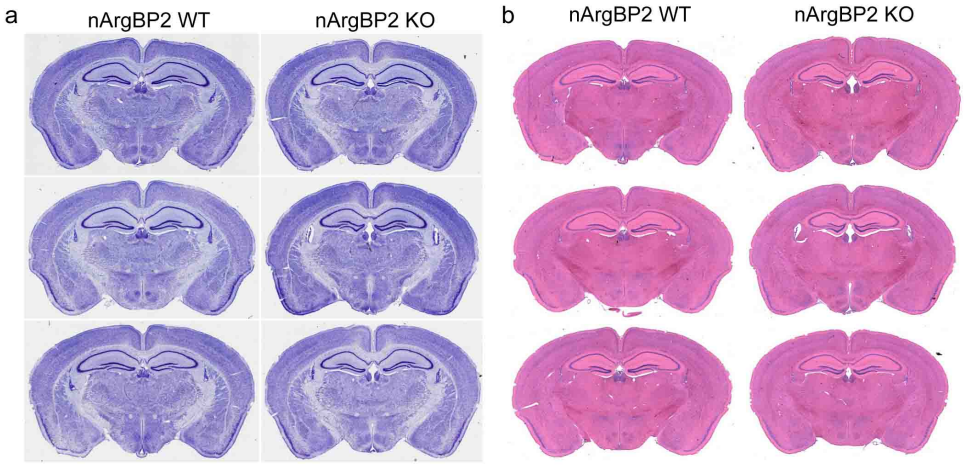

Supplemental Figure 2

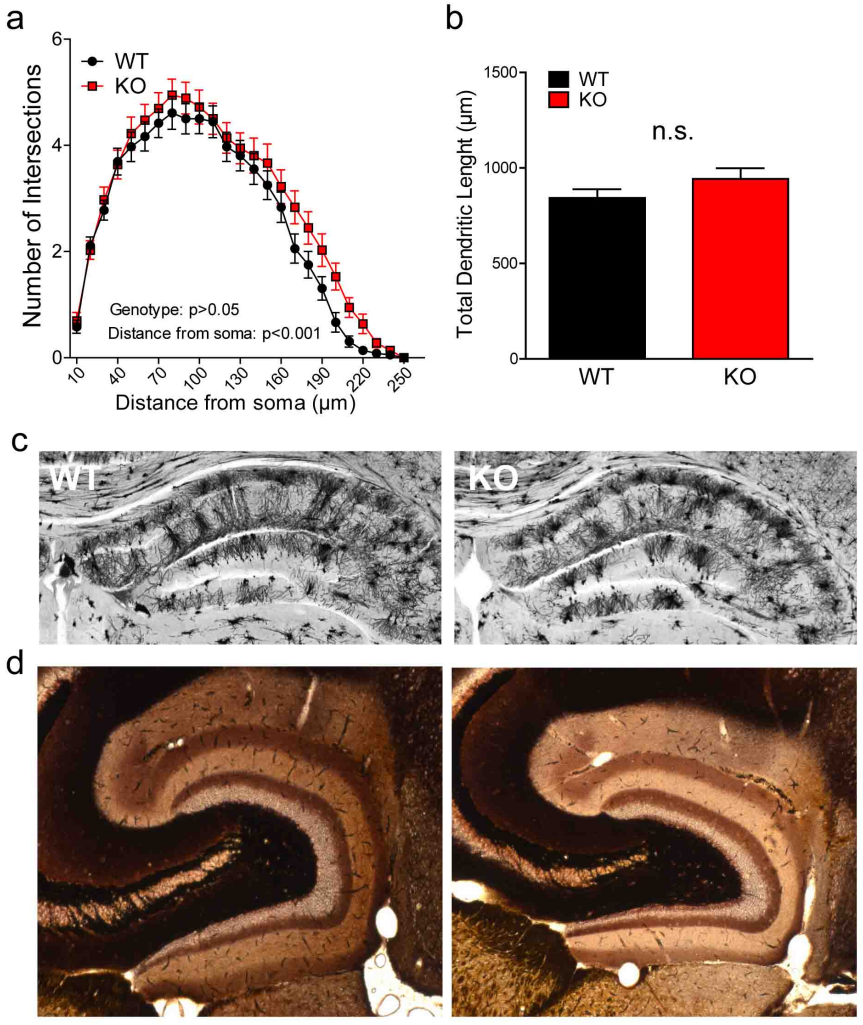

Supplementary Table 1

		Mean†	SEM	n
Lithium	WT	0.7438 mEq/L	0.05405 mEq/L	8
	KO	0.7278 mEq/L	0.05196 mEq/L	9
Valproic (bound + unbound)	WT	53.77 ug/mL	11.62 ug/mL	9
	KO	74.78 ug/mL	12.8 ug/mL	11

† Drug concentrations are not statistically different

Figure legends

Figure 1 – Increased levels of spontaneous activity in nArgBP2$^{-/-}$ mice during exploration of a novel environment. a, Gene structure and functional domains in the SORBS2 gene (top); targeted locus and position of Southern blot probe (middle); and targeting vector (bottom). b, Southern blot of wildtype (WT) and targeted ES cells (ES+) after digestion with XbaI; 5kb band is present in targeted ES clones. c, PCR with DNA from tail sample of wildtype ($^{+/+}$), heterozygous mutant (+/-) and homozygous nArgBP2 mutant mice ($^{-/-}$). d, Western blot from forebrain brain lysate, synaptosomal plasma membrane fraction (SPM) and PSD 2xTriton washed (2T) fractions in wildtype ($^{+/+}$) and knockout mice ($^{-/-}$) probed with anti-nArgBP2 (top) and β-tubulin antibodies (bottom). e-g, In an open field test for exploratory behavior in a novel environment, nArgBP2$^{-/-}$ mice, when compared to controls, displayed hyperactivity as measured by total distanced traveled (e), increased vertical exploratory behaviors (f), but similar distance traveled in the center of the open field (g). h, When analyzing stereotypies in the open field, nArgBP2$^{-/-}$ mice, when compared to controls, spent a larger amount of time performing repetitive movements. g-h;* $p<0.05$, **$p<0.01$, $p<0.001$, Two-way repeated measures ANOVA, data presented as means ± s.e.m. from n=18; 3-4 month old animals per group.

Figure 2 – Increased levels of activity in the home cage and disrupted circadian rhythms in nArgBP2$^{-/-}$ mice. a, When compared to controls, nArgBP2$^{-/-}$ mice displayed increased levels of activity in the running wheels during a 15 day period (light-dark). b-e, In the same running-wheel setup, both nArgBP2$^{-/-}$ and wildtype mice display normal entrainment to 12h light-12h dark cycles (Light-Dark Entrainment); after switching the animals to total darkness (“Free-Running” Circadian), nArgBP2$^{-/-}$ mice display a sharp reduction in internal circadian periodicity (e), and will occasionally lose all rhythmicity (d - bottom). f-g, Sensitivity to photonic cues is not lost during “dark-dark” and both nArgBP2$^{-/-}$ and wildtype mice display similar phase shifts after a 15min 300 lux pulse at both Circadian Time –CT- 14 (f) or CT 22 (g). * $p<0.05$, $p<0.001$, Two-way repeated measures ANOVA for a, Student’s t-test for e-g, data presented as means ± s.e.m. from n=10; 3-4 month old animals per group.

Figure 3 – Lithium treatment rescues circadian abnormalities in nArgBP2$^{-/-}$ mice. a-f, Cohorts of naïve wildtype (a) and nArgBP2$^{-/-}$ mice (b), lithium treated (b and e) or valproic acid treated (c and d) were tested for circadian rhythm in light-dark and dark-dark cycles. g, Lithium, but not valproic acid treatment, significantly rescue the circadian deficit in nArgBP2$^{-/-}$ mice. * $p<0.05$, Student's t-test, data presented as means ± s.e.m. from n=5-11 mice per group.

Figure 4 – nArgBP2$^{-/-}$ mice display lower levels of depressive-like behavior under basal conditions, but enhanced depressive-like behaviors after chronic mild stress. a, Naïve nArgBP2$^{-/-}$ mice, when compared to controls, display less time spent in immobility in the forced swim test. However, lithium treatment normalizes their response. b, Analyzing the same animals tested before lithium treatment and 4 weeks after treatment reveals an inverse trend between genotypes in the forced swim test, producing an anti-manic effect in nArgBP2$^{-/-}$ mice and a mild anti-depressive effect in wildtype controls. c-d, After subjecting nArgBP2$^{-/-}$ and wildtype mice to prolonged 24h light, both genotypes lose circadian rhythmicity (c). Additionally, testing the same animals after the stress paradigm in the forced swim test, revealed that the nArgBP2$^{-/-}$ mice spend more time in immobility when compared to controls (d). * $p<0.05$, Student's t-test, data presented as means ± s.e.m. from n=8-10 mice per group.

Figure 5 – Behavioral inflexibility in nArgBP2$^{-/-}$ mice. a-b, Latency to find the hidden platform (SW) decreases significantly across 5 days of training for both wildtype and nArgBP2$^{-/-}$ mice (a). In the probe trial, when compared to controls, nArgBP2$^{-/-}$ mice spent a similar amount of time in target quadrant (SW) (b). c, Representative heat maps examples from control (WT) and nArgBP2$^{-/-}$ (KO) during the probe trial. d-e, Latency to find the platform decreases significantly across subsequent 5 days of reversal training (platform switched to NE) for both wildtype and nArgBP2$^{-/-}$ mice (d). In the reversal probe trial, when compared to controls, nArgBP2$^{-/-}$ mice spent a larger percent of time in the previously correct quadrant (SW), but still display preference for the new target quadrant (NE). f, Representative example heat maps from control (WT) and nArgBP2$^{-/-}$ mice (KO) during the reversal probe trial. *$p<0.05$, Student's t-test, all data are presented as means ± s.e.m; n=9 for wildtype, n=10 for nArgBP2$^{-/-}$ mice.

Figure 6 – Increased field excitatory postsynaptic currents in nArgBP2$^{-/-}$ dentate gyrus. a-b, Immunohistochemistry in a wildtype mouse brain section stained with anti-nArgBP2 antibody .a-b, nArgBP2 is highly enriched in the cortex, striatum and dentate gyrus (a). Dentate gyrus 2x magnification displaying an enrichment of nArgBP2 in the outer molecular layer and illustrative representation of recording and stimulation electrode positioning. c-e, Outer molecular layer fEPSP amplitude is increased in nArgBP2$^{-/-}$ mice (red) when compared to controls (black) (c); NP1 amplitude (d) and PPR (e) are not significantly different between nArgBP2$^{-/-}$ and control mice in field recordings. ** $p<0.01$, *** $p<0.001$; Two-Way repeated measures ANOVA, with Bonferroni post hoc test for c and d, Student's t-test for e; all data presented as means ± s.e.m. from n= 34 slices/8 mice (WT) and n= 29 slices/8 mice (KO).

Figure 7 – Increased glutamatergic subunits in nArgBP2$^{-/-}$ striatal PSDs. a-f, PSD samples from nArgBP2$^{-/-}$ and controls were probed for PSD scaffolding proteins (a,b), glutamate receptor channel subunits (b-c) and signaling proteins (e-f). Significant changes were observed for NMDA receptor subunits, NR1, NR2B and AMPA receptor subunits, GluR1 and GluR2. * $p<0.05$, ** $p<0.01$, *** $p<0.001$, Student's t-test, data presented as means ± s.e.m. from n=3-9 samples per group.

Supplementary Figure 1 – Normal brain anatomy but enlarged ventricles in nArgBP2$^{-/-}$ mice. a-b, Thionin (a) and Hematoxylin and eosin (b) stain in three wildtype and three nArgBP2$^{-/-}$reveals no gross abnormal anatomical defects but slightly enlarged ventricles in nArgBP2 knockout mice.

Supplementary Figure 2 – Normal dendritic morphology and patterning in nArgBP2$^{-/-}$ dentate gyrus. a-b, Sholl analysis of Golgi stained neurons reveals a similar dendritic complexity between nArgBP2$^{-/-}$ and wildtype dentate granule cells (a); total dendritic length is not significantly different between genotypes (b). c, Example sections of wildtype (WT) and nArgBP2$^{-/-}$ (KO) dentate gyrus after Golgi staining. d, Timm staining reveals a normal layer patterning in dentate gyrus from nArgBP2$^{-/-}$ mice when compared to controls. Two-Way repeated measures ANOVA, with Bonferroni post hoc test for a, Student's t-test for b; all data presented as means ± s.e.m. from n= 36 slices/3 mice (WT) and n= 36 slices/3 mice (KO).

Supplementary Table 1 – Serum blood levels of lithium and valproic acid in nArgBP2$^{-/-}$ and wildtype mice. Sodium valproate at 20 g/kg in the chow yielded serum drug levels (bound + unbound) at concentrations similar to the therapeutic window for human patients (50 - 100 µg/mL). Lithium carbonate at 2.4 g/kg in the chow yielded serum drug levels at concentrations similar to the therapeutic window for BPD patients (0.6 -1.2 mEq/L).

References

Abe M, Herzog ED, Block GD (2000) Lithium lengthens the circadian period of individual suprachiasmatic nucleus neurons. Neuroreport 11:3261-3264.

Adams LJ, Mitchell PB, Fielder SL, Rosso A, Donald JA, Schofield PR (1998) A susceptibility locus for bipolar affective disorder on chromosome 4q35. Am J Hum Genet 62:1084-1091.

Alt A, Nisenbaum ES, Bleakman D, Witkin JM (2006) A role for AMPA receptors in mood disorders. Biochem Pharmacol 71:1273-1288.

American Psychiatric Association (2000) Diagnostic and statistical manual of mental disorders : DSM-IV-TR, 4th Edition. Washington, DC: American Psychiatric Association.

Aschoff J (1965) Response curves in circadian periodicity. In: Circadian Clocks, Circadian Clocks Edition, pp 95-111. Amsterdam: North-Holland.

Barabasi AL, Gulbahce N, Loscalzo J (2011) Network medicine: a network-based approach to human disease. Nat Rev Genet 12:56-68.

Bayes A, van de Lagemaat LN, Collins MO, Croning MD, Whittle IR, Choudhary JS, Grant SG (2011) Characterization of the proteome, diseases and evolution of the human postsynaptic density. Nat Neurosci 14:19-21.

Berkel S, Marshall CR, Weiss B, Howe J, Roeth R, Moog U, Endris V, Roberts W, Szatmari P, Pinto D, Bonin M, Riess A, Engels H, Sprengel R, Scherer SW, Rappold GA (2010) Mutations in the SHANK2 synaptic scaffolding gene in autism spectrum disorder and mental retardation. Nat Genet 42:489-491.

Blair IP, Adams LJ, Badenhop RF, Moses MJ, Scimone A, Morris JA, Ma L, Austin CP, Donald JA, Mitchell PB, Schofield PR (2002) A transcript map encompassing a susceptibility locus for bipolar affective disorder on chromosome 4q35. Mol Psychiatry 7:867-873.

Boardman L, van der Merweb L, Lochner C, Kinneara CJ, Seedatd S, Steind D, J,, Moolman-Smook JC, Hemmings SMJ (2010) Investigating SAPAP3 variants in the

etiology of obsessive-compulsive disorder and trichotillomania in the South African white population. Comprehensive Psychiatry (in press).

Cestra G, Toomre D, Chang S, De Camilli P (2005) The Abl/Arg substrate ArgBP2/nArgBP2 coordinates the function of multiple regulatory mechanisms converging on the actin cytoskeleton. Proc Natl Acad Sci U S A 102:1731-1736.

Craddock N, Jones I (1999) Genetics of bipolar disorder. J Med Genet 36:585-594.

Du J, Gray NA, Falke CA, Chen W, Yuan P, Szabo ST, Einat H, Manji HK (2004) Modulation of synaptic plasticity by antimanic agents: the role of AMPA glutamate receptor subunit 1 synaptic expression. J Neurosci 24:6578-6589.

Du J, Creson TK, Wu LJ, Ren M, Gray NA, Falke C, Wei Y, Wang Y, Blumenthal R, Machado-Vieira R, Yuan P, Chen G, Zhuo M, Manji HK (2008) The role of hippocampal GluR1 and GluR2 receptors in manic-like behavior. J Neurosci 28:68-79.

Duffy A, Alda M, Crawford L, Milin R, Grof P (2007) The early manifestations of bipolar disorder: a longitudinal prospective study of the offspring of bipolar parents. Bipolar Disord 9:828-838.

Dunner DL, Patrick V, Fieve RR (1977) Rapid cycling manic depressive patients. Compr Psychiatry 18:561-566.

Durand CM et al. (2007) Mutations in the gene encoding the synaptic scaffolding protein SHANK3 are associated with autism spectrum disorders. Nat Genet 39:25-27.

Feliciano C, Peca J, Zhang Q, Takai Y, Feng G (2011) Characterization of nArgBP2 mRNA localization and protein expression in the mouse brain. Submitted.

Feng G, Tintrup H, Kirsch J, Nichol MC, Kuhse J, Betz H, Sanes JR (1998) Dual requirement for gephyrin in glycine receptor clustering and molybdoenzyme activity. Science 282:1321-1324.

Goh KI, Cusick ME, Valle D, Childs B, Vidal M, Barabasi AL (2007) The human disease network. Proc Natl Acad Sci U S A 104:8685-8690.

Harvey AG (2008) Sleep and circadian rhythms in bipolar disorder: seeking synchrony, harmony, and regulation. Am J Psychiatry 165:820-829.

Jackson A, Cavanagh J, Scott J (2003) A systematic review of manic and depressive prodromes. J Affect Disord 74:209-217.

Jones SH (2001) Circadian rhythms, multilevel models of emotion and bipolar disorder--an initial step towards integration? Clin Psychol Rev 21:1193-1209.

Jope RS (2003) Lithium and GSK-3: one inhibitor, two inhibitory actions, multiple outcomes. Trends Pharmacol Sci 24:441-443.

Kawabe H, Hata Y, Takeuchi M, Ide N, Mizoguchi A, Takai Y (1999) nArgBP2, a novel neural member of ponsin/ArgBP2/vinexin family that interacts with synapse-associated

protein 90/postsynaptic density-95-associated protein (SAPAP). J Biol Chem 274:30914-30918.

Kennedy MB (2000) Signal-processing machines at the postsynaptic density. Science 290:750-754.

Kessler RC, McGonagle KA, Zhao S, Nelson CB, Hughes M, Eshleman S, Wittchen HU, Kendler KS (1994) Lifetime and 12-month prevalence of DSM-III-R psychiatric disorders in the United States. Results from the National Comorbidity Survey. Arch Gen Psychiatry 51:8-19.

Kimura A, Baumann CA, Chiang SH, Saltiel AR (2001) The sorbin homology domain: a motif for the targeting of proteins to lipid rafts. Proc Natl Acad Sci U S A 98:9098-9103.

Lenox RH, Gould TD, Manji HK (2002) Endophenotypes in bipolar disorder. Am J Med Genet 114:391-406.

Lowrey PL, Takahashi JS (2000) Genetics of the mammalian circadian system: Photic entrainment, circadian pacemaker mechanisms, and posttranslational regulation. Annu Rev Genet 34:533-562.

McGuffin P, Rijsdijk F, Andrew M, Sham P, Katz R, Cardno A (2003) The heritability of bipolar affective disorder and the genetic relationship to unipolar depression. Arch Gen Psychiatry 60:497-502.

Nagy A, Rossant J, Nagy R, Abramow-Newerly W, Roder JC (1993) Derivation of completely cell culture-derived mice from early-passage embryonic stem cells. Proc Natl Acad Sci U S A 90:8424-8428.

Oti M, Huynen MA, Brunner HG (2008) Phenome connections. Trends Genet 24:103-106.

Peca J, Feliciano C, Ting JT, Wang W, Wells MF, Venkatraman TN, Lascola CD, Fu Z, Feng G (2011a) Shank3 mutant mice display autistic-like behaviours and striatal dysfunction. Nature 472:437-442.

Pinto D et al. (2010) Functional impact of global rare copy number variation in autism spectrum disorders. Nature 466:368-372.

Refinetti R (2006) Circadian physiology, 2nd Edition. Boca Raton: CRC Press/Taylor & Francis Group.

Roybal K, Theobold D, Graham A, DiNieri JA, Russo SJ, Krishnan V, Chakravarty S, Peevey J, Oehrlein N, Birnbaum S, Vitaterna MH, Orsulak P, Takahashi JS, Nestler EJ, Carlezon WA, Jr., McClung CA (2007) Mania-like behavior induced by disruption of CLOCK. Proc Natl Acad Sci U S A 104:6406-6411.

Sanacora G, Zarate CA, Krystal JH, Manji HK (2008) Targeting the glutamatergic system to develop novel, improved therapeutics for mood disorders. Nat Rev Drug Discov 7:426-437.

Serretti A, Mandelli L (2008) The genetics of bipolar disorder: genome 'hot regions,' genes, new potential candidates and future directions. Mol Psychiatry 13:742-771.

Shaltiel G, Maeng S, Malkesman O, Pearson B, Schloesser RJ, Tragon T, Rogawski M, Gasior M, Luckenbaugh D, Chen G, Manji HK (2008) Evidence for the involvement of the kainate receptor subunit GluR6 (GRIK2) in mediating behavioral displays related to behavioral symptoms of mania. Mol Psychiatry 13:858-872.

Sheng M, Hoogenraad CC (2007) The postsynaptic architecture of excitatory synapses: a more quantitative view. Annu Rev Biochem 76:823-847.

Sierra P, Livianos L, Arques S, Castello J, Rojo L (2007) Prodromal symptoms to relapse in bipolar disorder. Aust N Z J Psychiatry 41:385-391.

Sudhof TC (2008) Neuroligins and neurexins link synaptic function to cognitive disease. Nature 455:903-911.

Tarpey P et al. (2004) Mutations in the DLG3 gene cause nonsyndromic X-linked mental retardation. Am J Hum Genet 75:318-324.

Vitaterna MH, King DP, Chang AM, Kornhauser JM, Lowrey PL, McDonald JD, Dove WF, Pinto LH, Turek FW, Takahashi JS (1994) Mutagenesis and mapping of a mouse gene, Clock, essential for circadian behavior. Science 264:719-725.

Wang B, Golemis EA, Kruh GD (1997) ArgBP2, a multiple Src homology 3 domain-containing, Arg/Abl-interacting protein, is phosphorylated in v-Abl-transformed cells and localized in stress fibers and cardiocyte Z-disks. J Biol Chem 272:17542-17550.

Welch JM, Wang D, Feng G (2004) Differential mRNA expression and protein localization of the SAP90/PSD-95-associated proteins (SAPAPs) in the nervous system of the mouse. J Comp Neurol 472:24-39.

Welch JM, Lu J, Rodriguiz RM, Trotta NC, Peca J, Ding JD, Feliciano C, Chen M, Adams JP, Luo J, Dudek SM, Weinberg RJ, Calakos N, Wetsel WC, Feng G (2007) Cortico-striatal synaptic defects and OCD-like behaviours in Sapap3-mutant mice. Nature 448:894-900.

Wilson GM, Flibotte S, Chopra V, Melnyk BL, Honer WG, Holt RA (2006) DNA copy-number analysis in bipolar disorder and schizophrenia reveals aberrations in genes involved in glutamate signaling. Hum Mol Genet 15:743-749.

Yin L, Wang J, Klein PS, Lazar MA (2006) Nuclear receptor Rev-erbalpha is a critical lithium-sensitive component of the circadian clock. Science 311:1002-1005.

Zuchner S, Wendland JR, Ashley-Koch AE, Collins AL, Tran-Viet KN, Quinn K, Timpano KC, Cuccaro ML, Pericak-Vance MA, Steffens DC, Krishnan KR, Feng G, Murphy DL (2009) Multiple rare SAPAP3 missense variants in trichotillomania and OCD. Mol Psychiatry 14:6-9.

Acknowledgments

We thank S. Chatterjee for helpful discussion and support. We thank The Poitras Center for Affective Disorders Research. This work was funded by a grant from NIMH/NIH (R01MH081201), a Hartwell Individual Biomedical Research Award from The Hartwell Foundation, a Simons Foundation Autism Research Initiative (SFARI) grant Award to G.F..; and doctoral fellowships from the Portuguese Foundation for Science and Technology to C.F. (SFRH/BD/15855/2005) and J.P. (SFRH/BD/15231/2004). C.F. would like to acknowledge the support from the ‘‘Programa Gulbenkian de Doutoramento em Biomedicina’’ (PGDB, Oeiras, Portugal).

Author Contributions

C.F., J.P. and J.T. executed and analyzed the experiments. C.F. and G.F designed the experiments and wrote the paper.

Chapter 5

Final Discussion

An emerging theory proposes that several neuropsychiatric and developmental brain disorders are indeed 'synapsopathies' — synaptic development disorders or dysfunctions in synaptic plasticity (Bear et al., 2008; Zoghbi, 2003). This has been further confirmed by the involvement of a very large number of genes that code for proteins of the PSD in as many as 133 neurological, psychiatric and genetic disorders that affect the nervous system (Bayes et al., 2011). The works presented here adds support to this hypothesis and explores the role of nArgBP2 and Shank3 *in vivo* and how mutations in these genes influence synaptic function and behavior.

We observed that mutant nArgBP2 mice display several phenotypes reminiscent of manic behavior, while challenging these animals with a form of chronic mild stress led them to display an increase in measures of depressive-like behavior. Predictive validity was also tested by administering two drugs commonly prescribed to BPD patients – Valproic acid and Lithium. From these, lithium was found to ameliorate several of the manic-like behavioral manifestations in nArgBP2$^{-/-}$ mice.

We also generated and characterized two mutant mouse lines for the Shank3 gene. In this work we found that the cortico-striatal circuitry is dysfunctional following mutations in the Shank3 gene and that behaviorally the animals display increased grooming behaviors and deficits in social interaction. From the two Shank3 lines generated, a grade effect was correlated with the severity of the genetic lesion, with the more severe of the two causing significant synaptic dysfunction and overt abnormal behavioral phenotypes.

Nevertheless, while we made contributions to further understand the role of these proteins, the consequences of their lesion at the genetic level and gained insights in the affected circuits, several more questions are waiting further investigation. Regarding nArgBP2, it will still be important to probe which cellular mechanism may be playing a role in the up-regulation in glutamate signaling. Also, could endogenous nArgBP2 function as a negative regulator for the synaptic expression and regulation of glutamate receptors? Why are the nArgBP2 mutant mice sensitive to lithium and not valproic acid? Could this be relevant for human treatments or drug specificity for a subtype of BPD? What is the exact role played by the nArgBP2 brain-specific exon, why is it preserved across evolution with extremely high degree of conservation and by

which mechanisms it is only expressed in the brain? Does nArgBP2 play a role in the molecular clock oscillations?

Regarding Shank3, we and others have now shown that indeed a dysfunction in this gene causes autistic-like behaviors in mice. Evidences presented also point to a dysfunction in cortico-striatal circuits which may be the proximal cause for the excessive grooming behavior. Nevertheless, it is not well establish if this is the main source for the deficiencies seen in social interaction. Therefore, these animals may provide a powerful tool to dissect the brain circuitry involved in the regulation of social interactions. Other questions that are still unaddressed and remain relevant include knowing if a genetic postnatal rescue of Shank3 will rescue the synaptic and behavioral abnormalities. Considerable progress has been made in this area for other disorders, also of a genetic origin and also considered to be developmental in nature. For example, advances have been made in showing that a postnatal rescue of MECP2 (Rett Syndrome) and FMRP (Fragile-X Syndrome) expression can ameliorate or delay several of the abnormalities seen in the mouse models for these disorders (Giacometti et al., 2007; Guo et al., 2011; Guy et al., 2007; Zeier et al., 2009). Therefore it would be interesting to understand if a similar phenomenon could occur for a Shank3 genetic rescue. If answered in the affirmative, this would further support the shift in paradigm now considering developmental disorder as potentially “reversible”.

More broadly, one aspect still eluding precise understanding is the fact that the same gene or genes in the same family can trigger different disorders. For genetic products producing interrelated and interacting proteins, this may be explained by better comprehending their expression pattern in the mammalian brain, and potentially addressing which particular circuits are affected, and hence, which of these circuits contribute to discrete phenotypes. However, the origin of different disorders by mutations in the same gene still requires further investigation. This, for example, is the case for Shank3 which has been strongly linked to autism, but also schizophrenia. Here the solution may reside at understanding local differences between expression of isoforms, gradation of the deleterious mutations or the potential effect of environmental and/or other genetic factors. The generation of knock-in animals that replicate discrete human mutations may also produce novel insights into these questions.

Our understanding of human disorders is increasing at a rapid pace. The synergy between findings stemming from better diagnostic protocols, human genetic

data and functional studies performed in animal models will continue to produce important insights into the fundamental basic neurobiological phenomena and hopefully also coalesce into advances for more effective therapies aimed at these disorders.

References

Abou Jamra R, Becker T, Georgi A, Feulner T, Schumacher J, Stromaier J, Schirmbeck F, Schulze TG, Propping P, Rietschel M, Nothen MM, Cichon S. 2008. Genetic variation of the FAT gene at 4q35 is associated with bipolar affective disorder. Mol Psychiatry 13(3):277-284.

Abrahams BS, Geschwind DH. 2008. Advances in autism genetics: on the threshold of a new neurobiology. Nat Rev Genet 9(5):341-355.

Aharon I, Etcoff N, Ariely D, Chabris CF, O'Connor E, Breiter HC. 2001. Beautiful faces have variable reward value: fMRI and behavioral evidence. Neuron 32(3):537-551.

Akiskal HS. 1983. Dysthymic disorder: psychopathology of proposed chronic depressive subtypes. Am J Psychiatry 140(1):11-20.

Akiskal HS, Djenderedjian AM, Rosenthal RH, Khani MK. 1977. Cyclothymic disorder: validating criteria for inclusion in the bipolar affective group. Am J Psychiatry 134(11):1227-1233.

Albin RL, Young AB, Penney JB. 1989. The functional anatomy of basal ganglia disorders. Trends Neurosci 12(10):366-375.

Altamura CA, Mauri MC, Ferrara A, Moro AR, D'Andrea G, Zamberlan F. 1993. Plasma and platelet excitatory amino acids in psychiatric disorders. Am J Psychiatry 150(11):1731-1733.

American Psychiatric Association. 2000. Diagnostic and statistical manual of mental disorders : DSM-IV-TR. Washington, DC: American Psychiatric Association. xxxvii, 943 p. p.

American Psychiatric Association. 2000. Diagnostic criteria from DSM-IV-TR. Washington, D.C.: American Psychiatric Association. xii, 370 p. p.

Andreasen NC, Rice J, Endicott J, Coryell W, Grove WM, Reich T. 1987. Familial rates of affective disorder. A report from the National Institute of Mental Health Collaborative Study. Arch Gen Psychiatry 44(5):461-469.

Anguelova M, Benkelfat C, Turecki G. 2003. A systematic review of association studies investigating genes coding for serotonin receptors and the serotonin transporter: I. Affective disorders. Mol Psychiatry 8(6):574-591.

Antelman SM, Caggiula AR, Kucinski BJ, Fowler H, Gershon S, Edwards DJ, Austin MC, Stiller R, Kiss S, Kocan D. 1998. The effects of lithium on a potential cycling model of bipolar disorder. Prog Neuropsychopharmacol Biol Psychiatry 22(3):495-510.

Antoch MP, Song EJ, Chang AM, Vitaterna MH, Zhao Y, Wilsbacher LD, Sangoram AM, King DP, Pinto LH, Takahashi JS. 1997. Functional identification of the mouse circadian Clock gene by transgenic BAC rescue. Cell 89(4):655-667.

Arnone D, Cavanagh J, Gerber D, Lawrie SM, Ebmeier KP, McIntosh AM. 2009. Magnetic resonance imaging studies in bipolar disorder and schizophrenia: meta-analysis. Br J Psychiatry 195(3):194-201.

Asperger H. 1944. Die autistischen Psychopathen im Kindesalter. Archiv für Psychiatrie und Nervenkrankheiten(117):76-136.

Aylward EH, Roberts-Twillie JV, Barta PE, Kumar AJ, Harris GJ, Geer M, Peyser CE, Pearlson GD. 1994. Basal ganglia volumes and white matter hyperintensities in patients with bipolar disorder. Am J Psychiatry 151(5):687-693.

Bailey A, Le Couteur A, Gottesman I, Bolton P, Simonoff E, Yuzda E, Rutter M. 1995. Autism as a strongly genetic disorder: evidence from a British twin study. Psychol Med 25(1):63-77.

Baird G, Simonoff E, Pickles A, Chandler S, Loucas T, Meldrum D, Charman T. 2006. Prevalence of disorders of the autism spectrum in a population cohort of children in South Thames: the Special Needs and Autism Project (SNAP). Lancet 368(9531):210-215.

Bangash MA, Park JM, Melnikova T, Wang D, Jeon SK, Lee D, Syeda S, Kim J, Kouser M, Schwartz J, Cui Y, Zhao X, Speed HE, Kee SE, Tu JC, Hu JH, Petralia RS, Linden DJ, Powell CM, Savonenko A, Xiao B, Worley PF. 2011. Enhanced Polyubiquitination of Shank3 and NMDA Receptor in a Mouse Model of Autism. Cell 145(5):758-772.

Barabasi AL, Gulbahce N, Loscalzo J. 2011. Network medicine: a network-based approach to human disease. Nat Rev Genet 12(1):56-68.

Barbier E, Wang JB. 2009. Anti-depressant and anxiolytic like behaviors in PKCI/HINT1 knockout mice associated with elevated plasma corticosterone level. BMC Neurosci 10:132.

Barbini B, Colombo C, Benedetti F, Campori E, Bellodi L, Smeraldi E. 1998. The unipolar-bipolar dichotomy and the response to sleep deprivation. Psychiatry Res 79(1):43-50.

Baron M, Mendlewicz J, Gruen R, Asnis L, Fieve RR. 1981. Assortative mating in affective disorders. J Affect Disord 3(2):167-171.

Baron MK, Boeckers TM, Vaida B, Faham S, Gingery M, Sawaya MR, Salyer D, Gundelfinger ED, Bowie JU. 2006. An architectural framework that may lie at the core of the postsynaptic density. Science 311(5760):531-535.

Bartels A, Zeki S. 2000. The neural basis of romantic love. Neuroreport 11(17):3829-3834.

Bartels A, Zeki S. 2004. The neural correlates of maternal and romantic love. Neuroimage 21(3):1155-1166.

Baum AE, Akula N, Cabanero M, Cardona I, Corona W, Klemens B, Schulze TG, Cichon S, Rietschel M, Nothen MM, Georgi A, Schumacher J, Schwarz M, Abou Jamra R, Hofels S, Propping P, Satagopan J, Detera-Wadleigh SD, Hardy J, McMahon FJ. 2008. A genome-wide association study implicates diacylglycerol kinase eta (DGKH) and several other genes in the etiology of bipolar disorder. Mol Psychiatry 13(2):197-207.

Bayes A, van de Lagemaat LN, Collins MO, Croning MD, Whittle IR, Choudhary JS, Grant SG. 2011. Characterization of the proteome, diseases and evolution of the human postsynaptic density. Nat Neurosci 14(1):19-21.

Bear MF, Dolen G, Osterweil E, Nagarajan N. 2008. Fragile X: translation in action. Neuropsychopharmacology 33(1):84-87.

Beaudet A. 2007. Autism: highly heritable but not inherited. Nature Medicine 13(5):534-536.

Belanoff JK, Flores BH, Kalezhan M, Sund B, Schatzberg AF. 2001. Rapid reversal of psychotic depression using mifepristone. J Clin Psychopharmacol 21(5):516-521.

Belmaker RH, Agam G. 2008. Major depressive disorder. N Engl J Med 358(1):55-68.

Benedetti F, Barbini B, Bernasconi A, Fulgosi MC, Colombo C, Dallaspezia S, Gavinelli C, Marino E, Pirovano A, Radaelli D, Smeraldi E. 2008. Serotonin 5-HT2A receptor gene variants influence antidepressant response to repeated total

sleep deprivation in bipolar depression. Prog Neuropsychopharmacol Biol Psychiatry 32(8):1863-1866.

Berkel S, Marshall CR, Weiss B, Howe J, Roeth R, Moog U, Endris V, Roberts W, Szatmari P, Pinto D, Bonin M, Riess A, Engels H, Sprengel R, Scherer SW, Rappold GA. 2010. Mutations in the SHANK2 synaptic scaffolding gene in autism spectrum disorder and mental retardation. Nat Genet 42(6):489-491.

Berson DM. 2007. Phototransduction in ganglion-cell photoreceptors. Pflugers Arch 454(5):849-855.

Berson DM, Dunn FA, Takao M. 2002. Phototransduction by retinal ganglion cells that set the circadian clock. Science 295(5557):1070-1073.

Bertrand J, Mars A, Boyle C, Bove F, Yeargin-Allsopp M, Decoufle P. 2001. Prevalence of autism in a United States population: the Brick Township, New Jersey, investigation. Pediatrics 108(5):1155-1161.

Beyer JL, Kuchibhatla M, Payne ME, Moo-Young M, Cassidy F, Macfall J, Krishnan KR. 2004. Hippocampal volume measurement in older adults with bipolar disorder. Am J Geriatr Psychiatry 12(6):613-620.

Bienvenu OJ, Wang Y, Shugart YY, Welch JM, Grados MA, Fyer AJ, Rauch SL, McCracken JT, Rasmussen SA, Murphy DL, Cullen B, Valle D, Hoehn-Saric R, Greenberg BD, Pinto A, Knowles JA, Piacentini J, Pauls DL, Liang KY, Willour VL, Riddle M, Samuels JF, Feng G, Nestadt G. 2009. Sapap3 and pathological grooming in humans: Results from the OCD collaborative genetics study. Am J Med Genet B Neuropsychiatr Genet 150B(5):710-720.

Blackwood DH, Fordyce A, Walker MT, St Clair DM, Porteous DJ, Muir WJ. 2001. Schizophrenia and affective disorders--cosegregation with a translocation at chromosome 1q42 that directly disrupts brain-expressed genes: clinical and P300 findings in a family. Am J Hum Genet 69(2):428-433.

Blair IP, Chetcuti AF, Badenhop RF, Scimone A, Moses MJ, Adams LJ, Craddock N, Green E, Kirov G, Owen MJ, Kwok JB, Donald JA, Mitchell PB, Schofield PR. 2006. Positional cloning, association analysis and expression studies provide convergent evidence that the cadherin gene FAT contains a bipolar disorder susceptibility allele. Mol Psychiatry 11(4):372-383.

Blumberg HP, Kaufman J, Martin A, Whiteman R, Zhang JH, Gore JC, Charney DS, Krystal JH, Peterson BS. 2003. Amygdala and hippocampal volumes in

adolescents and adults with bipolar disorder. Arch Gen Psychiatry 60(12):1201-1208.

Blumenfeld H. 2010. Neuroanatomy through clinical cases. Sunderland, Mass.: Sinauer Associates. xxiii, 1006 p. p.

Boardman L, van der Merweb L, Lochner C, Kinneara CJ, Seedatd S, Steind D, J,, Moolman-Smook JC, Hemmings SMJ. 2010. Investigating SAPAP3 variants in the etiology of obsessive-compulsive disorder and trichotillomania in the South African white population. Comprehensive Psychiatry (in press).

Bockers TM, Mameza MG, Kreutz MR, Bockmann J, Weise C, Buck F, Richter D, Gundelfinger ED, Kreienkamp HJ. 2001. Synaptic scaffolding proteins in rat brain. Ankyrin repeats of the multidomain Shank protein family interact with the cytoskeletal protein alpha-fodrin. J Biol Chem 276(43):40104-40112.

Bonaglia MC, Giorda R, Borgatti R, Felisari G, Gagliardi C, Selicorni A, Zuffardi O. 2001. Disruption of the ProSAP2 gene in a t(12;22)(q24.1;q13.3) is associated with the 22q13.3 deletion syndrome. Am J Hum Genet 69(2):261-268.

Bonaglia MC, Giorda R, Mani E, Aceti G, Anderlid BM, Baroncini A, Pramparo T, Zuffardi O. 2006. Identification of a recurrent breakpoint within the SHANK3 gene in the 22q13.3 deletion syndrome. J Med Genet 43(10):822-828.

Botto LD, May K, Fernhoff PM, Correa A, Coleman K, Rasmussen SA, Merritt RK, O'Leary LA, Wong LY, Elixson EM, Mahle WT, Campbell RM. 2003. A population-based study of the 22q11.2 deletion: phenotype, incidence, and contribution to major birth defects in the population. Pediatrics 112(1 Pt 1):101-107.

Boulton AA, Baker GB, Martin-Iverson MT. 1991. Animal models in psychiatry. Clifton, N.J.: Humana Press.

Bourgeron T. 2009. A synaptic trek to autism. Curr Opin Neurobiol 19(2):231-234.

Bozdagi O, Sakurai T, Papapetrou D, Wang X, Dickstein DL, Takahashi N, Kajiwara Y, Yang M, Katz AM, Scattoni ML, Harris MJ, Saxena R, Silverman JL, Crawley JN, Zhou Q, Hof PR, Buxbaum JD. 2010. Haploinsufficiency of the autism-associated Shank3 gene leads to deficits in synaptic function, social interaction, and social communication. Mol Autism 1(1):15.

Braff DL, Geyer MA. 1990. Sensorimotor gating and schizophrenia. Human and animal model studies. Arch Gen Psychiatry 47(2):181-188.

Braff DL, Geyer MA, Swerdlow NR. 2001. Human studies of prepulse inhibition of startle: normal subjects, patient groups, and pharmacological studies. Psychopharmacology (Berl) 156(2-3):234-258.

Brambilla P, Harenski K, Nicoletti MA, Mallinger AG, Frank E, Kupfer DJ, Keshavan MS, Soares JC. 2001. Anatomical MRI study of basal ganglia in bipolar disorder patients. Psychiatry Res 106(2):65-80.

Buchan H, Johnstone E, McPherson K, Palmer RL, Crow TJ, Brandon S. 1992. Who benefits from electroconvulsive therapy? Combined results of the Leicester and Northwick Park trials. Br J Psychiatry 160:355-359.

Bunger MK, Wilsbacher LD, Moran SM, Clendenin C, Radcliffe LA, Hogenesch JB, Simon MC, Takahashi JS, Bradfield CA. 2000. Mop3 is an essential component of the master circadian pacemaker in mammals. Cell 103(7):1009-1017.

Carlin RK, Bartelt DC, Siekevitz P. 1983. Identification of fodrin as a major calmodulin-binding protein in postsynaptic density preparations. J Cell Biol 96(2):443-448.

Carmichael ST, Price JL. 1995a. Limbic connections of the orbital and medial prefrontal cortex in macaque monkeys. J Comp Neurol 363(4):615-641.

Carmichael ST, Price JL. 1995b. Sensory and premotor connections of the orbital and medial prefrontal cortex of macaque monkeys. J Comp Neurol 363(4):642-664.

Cavada C, Company T, Tejedor J, Cruz-Rizzolo RJ, Reinoso-Suarez F. 2000. The anatomical connections of the macaque monkey orbitofrontal cortex. A review. Cereb Cortex 10(3):220-242.

Cerullo MA, Adler CM, Delbello MP, Strakowski SM. 2009. The functional neuroanatomy of bipolar disorder. Int Rev Psychiatry 21(4):314-322.

Cestra G, Toomre D, Chang S, De Camilli P. 2005. The Abl/Arg substrate ArgBP2/nArgBP2 coordinates the function of multiple regulatory mechanisms converging on the actin cytoskeleton. Proc Natl Acad Sci U S A 102(5):1731-1736.

Chakrabarti S, Fombonne E. 2005. Pervasive developmental disorders in preschool children: confirmation of high prevalence. Am J Psychiatry 162(6):1133-1141.

Chen G, Huang LD, Jiang YM, Manji HK. 1999. The mood-stabilizing agent valproate inhibits the activity of glycogen synthase kinase-3. J Neurochem 72(3):1327-1330.

Chih B, Engelman H, Scheiffele P. 2005. Control of excitatory and inhibitory synapse formation by neuroligins. Science 307(5713):1324-1328.

Ciaranello RD, Ciaranello AL. 1991. Genetics of major psychiatric disorders. Annu Rev Med 42:151-158.

Cichon S, Winge I, Mattheisen M, Georgi A, Karpushova A, Freudenberg J, Freudenberg-Hua Y, Babadjanova G, Van Den Bogaert A, Abramova LI, Kapiletti S, Knappskog PM, McKinney J, Maier W, Jamra RA, Schulze TG, Schumacher J, Propping P, Rietschel M, Haavik J, Nothen MM. 2008. Brain-specific tryptophan hydroxylase 2 (TPH2): a functional Pro206Ser substitution and variation in the 5'-region are associated with bipolar affective disorder. Hum Mol Genet 17(1):87-97.

Clay HB, Sillivan S, Konradi C. 2010. Mitochondrial dysfunction and pathology in bipolar disorder and schizophrenia. Int J Dev Neurosci.

Collins MO, Husi H, Yu L, Brandon JM, Anderson CN, Blackstock WP, Choudhary JS, Grant SG. 2006. Molecular characterization and comparison of the components and multiprotein complexes in the postsynaptic proteome. J Neurochem 97 Suppl 1:16-23.

Conn PJ, Pin JP. 1997. Pharmacology and functions of metabotropic glutamate receptors. Annu Rev Pharmacol Toxicol 37:205-237.

Craddock N, Jones I. 1999. Genetics of bipolar disorder. J Med Genet 36(8):585-594.

Damasio AR. 2005. Descartes' error : emotion, reason, and the human brain. London: Penguin. xxiii, 312 p. p.

Damasio AR, Maurer RG. 1978. A neurological model for childhood autism. Arch Neurol 35(12):777-786.

Daw NW, Stein PS, Fox K. 1993. The role of NMDA receptors in information processing. Annu Rev Neurosci 16:207-222.

Dean C, Scholl FG, Choih J, DeMaria S, Berger J, Isacoff E, Scheiffele P. 2003. Neurexin mediates the assembly of presynaptic terminals. Nat Neurosci 6(7):708-716.

Debruyne JP, Noton E, Lambert CM, Maywood ES, Weaver DR, Reppert SM. 2006. A clock shock: mouse CLOCK is not required for circadian oscillator function. Neuron 50(3):465-477.

DeBruyne JP, Weaver DR, Reppert SM. 2007. CLOCK and NPAS2 have overlapping roles in the suprachiasmatic circadian clock. Nat Neurosci 10(5):543-545.

Del Zompo M, De Luca V, Severino G, Ni X, Mulas S, Congiu D, Piccardi MP, Kennedy JL. 2007. Haplotype association study between DRD1 gene and bipolar type I affective disorder in two samples from Canada and Sardinia. Am J Med Genet B Neuropsychiatr Genet 144B(2):237-241.

DeLong MR. 1990. Primate models of movement disorders of basal ganglia origin. Trends Neurosci 13(7):281-285.

Detera-Wadleigh SD, McMahon FJ. 2006. G72/G30 in schizophrenia and bipolar disorder: review and meta-analysis. Biol Psychiatry 60(2):106-114.

Devriendt K, Fryns JP, Mortier G, van Thienen MN, Keymolen K. 1998. The annual incidence of DiGeorge/velocardiofacial syndrome. J Med Genet 35(9):789-790.

Diehl DJ, Gershon S. 1992. The role of dopamine in mood disorders. Compr Psychiatry 33(2):115-120.

Dingledine R, Borges K, Bowie D, Traynelis SF. 1999. The glutamate receptor ion channels. Pharmacol Rev 51(1):7-61.

Drevets WC, Price JL, Simpson JR, Jr., Todd RD, Reich T, Vannier M, Raichle ME. 1997. Subgenual prefrontal cortex abnormalities in mood disorders. Nature 386(6627):824-827.

Du J, Creson TK, Wu LJ, Ren M, Gray NA, Falke C, Wei Y, Wang Y, Blumenthal R, Machado-Vieira R, Yuan P, Chen G, Zhuo M, Manji HK. 2008. The role of hippocampal GluR1 and GluR2 receptors in manic-like behavior. J Neurosci 28(1):68-79.

Du J, Gray NA, Falke CA, Chen W, Yuan P, Szabo ST, Einat H, Manji HK. 2004. Modulation of synaptic plasticity by antimanic agents: the role of AMPA glutamate receptor subunit 1 synaptic expression. J Neurosci 24(29):6578-6589.

Du Y, Weed SA, Xiong WC, Marshall TD, Parsons JT. 1998. Identification of a novel cortactin SH3 domain-binding protein and its localization to growth cones of cultured neurons. Mol Cell Biol 18(10):5838-5851.

Duffy A, Alda M, Crawford L, Milin R, Grof P. 2007. The early manifestations of bipolar disorder: a longitudinal prospective study of the offspring of bipolar parents. Bipolar Disord 9(8):828-838.

Dunner DL, Patrick V, Fieve RR. 1977. Rapid cycling manic depressive patients. Compr Psychiatry 18(6):561-566.

Durand CM, Betancur C, Boeckers TM, Bockmann J, Chaste P, Fauchereau F, Nygren G, Rastam M, Gillberg IC, Anckarsater H, Sponheim E, Goubran-Botros H, Delorme R, Chabane N, Mouren-Simeoni MC, de Mas P, Bieth E, Roge B, Heron D, Burglen L, Gillberg C, Leboyer M, Bourgeron T. 2007. Mutations in the gene encoding the synaptic scaffolding protein SHANK3 are associated with autism spectrum disorders. Nat Genet 39(1):25-27.

Ebert D, Berger M. 1998. Neurobiological similarities in antidepressant sleep deprivation and psychostimulant use: a psychostimulant theory of antidepressant sleep deprivation. Psychopharmacology (Berl) 140(1):1-10.

Einat H. 2007. Different behaviors and different strains: potential new ways to model bipolar disorder. Neurosci Biobehav Rev 31(6):850-857.

El-Mallakh RS, El-Masri MA, Huff MO, Li XP, Decker S, Levy RS. 2003. Intracerebroventricular administration of ouabain as a model of mania in rats. Bipolar Disord 5(5):362-365.

Elashoff M, Higgs BW, Yolken RH, Knable MB, Weis S, Webster MJ, Barci BM, Torrey EF. 2007. Meta-analysis of 12 genomic studies in bipolar disorder. J Mol Neurosci 31(3):221-243.

Elias GM, Nicoll RA. 2007. Synaptic trafficking of glutamate receptors by MAGUK scaffolding proteins. Trends Cell Biol 17(7):343-352.

Endo T, Roth C, Landolt HP, Werth E, Aeschbach D, Achermann P, Borbely AA. 1998. Selective REM sleep deprivation in humans: effects on sleep and sleep EEG. Am J Physiol 274(4 Pt 2):R1186-1194.

Endo T, Schwierin B, Borbely AA, Tobler I. 1997. Selective and total sleep deprivation: effect on the sleep EEG in the rat. Psychiatry Res 66(2-3):97-110.

Eslinger PJ, Damasio AR. 1985. Severe disturbance of higher cognition after bilateral frontal lobe ablation: patient EVR. Neurology 35(12):1731-1741.

Etherton MR, Blaiss CA, Powell CM, Sudhof TC. 2009. Mouse neurexin-1alpha deletion causes correlated electrophysiological and behavioral changes consistent with cognitive impairments. Proc Natl Acad Sci U S A 106(42):17998-18003.

Farmer A, McGuffin P. 1989. The classification of the depressions. Contemporary confusion revisited. Br J Psychiatry 155:437-443.

Farr CD, Gafken PR, Norbeck AD, Doneanu CE, Stapels MD, Barofsky DF, Minami M, Saugstad JA. 2004. Proteomic analysis of native metabotropic glutamate receptor 5 protein complexes reveals novel molecular constituents. J Neurochem 91(2):438-450.

Ferreira MA, O'Donovan MC, Meng YA, Jones IR, Ruderfer DM, Jones L, Fan J, Kirov G, Perlis RH, Green EK, Smoller JW, Grozeva D, Stone J, Nikolov I, Chambert K, Hamshere ML, Nimgaonkar VL, Moskvina V, Thase ME, Caesar S, Sachs GS, Franklin J, Gordon-Smith K, Ardlie KG, Gabriel SB, Fraser C, Blumenstiel B, Defelice M, Breen G, Gill M, Morris DW, Elkin A, Muir WJ, McGhee KA, Williamson R, MacIntyre DJ, MacLean AW, St CD, Robinson M, Van Beck M, Pereira AC, Kandaswamy R, McQuillin A, Collier DA, Bass NJ, Young AH, Lawrence J, Ferrier IN, Anjorin A, Farmer A, Curtis D, Scolnick EM, McGuffin P, Daly MJ, Corvin AP, Holmans PA, Blackwood DH, Gurling HM, Owen MJ, Purcell SM, Sklar P, Craddock N. 2008. Collaborative genome-wide association analysis supports a role for ANK3 and CACNA1C in bipolar disorder. Nat Genet 40(9):1056-1058.

Ford DE, Kamerow DB. 1989. Epidemiologic study of sleep disturbances and psychiatric disorders. An opportunity for prevention? JAMA 262(11):1479-1484.

Francis PT, Poynton A, Lowe SL, Najlerahim A, Bridges PK, Bartlett JR, Procter AW, Bruton CJ, Bowen DM. 1989. Brain amino acid concentrations and Ca2+-dependent release in intractable depression assessed antemortem. Brain Res 494(2):315-324.

Franklin TR, Druhan JP. 2000. Involvement of the nucleus accumbens and medial prefrontal cortex in the expression of conditioned hyperactivity to a cocaine-associated environment in rats. Neuropsychopharmacology 23(6):633-644.

Frazier JA, Chiu S, Breeze JL, Makris N, Lange N, Kennedy DN, Herbert MR, Bent EK, Koneru VK, Dieterich ME, Hodge SM, Rauch SL, Grant PE, Cohen BM, Seidman LJ, Caviness VS, Biederman J. 2005. Structural brain magnetic resonance imaging of limbic and thalamic volumes in pediatric bipolar disorder. Am J Psychiatry 162(7):1256-1265.

Frey BN, Andreazza AC, Rosa AR, Martins MR, Valvassori SS, Reus GZ, Hatch JP, Quevedo J, Kapczinski F. 2006a. Lithium increases nerve growth factor levels in

the rat hippocampus in an animal model of mania. Behav Pharmacol 17(4):311-318.

Frey BN, Valvassori SS, Reus GZ, Martins MR, Petronilho FC, Bardini K, Dal-Pizzol F, Kapczinski F, Quevedo J. 2006b. Effects of lithium and valproate on amphetamine-induced oxidative stress generation in an animal model of mania. J Psychiatry Neurosci 31(5):326-332.

Frye MA, Tsai GE, Huggins T, Coyle JT, Post RM. 2007. Low cerebrospinal fluid glutamate and glycine in refractory affective disorder. Biol Psychiatry 61(2):162-166.

Gauthier J, Spiegelman D, Piton A, Lafreniere RG, Laurent S, St-Onge J, Lapointe L, Hamdan FF, Cossette P, Mottron L, Fombonne E, Joober R, Marineau C, Drapeau P, Rouleau GA. 2009. Novel de novo SHANK3 mutation in autistic patients. Am J Med Genet B Neuropsychiatr Genet 150B(3):421-424.

Geschwind DH. 2009. Advances in autism. Annu Rev Med 60:367-380.

Gessa GL, Pani L, Fadda P, Fratta W. 1995. Sleep deprivation in the rat: an animal model of mania. Eur Neuropsychopharmacol 5 Suppl:89-93.

Giacometti E, Luikenhuis S, Beard C, Jaenisch R. 2007. Partial rescue of MeCP2 deficiency by postnatal activation of MeCP2. Proc Natl Acad Sci U S A 104(6):1931-1936.

Goddard GV, McIntyre DC, Leech CK. 1969. A permanent change in brain function resulting from daily electrical stimulation. Exp Neurol 25(3):295-330.

Goel N, Lee TM. 1997. Social cues modulate free-running circadian activity rhythms in the diurnal rodent, Octodon degus. Am J Physiol 273(2 Pt 2):R797-804.

Goh KI, Cusick ME, Valle D, Childs B, Vidal M, Barabasi AL. 2007. The human disease network. Proc Natl Acad Sci U S A 104(21):8685-8690.

Goldin LR, Gershon ES, Targum SD, Sparkes RS, McGinniss M. 1983. Segregation and linkage analyses in families of patients with bipolar, unipolar, and schizoaffective mood disorders. Am J Hum Genet 35(2):274-287.

Gould TD, Zarate CA, Manji HK. 2004. Glycogen synthase kinase-3: a target for novel bipolar disorder treatments. J Clin Psychiatry 65(1):10-21.

Gould TJ, Keith RA, Bhat RV. 2001. Differential sensitivity to lithium's reversal of amphetamine-induced open-field activity in two inbred strains of mice. Behav Brain Res 118(1):95-105.

Grace SL, Evindar A, Stewart DE. 2003. The effect of postpartum depression on child cognitive development and behavior: a review and critical analysis of the literature. Arch Womens Ment Health 6(4):263-274.

Graybiel AM. 2008. Habits, rituals, and the evaluative brain. Annu Rev Neurosci 31:359-387.

Greenwood TA, Alexander M, Keck PE, McElroy S, Sadovnick AD, Remick RA, Kelsoe JR. 2001. Evidence for linkage disequilibrium between the dopamine transporter and bipolar disorder. Am J Med Genet 105(2):145-151.

Greenwood TA, Schork NJ, Eskin E, Kelsoe JR. 2006. Identification of additional variants within the human dopamine transporter gene provides further evidence for an association with bipolar disorder in two independent samples. Mol Psychiatry 11(2):125-133, 115.

Grigoroiu-Serbanescu M, Diaconu CC, Herms S, Bleotu C, Vollmer J, Muhleisen TW, Prelipceanu D, Priebe L, Mihailescu R, Georgescu MJ, Sima D, Grimberg M, Nothen MM, Cichon S. 2008. Investigation of the tryptophan hydroxylase 2 gene in bipolar I disorder in the Romanian population. Psychiatr Genet 18(5):240-247.

Gruber SA, Rogowska J, Yurgelun-Todd DA. 2004. Decreased activation of the anterior cingulate in bipolar patients: an fMRI study. J Affect Disord 82(2):191-201.

Guo W, Allan AM, Zong R, Zhang L, Johnson EB, Schaller EG, Murthy AC, Goggin SL, Eisch AJ, Oostra BA, Nelson DL, Jin P, Zhao X. 2011. Ablation of Fmrp in adult neural stem cells disrupts hippocampus-dependent learning. Nat Med 17(5):559-565.

Guy J, Gan J, Selfridge J, Cobb S, Bird A. 2007. Reversal of neurological defects in a mouse model of Rett syndrome. Science 315(5815):1143-1147.

Haber SN, Kunishio K, Mizobuchi M, Lynd-Balta E. 1995. The orbital and medial prefrontal circuit through the primate basal ganglia. J Neurosci 15(7 Pt 1):4851-4867.

Hallett M. 2000. Transcranial magnetic stimulation and the human brain. Nature 406(6792):147-150.

Hardin PE, Hall JC, Rosbash M. 1990. Feedback of the Drosophila period gene product on circadian cycling of its messenger RNA levels. Nature 343(6258):536-540.

Harvey AG. 2001. Insomnia: symptom or diagnosis? Clin Psychol Rev 21(7):1037-1059.

Harvey AG. 2008. Sleep and circadian rhythms in bipolar disorder: seeking synchrony, harmony, and regulation. Am J Psychiatry 165(7):820-829.

Harvey AG. 2011. Sleep and Circadian Functioning: Critical Mechanisms in the Mood Disorders. Annu Rev Clin Psychol 7(8).

Harvey M, Gagne B, Labbe M, Barden N. 2007. Polymorphisms in the neuronal isoform of tryptophan hydroxylase 2 are associated with bipolar disorder in French Canadian pedigrees. Psychiatr Genet 17(1):17-22.

Hashimoto K, Sawa A, Iyo M. 2007. Increased levels of glutamate in brains from patients with mood disorders. Biol Psychiatry 62(11):1310-1316.

Hashimoto R, Hough C, Nakazawa T, Yamamoto T, Chuang DM. 2002. Lithium protection against glutamate excitotoxicity in rat cerebral cortical neurons: involvement of NMDA receptor inhibition possibly by decreasing NR2B tyrosine phosphorylation. J Neurochem 80(4):589-597.

Hayashi MK, Tang C, Verpelli C, Narayanan R, Stearns MH, Xu RM, Li H, Sala C, Hayashi Y. 2009. The postsynaptic density proteins Homer and Shank form a polymeric network structure. Cell 137(1):159-171.

Haznedar MM, Roversi F, Pallanti S, Baldini-Rossi N, Schnur DB, Licalzi EM, Tang C, Hof PR, Hollander E, Buchsbaum MS. 2005. Fronto-thalamo-striatal gray and white matter volumes and anisotropy of their connections in bipolar spectrum illnesses. Biol Psychiatry 57(7):733-742.

Heils A, Teufel A, Petri S, Stober G, Riederer P, Bengel D, Lesch KP. 1996. Allelic variation of human serotonin transporter gene expression. J Neurochem 66(6):2621-2624.

Hirayasu Y, Shenton ME, Salisbury DF, Kwon JS, Wible CG, Fischer IA, Yurgelun-Todd D, Zarate C, Kikinis R, Jolesz FA, McCarley RW. 1999. Subgenual cingulate cortex volume in first-episode psychosis. Am J Psychiatry 156(7):1091-1093.

Hodgkinson CA, Goldman D, Jaeger J, Persaud S, Kane JM, Lipsky RH, Malhotra AK. 2004. Disrupted in schizophrenia 1 (DISC1): association with schizophrenia, schizoaffective disorder, and bipolar disorder. Am J Hum Genet 75(5):862-872.

Hopkins J, Marcus M, Campbell SB. 1984. Postpartum depression: a critical review. Psychol Bull 95(3):498-515.

Hung AY, Futai K, Sala C, Valtschanoff JG, Ryu J, Woodworth MA, Kidd FL, Sung CC, Miyakawa T, Bear MF, Weinberg RJ, Sheng M. 2008. Smaller dendritic spines,

weaker synaptic transmission, but enhanced spatial learning in mice lacking Shank1. J Neurosci 28(7):1697-1708.

Husi H, Grant SG. 2001. Isolation of 2000-kDa complexes of N-methyl-D-aspartate receptor and postsynaptic density 95 from mouse brain. J Neurochem 77(1):281-291.

Husi H, Ward MA, Choudhary JS, Blackstock WP, Grant SG. 2000. Proteomic analysis of NMDA receptor-adhesion protein signaling complexes. Nat Neurosci 3(7):661-669.

Hwang J, Lyoo IK, Dager SR, Friedman SD, Oh JS, Lee JY, Kim SJ, Dunner DL, Renshaw PF. 2006. Basal ganglia shape alterations in bipolar disorder. Am J Psychiatry 163(2):276-285.

Ichtchenko K, Hata Y, Nguyen T, Ullrich B, Missler M, Moomaw C, Sudhof TC. 1995. Neuroligin 1: a splice site-specific ligand for beta-neurexins. Cell 81(3):435-443.

Insel TR. 2009. Disruptive insights in psychiatry: transforming a clinical discipline. J Clin Invest 119(4):700-705.

Irie M, Hata Y, Takeuchi M, Ichtchenko K, Toyoda A, Hirao K, Takai Y, Rosahl TW, Sudhof TC. 1997. Binding of neuroligins to PSD-95. Science 277(5331):1511-1515.

Ishizuka K, Paek M, Kamiya A, Sawa A. 2006. A review of Disrupted-In-Schizophrenia-1 (DISC1): neurodevelopment, cognition, and mental conditions. Biol Psychiatry 59(12):1189-1197.

Jackson A, Cavanagh J, Scott J. 2003. A systematic review of manic and depressive prodromes. J Affect Disord 74(3):209-217.

Jacquemont ML, Sanlaville D, Redon R, Raoul O, Cormier-Daire V, Lyonnet S, Amiel J, Le Merrer M, Heron D, de Blois MC, Prieur M, Vekemans M, Carter NP, Munnich A, Colleaux L, Philippe A. 2006. Array-based comparative genomic hybridisation identifies high frequency of cryptic chromosomal rearrangements in patients with syndromic autism spectrum disorders. J Med Genet 43(11):843-849.

Jamain S, Quach H, Betancur C, Rastam M, Colineaux C, Gillberg IC, Soderstrom H, Giros B, Leboyer M, Gillberg C, Bourgeron T. 2003. Mutations of the X-linked genes encoding neuroligins NLGN3 and NLGN4 are associated with autism. Nat Genet 34(1):27-29.

Jamain S, Radyushkin K, Hammerschmidt K, Granon S, Boretius S, Varoqueaux F, Ramanantsoa N, Gallego J, Ronnenberg A, Winter D, Frahm J, Fischer J, Bourgeron T, Ehrenreich H, Brose N. 2008. Reduced social interaction and ultrasonic communication in a mouse model of monogenic heritable autism. Proc Natl Acad Sci U S A 105(5):1710-1715.

James NM, Chapman CJ. 1975. A genetic study of bipolar affective disorder. Br J Psychiatry 126:449-456.

Jones SH. 2001. Circadian rhythms, multilevel models of emotion and bipolar disorder--an initial step towards integration? Clin Psychol Rev 21(8):1193-1209.

Jones SH, Hare DJ, Evershed K. 2005. Actigraphic assessment of circadian activity and sleep patterns in bipolar disorder. Bipolar Disord 7(2):176-186.

Jones SR, Gainetdinov RR, Wightman RM, Caron MG. 1998. Mechanisms of amphetamine action revealed in mice lacking the dopamine transporter. J Neurosci 18(6):1979-1986.

Jouvet D, Vimont P, Delorme F. 1964. [Study of Selective Deprivation of the Paradoxal Phase of Sleep in the Cat]. J Physiol (Paris) 56:381.

Judd LL, Akiskal HS, Maser JD, Zeller PJ, Endicott J, Coryell W, Paulus MP, Kunovac JL, Leon AC, Mueller TI, Rice JA, Keller MB. 1998. A prospective 12-year study of subsyndromal and syndromal depressive symptoms in unipolar major depressive disorders. Arch Gen Psychiatry 55(8):694-700.

Kaladchibachi SA, Doble B, Anthopoulos N, Woodgett JR, Manoukian AS. 2007. Glycogen synthase kinase 3, circadian rhythms, and bipolar disorder: a molecular link in the therapeutic action of lithium. J Circadian Rhythms 5:3.

Kalynchuk LE, Pinel JP, Treit D. 1998. Long-term kindling and interictal emotionality in rats: effect of stimulation site. Brain Res 779(1-2):149-157.

Kanazawa T, Glatt SJ, Kia-Keating B, Yoneda H, Tsuang MT. 2007. Meta-analysis reveals no association of the Val66Met polymorphism of brain-derived neurotrophic factor with either schizophrenia or bipolar disorder. Psychiatr Genet 17(3):165-170.

Kandel ER, Schwartz JH, Jessell TM. 2000. Principles of neural science. New York: McGraw-Hill, Health Professions Division. xli, 1414 p. p.

Kanner L. 1943. Autistic disturbances of affective contact. Nervous Child(2):217-250.

Kato T, Kato N. 2000. Mitochondrial dysfunction in bipolar disorder. Bipolar Disord 2(3 Pt 1):180-190.

Kawabe H, Hata Y, Takeuchi M, Ide N, Mizoguchi A, Takai Y. 1999. nArgBP2, a novel neural member of ponsin/ArgBP2/vinexin family that interacts with synapse-associated protein 90/postsynaptic density-95-associated protein (SAPAP). J Biol Chem 274(43):30914-30918.

Kemp JM, Powell TP. 1970. The cortico-striate projection in the monkey. Brain 93(3):525-546.

Kendell RE. 1987. Diagnosis and classification of functional psychoses. Br Med Bull 43(3):499-513.

Kendler KS, Prescott CA. 1999. A population-based twin study of lifetime major depression in men and women. Arch Gen Psychiatry 56(1):39-44.

Kennedy MB. 2000. Signal-processing machines at the postsynaptic density. Science 290(5492):750-754.

Kennedy MB, Bennett MK, Erondu NE. 1983. Biochemical and immunochemical evidence that the "major postsynaptic density protein" is a subunit of a calmodulin-dependent protein kinase. Proc Natl Acad Sci U S A 80(23):7357-7361.

Kessler RC, McGonagle KA, Swartz M, Blazer DG, Nelson CB. 1993. Sex and depression in the National Comorbidity Survey. I: Lifetime prevalence, chronicity and recurrence. J Affect Disord 29(2-3):85-96.

Kessler RC, McGonagle KA, Zhao S, Nelson CB, Hughes M, Eshleman S, Wittchen HU, Kendler KS. 1994. Lifetime and 12-month prevalence of DSM-III-R psychiatric disorders in the United States. Results from the National Comorbidity Survey. Arch Gen Psychiatry 51(1):8-19.

Kim-Cohen J, Caspi A, Moffitt TE, Harrington H, Milne BJ, Poulton R. 2003. Prior juvenile diagnoses in adults with mental disorder: developmental follow-back of a prospective-longitudinal cohort. Arch Gen Psychiatry 60(7):709-717.

Kim E, Naisbitt S, Hsueh YP, Rao A, Rothschild A, Craig AM, Sheng M. 1997. GKAP, a novel synaptic protein that interacts with the guanylate kinase-like domain of the PSD-95/SAP90 family of channel clustering molecules. J Cell Biol 136(3):669-678.

Kim HG, Kishikawa S, Higgins AW, Seong IS, Donovan DJ, Shen Y, Lally E, Weiss LA, Najm J, Kutsche K, Descartes M, Holt L, Braddock S, Troxell R, Kaplan L, Volkmar F, Klin A, Tsatsanis K, Harris DJ, Noens I, Pauls DL, Daly MJ, MacDonald ME, Morton CC, Quade BJ, Gusella JF. 2008. Disruption of neurexin 1 associated with autism spectrum disorder. Am J Hum Genet 82(1):199-207.

Kim JS, Schmid-Burgk W, Claus D, Kornhuber HH. 1982. Increased serum glutamate in depressed patients. Arch Psychiatr Nervenkr 232(4):299-304.

Kimber WL, Hsieh P, Hirotsune S, Yuva-Paylor L, Sutherland HF, Chen A, Ruiz-Lozano P, Hoogstraten-Miller SL, Chien KR, Paylor R, Scambler PJ, Wynshaw-Boris A. 1999. Deletion of 150 kb in the minimal DiGeorge/velocardiofacial syndrome critical region in mouse. Hum Mol Genet 8(12):2229-2237.

Kimura A, Baumann CA, Chiang SH, Saltiel AR. 2001. The sorbin homology domain: a motif for the targeting of proteins to lipid rafts. Proc Natl Acad Sci U S A 98(16):9098-9103.

King DP, Zhao Y, Sangoram AM, Wilsbacher LD, Tanaka M, Antoch MP, Steeves TD, Vitaterna MH, Kornhauser JM, Lowrey PL, Turek FW, Takahashi JS. 1997. Positional cloning of the mouse circadian clock gene. Cell 89(4):641-653.

Kioka N, Ueda K, Amachi T. 2002. Vinexin, CAP/ponsin, ArgBP2: a novel adaptor protein family regulating cytoskeletal organization and signal transduction. Cell Struct Funct 27(1):1-7.

Kitayama S, Shimada S, Xu H, Markham L, Donovan DM, Uhl GR. 1992. Dopamine transporter site-directed mutations differentially alter substrate transport and cocaine binding. Proc Natl Acad Sci U S A 89(16):7782-7785.

Klein PS, Melton DA. 1996. A molecular mechanism for the effect of lithium on development. Proc Natl Acad Sci U S A 93(16):8455-8459.

Kokoshka JM, Vaughan RA, Hanson GR, Fleckenstein AE. 1998. Nature of methamphetamine-induced rapid and reversible changes in dopamine transporters. Eur J Pharmacol 361(2-3):269-275.

Konopka RJ, Benzer S. 1971. Clock mutants of Drosophila melanogaster. Proc Natl Acad Sci U S A 68(9):2112-2116.

Koob GF, Bloom FE. 1988. Cellular and molecular mechanisms of drug dependence. Science 242(4879):715-723.

Krach S, Paulus FM, Bodden M, Kircher T. 2010. The rewarding nature of social interactions. Front Behav Neurosci 4:22.

Kucinski BJ, Antelman SM, Caggiula AR, Fowler H, Gershon S, Edwards DJ, Austin MC. 1998. Oscillatory effects of repeated morphine on shock-induced hypoalgesia and beta-endorphin. Synapse 30(1):30-37.

Kuribara H, Uchihashi Y. 1993. Dopamine antagonists can inhibit methamphetamine sensitization, but not cocaine sensitization, when assessed by ambulatory activity in mice. J Pharm Pharmacol 45(12):1042-1045.

La Malfa G, Lassi S, Bertelli M, Salvini R, Placidi GF. 2004. Autism and intellectual disability: a study of prevalence on a sample of the Italian population. J Intellect Disabil Res 48(Pt 3):262-267.

Lange KJ, McInnis MG. 2002. Studies of anticipation in bipolar affective disorder. CNS Spectr 7(3):196-202.

Lasky-Su JA, Faraone SV, Glatt SJ, Tsuang MT. 2005. Meta-analysis of the association between two polymorphisms in the serotonin transporter gene and affective disorders. Am J Med Genet B Neuropsychiatr Genet 133B(1):110-115.

Lau JY, Eley TC. 2010. The genetics of mood disorders. Annu Rev Clin Psychol 6:313-337.

Laumonnier F, Bonnet-Brilhault F, Gomot M, Blanc R, David A, Moizard MP, Raynaud M, Ronce N, Lemonnier E, Calvas P, Laudier B, Chelly J, Fryns JP, Ropers HH, Hamel BC, Andres C, Barthelemy C, Moraine C, Briault S. 2004. X-linked mental retardation and autism are associated with a mutation in the NLGN4 gene, a member of the neuroligin family. Am J Hum Genet 74(3):552-557.

Lawrence NS, Williams AM, Surguladze S, Giampietro V, Brammer MJ, Andrew C, Frangou S, Ecker C, Phillips ML. 2004. Subcortical and ventral prefrontal cortical neural responses to facial expressions distinguish patients with bipolar disorder and major depression. Biol Psychiatry 55(6):578-587.

Lax P, Zamora S, Madrid JA. 1999. Food-entrained feeding and locomotor circadian rhythms in rats under different lighting conditions. Chronobiol Int 16(3):281-291.

LeDoux JE. 2000. Emotion circuits in the brain. Annu Rev Neurosci 23:155-184.

Lesch KP, Bengel D, Heils A, Sabol SZ, Greenberg BD, Petri S, Benjamin J, Muller CR, Hamer DH, Murphy DL. 1996. Association of anxiety-related traits with a

polymorphism in the serotonin transporter gene regulatory region. Science 274(5292):1527-1531.

Leung LS, Ma J, McLachlan RS. 2000. Behaviors induced or disrupted by complex partial seizures. Neurosci Biobehav Rev 24(7):763-775.

Levine J, Panchalingam K, Rapoport A, Gershon S, McClure RJ, Pettegrew JW. 2000. Increased cerebrospinal fluid glutamine levels in depressed patients. Biol Psychiatry 47(7):586-593.

Leyfer OT, Folstein SE, Bacalman S, Davis NO, Dinh E, Morgan J, Tager-Flusberg H, Lainhart JE. 2006. Comorbid psychiatric disorders in children with autism: interview development and rates of disorders. J Autism Dev Disord 36(7):849-861.

Li R, el-Mallakh RS, Harrison L, Changaris DG, Levy RS. 1997. Lithium prevents ouabain-induced behavioral changes. Toward an animal model for manic depression. Mol Chem Neuropathol 31(1):65-72.

Lim S, Naisbitt S, Yoon J, Hwang JI, Suh PG, Sheng M, Kim E. 1999. Characterization of the Shank family of synaptic proteins. Multiple genes, alternative splicing, and differential expression in brain and development. J Biol Chem 274(41):29510-29518.

Lim S, Sala C, Yoon J, Park S, Kuroda S, Sheng M, Kim E. 2001. Sharpin, a novel postsynaptic density protein that directly interacts with the shank family of proteins. Mol Cell Neurosci 17(2):385-397.

Linghu B, Snitkin ES, Hu Z, Xia Y, Delisi C. 2009. Genome-wide prioritization of disease genes and identification of disease-disease associations from an integrated human functional linkage network. Genome Biol 10(9):R91.

Lipina TV, Niwa M, Jaaro-Peled H, Fletcher PJ, Seeman P, Sawa A, Roder JC. 2010. Enhanced dopamine function in DISC1-L100P mutant mice: implications for schizophrenia. Genes Brain Behav 9(7):777-789.

Lopez Leon S, Croes EA, Sayed-Tabatabaei FA, Claes S, Van Broeckhoven C, van Duijn CM. 2005. The dopamine D4 receptor gene 48-base-pair-repeat polymorphism and mood disorders: a meta-analysis. Biol Psychiatry 57(9):999-1003.

Lopez VA, Detera-Wadleigh S, Cardona I, Kassem L, McMahon FJ. 2007. Nested association between genetic variation in tryptophan hydroxylase II, bipolar affective disorder, and suicide attempts. Biol Psychiatry 61(2):181-186.

Lyons MJ, Eisen SA, Goldberg J, True W, Lin N, Meyer JM, Toomey R, Faraone SV, Merla-Ramos M, Tsuang MT. 1998. A registry-based twin study of depression in men. Arch Gen Psychiatry 55(5):468-472.

Machado-Vieira R, Kapczinski F, Soares JC. 2004. Perspectives for the development of animal models of bipolar disorder. Prog Neuropsychopharmacol Biol Psychiatry 28(2):209-224.

Malatynska E, Knapp RJ. 2005. Dominant-submissive behavior as models of mania and depression. Neurosci Biobehav Rev 29(4-5):715-737.

Malatynska E, Pinhasov A, Crooke JJ, Smith-Swintosky VL, Brenneman DE. 2007. Reduction of dominant or submissive behaviors as models for antimanic or antidepressant drug testing: technical considerations. J Neurosci Methods 165(2):175-182.

Malenka RC, Nicoll RA. 1993. NMDA-receptor-dependent synaptic plasticity: multiple forms and mechanisms. Trends Neurosci 16(12):521-527.

Malhi GS, Lagopoulos J, Ward PB, Kumari V, Mitchell PB, Parker GB, Ivanovski B, Sachdev P. 2004. Cognitive generation of affect in bipolar depression: an fMRI study. Eur J Neurosci 19(3):741-754.

Malinow R, Malenka RC. 2002. AMPA receptor trafficking and synaptic plasticity. Annu Rev Neurosci 25:103-126.

Manji HK, Moore GJ, Rajkowska G, Chen G. 2000. Neuroplasticity and cellular resilience in mood disorders. Mol Psychiatry 5(6):578-593.

Mansour HA, Wood J, Logue T, Chowdari KV, Dayal M, Kupfer DJ, Monk TH, Devlin B, Nimgaonkar VL. 2006. Association study of eight circadian genes with bipolar I disorder, schizoaffective disorder and schizophrenia. Genes Brain Behav 5(2):150-157.

Mathews CA, Reus VI. 2001. Assortative mating in the affective disorders: a systematic review and meta-analysis. Compr Psychiatry 42(4):257-262.

Mauri MC, Ferrara A, Boscati L, Bravin S, Zamberlan F, Alecci M, Invernizzi G. 1998. Plasma and platelet amino acid concentrations in patients affected by major

depression and under fluvoxamine treatment. Neuropsychobiology 37(3):124-129.

McCrae CS, Lichstein KL. 2001. Secondary insomnia: diagnostic challenges and intervention opportunities. Sleep Med Rev 5(1):47-61.

McGuffin P, Katz R, Aldrich J, Bebbington P. 1988. The Camberwell Collaborative Depression Study. II. Investigation of family members. Br J Psychiatry 152:766-774.

McGuffin P, Katz R, Watkins S, Rutherford J. 1996. A hospital-based twin register of the heritability of DSM-IV unipolar depression. Arch Gen Psychiatry 53(2):129-136.

McInnis MG, McMahon FJ, Chase GA, Simpson SG, Ross CA, DePaulo JR, Jr. 1993. Anticipation in bipolar affective disorder. Am J Hum Genet 53(2):385-390.

McMahon FJ, Stine OC, Meyers DA, Simpson SG, DePaulo JR. 1995. Patterns of maternal transmission in bipolar affective disorder. Am J Hum Genet 56(6):1277-1286.

Meerding WJ, Bonneux L, Polder JJ, Koopmanschap MA, van der Maas PJ. 1998. Demographic and epidemiological determinants of healthcare costs in Netherlands: cost of illness study. BMJ 317(7151):111-115.

Meltzer HY. 1987. Psychopharmacology : the third generation of progress. Neuropsychopharmacology ACo, editor. New York: Raven Press. xliii, 1780 p. p.

Merikangas KR, Weissman MM, Prusoff BA, John K. 1988. Assortative mating and affective disorders: psychopathology in offspring. Psychiatry 51(1):48-57.

Missler M, Fernandez-Chacon R, Sudhof TC. 1998. The making of neurexins. J Neurochem 71(4):1339-1347.

Mitani H, Shirayama Y, Yamada T, Maeda K, Ashby CR, Jr., Kawahara R. 2006. Correlation between plasma levels of glutamate, alanine and serine with severity of depression. Prog Neuropsychopharmacol Biol Psychiatry 30(6):1155-1158.

Modell JG, Mountz JM, Curtis GC, Greden JF. 1989. Neurophysiologic dysfunction in basal ganglia/limbic striatal and thalamocortical circuits as a pathogenetic mechanism of obsessive-compulsive disorder. J Neuropsychiatry Clin Neurosci 1(1):27-36.

Moessner R, Marshall CR, Sutcliffe JS, Skaug J, Pinto D, Vincent J, Zwaigenbaum L, Fernandez B, Roberts W, Szatmari P, Scherer SW. 2007. Contribution of SHANK3 mutations to autism spectrum disorder. Am J Hum Genet 81(6):1289-1297.

Montkowski A, Barden N, Wotjak C, Stec I, Ganster J, Meaney M, Engelmann M, Reul JM, Landgraf R, Holsboer F. 1995. Long-term antidepressant treatment reduces behavioural deficits in transgenic mice with impaired glucocorticoid receptor function. J Neuroendocrinol 7(11):841-845.

Naisbitt S, Kim E, Tu JC, Xiao B, Sala C, Valtschanoff J, Weinberg RJ, Worley PF, Sheng M. 1999. Shank, a novel family of postsynaptic density proteins that binds to the NMDA receptor/PSD-95/GKAP complex and cortactin. Neuron 23(3):569-582.

Namima M, Sugihara K, Watanabe Y, Sasa H, Umekage T, Okamoto K. 1999. Quantitative analysis of the effects of lithium on the reverse tolerance and the c-Fos expression induced by methamphetamine in mice. Brain Res Brain Res Protoc 4(1):11-18.

Nicoll RA, Tomita S, Bredt DS. 2006. Auxiliary subunits assist AMPA-type glutamate receptors. Science 311(5765):1253-1256.

Nievergelt CM, Kripke DF, Barrett TB, Burg E, Remick RA, Sadovnick AD, McElroy SL, Keck PE, Jr., Schork NJ, Kelsoe JR. 2006. Suggestive evidence for association of the circadian genes PERIOD3 and ARNTL with bipolar disorder. Am J Med Genet B Neuropsychiatr Genet 141B(3):234-241.

NIH. 2005. NIH State-of-the-Science Conference Statement on manifestations and management of chronic insomnia in adults. NIH Consens State Sci Statements 22(2):1-30.

NIMH USDoHaHS, National Institute of Mental Health. 1992. Epidemiologic Catchment Area Study, 1980-1985: [United States]. In: Dept. of Health and Human Services NIoMH, editor. Ann Arbor, MI: nter-university Consortium for Political and Social Research.

Noga JT, Vladar K, Torrey EF. 2001. A volumetric magnetic resonance imaging study of monozygotic twins discordant for bipolar disorder. Psychiatry Res 106(1):25-34.

Nonaka S, Hough CJ, Chuang DM. 1998. Chronic lithium treatment robustly protects neurons in the central nervous system against excitotoxicity by inhibiting N-methyl-D-aspartate receptor-mediated calcium influx. Proc Natl Acad Sci U S A 95(5):2642-2647.

Nylander PO, Engstrom C, Chotai J, Wahlstrom J, Adolfsson R. 1994. Anticipation in Swedish families with bipolar affective disorder. J Med Genet 31(9):686-689.

O'Brien RJ, Lau LF, Huganir RL. 1998. Molecular mechanisms of glutamate receptor clustering at excitatory synapses. Curr Opin Neurobiol 8(3):364-369.

O'Tuathaigh CM, Babovic D, O'Meara G, Clifford JJ, Croke DT, Waddington JL. 2007. Susceptibility genes for schizophrenia: characterisation of mutant mouse models at the level of phenotypic behaviour. Neurosci Biobehav Rev 31(1):60-78.

OECD. 2008. Mental Health in OECD Countries. http://wwwoecdorg.

Ohara K, Suzuki Y, Ushimi Y, Yoshida K. 1998. Anticipation and imprinting in Japanese familial mood disorders. Psychiatry Res 79(3):191-198.

Okabe S. 2007. Molecular anatomy of the postsynaptic density. Mol Cell Neurosci 34(4):503-518.

Oti M, Brunner HG. 2007. The modular nature of genetic diseases. Clin Genet 71(1):1-11.

Oti M, Huynen MA, Brunner HG. 2008. Phenome connections. Trends Genet 24(3):103-106.

Palay SL. 1956a. Structure and function in the neuron. Prog Neurobiol 1:64-82.

Palay SL. 1956b. Synapses in the central nervous system. J Biophys Biochem Cytol 2(4 Suppl):193-202.

Palay SL, Palade GE. 1955. The fine structure of neurons. J Biophys Biochem Cytol 1(1):69-88.

Palo OM, Antila M, Silander K, Hennah W, Kilpinen H, Soronen P, Tuulio-Henriksson A, Kieseppa T, Partonen T, Lonnqvist J, Peltonen L, Paunio T. 2007. Association of distinct allelic haplotypes of DISC1 with psychotic and bipolar spectrum disorders and with underlying cognitive impairments. Hum Mol Genet 16(20):2517-2528.

Papolos DF, Faedda GL, Veit S, Goldberg R, Morrow B, Kucherlapati R, Shprintzen RJ. 1996. Bipolar spectrum disorders in patients diagnosed with velo-cardio-facial

syndrome: does a hemizygous deletion of chromosome 22q11 result in bipolar affective disorder? Am J Psychiatry 153(12):1541-1547.

Patel A, Knapp M. 1998. Costs of mental illness in England. Mental Health Research Review 5.

Paylor R, Lindsay E. 2006. Mouse models of 22q11 deletion syndrome. Biol Psychiatry 59(12):1172-1179.

Paylor R, McIlwain KL, McAninch R, Nellis A, Yuva-Paylor LA, Baldini A, Lindsay EA. 2001. Mice deleted for the DiGeorge/velocardiofacial syndrome region show abnormal sensorimotor gating and learning and memory impairments. Hum Mol Genet 10(23):2645-2650.

Payne JL, Quiroz JA, Zarate CA, Jr., Manji HK. 2002. Timing is everything: does the robust upregulation of noradrenergically regulated plasticity genes underlie the rapid antidepressant effects of sleep deprivation? Biol Psychiatry 52(10):921-926.

Peca J, Feliciano C, Ting JT, Wang W, Wells MF, Venkatraman TN, Lascola CD, Fu Z, Feng G. 2011. Shank3 mutant mice display autistic-like behaviours and striatal dysfunction. Nature.

Pepin MC, Pothier F, Barden N. 1992. Impaired type II glucocorticoid-receptor function in mice bearing antisense RNA transgene. Nature 355(6362):725-728.

Perry W, Minassian A, Feifel D, Braff DL. 2001. Sensorimotor gating deficits in bipolar disorder patients with acute psychotic mania. Biol Psychiatry 50(6):418-424.

Petrides G, Fink M, Husain MM, Knapp RG, Rush AJ, Mueller M, Rummans TA, O'Connor KM, Rasmussen KG, Jr., Bernstein HJ, Biggs M, Bailine SH, Kellner CH. 2001. ECT remission rates in psychotic versus nonpsychotic depressed patients: a report from CORE. J ECT 17(4):244-253.

Phelan MC, Rogers RC, Saul RA, Stapleton GA, Sweet K, McDermid H, Shaw SR, Claytor J, Willis J, Kelly DP. 2001. 22q13 deletion syndrome. Am J Med Genet 101(2):91-99.

Pine DS, Cohen P, Gurley D, Brook J, Ma Y. 1998. The risk for early-adulthood anxiety and depressive disorders in adolescents with anxiety and depressive disorders. Arch Gen Psychiatry 55(1):56-64.

Pinto D, Pagnamenta AT, Klei L, Anney R, Merico D, Regan R, Conroy J, Magalhaes TR, Correia C, Abrahams BS, Almeida J, Bacchelli E, Bader GD, Bailey AJ,

Baird G, Battaglia A, Berney T, Bolshakova N, Bolte S, Bolton PF, Bourgeron T, Brennan S, Brian J, Bryson SE, Carson AR, Casallo G, Casey J, Chung BH, Cochrane L, Corsello C, Crawford EL, Crossett A, Cytrynbaum C, Dawson G, de Jonge M, Delorme R, Drmic I, Duketis E, Duque F, Estes A, Farrar P, Fernandez BA, Folstein SE, Fombonne E, Freitag CM, Gilbert J, Gillberg C, Glessner JT, Goldberg J, Green A, Green J, Guter SJ, Hakonarson H, Heron EA, Hill M, Holt R, Howe JL, Hughes G, Hus V, Igliozzi R, Kim C, Klauck SM, Kolevzon A, Korvatska O, Kustanovich V, Lajonchere CM, Lamb JA, Laskawiec M, Leboyer M, Le Couteur A, Leventhal BL, Lionel AC, Liu XQ, Lord C, Lotspeich L, Lund SC, Maestrini E, Mahoney W, Mantoulan C, Marshall CR, McConachie H, McDougle CJ, McGrath J, McMahon WM, Merikangas A, Migita O, Minshew NJ, Mirza GK, Munson J, Nelson SF, Noakes C, Noor A, Nygren G, Oliveira G, Papanikolaou K, Parr JR, Parrini B, Paton T, Pickles A, Pilorge M, Piven J, Ponting CP, Posey DJ, Poustka A, Poustka F, Prasad A, Ragoussis J, Renshaw K, Rickaby J, Roberts W, Roeder K, Roge B, Rutter ML, Bierut LJ, Rice JP, Salt J, Sansom K, Sato D, Segurado R, Sequeira AF, Senman L, Shah N, Sheffield VC, Soorya L, Sousa I, Stein O, Sykes N, Stoppioni V, Strawbridge C, Tancredi R, Tansey K, Thiruvahindrapduram B, Thompson AP, Thomson S, Tryfon A, Tsiantis J, Van Engeland H, Vincent JB, Volkmar F, Wallace S, Wang K, Wang Z, Wassink TH, Webber C, Weksberg R, Wing K, Wittemeyer K, Wood S, Wu J, Yaspan BL, Zurawiecki D, Zwaigenbaum L, Buxbaum JD, Cantor RM, Cook EH, Coon H, Cuccaro ML, Devlin B, Ennis S, Gallagher L, Geschwind DH, Gill M, Haines JL, Hallmayer J, Miller J, Monaco AP, Nurnberger JI, Jr., Paterson AD, Pericak-Vance MA, Schellenberg GD, Szatmari P, Vicente AM, Vieland VJ, Wijsman EM, Scherer SW, Sutcliffe JS, Betancur C. 2010. Functional impact of global rare copy number variation in autism spectrum disorders. Nature 466(7304):368-372.

Post RM, Weiss SR. 1998. Sensitization and kindling phenomena in mood, anxiety, and obsessive-compulsive disorders: the role of serotonergic mechanisms in illness progression. Biol Psychiatry 44(3):193-206.

Post RM, Weiss SRB, Leverich GS, Smith M, Zhang L-X. 2001. Sensitization and kindling-like phenomena in bipolar disorder: implications for psychopharmacology. Clinical Neuroscience Research 1(1-2):69-81.

Prasad C, Prasad AN, Chodirker BN, Lee C, Dawson AK, Jocelyn LJ, Chudley AE. 2000. Genetic evaluation of pervasive developmental disorders: the terminal 22q13 deletion syndrome may represent a recognizable phenotype. Clin Genet 57(2):103-109.

Precht KS, Lese CM, Spiro RP, Huttenlocher PR, Johnston KM, Baker JC, Christian SL, Kittikamron K, Ledbetter DH. 1998. Two 22q telomere deletions serendipitously detected by FISH. J Med Genet 35(11):939-942.

Prickaerts J, Moechars D, Cryns K, Lenaerts I, van Craenendonck H, Goris I, Daneels G, Bouwknecht JA, Steckler T. 2006. Transgenic mice overexpressing glycogen synthase kinase 3beta: a putative model of hyperactivity and mania. J Neurosci 26(35):9022-9029.

Prybylowski K, Wenthold RJ. 2004. N-Methyl-D-aspartate receptors: subunit assembly and trafficking to the synapse. J Biol Chem 279(11):9673-9676.

Purves D. 2008. Neuroscience. Sunderland, Mass.: Sinauer. xvii, 857, G-816, IC-857, I-829 p. p.

Quitsch A, Berhorster K, Liew CW, Richter D, Kreienkamp HJ. 2005. Postsynaptic shank antagonizes dendrite branching induced by the leucine-rich repeat protein Densin-180. J Neurosci 25(2):479-487.

Racine RJ. 1972. Modification of seizure activity by electrical stimulation. II. Motor seizure. Electroencephalogr Clin Neurophysiol 32(3):281-294.

Rademacher L, Krach S, Kohls G, Irmak A, Grunder G, Spreckelmeyer KN. 2010. Dissociation of neural networks for anticipation and consumption of monetary and social rewards. Neuroimage 49(4):3276-3285.

Reich T, Clayton PJ, Winokur G. 1969. Family history studies: V. The genetics of mania. Am J Psychiatry 125(10):1358-1369.

Reich T, Van Eerdewegh P, Rice J, Mullaney J, Endicott J, Klerman GL. 1987. The familial transmission of primary major depressive disorder. J Psychiatr Res 21(4):613-624.

Rice DP. 1990. The economic costs of alcohol and drug abuse and mental illness, 1985. Rockville, Md.: U.S. Dept. of Health and Human Services, Public Health Service, Alcohol, Drug Abuse, and Mental Health Administration. xi, 296 p. p.

Rich BA, Vinton DT, Roberson-Nay R, Hommer RE, Berghorst LH, McClure EB, Fromm SJ, Pine DS, Leibenluft E. 2006. Limbic hyperactivation during processing of

neutral facial expressions in children with bipolar disorder. Proc Natl Acad Sci U S A 103(23):8900-8905.

Ridder S, Chourbaji S, Hellweg R, Urani A, Zacher C, Schmid W, Zink M, Hortnagl H, Flor H, Henn FA, Schutz G, Gass P. 2005. Mice with genetically altered glucocorticoid receptor expression show altered sensitivity for stress-induced depressive reactions. J Neurosci 25(26):6243-6250.

Riemann D, Voderholzer U. 2003. Primary insomnia: a risk factor to develop depression? J Affect Disord 76(1-3):255-259.

Ritz MC, Lamb RJ, Goldberg SR, Kuhar MJ. 1987. Cocaine receptors on dopamine transporters are related to self-administration of cocaine. Science 237(4819):1219-1223.

Ronty M, Taivainen A, Moza M, Kruh GD, Ehler E, Carpen O. 2005. Involvement of palladin and alpha-actinin in targeting of the Abl/Arg kinase adaptor ArgBP2 to the actin cytoskeleton. Exp Cell Res 310(1):88-98.

Rosen LN, Targum SD, Terman M, Bryant MJ, Hoffman H, Kasper SF, Hamovit JR, Docherty JP, Welch B, Rosenthal NE. 1990. Prevalence of seasonal affective disorder at four latitudes. Psychiatry Res 31(2):131-144.

Rosenberg RE, Law JK, Yenokyan G, McGready J, Kaufmann WE, Law PA. 2009. Characteristics and concordance of autism spectrum disorders among 277 twin pairs. Arch Pediatr Adolesc Med 163(10):907-914.

Rosenthal NE, Sack DA, Gillin JC, Lewy AJ, Goodwin FK, Davenport Y, Mueller PS, Newsome DA, Wehr TA. 1984. Seasonal affective disorder. A description of the syndrome and preliminary findings with light therapy. Arch Gen Psychiatry 41(1):72-80.

Rotondo A, Mazzanti C, Dell'Osso L, Rucci P, Sullivan P, Bouanani S, Gonnelli C, Goldman D, Cassano GB. 2002. Catechol o-methyltransferase, serotonin transporter, and tryptophan hydroxylase gene polymorphisms in bipolar disorder patients with and without comorbid panic disorder. Am J Psychiatry 159(1):23-29.

Roussignol G, Ango F, Romorini S, Tu JC, Sala C, Worley PF, Bockaert J, Fagni L. 2005. Shank expression is sufficient to induce functional dendritic spine synapses in aspiny neurons. J Neurosci 25(14):3560-3570.

Roybal K, Theobold D, Graham A, DiNieri JA, Russo SJ, Krishnan V, Chakravarty S, Peevey J, Oehrlein N, Birnbaum S, Vitaterna MH, Orsulak P, Takahashi JS, Nestler EJ, Carlezon WA, Jr., McClung CA. 2007. Mania-like behavior induced by disruption of CLOCK. Proc Natl Acad Sci U S A 104(15):6406-6411.

Rudenko G, Nguyen T, Chelliah Y, Sudhof TC, Deisenhofer J. 1999. The structure of the ligand-binding domain of neurexin Ibeta: regulation of LNS domain function by alternative splicing. Cell 99(1):93-101.

Sack RL, Brandes RW, Kendall AR, Lewy AJ. 2000. Entrainment of free-running circadian rhythms by melatonin in blind people. N Engl J Med 343(15):1070-1077.

Sanacora G, Zarate CA, Krystal JH, Manji HK. 2008. Targeting the glutamatergic system to develop novel, improved therapeutics for mood disorders. Nat Rev Drug Discov 7(5):426-437.

Satcher DS. 2000. Executive summary: a report of the Surgeon General on mental health. Public Health Rep 115(1):89-101.

Schatzberg AF, Rothschild AJ, Langlais PJ, Bird ED, Cole JO. 1985. A corticosteroid/dopamine hypothesis for psychotic depression and related states. J Psychiatr Res 19(1):57-64.

Schatzberg AF, Rothschild AJ, Stahl JB, Bond TC, Rosenbaum AH, Lofgren SB, MacLaughlin RA, Sullivan MA, Cole JO. 1983. The dexamethasone suppression test: identification of subtypes of depression. Am J Psychiatry 140(1):88-91.

Schwartz WJ, Zimmerman P. 1990. Circadian timekeeping in BALB/c and C57BL/6 inbred mouse strains. J Neurosci 10(11):3685-3694.

Scott-Van Zeeland AA, Dapretto M, Ghahremani DG, Poldrack RA, Bookheimer SY. 2010. Reward processing in autism. Autism Res 3(2):53-67.

Scott LJ, Muglia P, Kong XQ, Guan W, Flickinger M, Upmanyu R, Tozzi F, Li JZ, Burmeister M, Absher D, Thompson RC, Francks C, Meng F, Antoniades A, Southwick AM, Schatzberg AF, Bunney WE, Barchas JD, Jones EG, Day R, Matthews K, McGuffin P, Strauss JS, Kennedy JL, Middleton L, Roses AD, Watson SJ, Vincent JB, Myers RM, Farmer AE, Akil H, Burns DK, Boehnke M. 2009. Genome-wide association and meta-analysis of bipolar disorder in individuals of European ancestry. Proc Natl Acad Sci U S A 106(18):7501-7506.

Sebat J, Lakshmi B, Malhotra D, Troge J, Lese-Martin C, Walsh T, Yamrom B, Yoon S, Krasnitz A, Kendall J, Leotta A, Pai D, Zhang R, Lee YH, Hicks J, Spence SJ, Lee AT, Puura K, Lehtimaki T, Ledbetter D, Gregersen PK, Bregman J, Sutcliffe JS, Jobanputra V, Chung W, Warburton D, King MC, Skuse D, Geschwind DH, Gilliam TC, Ye K, Wigler M. 2007. Strong association of de novo copy number mutations with autism. Science 316(5823):445-449.

Serretti A, Mandelli L. 2008. The genetics of bipolar disorder: genome 'hot regions,' genes, new potential candidates and future directions. Mol Psychiatry 13(8):742-771.

Shaldivin A, Kaptsan A, Belmaker RH, Einat H, Grisaru N. 2001. Transcranial magnetic stimulation in an amphetamine hyperactivity model of mania. Bipolar Disord 3(1):30-34.

Shapiro L, Love J, Colman DR. 2007. Adhesion molecules in the nervous system: structural insights into function and diversity. Annu Rev Neurosci 30:451-474.

Sheng M, Hoogenraad CC. 2007. The postsynaptic architecture of excitatory synapses: a more quantitative view. Annu Rev Biochem 76:823-847.

Shih RA, Belmonte PL, Zandi PP. 2004. A review of the evidence from family, twin and adoption studies for a genetic contribution to adult psychiatric disorders. Int Rev Psychiatry 16(4):260-283.

Sierra P, Livianos L, Arques S, Castello J, Rojo L. 2007. Prodromal symptoms to relapse in bipolar disorder. Aust N Z J Psychiatry 41(5):385-391.

Sklar P, Gabriel SB, McInnis MG, Bennett P, Lim YM, Tsan G, Schaffner S, Kirov G, Jones I, Owen M, Craddock N, DePaulo JR, Lander ES. 2002. Family-based association study of 76 candidate genes in bipolar disorder: BDNF is a potential risk locus. Brain-derived neutrophic factor. Mol Psychiatry 7(6):579-593.

Sklar P, Smoller JW, Fan J, Ferreira MA, Perlis RH, Chambert K, Nimgaonkar VL, McQueen MB, Faraone SV, Kirby A, de Bakker PI, Ogdie MN, Thase ME, Sachs GS, Todd-Brown K, Gabriel SB, Sougnez C, Gates C, Blumenstiel B, Defelice M, Ardlie KG, Franklin J, Muir WJ, McGhee KA, MacIntyre DJ, McLean A, VanBeck M, McQuillin A, Bass NJ, Robinson M, Lawrence J, Anjorin A, Curtis D, Scolnick EM, Daly MJ, Blackwood DH, Gurling HM, Purcell SM. 2008. Whole-genome association study of bipolar disorder. Mol Psychiatry 13(6):558-569.

Smeraldi E, Negri F, Melica AM. 1977. A genetic study of affective disorders. Acta Psychiatr Scand 56(5):382-398.

Smith EN, Bloss CS, Badner JA, Barrett T, Belmonte PL, Berrettini W, Byerley W, Coryell W, Craig D, Edenberg HJ, Eskin E, Foroud T, Gershon E, Greenwood TA, Hipolito M, Koller DL, Lawson WB, Liu C, Lohoff F, McInnis MG, McMahon FJ, Mirel DB, Murray SS, Nievergelt C, Nurnberger J, Nwulia EA, Paschall J, Potash JB, Rice J, Schulze TG, Scheftner W, Panganiban C, Zaitlen N, Zandi PP, Zollner S, Schork NJ, Kelsoe JR. 2009. Genome-wide association study of bipolar disorder in European American and African American individuals. Mol Psychiatry 14(8):755-763.

Sodhi M, Wood KH, Meador-Woodruff J. 2008. Role of glutamate in schizophrenia: integrating excitatory avenues of research. Expert Rev Neurother 8(9):1389-1406.

Soronen P, Ollila HM, Antila M, Silander K, Palo OM, Kieseppa T, Lonnqvist J, Peltonen L, Tuulio-Henriksson A, Partonen T, Paunio T. 2010. Replication of GWAS of bipolar disorder: association of SNPs near CDH7 with bipolar disorder and visual processing. Mol Psychiatry 15(1):4-6.

Spreckelmeyer KN, Krach S, Kohls G, Rademacher L, Irmak A, Konrad K, Kircher T, Grunder G. 2009. Anticipation of monetary and social reward differently activates mesolimbic brain structures in men and women. Soc Cogn Affect Neurosci 4(2):158-165.

Starke K. 1981. Presynaptic receptors. Annu Rev Pharmacol Toxicol 21:7-30.

Steketee JD, Kalivas PW. 1992. Microinjection of the D2 agonist quinpirole into the A10 dopamine region blocks amphetamine-, but not cocaine-stimulated motor activity. J Pharmacol Exp Ther 261(2):811-818.

Stephen MDS, Paul PDM, Cummings JL, editors. 1997. The Neuropsychiatry of Limbic and Subcortical Disorders: American Psychiatric Publishing, Inc.

Strakowski SM, Adler CM, DelBello MP. 2002a. Volumetric MRI studies of mood disorders: do they distinguish unipolar and bipolar disorder? Bipolar Disord 4(2):80-88.

Strakowski SM, Delbello MP, Adler CM. 2005. The functional neuroanatomy of bipolar disorder: a review of neuroimaging findings. Mol Psychiatry 10(1):105-116.

Strakowski SM, DelBello MP, Sax KW, Zimmerman ME, Shear PK, Hawkins JM, Larson ER. 1999. Brain magnetic resonance imaging of structural abnormalities in bipolar disorder. Arch Gen Psychiatry 56(3):254-260.

Strakowski SM, DelBello MP, Zimmerman ME, Getz GE, Mills NP, Ret J, Shear P, Adler CM. 2002b. Ventricular and periventricular structural volumes in first- versus multiple-episode bipolar disorder. Am J Psychiatry 159(11):1841-1847.

Strasser HC, Lilyestrom J, Ashby ER, Honeycutt NA, Schretlen DJ, Pulver AE, Hopkins RO, Depaulo JR, Potash JB, Schweizer B, Yates KO, Kurian E, Barta PE, Pearlson GD. 2005. Hippocampal and ventricular volumes in psychotic and nonpsychotic bipolar patients compared with schizophrenia patients and community control subjects: a pilot study. Biol Psychiatry 57(6):633-639.

Sudhof TC. 2008. Neuroligins and neurexins link synaptic function to cognitive disease. Nature 455(7215):903-911.

Sullivan PF, Neale MC, Kendler KS. 2000. Genetic epidemiology of major depression: review and meta-analysis. Am J Psychiatry 157(10):1552-1562.

Swayze VW, 2nd, Andreasen NC, Alliger RJ, Yuh WT, Ehrhardt JC. 1992. Subcortical and temporal structures in affective disorder and schizophrenia: a magnetic resonance imaging study. Biol Psychiatry 31(3):221-240.

Tabuchi K, Blundell J, Etherton MR, Hammer RE, Liu X, Powell CM, Sudhof TC. 2007. A neuroligin-3 mutation implicated in autism increases inhibitory synaptic transmission in mice. Science 318(5847):71-76.

Takahashi JS, Hong HK, Ko CH, McDearmon EL. 2008. The genetics of mammalian circadian order and disorder: implications for physiology and disease. Nat Rev Genet 9(10):764-775.

Takeuchi M, Hata Y, Hirao K, Toyoda A, Irie M, Takai Y. 1997. SAPAPs. A family of PSD-95/SAP90-associated proteins localized at postsynaptic density. J Biol Chem 272(18):11943-11951.

Tarpey P, Parnau J, Blow M, Woffendin H, Bignell G, Cox C, Cox J, Davies H, Edkins S, Holden S, Korny A, Mallya U, Moon J, O'Meara S, Parker A, Stephens P, Stevens C, Teague J, Donnelly A, Mangelsdorf M, Mulley J, Partington M, Turner G, Stevenson R, Schwartz C, Young I, Easton D, Bobrow M, Futreal PA, Stratton MR, Gecz J, Wooster R, Raymond FL. 2004. Mutations in the DLG3

gene cause nonsyndromic X-linked mental retardation. Am J Hum Genet 75(2):318-324.

Trimble WS, Linial M, Scheller RH. 1991. Cellular and molecular biology of the presynaptic nerve terminal. Annu Rev Neurosci 14:93-122.

Trzebiatowska-Trzeciak O. 1977. Genetical analysis of unipolar and bipolar endogenous affective psychoses. Br J Psychiatry 131:478-485.

Tu JC, Xiao B, Naisbitt S, Yuan JP, Petralia RS, Brakeman P, Doan A, Aakalu VK, Lanahan AA, Sheng M, Worley PF. 1999. Coupling of mGluR/Homer and PSD-95 complexes by the Shank family of postsynaptic density proteins. Neuron 23(3):583-592.

Tuchman R, Rapin I. 2002. Epilepsy in autism. Lancet Neurol 1(6):352-358.

Ushkaryov YA, Petrenko AG, Geppert M, Sudhof TC. 1992. Neurexins: synaptic cell surface proteins related to the alpha-latrotoxin receptor and laminin. Science 257(5066):50-56.

Vale AL, Ratcliffe F. 1987. Effect of lithium administration on rat brain 5-hydroxyindole levels in a possible animal model for mania. Psychopharmacology (Berl) 91(3):352-355.

van de Lagemaat LN, Grant SG. 2010. Genome variation and complexity in the autism spectrum. Neuron 67(1):8-10.

Van Den Bogaert A, Sleegers K, De Zutter S, Heyrman L, Norrback KF, Adolfsson R, Van Broeckhoven C, Del-Favero J. 2006. Association of brain-specific tryptophan hydroxylase, TPH2, with unipolar and bipolar disorder in a Northern Swedish, isolated population. Arch Gen Psychiatry 63(10):1103-1110.

van Driel MA, Bruggeman J, Vriend G, Brunner HG, Leunissen JA. 2006. A text-mining analysis of the human phenome. Eur J Hum Genet 14(5):535-542.

Vera GH. 1998. Prevalence of seasonal affective disorder. Br J Psychiatry 173:270.

Vitaterna MH, King DP, Chang AM, Kornhauser JM, Lowrey PL, McDonald JD, Dove WF, Pinto LH, Turek FW, Takahashi JS. 1994. Mutagenesis and mapping of a mouse gene, Clock, essential for circadian behavior. Science 264(5159):719-725.

Vollrath M, Wicki W, Angst J. 1989. The Zurich study. VIII. Insomnia: association with depression, anxiety, somatic syndromes, and course of insomnia. Eur Arch Psychiatry Neurol Sci 239(2):113-124.

Wakefield JC, Schmitz MF, First MB, Horwitz AV. 2007. Extending the bereavement exclusion for major depression to other losses: evidence from the National Comorbidity Survey. Arch Gen Psychiatry 64(4):433-440.

Wallis JD. 2007. Orbitofrontal cortex and its contribution to decision-making. Annu Rev Neurosci 30:31-56.

Walther DJ, Peter JU, Bashammakh S, Hortnagl H, Voits M, Fink H, Bader M. 2003. Synthesis of serotonin by a second tryptophan hydroxylase isoform. Science 299(5603):76.

Wang B, Golemis EA, Kruh GD. 1997. ArgBP2, a multiple Src homology 3 domain-containing, Arg/Abl-interacting protein, is phosphorylated in v-Abl-transformed cells and localized in stress fibers and cardiocyte Z-disks. J Biol Chem 272(28):17542-17550.

Wang X, McCoy PA, Rodriguiz RM, Pan Y, Je HS, Roberts AC, Kim CJ, Berrios J, Colvin JS, Bousquet-Moore D, Lorenzo I, Wu G, Weinberg RJ, Ehlers MD, Philpot BD, Beaudet AL, Wetsel WC, Jiang YH. 2011. Synaptic dysfunction and abnormal behaviors in mice lacking major isoforms of Shank3. Hum Mol Genet.

Wehr TA, Goodwin FK. 1979. Rapid cycling in manic-depressives induced by tricyclic antidepressants. Arch Gen Psychiatry 36(5):555-559.

Wehr TA, Wirz-Justice A, Goodwin FK, Duncan W, Gillin JC. 1979. Phase advance of the circadian sleep-wake cycle as an antidepressant. Science 206(4419):710-713.

Wei Q, Lu XY, Liu L, Schafer G, Shieh KR, Burke S, Robinson TE, Watson SJ, Seasholtz AF, Akil H. 2004. Glucocorticoid receptor overexpression in forebrain: a mouse model of increased emotional lability. Proc Natl Acad Sci U S A 101(32):11851-11856.

Weissman MM, Bland R, Joyce PR, Newman S, Wells JE, Wittchen HU. 1993. Sex differences in rates of depression: cross-national perspectives. J Affect Disord 29(2-3):77-84.

Weissman MM, Gershon ES, Kidd KK, Prusoff BA, Leckman JF, Dibble E, Hamovit J, Thompson WD, Pauls DL, Guroff JJ. 1984. Psychiatric disorders in the relatives of probands with affective disorders. The Yale University--National Institute of Mental Health Collaborative Study. Arch Gen Psychiatry 41(1):13-21.

Welch JM, Lu J, Rodriguiz RM, Trotta NC, Peca J, Ding JD, Feliciano C, Chen M, Adams JP, Luo J, Dudek SM, Weinberg RJ, Calakos N, Wetsel WC, Feng G. 2007. Cortico-striatal synaptic defects and OCD-like behaviours in Sapap3-mutant mice. Nature 448(7156):894-900.

Welch JM, Wang D, Feng G. 2004. Differential mRNA expression and protein localization of the SAP90/PSD-95-associated proteins (SAPAPs) in the nervous system of the mouse. J Comp Neurol 472(1):24-39.

WHO. 2004a. International statistical classification of diseases and related health problems. Geneva: World Health Organization.

WHO WHO. 2001. The World Health Report 2001: Mental Health: New Understanding, New Hope.

WHO WHO. 2004b. The global burden of disease: 2004 update, Part 3, Disease incidence, prevalence and disability.

Wilson HL, Wong AC, Shaw SR, Tse WY, Stapleton GA, Phelan MC, Hu S, Marshall J, McDermid HE. 2003. Molecular characterisation of the 22q13 deletion syndrome supports the role of haploinsufficiency of SHANK3/PROSAP2 in the major neurological symptoms. J Med Genet 40(8):575-584.

Wisniowiecka-Kowalnik B, Nesteruk M, Peters SU, Xia Z, Cooper ML, Savage S, Amato RS, Bader P, Browning MF, Haun CL, Duda AW, 3rd, Cheung SW, Stankiewicz P. 2010. Intragenic rearrangements in NRXN1 in three families with autism spectrum disorder, developmental delay, and speech delay. Am J Med Genet B Neuropsychiatr Genet 153B(5):983-993.

WTCCC. 2007. Genome-wide association study of 14,000 cases of seven common diseases and 3,000 shared controls. Nature 447(7145):661-678.

Wu JC, Kelsoe JR, Schachat C, Bunney BG, DeModena A, Golshan S, Gillin JC, Potkin SG, Bunney WE. 2009. Rapid and sustained antidepressant response with sleep deprivation and chronotherapy in bipolar disorder. Biol Psychiatry 66(3):298-301.

Yehuda R, Boisoneau D, Mason JW, Giller EL. 1993. Glucocorticoid receptor number and cortisol excretion in mood, anxiety, and psychotic disorders. Biol Psychiatry 34(1-2):18-25.

Yucel K, Taylor VH, McKinnon MC, Macdonald K, Alda M, Young LT, MacQueen GM. 2008. Bilateral hippocampal volume increase in patients with bipolar disorder and short-term lithium treatment. Neuropsychopharmacology 33(2):361-367.

Yurgelun-Todd DA, Gruber SA, Kanayama G, Killgore WD, Baird AA, Young AD. 2000. fMRI during affect discrimination in bipolar affective disorder. Bipolar Disord 2(3 Pt 2):237-248.

Yurgelun-Todd DA, Ross AJ. 2006. Functional magnetic resonance imaging studies in bipolar disorder. CNS Spectr 11(4):287-297.

Zarate CA, Manji HK. 2009. Bipolar depression : molecular neurobiology, clinical diagnosis, and pharmacotherapy. Basel ; Boston: Birkhäuser. xii, 279 p. p.

Zeier Z, Kumar A, Bodhinathan K, Feller JA, Foster TC, Bloom DC. 2009. Fragile X mental retardation protein replacement restores hippocampal synaptic function in a mouse model of fragile X syndrome. Gene Ther 16(9):1122-1129.

Zoghbi HY. 2003. Postnatal neurodevelopmental disorders: meeting at the synapse? Science 302(5646):826-830.

Zuchner S, Wendland JR, Ashley-Koch AE, Collins AL, Tran-Viet KN, Quinn K, Timpano KC, Cuccaro ML, Pericak-Vance MA, Steffens DC, Krishnan KR, Feng G, Murphy DL. 2009. Multiple rare SAPAP3 missense variants in trichotillomania and OCD. Mol Psychiatry 14(1):6-9.

Appendix 1

ARTICLES

Cortico-striatal synaptic defects and OCD-like behaviours in *Sapap3*-mutant mice

Jeffrey M. Welch[1]*, Jing Lu[1,4]*, Ramona M. Rodriguiz[2], Nicholas C. Trotta[1], Joao Peca[1,5], Jin-Dong Ding[6], Catia Feliciano[1,7], Meng Chen[3], J. Paige Adams[8], Jianhong Luo[4], Serena M. Dudek[8], Richard J. Weinberg[6], Nicole Calakos[1,3], William C. Wetsel[2] & Guoping Feng[1]

Obsessive-compulsive disorder (OCD) is an anxiety-spectrum disorder characterized by persistent intrusive thoughts (obsessions) and repetitive actions (compulsions). Dysfunction of cortico-striato-thalamo-cortical circuitry is implicated in OCD, although the underlying pathogenic mechanisms are unknown. SAP90/PSD95-associated protein 3 (SAPAP3; also known as DLGAP3) is a postsynaptic scaffolding protein at excitatory synapses that is highly expressed in the striatum. Here we show that mice with genetic deletion of *Sapap3* exhibit increased anxiety and compulsive grooming behaviour leading to facial hair loss and skin lesions; both behaviours are alleviated by a selective serotonin reuptake inhibitor. Electrophysiological, structural and biochemical studies of *Sapap3*-mutant mice reveal defects in cortico-striatal synapses. Furthermore, lentiviral-mediated selective expression of *Sapap3* in the striatum rescues the synaptic and behavioural defects of *Sapap3*-mutant mice. These findings demonstrate a critical role for SAPAP3 at cortico-striatal synapses and emphasize the importance of cortico-striatal circuitry in OCD-like behaviours.

OCD, a common and incapacitating psychiatric disorder, affects ~2 per cent of the world population[1,2]. OCD is characterized by persistent intrusive thoughts (obsessions), repetitive actions (compulsions) and excessive anxiety. Clinical expression of OCD is heterogeneous in the types of obsessions and compulsions, heritability and co-morbid conditions, probably reflecting heterogeneity in the underlying pathology[3]. In addition, there are many disorders that share features with OCD, termed 'OC-spectrum disorders', which include Tourette's syndrome, trichotillomania and body dysmorphic disorder.

The neurobiological basis of OCD is unclear. However, lesions, functional neuro-imaging, and neuropsychological studies have indicated that the cortico-striato-thalamo-cortical circuitry may have a key role in the pathogenesis of OCD[3–5]. Familial studies of OCD indicate that the risk to first degree relatives is 3–12 times greater than the general population, similar to familial risk rates observed for bipolar disorder and schizophrenia[6–8]. In addition, concordance for OCD is greater among pairs of monozygotic (80–87%) than dizygotic (47–50%) twins[9,10]. However, no genetic factors have yet been identified as a cause of OCD, presumably reflecting aetiological heterogeneity within the disorder. Although many of the symptoms of OCD can be ameliorated by enhancing serotonin neurotransmission, it is not clear at the cellular level whether defects in the serotonergic system are the primary cause[3–5]. Indeed, dopaminergic and glutamatergic neurotransmitter systems have also been implicated[5,11]. Here we show that targeted deletion of *Sapap3* in mice leads to a behavioural phenotype similar to OCD: compulsive over-grooming behaviour, increased anxiety, and response to selective serotonin reuptake inhibitors. In these mutant mice, we have identified defects at cortico-striatal synapses, part of the circuitry implicated in OCD, and we show that selective expression of *Sapap3* in the striatum rescues the synaptic and behavioural defects. These findings indicate that defects in excitatory transmission at cortico-striatal synapses may underlie some aspects of OCD.

Sapap3$^{-/-}$ mice exhibit self-inflicted facial lesions

SAPAP family proteins were originally identified as postsynaptic density (PSD) components that interact with the PSD95 and Shank families of proteins[12,13], two other multi-domain postsynaptic scaffolding proteins at excitatory synapses. Together, these three groups of proteins are thought to form a key scaffolding complex that regulates the trafficking and targeting of neurotransmitter receptors and signalling molecules to the postsynaptic membrane of excitatory synapses[14–16]. There are four highly homologous genes encoding members of the SAPAP family[13]. Of these, *Sapap1*, *3* and *4* are highly, but differentially, expressed in several regions of the brain[17,18]. Notably, *Sapap3* is the only member highly expressed in the striatum. To facilitate study of the *in vivo* function of SAPAP proteins at synapses, we generated knockout mice for the *Sapap3* gene using homologous recombination in mouse embryonic stem cells (Supplementary Fig. 1a–d). Mice homozygous for the *Sapap3* deletion (*Sapap3*$^{-/-}$) were born at the expected mendelian rate, grew to adulthood with body weights similar to wild-type mice, and were fertile. Anatomical and histological analyses of brain showed that *Sapap3*$^{-/-}$ mice were grossly normal (data not shown).

By the age of 4–6 months, however, *Sapap3*$^{-/-}$ mice developed lesions on their head, neck and snout regions (Fig. 1a). This phenotype was 100% penetrant. Lesions were usually first noticed as a patch of hairless skin under the eyes, or swelling of the snout, progressing to relatively symmetric bilateral lesions encompassing large parts of the neck and head. *Sapap3*$^{-/-}$ mice developed lesions regardless of

[1]Department of Neurobiology, [2]Departments of Psychiatry and Behavioral Sciences, Cell Biology, Neurobiology, and Mouse Behavioral and Neuroendocrine Analysis Core Facility, [3]Division of Neurology, Center for Translational Neuroscience, Duke University Medical Center, Durham, North Carolina 27710, USA. [4]Department of Neurobiology, Zhejiang University School of Medicine, Hangzhou, Zhejiang 310058, China. [5]Center for Neuroscience and Cell Biology, University of Coimbra, 3004-517 Coimbra, Portugal. [6]Department of Cell and Developmental Biology, Neuroscience Center, University of North Carolina, Chapel Hill, North Carolina 27599, USA. [7]Gulbenkian PhD Programme in Biomedicine, Gulbenkian Science Institute, 2781-901 Oeiras, Portugal. [8]National Institute of Environmental Health Sciences, National Institutes of Health, Research Triangle Park, North Carolina 27709, USA. *These authors contributed equally to this work.

whether they were housed alone or with cage mates. Lesions were not observed on wild-type or heterozygous mice even when housed in the same cage with *Sapap3*$^{-/-}$ mice from birth, thereby excluding the possibility that lesions were caused by allogrooming or were the result of aggressive encounters with other *Sapap3*$^{-/-}$ mice. In fact, *Sapap3*$^{-/-}$ mice were not observed to behave aggressively, but were often seen engaged in self-grooming whether they were housed alone or in groups.

Given the obvious lesions on the *Sapap3*$^{-/-}$ mice, we tested the possibility that their lesions might be caused by peripheral cutaneous defects, such as inflammation or abnormal afferent sensation. We examined facial skin from pre-lesion *Sapap3*$^{-/-}$ mice that exhibited increased grooming. Histological analysis of skin did not reveal any anatomical differences among wild-type, *Sapap3*$^{+/-}$ and *Sapap3*$^{-/-}$ mice, and no lymphocytic or granulocytic infiltration was observed (Supplementary Fig. 1e, f). We did, however, find lymphocytic/granulocytic infiltration in skin with lesions, probably owing to injury and infection (Supplementary Fig. 1g). No differences were detected in sensory innervation among wild-type, *Sapap3*$^{+/-}$ and *Sapap3*$^{-/-}$ mice; hair-nerve end organs, lobular corpuscle-like nerve endings, and free epidermal nerve endings were present and not different between *Sapap3*$^{-/-}$ and control mice (Supplementary Fig. 1h, i). Thus, our examination revealed no obvious peripheral defects that would indicate a cause for the lesions. Together, these findings raised the possibility that *Sapap3*$^{-/-}$ mice have excessive and injurious self-grooming behaviour.

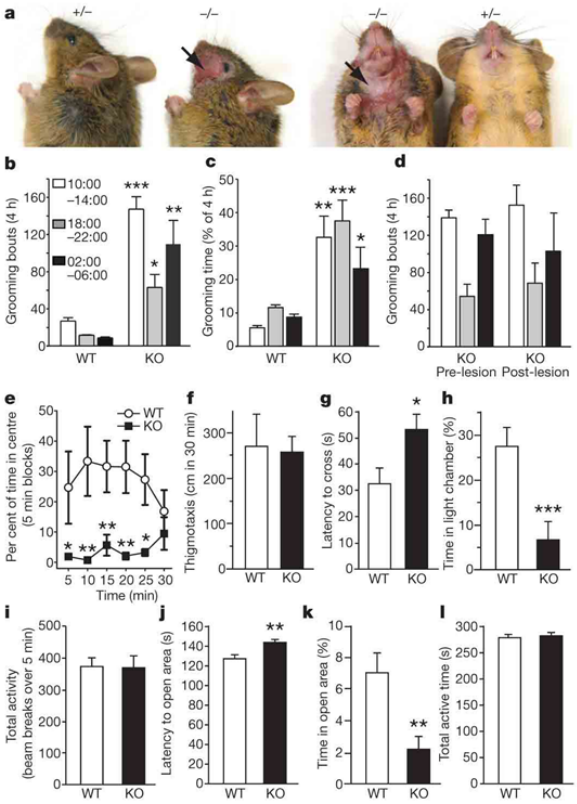

Figure 1 | Facial lesions, excessive grooming and anxiety-like behaviours in *Sapap3*-mutant mice. **a**, *Sapap3*$^{-/-}$ mice have facial and neck skin lesions (arrows). **b**, **c**, *Sapap3*$^{-/-}$ mice (KO) showed more grooming bouts (**b**) and spent more time in self-grooming (**c**) than wild-type mice (WT) at all times examined. **d**, Pre-lesion and post-lesion groups of *Sapap3*$^{-/-}$ mice showed similar degrees of increased grooming. **e**, **f**, In the open field test, *Sapap3*$^{-/-}$ mice spent less time in the centre (**e**), whereas locomotion along the perimeter was comparable to wild-type controls (**f**). **g–i**, In the dark–light emergence test, *Sapap3*$^{-/-}$ mice took longer to cross from the dark to the brightly lit chamber (**g**) and spent less time in the brightly lit chamber (**h**), whereas total activity in both chambers was similar (**i**). **j–l**, In the elevated zero maze, *Sapap3*$^{-/-}$ mice took longer to cross into the open areas (**j**) and spent less time in these areas than wild-type controls (**k**), whereas total activity in both open and closed areas was similar (**l**). $^{*}P < 0.05$, $^{**}P < 0.01$, $^{***}P < 0.001$, repeated measures ANOVA for **b**–**e** and two-tailed *t*-test for **f**–**l**; all data are presented as means ± s.e.m. from 8–9 mice per genotype; Cohen's kappa for intra-observer agreement exceeded 0.92.

OCD-like behaviours of *Sapap3*$^{-/-}$ mice

To determine whether *Sapap3*$^{-/-}$ mice groom excessively, we continuously videotaped habituated, individually housed mice for 24 h. Isolated *Sapap3*$^{-/-}$ mice showed dramatically increased grooming bouts and spent significantly more time self-grooming than wild-type litter mates (Fig. 1b, c). The increased grooming was present throughout the day, including the period when mice usually sleep (10:00–14:00). Both mutant mice with facial lesions and mice yet to develop lesions showed similar degrees of increased grooming (Fig. 1d), indicating that the lesion itself was not the cause of increased grooming. We thus conclude that *Sapap3*$^{-/-}$ mice have excessive and injurious levels of self-grooming, a phenotype reminiscent of compulsive behaviours.

Because the *Sapap3*$^{-/-}$ mice exhibited a compulsive-like behaviour, we considered whether their phenotypes further resemble OC-spectrum disorders. We therefore examined other OCD-like behaviours that are measurable in mice, such as increased anxiety and response to typical pharmacological agents. To test whether *Sapap3*$^{-/-}$ mice exhibit increased anxiety, we conducted open field, dark–light emergence, and elevated zero maze tests. In the open field, mice with anxiety-like phenotypes tend to stay along the walls, avoiding the centre zone. *Sapap3*$^{-/-}$ mice spent much less time exploring the centre area than wild-type litter mates (Fig. 1e). However, activities along the walls and corners, areas believed to be less stressful, were not different between wild-type and *Sapap3*$^{-/-}$ mice (Fig. 1f). In the dark–light emergence test, the latency to cross from a dark into a brightly lit chamber (a stressful environment), and the time spent in the brightly lit chamber were examined. *Sapap3*$^{-/-}$ mice took longer to cross from the dark to the lit chamber and spent less time in the lit chamber than wild-type controls (Fig. 1g, h), even though total activity in the chambers was similar between wild-type and *Sapap3*$^{-/-}$ mice (Fig. 1i). Finally, in the elevated zero maze test, we found that *Sapap3*$^{-/-}$ mice took longer to cross into the open areas (riskier environment) and spent significantly less time exploring the open areas compared with wild-type controls (Fig. 1j, k), whereas total activity was not different between the two genotypes (Fig. 1l). Together, these results indicate that *Sapap3*$^{-/-}$ mice have an anxiety-like phenotype.

We next evaluated whether drugs used to treat OCD would be effective in reducing the abnormal behaviour in *Sapap3*$^{-/-}$ mice. Selective serotonin reuptake inhibitors are a first-line treatment for OCD; although their mechanism of action is not well understood, these drugs alleviate symptoms in approximately 50% of OCD patients[3]. Fluoxetine treatment for 6 days (once per day at 5 mg kg^{-1}, intraperitoneally) did not affect grooming behaviour of wild-type mice. However, this treatment significantly reduced the excessive grooming in *Sapap3*$^{-/-}$ mice (Fig. 2a). Furthermore, fluoxetine dramatically reduced anxiety-like behaviours in *Sapap3*$^{-/-}$ mice in the dark–light emergence test without affecting their total activity (Fig. 2b, c). In contrast, a single injection of fluoxetine (5 mg kg^{-1}, intraperitoneally) had no effects on their excessive grooming behaviour (Fig. 2d). Thus, *Sapap3*$^{-/-}$ mice exhibit compulsive-like grooming and increased anxiety, both of which are alleviated by 6 days of fluoxetine treatment.

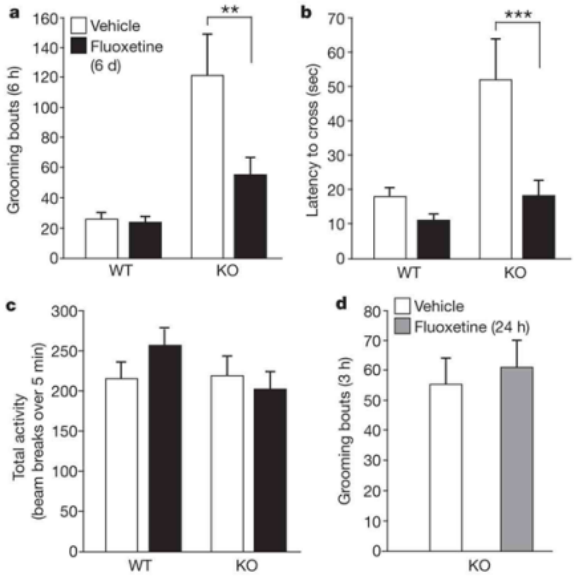

Figure 2 | Fluoxetine treatment alleviates excessive grooming and anxiety-like behaviour. **a**, Daily fluoxetine treatment over six days reduced grooming behaviour in *Sapap3*$^{-/-}$ mice. **b**, **c**, Given over 6 days, fluoxetine alleviated anxiety-like behaviour of *Sapap3*$^{-/-}$ mice in the dark–light emergence test (**b**) without affecting their total activity (**c**). **d**, A single injection of fluoxetine had no effect on the grooming behaviour of *Sapap3*$^{-/-}$ mice. $^{**}P < 0.01$, $^{***}P < 0.001$, repeated measures ANOVA; all data are presented as means ± s.e.m. from 9–11 mice per group; Cohen's kappa for intra-observer agreement exceeded 0.92.

Altered cortico-striatal synaptic transmission

The observations that SAPAP3 is the only member of the SAPAP family highly expressed in the striatum (Fig. 3a) and that *Sapap3*$^{-/-}$ mice show OCD-like behaviours indicate that there may be defects in striatal neurotransmission in *Sapap3*$^{-/-}$ mice. Because SAPAPs are postsynaptic proteins of excitatory synapses[12,17] and directly bind PSD95 family proteins, which are known to regulate the trafficking of both AMPA- and NMDA-type glutamate receptors (AMPAR and NMDAR, respectively)[19–21], we focused on cortico-striatal synapses, which constitute the large majority of glutamatergic synapses in the striatum. We performed extracellular recordings from acute striatal brain slices. A field recording electrode was placed in the dorso-lateral striatum and a stimulating electrode was placed nearby in the corpus callosum. Recordings were obtained in the presence of picrotoxin, a GABA $(\gamma\text{-aminobutyric acid})_A$ receptor antagonist, to block contaminating responses from intra-striatal GABAergic circuitry. We found that field excitatory postsynaptic potentials (fEPSPs) were significantly reduced in *Sapap3*$^{-/-}$ mice compared with wild-type litter mates (Fig. 3b). Axonal excitability and presynaptic function were not different from wild type, as indicated by the slope of the input–output curves normalized to the peak response, the relationship of stimulation intensity to the amplitude of the action potential component (NP1; Supplementary Fig. 2a, b), and paired-pulse ratios (Fig. 3c), indicating that the reduction in total field responses was probably due to a postsynaptic impairment in synaptic transmission.

We next evaluated NMDAR-dependent responses by recording in the presence of an AMPAR antagonist (NBQX) and the NMDAR co-factor glycine, in the absence of magnesium. Surprisingly, in contrast to the reduction we observed in the total fEPSP amplitude, which is dominated by AMPAR transmission under these conditions, the NMDAR-dependent fEPSPs were elevated in *Sapap3*$^{-/-}$ mice (Fig. 3d, e). These findings indicate a differential effect of *Sapap3* deletion on extracellular field potentials that are dependent on AMPAR and NMDAR activity. We further tested whether the synaptic defects are unique to the striatum by examining synaptic transmission in the hippocampus, in which *Sapap1*, *3* and *4* are highly expressed[17,18]. We found no defects in CA3–CA1 hippocampal basal synaptic transmission in *Sapap3*$^{-/-}$ mice (Supplementary Fig. 2c, d), probably reflecting functional redundancy or compensation by other members of the SAPAP family. Together, these findings identify an important role for SAPAP3 in postsynaptic glutamatergic synaptic function at cortico-striatal synapses.

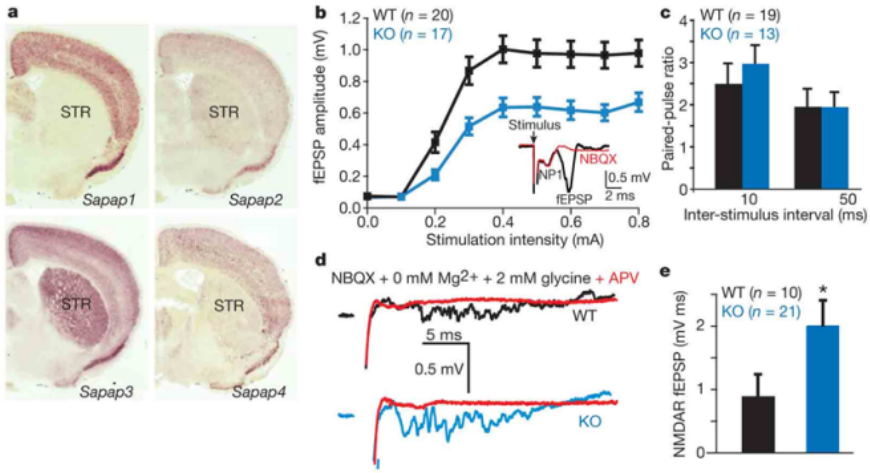

Figure 3 | Altered cortico-striatal synaptic transmission in *Sapap3*-mutant mice. **a**, Only *Sapap3* messenger RNA is highly expressed in the striatum (STR). **b**, Cortico-striatal field potential recordings of acute brain slices show decreased fEPSPs in *Sapap3*$^{-/-}$ mice. $P < 0.001$, repeated measures ANOVA. Inset shows a typical field recording (black trace) and sensitivity to NBQX (red trace). NP1, negative peak 1. **c**, Paired-pulse ratios (slope of fEPSP no. 2/slope fEPSP no. 1) are similar between wild-type and *Sapap3*$^{-/-}$ mice. **d**, Example traces of NMDAR-dependent fEPSPs recorded in the presence of 50 μM NBQX, 0 mM Mg^{2+} and 2 mM glycine. Sensitivity to APV is indicated by the red trace. **e**, NMDAR fEPSP area is increased in *Sapap3*$^{-/-}$ mice. $^{*}P < 0.05$, two-tailed *t*-test; number of recordings in parentheses. All data are presented as means ± s.e.m.

Altered NMDAR composition of the PSD in striatum

To investigate the potential role of SAPAP3 in postsynaptic assembly, we examined the levels of a select group of PSD proteins that directly or indirectly interact with SAPAPs, using biochemically purified PSD fractions from the striatum of wild-type and *Sapap3*$^{-/-}$ mice. We found no significant differences in the levels of PSD95, PSD93 or Shank proteins in the striatal PSD between the genotypes (Fig. 4a, b). However, the level of NR1, the obligatory subunit of the NMDAR, was significantly increased (Fig. 4a, b). This result is consistent with our data from extracellular recordings in the striatum, which showed increased NMDAR field potential responses. Although we cannot exclude the possibility that the larger NMDAR-dependent fEPSPs include a contribution from activated conductances other than NMDARs (a limitation of extracellular recordings), our electrophysiological data in combination with these biochemical findings indicate that an increase in NMDARs in the PSD may result in increased synaptic NMDAR activity in *Sapap3*$^{-/-}$ mice. Interestingly, we also found that the level of NR2B, the 'juvenile' subunit of the NMDAR, was significantly increased in the PSD of *Sapap3*$^{-/-}$ mice, whereas NR2A, the 'adult' subunit, was significantly reduced (Fig. 4a, b). In contrast, we found no significant changes in the overall levels of NR1, NR2A and NR2B subunits in the total striatal lysate (Supplementary Fig. 3a, b), suggesting that the changes in these subunits occur exclusively at the PSD. Synaptic NMDARs are known to undergo a developmental switch from predominantly NR1/NR2B to NR1/NR2A or NR1/NR2A/NR2B during the first two postnatal weeks of life[22–27]. Although the underlying molecular mechanisms of this developmental switch are not well understood, postsynaptic scaffolding proteins, including the PSD95 and SAPAP family of proteins, have been implicated in this process[28–31]. Our data indicate that the NMDAR subunit composition at cortico-striatal synapses of adult *Sapap3*$^{-/-}$ mice is similar to that of wild-type juvenile mice[27,28], indicating that SAPAP3 may play an important part in synaptic NMDAR subunit switching and maturation at cortico-striatal synapses.

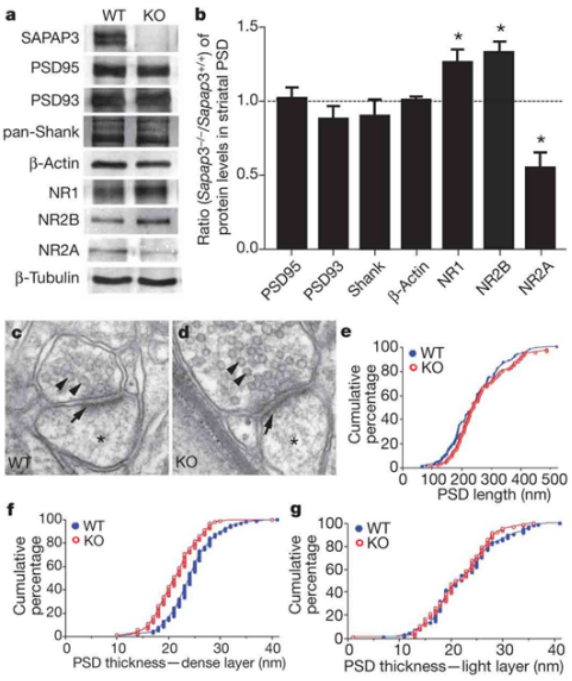

Figure 4 | Structural and biochemical analyses of cortico-striatal synapses in *Sapap3*-mutant mice. **a**, **b**, The levels of PSD95 (DLG4), PSD93 (DLG2) and Shank (SHANK1-3) in striatal PSD fractions are not affected in *Sapap3*$^{-/-}$ mice. The levels of NR1 (GRIN1) and NR2B (GRIN2B) subunits are increased, whereas that of NR2A (GRIN2A) is decreased. β-actin and β-tubulin were used as loading controls. $^*P < 0.05$, two-tailed *t*-test. All data are presented as means ± s.e.m. **c**, **d**, Electron micrographs show the presence of synaptic vesicles (arrowheads), postsynaptic densities (arrows) and dendritic spines (asterisks). **e**, The length of the PSD is not significantly different in wild-type and *Sapap3*$^{-/-}$ mice. **f**, **g**, The thickness of the dense layer (**f**) of the PSD in *Sapap3*$^{-/-}$ mice, but not the light layer (**g**), is reduced. $P < 0.001$, two-tailed *t*-test; $n = 94$ for wild type and $n = 92$ for *Sapap3*$^{-/-}$ mice.

Structure of cortico-striatal synapses in *Sapap3*$^{-/-}$ mice

To determine whether these electrophysiological and biochemical defects are accompanied by morphological changes, we examined the spine density of medium spiny neurons in the striatum using both Golgi staining and DiI filling by Diolistics. We found similar spine densities on medium spiny neurons in *Sapap3*$^{-/-}$ and wild-type mice at postnatal day (P)21 (Supplementary Fig. 3c–e) and in adults (data not shown), indicating that spine formation and maintenance were not affected by the lack of SAPAP3 proteins.

We next examined whether deletion of *Sapap3* affects PSD ultrastructure at cortico-striatal synapses using electron microscopic analysis to measure the length and thickness of the PSD in the striatum (Fig. 4c, d). We found no significant difference in length of the PSD between *Sapap3*$^{-/-}$ and wild-type mice (Fig. 4e). The PSD is reported to exhibit a laminar organization: NMDARs, scaffolding proteins and signalling proteins reside in the electron-dense layer near the synaptic membrane, whereas proteins linked to trafficking and the actin cytoskeleton reside in the filamentous fringe towards the cytoplasm[32]. Accordingly, we independently measured the thickness of the 'dense layer' and the fringe 'light layer'. We found a small but significant reduction in thickness of the dense layer but not the light layer (Fig. 4f, g) of the PSD in striatal synapses in *Sapap3*$^{-/-}$ mice, suggesting a subtle defect in the structure of the postsynaptic complex. This finding is consistent with the proposed role of SAPAP3 as a postsynaptic scaffolding protein at excitatory synapses[12,17].

Rescue by striatal-specific expression of *Sapap3*

Our findings of altered cortico-striatal synaptic function and structure in *Sapap3*-mutant mice, along with pre-existing evidence for the role of striatal circuitry in the pathogenesis of OC-spectrum disorders led us to ask whether loss of SAPAP3 in the striatum was critical for the phenotypes of *Sapap3*$^{-/-}$ mice. We therefore investigated whether selective expression of SAPAP3 in the striatum was sufficient to rescue the phenotypes of *Sapap3*$^{-/-}$ mice. We generated lentiviral vectors that express either green fluorescent protein (GFP) alone or a GFP–SAPAP3 fusion protein. GFP was fused to SAPAP3 at the amino terminus, a region with no known protein–protein interaction sites or motifs. As expected, GFP–SAPAP3 fusion proteins properly localized to synapses when transfected into cultured neurons (Supplementary Fig. 4a).

Lentiviruses expressing either GFP or GFP–SAPAP3 were delivered to the striatum of *Sapap3*$^{-/-}$ mice by bilateral microinjections at P7. To minimize injury and maximize lentiviral infection, we gave injections at one anterior and one posterior site per hemisphere and delivered lentivirus to 8 locations per hemisphere by injection of lentivirus along the needle path (Fig. 5a; see Methods). Sustained expression of GFP and GFP–SAPAP3 was observed in both dorsal and ventral striatum in post-mortem examination of brains at the end of the study (Fig. 5b–e, and Supplementary Fig. 4b, c).

At 4–6 months after injection, behavioural analyses were conducted to assess grooming, facial lesions and anxiety-like behaviours. When examined by continuous videotaping, excessive grooming was markedly reduced in *Sapap3*$^{-/-}$ mice injected with lentivirus encoding GFP–SAPAP3 in comparison to *Sapap3*$^{-/-}$ mice injected with the control *GFP* lentivirus (Fig. 5f). Moreover, facial

lesion severity was also significantly reduced in *Sapap3*$^{-/-}$ mice injected with *GFP–Sapap3* lentivirus (Fig. 5g, h). All eight *Sapap3*$^{-/-}$ mice injected with the control *GFP* lentivirus developed open skin lesions (six with large lesions, one with medium, and one with small open wounds). In contrast, only three of the eight *Sapap3*$^{-/-}$ mice injected with GFP–SAPAP3 developed open skin lesions (one with large, one with medium, and one with small open wounds), whereas two had small hairless patches and three had normal skin conditions (Fig. 5i). Furthermore, *Sapap3*$^{-/-}$ mice injected with lentivirus encoding GFP–SAPAP3 also showed reduced anxiety-like behaviour in the dark–light emergence test (Fig. 5j, k), with no change in total activity (data not shown). Finally, lentiviral-mediated expression of GFP–SAPAP3 in the striatum also rescued defects in cortico-striatal synaptic transmission in *Sapap3*$^{-/-}$ mice (Fig. 5l, m). Together, these data show that early postnatal expression of GFP–SAPAP3 selectively in the striatum is sufficient to alleviate the major manifestations of the OCD-like phenotype in *Sapap3*$^{-/-}$ mice.

Discussion

Although dysfunction of cortico-striato-thalamo-cortical circuitry has been widely implicated in OC-spectrum disorders, the nature of this dysfunction remains unclear. Our study of *Sapap3*-mutant mice has identified an important role for SAPAP3 at cortico-striatal synapses and, although there are inherent limitations of evaluating thought content in mice, our study further indicates that cortico-striatal synaptic defects may be central to the genesis of OCD-like behaviours. These conclusions are supported by several lines of evidence. First, *Sapap3*$^{-/-}$ mice exhibit OCD-like behaviours: excessive time spent performing a ritualistic action to the point of being self-injurious, increased anxiety-like behaviours, and response of these manifestations to a selective serotonin reuptake inhibitor. Second, SAPAP3 protein is localized to excitatory, but not inhibitory, synapses[15]. Third, *Sapap3* is the only member of the *Sapap* family that is highly expressed in the striatum. Fourth, *Sapap3*-mutant mice have reduced cortico-striatal synaptic transmission and an NMDAR subunit composition suggestive of immature cortico-striatal synapses. Finally, selective expression of *Sapap3* in the striatum of *Sapap3*$^{-/-}$ mice rescues the synaptic defects and OCD-like behaviours.

Anxiety is attributed primarily to dysfunction of the amygdala and ventral hippocampus. Interestingly, SAPAP3, unlike SAPAP1 and SAPAP4, is not highly expressed in the amygdala (Supplementary Fig. 5a–d), whereas all four members of the SAPAP family are expressed in the ventral hippocampus (Supplementary Fig. 5e–h), suggesting that anxiety-like behaviour in *Sapap3*$^{-/-}$ mice is unlikely to be due to the lack of SAPAP3 in amygdala or ventral hippocampus. The unique expression of SAPAP3 in the striatum and the alleviation of the anxiety-like behaviour by lentiviral-mediated expression of GFP–SAPAP3 in the striatum suggest that the anxiety-like behaviour in *Sapap3*$^{-/-}$ mice originates from striatal defects. Because the amygdala projects to the striatum, it is also possible that some functions of amygdalar-striatal projections are impaired in *Sapap3*$^{-/-}$ mice. Additionally, our video surveillance data indicate that *Sapap3*-mutant mice have a disrupted sleep pattern (Supplementary Fig. 6), which is alleviated by fluoxetine treatment (Supplementary Fig. 7). This sleep disturbance may also contribute to the anxiety-like behaviour in *Sapap3*$^{-/-}$ mice.

A principal role of the striatum is to integrate the various inputs arriving from the cortex and use this information to select certain motor and/or cognitive programs (decision making), which are subsequently carried out through the direct and indirect pathways of

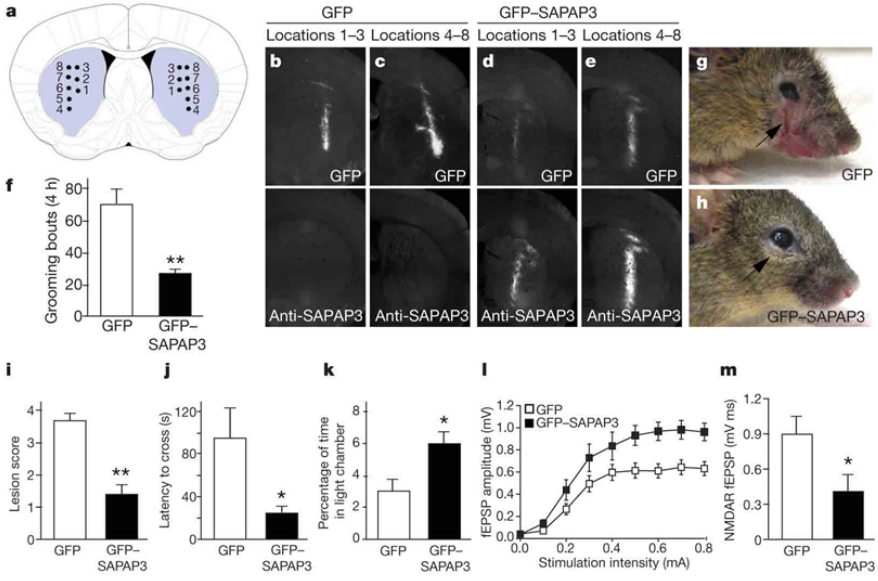

Figure 5 | Lentiviral-mediated rescue of behavioural and synaptic defects in *Sapap3*-mutant mice. **a**, Diagram showing the approximate locations of microinjections in the striatum of *Sapap3*$^{-/-}$ mice. Injection site 1, locations 1–3 are more anterior than injection site 2, locations 4–8. **b–c**, Brain sections from a *Sapap3*$^{-/-}$ mouse injected with *GFP* lentivirus show GFP fluorescence (**b**, **c**, upper panels) and an absence of SAPAP3 staining (**b**, **c**, lower panels). **d–e**, Brain sections from a *Sapap3*$^{-/-}$ mouse injected with lentivirus encoding GFP–SAPAP3 show both GFP fluorescence (**d**, **e**, upper panels) and SAPAP3 immunostaining (**d**, **e**, lower panels). **f**, Compared with *Sapap3*$^{-/-}$ mice with GFP, *Sapap3*$^{-/-}$ mice with GFP–SAPAP3 showed significantly reduced over-grooming behaviour. $^{**}P < 0.01$, two-tailed *t*-test; $n = 8$ mice per group for **f**, **i–k**. **g**, **h**, *Sapap3*$^{-/-}$ mice with GFP–SAPAP3 (**h**) had reduced severity of facial lesions when compared to *Sapap3*$^{-/-}$ mice with GFP (**g**). **i**, Semi-quantitative lesion scores. $^{**}P < 0.01$, Mann–Whitney U test. **j**, **k**, Reduced anxiety-like behaviours in *Sapap3*$^{-/-}$ mice injected with *GFP–Sapap3* lentivirus in the dark–light emergence test, including decreased latency to cross from the dark to light chamber (**j**) and increased time in the light chamber (**k**). $^{*}P < 0.05$, two-tailed *t*-test. **l**, **m**, Field recordings from infected striatal areas of P21–P25 *Sapap3*$^{-/-}$ mice with GFP–SAPAP3 showed an increase in cortico-striatal fEPSP amplitude (**l**) and a reduction of NMDAR-dependent fEPSP area (**m**). $P < 0.001$, repeated measures ANOVA for **l**; $^{*}P < 0.05$, two-tailed *t*-test for **m**; *n* is 12 and 10 for **l**, and 10 and 9 for **m** for *GFP*-injected and *GFP–Sapap3* injected mice, respectively. All data are presented as means ± s.e.m.

the basal ganglia[4]. A prominent model for OCD is that an activity imbalance between the direct and indirect pathways leads to behavioural abnormalities of OCD[3], and recent studies have shown that the two pathways are differentially regulated at cortico-striatal synapses[33–35]. We have identified defects in both AMPAR- and NMDAR-dependent synaptic transmission at cortico-striatal synapses. These data are from extracellular field recordings, representing a population average of the effects on individual neurons. If the observed effects are differentially manifested by medium spiny neurons in the direct or indirect pathway, an imbalance in activity could be readily envisioned.

Studies of the mechanisms of OC-spectrum disorders have mostly focused on the serotonergic and dopaminergic systems. However, recent genetic association studies of OCD in humans have implicated genes important for glutamatergic neurotransmission[36–38]. Together with our study of SAPAP3 in mice, these observations raise the possibility that defects in excitatory synaptic transmission in the cortico-striatal circuit may contribute to the pathogenesis of OC-spectrum disorders in humans.

METHODS SUMMARY

Behavioural analysis. *Sapap3*-knockout mice were generated by homologous recombination in R1 embryonic stem cells using standard procedures[39]. Adult mice, age 4–8 months, were used for behavioural analyses. For analyses of grooming behaviours[40], habituated, individually housed animals were videotaped for 24 h under 700 lx (day) and ~2 lx (red light at night) illumination. Tests for anxiety-like behaviours were performed as described[41,42]. All experiments were done blind to genotypes. Because of the presence of obvious facial lesions in *Sapap3*-mutant mice, it is impossible to perform video decoding in a blind manner. To avoid bias, trained individuals unfamiliar with the project (listed in the Acknowledgements) were recruited to decode the videos.

Cortico-striatal electrophysiology. Acute sagittal brain slices (300 μm) from P17–P25 mice were used for all experiments. The field recording electrode was placed in the dorso-lateral striatum and a monopolar stimulation electrode was placed in the corpus callosum. All recordings were performed at 30–32 °C and in the presence of picrotoxin and all data were collected and analysed before unblinding of genotypes.

Stereotaxic injection. One-week-old $Sapap3^{-/-}$ mice were anaesthetized and placed in a mouse head holder. *GFP* lentivirus or *GFP–Sapap3* lentivirus was bilaterally injected into the striatum through 2 sites at 8 locations per hemisphere. Behavioural analyses were performed 4–6 months after injection.

Full Methods and any associated references are available in the online version of the paper at www.nature.com/nature.

Received 30 May; accepted 16 July 2007.

1. Karno, M., Golding, J. M., Sorenson, S. B. & Burnam, M. A. The epidemiology of obsessive-compulsive disorder in five US communities. *Arch. Gen. Psychiatry* **45,** 1094–1099 (1988).
2. Torres, A. R. *et al.* Obsessive-compulsive disorder: prevalence, comorbidity, impact, and help-seeking in the British national psychiatric morbidity survey of 2000. *Am. J. Psychiatry* **163,** 1978–1985 (2006).
3. Swedo, S. E. & Snider, L. A. in *Neurobiology of Mental Illness* (eds Nestler, E. J & Charney, D.S.) 628–638 (Oxford Univ. Press, New York, 2004).
4. Graybiel, A. M. & Rauch, S. L. Toward a neurobiology of obsessive-compulsive disorder. *Neuron* **28,** 343–347 (2000).
5. Aouizerate, B. *et al.* Pathophysiology of obsessive-compulsive disorder: a necessary link between phenomenology, neuropsychology, imagery and physiology. *Prog. Neurobiol.* **72,** 195–221 (2004).
6. Hanna, G. L. *et al.* Genome-wide linkage analysis of families with obsessive-compulsive disorder ascertained through pediatric probands. *Am. J. Med. Genet.* **114,** 541–552 (2002).
7. Shugart, Y. Y. *et al.* Genomewide linkage scan for obsessive-compulsive disorder: evidence for susceptibility loci on chromosomes 3q, 7p, 1q, 15q, and 6q. *Mol. Psychiatry* **11,** 763–770 (2006).
8. Nestadt, G. *et al.* A family study of obsessive-compulsive disorder. *Arch. Gen. Psychiatry* **57,** 358–363 (2000).
9. Inouye, E. Similar and dissimilar manifestations of obsessive-compulsive neurosis in monozygotic twins. *Am. J. Psychiatry* **121,** 1171–1175 (1965).
10. Carey, G. & Gottesman, I. I. in *Anxiety: New Research and Changing Concepts* (eds Klein, D.F. & Rabkin J.) 117–136 (Raven Press, New York, 1981).
11. Chakrabarty, K., Bhattacharyya, S., Christopher, R. & Khanna, S. Glutamatergic dysfunction in OCD. *Neuropsychopharmacology* **30,** 1735–1740 (2005).
12. Kim, E. *et al.* GKAP, a novel synaptic protein that interacts with the guanylate kinase-like domain of the PSD-95/SAP90 family of channel clustering molecules. *J. Cell Biol.* **136,** 669–678 (1997).
13. Takeuchi, M. *et al.* SAPAPs. A family of PSD-95/SAP90-associated proteins localized at postsynaptic density. *J. Biol. Chem.* **272,** 11943–11951 (1997).
14. Scannevin, R. H. & Huganir, R. L. Postsynaptic organization and regulation of excitatory synapses. *Nature Rev. Neurosci.* **1,** 133–141 (2000).
15. Kim, E. & Sheng, M. PDZ domain proteins of synapses. *Nature Rev. Neurosci.* **5,** 771–781 (2004).
16. Funke, L., Dakoji, S. & Bredt, D. S. Membrane-associated guanylate kinases regulate adhesion and plasticity at cell junctions. *Annu. Rev. Biochem.* **74,** 219–245 (2005).
17. Welch, J. W., Wang, D. & Feng, G. Differential mRNA expression and protein localization of the SAP90/PSD-95-associated proteins (SAPAPs) in the nervous system of the mouse. *J. Comp. Neurol.* **472,** 24–39 (2004).
18. Kindler, S., Rehbein, M., Classen, B., Richter, D. & Bockers, T. M. Distinct spatiotemporal expression of *SAPAP* transcripts in the developing rat brain: a novel dendritically localized mRNA. *Brain Res. Mol. Brain Res.* **126,** 14–21 (2004).
19. Malinow, R. & Malenka, R. C. AMPA receptor trafficking and synaptic plasticity. *Annu. Rev. Neurosci.* **25,** 103–126 (2002).
20. Prybylowski, K. & Wenthold, R. J. *N*-Methyl-D-aspartate receptors: subunit assembly and trafficking to the synapse. *J. Biol. Chem.* **279,** 9673–9676 (2004).
21. Nicoll, R. A., Tomita, S. & Bredt, D. S. Auxiliary subunits assist AMPA-type glutamate receptors. *Science* **311,** 1253–1256 (2006).
22. Sheng, M., Cummings, J., Roldan, L. A., Jan, Y. N. & Jan, L. Y. Changing subunit composition of heteromeric NMDA receptors during development of rat cortex. *Nature* **368,** 144–147 (1994).
23. Shi, J., Aamodt, S. M. & Constantine-Paton, M. Temporal correlations between functional and molecular changes in NMDA receptors and GABA neurotransmission in the superior colliculus. *J. Neurosci.* **17,** 6264–6276 (1997).
24. Stocca, G. & Vicini, S. Increased contribution of NR2A subunit to synaptic NMDA receptors in developing rat cortical neurons. *J. Physiol.* **507,** 13–24 (1998).
25. Tovar, K. R. & Westbrook, G. L. The incorporation of NMDA receptors with a distinct subunit composition at nascent hippocampal synapses *in vitro*. *J. Neurosci.* **19,** 4180–4188 (1999).
26. Chapman, D. E., Keefe, K. A. & Wilcox, K. S. Evidence for functionally distinct synaptic NMDA receptors in ventromedial versus dorsolateral striatum. *J. Neurophysiol.* **89,** 69–80 (2003).
27. Li, L., Murphy, T. H., Hayden, M. R. & Raymond, L. A. Enhanced striatal NR2B-containing methyl-D-aspartate receptor-mediated synaptic currents in a mouse model of Huntington disease. *J. Neurophysiol.* **92,** 2738–2746 (2004).
28. Sans, N. *et al.* A developmental change in NMDA receptor-associated proteins at hippocampal synapses. *J. Neurosci.* **20,** 1260–1271 (2000).
29. Barria, A. & Malinow, R. Subunit-specific NMDA receptor trafficking to synapses. *Neuron* **35,** 345–353 (2002).
30. Prybylowski, K. *et al.* The synaptic localization of NR2B-containing NMDA receptors is controlled by interactions with PDZ proteins and AP-2. *Neuron* **47,** 845–857 (2005).
31. van Zundert, B., Yoshii, A. & Constantine-Paton, M. Receptor compartmentalization and trafficking at glutamate synapses: a developmental proposal. *Trends Neurosci.* **27,** 428–437 (2004).
32. Valtschanoff, J. G. & Weinberg, R. J. Laminar organization of the NMDA receptor complex within the postsynaptic density. *J. Neurosci.* **21,** 1211–1217 (2001).
33. Day, M. *et al.* Selective elimination of glutamatergic synapses on striatopallidal neurons in Parkinson disease models. *Nature Neurosci.* **9,** 251–259 (2006).
34. Kreitzer, A. C. & Malenka, R. C. Endocannabinoid-mediated rescue of striatal LTD and motor deficits in Parkinson's disease models. *Nature* **445,** 643–647 (2007).
35. Surmeier, D. J., Ding. J., Day, M., Wang, Z. & Shen, W. D1 and D2 dopamine-receptor modulation of striatal glutamatergic signaling in striatal medium spiny neurons. *Trends Neurosci.* **30,** 228–235 (2007).
36. Arnold, P. D. *et al.* Association of a glutamate (NMDA) subunit receptor gene (*GRIN2B*) with obsessive-compulsive disorder: a preliminary study. *Psychopharmacology* **174,** 530–538 (2004).
37. Arnold, P. D., Sicard, T., Burroughs, E., Richter, M. A. & Kennedy, J. L. Glutamate transporter gene *SLC1A1* associated with obsessive-compulsive disorder. *Arch. Gen. Psychiatry* **63,** 769–776 (2006).
38. Dickel, D. E. *et al.* Association testing of the positional and functional candidate gene *SLC1A1/EAAC1* in early-onset obsessive-compulsive disorder. *Arch. Gen. Psychiatry* **63,** 778–785 (2006).
39. Feng, G. *et al.* Dual requirement for gephyrin in glycine receptor clustering and molybdoenzyme activity. *Science* **282,** 1321–1324 (1998).
40. Greer, J. M. & Capecchi, M. R. Hoxb8 is required for normal grooming behavior in mice. *Neuron* **33,** 23–34 (2002).
41. Pogorelov, V. M., Rodriguiz, R. M., Insco, M. L., Caron, M. G. & Wetsel, W. C. Novelty seeking and stereotypic activation of behavior in mice with disruption of the *DAT1* gene. *Neuropsychopharmacology* **30,** 1818–1831 (2005).
42. Weisstaub, N. V. *et al.* Cortical 5-HT2A receptor signaling modulates anxiety-like behaviors in mice. *Science* **313,** 536–540 (2006).
43. Bakeman, R. & Gottman, J. M. in *Observing Interaction: An Introduction to Sequential Analyses* 56–90 (Cambridge Univ. Press, New York, 1997).
44. Treit, D. & Fundytus, M. Thigmotaxis as a test for anxiolytic activity in rats. *Pharmacol. Biochem. Behav.* **31,** 959–962 (1988).

45. Crawley, J. N. & Goodwin, F. K. Preliminary report of a simple animal behavior model for the anxiolytic effects of benzodiazepines. *Pharmacol. Biochem. Behav.* **12,** 167–170 (1980).
46. Feng, G. *et al.* Imaging neuronal subsets in transgenic mice expressing multiple spectral variants of GFP. *Neuron* **28,** 41–51 (2000).
47. Gan, W. B., Grutzendler, J., Wong, W. T., Wong, R. O. & Lichtman, J. W. Multicolor "DiOlistic" labeling of the nervous system using lipophilic dye combinations. *Neuron* **27,** 219–225 (2000).
48. Lois, C., Hong, E. J., Pease, S., Brown, E. J. & Baltimore, D. Germline transmission and tissue-specific expression of transgenes delivered by lentiviral vectors. *Science* **295,** 868–872 (2002).
49. Parker, M. J., Zhao, S., Bredt, D. S., Sanes, J. R. & Feng, G. PSD93 regulates synaptic stability at neuronal cholinergic synapses. *J. Neurosci.* **24,** 378–388 (2004).
50. Lau, L. F. & Huganir, R. L. Differential tyrosine phosphorylation of *N*-methyl-D-aspartate receptor subunits. *J. Biol. Chem.* **270,** 20036–20041 (1995).

Supplementary Information is linked to the online version of the paper at www.nature.com/nature.

Acknowledgements We thank J. Gross, K. Phend and L. Qiu for technical assistance, and L. Phillips, L. Nguyen, S. Greeter, J. Wilkins and M. Fukui for assistance in behavioural testing and decoding of video tapes. We thank M. Ehlers for the anti-NR2B antibody and E. Kim for the anti-Shank antibody. We also thank M. Caron, M. Ehlers, Z. He, J. Sanes, F. Wang, A. West and members of the Feng laboratory for critical reading of the manuscript. This work was supported by grants from NINDS and NIMH to G.F., R.J.W. and N.C.; by unrestricted funds to W.C.W.; and by the Intramural Research Program of NIEHS to S.M.D. J.M.W. was supported by an NSF pre-doctoral fellowship and an NIH National Research Service Award. N.C. is a recipient of a Klingenstein Fellowship in the Neurosciences and a NARSAD Young Investigator Award. G.F. is a recipient of a Sloan Fellowship, a Klingenstein Fellowship in the Neurosciences, an EJLB Foundation Scholar Research Program Award, a McKnight Neuroscience of Brain Disorders Award and a Hartwell Foundation Individual Biomedical Research Award.

Author Contributions J.M.W., J. Lu, R.M.R., N.C.T., J.P., J.-D.D., C.F., M.C. and J.P.A. participated in the design, analysis and execution of experiments. G.F., N.C., W.C.W., J.M.W., R.J.W., S.M.D. and J. Luo participated in the design, analysis and interpretation of experiments.

Author Information Reprints and permissions information is available at www.nature.com/reprints. The authors declare no competing financial interests. Correspondence and requests for materials should be addressed to G.F. (feng@neuro.duke.edu).

METHODS

Mice. A targeting vector was designed to replace exon 3 (containing the translation initiation codon) of the *Sapap3* gene with a *NEO* cassette. Genotypes were determined by PCR of mouse tail DNA, using primer F1 (ATTGGTAGGCAATACCAACAGG) and R1 (GCAAAGGCTCTTCATATTGTTGG) for the wild-type allele (147 base pairs), and F1 and R2 (CTTTGTGGTTCTAAGTACTGTGG; in neo cassette) for the mutant allele (222 base pairs). Primer locations are indicated in Supplementary Fig. 1.

Grooming behaviour[40]**.** Because behaviours were most representative at the times 02:00–06:00, 10:00–14:00 and 18:00–22:00, these segments were selected for analyses using Noldus Observer software (Leesburg). The total amount of time in each 4-h segment spent grooming, eating, sleeping, rearing, digging or pushing bedding (shifting) was determined, along with general states of activity. Grooming included all sequences of face-wiping, scratching/rubbing of head and ears, and full-body grooming. Bouts of behaviour lasted at least 3 s; pauses longer than 3 s constituted a new bout. Observer reliability was determined with Cohen's kappa[43].

Anxiety-like behaviours[41,42]**.** Zero maze: an elevated zero maze[41] was indirectly illuminated at 60 lx. Testing commenced with an animal being introduced into a closed area of the maze. Behaviour was video-taped for 5 min and subsequently scored by trained observers using the Noldus Observer (Nodus Information Technology). Anxiety-like behaviour was deduced on the basis of the percentage of time spent in the open areas and the latency to enter the open areas. Total activity time in the maze was an indicator of motor activity. Observer reliability was determined with Cohen's Kappa.

Open field: spontaneous locomotor activity was evaluated over 30 min in an automated Omnitech Digiscan apparatus (AccuScan Instruments) as described[44]. Locomotor activity was assessed as total distance travelled (cm). Anxiety-like behaviour was defined by the percentage of time spent in the centre as contrasted with the percentage of time spent in the perimeter (thigmotaxis) of the open field.

Dark–light emergence test[45]: Mice were adapted in an adjacent room to low light conditions (~40 lx) and the test room was initially under similar illumination. Testing was conducted in a two-chambered test apparatus (Med-Associates), with one side draped in black cloth (for example, dark-chamber) and the other illuminated at ~1,400 lx (for example, light-chamber) with a 170 mA high intensity house light and overhead fluorescent lamps. Immediately on placing the mice into the darkened chamber, the lighted chamber was illuminated and the door between the two chambers was opened. The mice were allowed to freely explore the apparatus for 5 min. The latency to emerge from the darkened into the lighted chamber and the percentage of time spent in the illuminated chamber were used as indices of anxiety-like behaviours. Total motor activity in the two chambers was measured by infrared beam-breaks.

Fluoxetine treatment. Adult mice 4–6 months of age were injected with fluoxetine (5 mg kg^{-1}, intraperitoneally) once a day for one or six days and behaviours were tested 24 h after the final injection. Grooming and anxiety-like behaviours were tested as described above.

Skin analyses. Haematoxylin and eosin staining was performed on facial skin below the eyes by following a standard protocol. For visualization of sensory nerves in skin, *Sapap3*-mutant mice were crossed with Thy1GFP-J mice[46]. Mice were perfused transcardially with saline and 4% paraformaldehyde, and skin from just below the eyes was dissected and post-fixed for 24 h. Confocal images were taken from 50-μm cryosections. Skin lesions were scored as follows: 0, normal skin; 1, hairless patches; 2, small open-wound lesions, length <2 mm; 3, moderate open-wound lesions, length 2–4 mm; 4, large open-wound lesions, length >4 mm.

Cortico-striatal electrophysiology. Recording perfusion solution contained (in mM): 119 NaCl, 2.5 KCl, 1.2 NaH_2PO_4, 26 $NaHCO_3$, 1 $MgCl_2$, 2 $CaCl_2$ and 0.1 picrotoxin ($GABA_A$ receptor antagonist). Slicing and recovery solutions were identical to perfusion solution except for containing 0.5 $CaCl_2$ and no picrotoxin. APV (50 μM) and NBQX (50 μM) were obtained from Tocris. Solutions were continuously equilibrated with 95% O_2 and 5% CO_2 (pH 7.4) and perfusion flow rate was 2 ml min^{-1}. Slices were allowed to recover for a minimum of 1 h at 30–32 °C, following slicing. All recordings were performed at 30–32 °C.

The field recording electrode was placed in the dorso-lateral striatum and a monopolar stimulation electrode was placed in the corpus callosum. Current was delivered to the stimulating electrode using an AMPI. Stimulus Isolator (AMPI) for 150 μs. Three distinct components were resolved in the majority of recordings: stimulation artefact, negative peak 1 (NP1, action-potential-derived on the basis of latency, resistance to NBQX and picrotoxin, and sensitivity to tetrodotoxin) and negative peak 2 (NP2, fEPSP based on latency and sensitivity to NBQX; in addition, sensitivity to tetrodotoxin indicates the response is not due to direct activation by stimulating electrode current). The callosal stimulation site was chosen over an intra-striatal site to minimize activation of non-cortical axons. Data were acquired at 20 kHz and filtered at 2 kHz using MultiClamp 700B amplifier and pClamp 10.0 software (Axon Instruments). Data were analysed offline using Clampfit 10.0 (Axon Instruments). Five consecutive responses were averaged before measuring amplitude, slope or area in the respective assays. When amplitudes are reported, similar conclusions were obtained by slope analysis. Paired-pulse responses were evoked using a stimulation intensity that yielded the maximal fEPSP response. Slope values used for paired-pulse ratios refer to slope during the period from 20–80% of the peak response. NMDAR fEPSPs were evoked using the same stimulation intensity that yielded the maximal fEPSP response under the basal recording conditions used to generate the input–output curves. The area of NMDAR field potential responses was measured during a standard 20-ms time window beginning approximately 8 ms after stimulation. All data were collected and analysed before unblinding of genotypes. In addition, NMDAR field potential recordings and correlative PSD biochemical studies were performed in two different laboratories and were unblinded at the same time.

For *in vivo* viral expression rescue experiments, the same slicing, recording, and analysis methods were used as described above except that the stimulating and recording electrodes were placed within the fluorescent green tissue. Only slices where green cells were visible in the dorsolateral recording region were used. Viral rescue experiments were performed and analysed blind to the viral identity.

Diolistics. 'Bullets' were prepared by coating tungsten particles (Bio-rad) with DiI (Molecular Probes-Invitrogen) dissolved in methylene chloride as described[47]. Mice were perfused transcardially, first with normal saline, and then with buffered 4% paraformaldehyde. Fixed mice were decapitated and the head was allowed to post-fix for 24–48 h in buffered 4% paraformaldehyde at 4 °C. Brains were dissected and 250 μm coronal slices were cut on a vibratome.

Diolistic filling of individual cells was performed using a standard Bio-Rad biolistic system. Slices were placed into the interior chamber of a Falcon organ tissue culture dish (catalogue number 3,037) and excess buffer was removed. A Millipore 3.0-μm Isopore filter (catalogue number TSTP04704) was placed to rest on top of the tissue culture dish and a Kimwipe was placed on top of the Millipore filter. Bullets were shot through the Kimwipe and filter barrier using a helium charge of 552 kPa (80 psi). Individual labelling of 3–15 striatal medium spiny neurons was successful in approximately 50% of slices. Following the diolistic procedure, slices were allowed to incubate in buffer at 4 °C for 1–2 h. Following incubation, slices were immediately mounted and imaged on a confocal microscope.

Lentivirus production and stereotaxic injection. The lentivirus vector was based on FUGW[48] and modified by replacing the ubiquitin promoter with a CMV promoter to improve neuronal expression. GFP was fused to the amino terminus of SAPAP3 to generate the GFP–SAPAP3 fusion protein. The complementary DNA clone encoding GFP or GFP–SAPAP3 was placed downstream of the CMV promoter between *Bam*HI and *Eco*RI sites[48]. Viral particles were produced by transient transfection of 293T cells with the lentiviral vector encoding GFP or GFP–SAPAP3 along with the envelope (VSVg) and packaging (Δ8.9) vectors. High titre viral suspensions were obtained by ultra-centrifugation at 77,000*g* for 90 min.

One-week-old $Sapap3^{-/-}$ mice were anaesthetized with a mixture of ketamine and xylazine (intraperitoneally), and placed in a mouse head holder (David Kopf Instruments). Lentivirus encoding GFP or GFP–SAPAP3 was bilaterally injected into the striatum through two sites at eight locations per hemisphere. At each of the injection sites, the microinjection needle was advanced to the deepest (ventral) position for the first injection; additional injections were made every 0.3 mm while withdrawing the injection needle. The coordinates from Bregma were: injection site 1, location 1–3: anterior 0.5 mm, mediolateral 1.4 mm, dorsoventral 2.8, 2.5, 2.2 mm; injection site 2, location 4–8: anterior 0.2 mm, mediolateral 1.7 mm, dorsoventral 3.3, 3.0, 2.7, 2.4, 2.1 mm. For each injection location, 90 nl of virus was injected using Nanoject II (Drummond Scientific), and the needle was left in place for 3 min after each injection.

Electron microscopic analysis. Striatal tissues for electron microscopic analysis were processed and quantitatively analysed according to protocols previously described[32]. Synapses with clear membranes (likely to be cut orthogonal to the plane of the synaptic membrane) were photographed at ×15,000 magnification. Data collection and analysis were performed by observers blinded to genotypes. For every clearly defined synapse, data for PSD length and PSD thickness were collected.

PSD preparation and western blot. PSD fractions of the striatum were prepared as described[17,49], separated by SDS–PAGE and probed with specific antibodies. The relative amount of β-tubulin and β-actin were used as loading controls for quantification. Antibodies for SAPAP3, PSD95, PSD93, Shank and NR2B have been described previously[17,49,50]. Antibodies for NR1 (mouse monoclonal) and NR2A (rabbit polyclonal) were from BD Biosciences and Upstate, respectively.

Figure S1

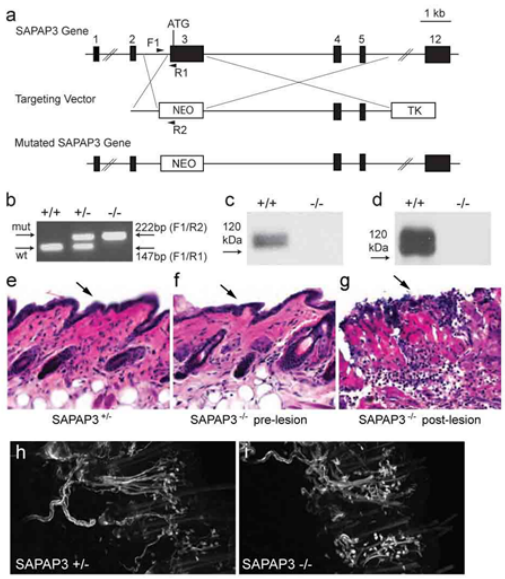

Figure S1: Generation and initial characterization of SAPAP3 knockout mice. a, Strategy for generating SAPAP3 knockout mice. The SAPAP3 gene contains 12 exons; exon 3 that includes the translation initiation codon (ATG) was replaced by a neomycin cassette (NEO). TK, thymidine kinase cassette. Locations of PCR primers for genotyping are indicated by arrowheads (F1, R1, and R2). **b,** PCR screening of mouse tail DNA (+/+, wildtype; +/-, heterozygote; -/-, homozygous mutant). **c, d,** Immunoblots of brain lysate (c) and PSD fractions (d) probed with a SAPAP3-specific antibody showing the absence of SAPAP3 proteins in SAPAP3$^{-/-}$ mice. **e, f,** H&E staining shows normal skin morphology from pre-lesion SAPAP3-/- mice. **g,** Only post-lesion skin from SAPAP3$^{-/-}$ mice showed damaged epidermis (arrow) and infiltration of lymphocytes/granulocytes, likely due to injury and infection. **h, i,** Comparable sensory innervation in facial skin of SAPAP3$^{+/-}$ and SAPAP3$^{-/-}$ mice (crossed to Thy1GFP-J mice) revealed by GFPlabeled sensory nerves and nerve terminals.

Figure S2

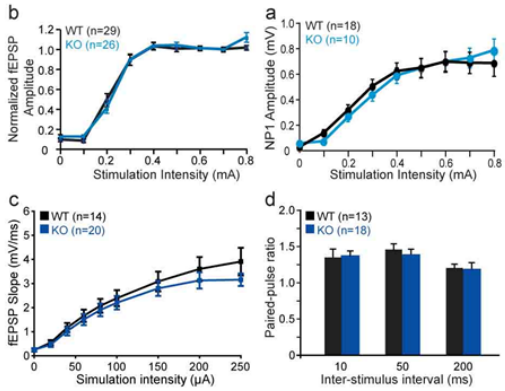

Figure S2: Additional electrophysiological characterization of SAPAP3 mutant mice. a, Input-output curve normalized to maximal response from cortico-striatal field potential recordings of acute brain slices shows identical slopes for wildtype (WT) and SAPAP3$^{-/-}$ (KO) mice. **b**, cortico-striatal field potential recordings of acute brain slices shows normal relationship between stimulation intensity and NP1 (action potential derived) amplitude between wildtype and SAPAP3$^{-/-}$ mice. **c, d**, Basic synaptic transmission in the hippocampus of SAPAP3$^{-/-}$ mice is normal. Hippocampal slices were prepared from SAPAP3$^{-/-}$ mice and wildtype littermate controls, and field recordings were performed from the dorsal hippocampus. No difference in synaptic transmission was observed between wildtype and SAPAP3$^{-/-}$ animals, as shown using different stimulus intensities (**c**). In addition, no difference in presynaptic function in the hippocampus was observed between wildtype and SAPAP3$^{-/-}$ animals, as indicated by normal paired-pulse ratios (**d**).

Figure S3

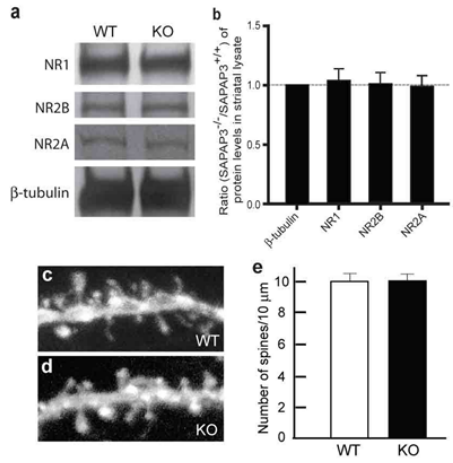

Figure S3: Biochemical and structural analysis of cortico-strial synapses in SAPAP3 mutant mice. a, Total protein lysates were prepared from the striatum of adult wildtype and SAPAP3$^{-/-}$ mice and probed with antibodies specific to NR1, NR2A or NR2B subunit of the NMDAR. Antibodies to β-tubulin were used for loading controls. **b**, Quantification of the relative levels of NR1, NR2A and NR2B in wildtype and SAPAP3$^{-/-}$ total striatal lysates. No significant differences were detected between genotypes in the total levels of NR1, NR2A and NR2B in striatal lysates. **c, d,** Morphology of MSNs in the fixed brain slices of wildtype (**c**) and SAPAP3$^{-/-}$ (**d**) mice was revealed with DiI filling by Diolistics. e, Similar spine densities on medium spiny neurons of wildtype and SAPAP3$^{-/-}$ mice. Data were collected from 21 and 26 dendrites from P21 wildtype and SAPAP3$^{-/-}$ mice, respectively.

Figure S4

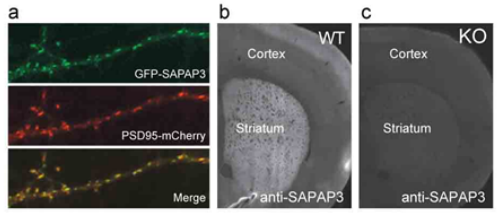

Figure S4: Characterization of the GFP-SAPAP3 construct and the anti-SAPAP3 antibody. a, GFP-SAPAP3 and PSD95-mCherry (to mark excitatory synapses) plasmid constructs were cotransfected into cultured hippocampal neurons. GFP-SAPAP3 (top) and PSD95-mCherry (middle) fusion proteins are precisely colocalized (bottom), indicating that GFP-SAPAP3 proteins are targeted to synapses. **b, c**, immunostaining of coronal brain sections from wildtype (**b**) and SAPAP3$^{-/-}$ (**c**) mice show the specificity of the anti-SAPAP3 antibody.

Figure S5

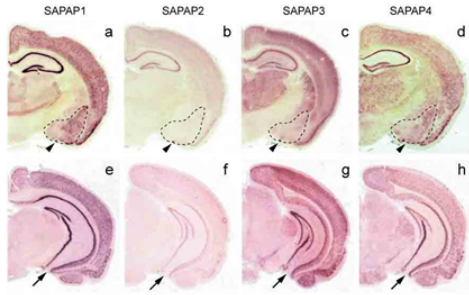

Figure S5: Expression of SAPAPs in the hippocampus and amygdala. a-d, *In situ* hybridization showing that mRNA of SAPAP1 and 4, but not SAPAP3, are highly expressed in the amygdala (dotted line and arrowheads). **e-h**, *In situ* hybridization showing that mRNA of SAPAP1, 3 and 4 are highly expressed in both the dorsal and ventral hippocampus (arrows).

Figure S6

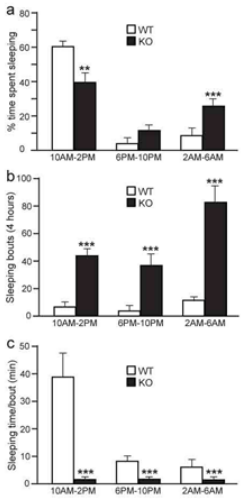

Figure S6: Disrupted sleeping patterns in SAPAP3 mutant mice. a, 24 hour video taping showed that SAPAP3$^{-/-}$ mice slept less during the normal sleeping period (10AM to 2PM) and slept more during the activity time (2AM to 6AM). Most strikingly, SAPAP3$^{-/-}$ mice showed significantly increased sleeping bouts (**b**), and thus sleeping time per sleeping bout was dramatically reduced (**c**), indicating their sleep was frequently disrupted. Data were collected from the same groups of mice shown in Fig. 1b, c in the main text. $p<0.001$ for a and c, and $p<0.01$ for b with repeated measures ANOVA (time block x genotype); **p< 0.02, ***p< 0.001, Bonferroni corrected pair-wise comparisons (post-hoc tests).

Figure S7

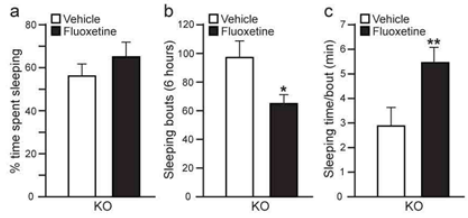

Figure S7: Sleep was less disrupted in fluoxetine-treated SAPAP3$^{-/-}$ mice. Data (1pm-7pm) were collected from the same groups of mice shown in Fig. 2a-c in the main text, which were treated once a day with vehicle or fluoxetine (5 mg/kg, i.p.) for 6 days. Fluoxetine significantly reduced the number of sleeping bouts (b) and increased sleeping time per bout (c). *p< 0.05, **p< 0.01, two-tailed t-test.

ITQB-UNL | Av. da República, 2780-157 Oeiras, Portugal
Tel (+351) 214 469 100
Fax (+351) 214 411 277

www.itqb.unl.pt